Investigating the role of wind disturbance in tropical forests through a forest dynamics model and satellite observations

E-Ping Rau

Université Fédérale
Toulouse Midi-Pyrénées

THÈSE

En vue de l'obtention du
DOCTORAT DE L'UNIVERSITÉ DE TOULOUSE

Délivré par l'Université Toulouse 3 - Paul Sabatier

Présentée et soutenue par

E-Ping RAU

Le 18 janvier 2022

Rôle de la perturbation par le vent dans les forêts tropicales via un modèle dynamique de végétation et lobservation satellitaire

---

Ecole doctorale : **SEVAB - Sciences Ecologiques, Vétérinaires, Agronomiques et Bioingenieries**

Spécialité : **Ecologie, biodiversité et évolution**

Unité de recherche :
EDB - Evolution et Diversité Biologique

Thèse dirigée par
Jérôme CHAVE

Jury

M. Benoit COURBAUD, Rapporteur
M. Hank SHUGART, Rapporteur
Mme Isabelle MARECHAUX, Examinatrice
M. Thierry KOLECK, Examinateur
M. Jérôme CHAVE, Directeur de thèse
M. Christophe THEBAUD, Président

UNIVERSITÉ ET LABORATOIRES

Cette thèse a été réalisée au sein du laboratoire :

Évolution & Diversité Biologique du CNRS
(UMR 5174, CNRS, Université Paul Sabatier, IRD)
118 route de Narbonne
31062 Toulouse (France)

Elle a été financée par :

La **Région Occitanie** et le **Centre National d'Études Spatiales**

樹頭徛予在，毋驚樹尾做風颱。

Tshiū-thâu khiā hōo tsāi, m̄ kiann tshiū-bué tsò hong-thai.

“If the root firmly anchored, there is no need to fear typhoons passing over the treetop.”

Metaphor for the importance of building a good foundation.

- *Taiwanese idiom (Taiwanese Hokkien)*

毋驚七月半个鬼，只怕七月半个水。

M̂-kiang tshit-ngia̍t-pàn kài kúi, chí phà tshit-ngia̍t-pàn kài shúi.

“Fear not the ghost of mid-July*, but do fear the flood in mid-July*.”

Conventional observation of the severity of flooding and landslides due to the heavy precipitations brought by typhoons in July.

- *Taiwanese idiom (Taiwaense Hakka, Hóiliu̍k dialect)*

*July in Lunar Calendar is traditional Ghost Month; it corresponds to late August - early September in Gregorian Calendar.

“…and all nature’s wildness tells the same story. Storms of every sort, torrents, earthquakes, cataclysms, ‘convulsions of nature,’ etc., however mysterious and lawless at first sight they may seem, are only harmonious notes in the song of creation, varied expressions of God’s love.”

- John Muir, *Our National Parks*, *Chapter 4: The Fountains and Streams of the Yosemite National Park*

Remerciements / Acknowledgment

Doing a PhD has truly been a long, winding and fascinating ride, one which you rarely see the entire picture of when you were in it. Three years of sifting through bibliography from almost fifty years ago to only last month, going over the model code and correcting errors sometimes involving one single arithmetic sign, making sense of the output graphs and making them prettier, revising and polishing paragraphs of texts, lying in bed at night thinking over hard-to-answer questions, practicing speeches in front of the screen: at the end of the maze, all were condensed in a hundred-page report, 45 minutes of presentation and about one hour of Qs and As. But it was so much more than that. Doing a PhD was troubleshooting and learning to find help, asking the right questions and knowing the limits to our answers, putting information into perspective, and above all, staying curious and motivated to invest time and energy to explore new horizons. I cherish being given this chance to challenge myself, and my gratitude is immense towards all of those who has made this experience possible and rewarding.

First and foremost, I cannot express enough thanks to my advisor Jérôme Chave, who was willing to believe in me, accompany and guide me on this exciting but unchartered journey. Every time I was plagued with self-doubt and started to lose track or focus, a discussion with you never failed to clear the clouds for me, which is especially precious knowing the number of tasks you juggle at the same time. I give equal thanks to present and former teammates, in particular Isabelle Maréchaux and Fabian Fischer with their modeling expertise and Nicholas Labrière with his remote sensing expertise, who were always willing to teach me with patience even when it involved basic concepts; I also enjoyed and appreciated discussing with Julian Donalds and Tony Shengli Tao as well as their valuable feedbacks and insights. Numerous collaborators have also substantially contributed to my PhD projects: I would like to particularly thank Barry Gardiner for his generous help on the windthrow risk model.

There are too many colleagues in the lab that I would like to thank in person to list: researchers (contractual or permanent), technicians, informaticians and secretaries alike, I owe my very pleasant lab life to your support and kindness: special thanks to Dominique Pantalacci, Véronique Cassin, Elisabeth Louw, Pierre Solbès and Julien Corrège for being the backbone of the doctoral school and the lab. I would like to give a shout-out to as many past and present PhD students as possible after all: Kévin, Marine, Isa, Juan, Iris, Églantine, Maëva, Luana, Alex, Sean, Pauline, Opale, Thomas, Déborah, Paul, Alexandre, Valentin, Laurine, Amandine, Piotr, Shenpu, Julie, Laura and Julia, whether our interactions were long or brief, your presence makes me feel like in a big, caring and constantly evolving family (and

any omission in this list of “family members” would be entirely of my fault!). A special mention to Alex for introducing me to the opportunities of both organizing the Journal Club and becoming student representative at SEVAB, and for being a great friend in general: your presence always creates a positive force around you, and I recall with fondness the many bottles or pints that we toasted during the beer party or at Dubliner’s. Another one goes to Yves, for being my trustworthy partner as Lab Council representative. On this note, I am also grateful for having had the opportunity to be a Lab Council representative and SEVAB student representative, and to work alongside all the fellow student representatives: this experience has opened my eyes to the fact that we, as PhD students, can and should also be an active force to make our working environment better, and gave me inspirations to what I could do as a person in the future.

My journey of research at Toulouse did not start with PhD. The two years that I have spent at the university and in the lab as a master’s student has trained me and made me even more aware and interested in the many wonderful mysteries ecology has to offer, and I would like to thank Christophe Thébaud and Emmanuelle Cam for the organization of the courses, as well as the many teachers in the program, notably Pierrick Blanchard, Christophe Andalo and Mélanie Roy.

Of course, I can never downplay the importance of the emotional support that my family provided: weekends after weekends without fail, talking with parents and my brother about everything over video meetings, from the profound to the banal, keeps me connected to the reality and the palpable simplicity of my life and joyous moments. My friends back in Taiwan have been a great help as well: if I was able to feel a shred of normalcy during these past two years of uncertainty and isolation, it was in large part thanks to the uninterrupted interaction with you all on the internet - in this respect, I unflinchingly acknowledge and salute the benefit of internet and social media. And finally, big thanks and hugs to William and Philippe: without your love, faith and care, always being there to listen to me and encourage me, some of the darkest hours during my study would have been much less easy to overcome. My love goes out to you.

And in the end, I guess I also have the city of Toulouse to thank for, for all the memories that you were able to offer! I shall miss the unexpectedly dazzling sunset in all its splendid color palettes that I have seen countless times on the way back home in the bus, as well as the bicycle rides along the canal.

Résumé

Les perturbations naturelles ont une influence importante sur la structure, la composition et le fonctionnement des forêts tropicales et un rôle dans la régulation des cycles biogéochimiques. La fréquence et l'intensité des perturbations naturelles sont modifiés par les changements climatiques : une meilleure connaissance de leur mécanisme d'action est nécessaire pour prédire les conséquences de cette modification. La modélisation permet d'évaluer le rôle de chacun des processus écologiques et leur lien avec les facteurs environnementaux. Les outils de la télédétection nous informent sur la structure et le fonctionnement des forêts à large échelle, et peuvent être utiles à la calibration et la validation des modèles de végétation. Dans cette thèse, j'ai employé ces deux approches pour examiner comment les forêts tropicales sont façonnées par les perturbations naturelles, notamment le vent, qui est un facteur majeur de perturbation dans de nombreuses régions tropicales.

Dans un premier temps, j'ai évalué la transférabilité d'un modèle individu-centré et spatialement explicite via un test de sensibilité et la calibration des paramètres globaux. Le modèle prédit correctement la structure de la forêt sur deux sites contrastés, et sa réponse est cohérente avec les variations du forçage climatique. La calibration d'un petit nombre de paramètres clés a été nécessaire, dont notamment celui qui contrôle la mortalité.

Pour étudier la sensibilité du modèle à la mortalité, j'ai mis en œuvre un module de dégâts de vents fondé sur les principes biophysiques et couplé avec la vitesse de vent, afin de modéliser les réponses de la forêt aux évènements de vent extrême. Avec l'augmentation du niveau de perturbation, la hauteur de la canopée diminue de manière constante mais la biomasse montre une réponse non-linéaire. L'intensité du vent a un fort impact sur la hauteur de la canopée et la biomasse, mais pas la fréquence des évènements de vent extrême.

Finalement, j'ai testé si les données radar des satellites Sentinel-1 pourraient servir à détecter les trouées dues aux perturbations naturelles en Guyane française. Les données Sentinel-1 détectent plus de trouées naturelles au-dessus de 0.2 ha que les données satellitaires optiques, et elles présentent un patron spatial cohérent avec les images optiques. Le niveau de perturbation ne varie pas en fonction de l'altitude. Nous avons trouvé plus de perturbations pendant les saisons sèches, ce qui pourrait être dû à la réponse tardive des précipitations plutôt qu'à la réponse directe de la sècheresse.

En conclusion, cette thèse démontre que l'intégration entre la modélisation et la télédétection éclairent les effets des perturbations naturelles sur les forêts tropicales. Les résultats qui en découlent peuvent servir à étudier d'autres types de perturbations et leurs interactions sur une large échelle.

Abstract

Natural disturbances have an important influence on the structure, composition and functioning of tropical forests and a role in the regulation of biogeochemical cycles. The frequency and intensity of natural disturbances are modified by climate change: a better knowledge of their mechanism of action is necessary to predict the consequences of this modification. Modeling allows us to evaluate the role of each of the ecological processes and their link with environmental factors. Remote sensing tools inform us about the structure and functioning of forests at large scales, and can be useful for the calibration and validation of vegetation models. In this thesis, I employed both approaches to examine how tropical forests are shaped by natural disturbances, particularly wind, which is a major disturbance factor in many tropical regions.

First, I evaluated the transferability of a spatially explicit, individual-based model via sensitivity testing and calibration of global parameters. The model correctly predicts forest structure at two contrasting sites, and its response is consistent with variations in climate forcing. Calibration of a small number of key parameters was required, including the parameter controlling mortality and crown allometry.

To investigate the sensitivity of the model to mortality, I implemented a wind damage module based on biophysical principles and coupled with wind speed to model forest responses to extreme wind events. With increasing disturbance level, canopy height decreased steadily but biomass showed a non-linear response. Wind intensity had a strong impact on canopy height and biomass, but not the frequency of extreme wind events.

Finally, I tested whether radar data from Sentinel-1 satellites could be used to detect gaps due to natural disturbances in French Guiana. The Sentinel-1 data detected more natural gaps above 0.2 ha than the optical satellite data, and they showed a spatial pattern consistent with the optical images. The level of disturbance did not vary with altitude. We found more disturbance during dry seasons, which could be due to the delayed response of precipitation rather than the direct response of drought.

In conclusion, this thesis demonstrates that the integration between modeling and remote sensing sheds light on the effects of natural disturbances on tropical forests. The resulting results can be used to study other types of disturbances and their interactions on a large scale.

Table des matières

GENERAL INTRODUCTION

Forests, which are a rich reservoir for biodiversity and play an essential role in the global biosphere and biogeochemical cycles, are increasingly threatened by human activities and climate change. Natural disturbances, while being an integral element of the forest dynamics, are also being altered by climate change. Wind, and in particular tropical cyclones, is a major disturbance force that can cause considerable tree mortality, and tropical cyclones have been shown to be related to forest properties worldwide. However, knowledge on the mechanisms by which cyclonic winds drive forest structure and dynamics remains insufficient, due to the limitations of empirical studies, whose results are inconsistent and contingent on multiple factors. In order to predict and anticipate how changes in wind disturbance patterns will influence forest cover, structure, diversity and functioning in the future, we need both sufficient observational data on current forest disturbances, and a comprehensive understanding on how wind disturbance affects forests, including tree mortality.

Studying the consequences of natural disturbances on forests have been facilitated by computer models that include detailed representations of individual-level processes. However, the realism and transferability of such highly detailed models need to be assessed and improved to make sure they are applicable over a large scale at different sites: this depends on a mechanistic representation of key biological processes in a forest and on the availability of spatially distributed data on climate and plant functional composition. In addition, tree mortality needs to be explicitly coupled to wind disturbances in the models to allow for explorations on the effects of changing disturbance patterns. Model improvement on wind-induced tree mortality needs to be implemented in particular for species-rich, structurally complex tropical forests, because they are the ecosystems most impacted by climate change and human activities, but also the least understood.

Finally, global-scale forest monitoring with high spatial and temporal precision is increasingly possible with advances in remote sensing technology and satellite data collection. Near-real time monitoring of natural disturbance events remains challenging, but it is worthwhile to address how remote sensing could further contribute to characterization of fine-scale disturbance patterns, which may help constrain forest model parameterization, and/or serve to validate model products.

In this thesis, I studied wind disturbance from the perspectives of forest modeling and remote sensing. I examined the transferability of the spatially explicit individual-based model TROLL (Chave, 1999; Maréchaux and Chave, 2017) by calibrating a number of empirical parameters at two contrasting forest sites through model inversion, and by examining model responses to variations in a range of globally consistent climate forcing. I then implemented a mechanistic model of wind-induced tree mortality, ForestGALES (Gardiner et al., 2008,

2000; Hale et al., 2015), into the TROLL model, in order to investigate the long-term impacts of recurrent wind disturbances on forest structure and dynamics. I also explored the potential to assess natural disturbances using synthetic aperture radar (SAR) data from the Sentinel-1 satellite, with near-real time coverage (once every 12 days) at a fine spatial resolution (10 × 10 meters). Using the data set treated by a deforestation detection algorithm (Ballère et al., 2021; Bouvet et al., 2018), I devised a protocol to select formation of natural forest gaps in French Guiana from 2016 to 2019 using GIS tools, and analyze their spatiotemporal pattern and dynamics. Figure *1* summarizes the different research topics to which I attempted to contribute in this thesis.

I describe in detail the various methods and approaches used in this work and how they connect to each other and to the research topics, and present the results in the form of three scientific articles and manuscripts. Finally, I summarize and contextualize the results from the three articles, describe the limitations and caveats of these studies, and highlight future perspectives.

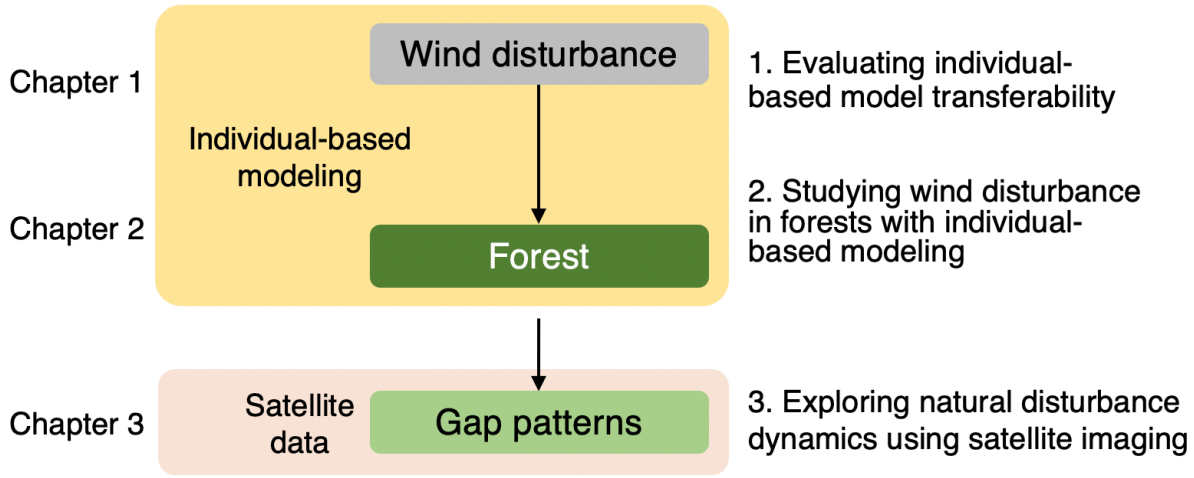

Figure 1. Basic roadmap of summarized research topics of the thesis and corresponding chapters.

Forest and the Wind of Change

Why forests are important

Forests are an essential part of our biosphere. They harbor the majority of terrestrial biodiversity on Earth, and account for the majority of terrestrial gross primary production (GPP), total plant biomass, and living carbon stocks (Pan et al., 2013). In addition, forests participate in the water cycle by replenishing atmospheric moisture, promoting local cooling and rainfall, and enhancing groundwater retention and filtration (Ellison et al., 2017), which indirectly provides benefits to nearby agricultural systems (Cohn, 2017). Forests provide

invaluable resources such as timber, food, medicinal plants and fresh water (Brandon, 2015), and also represent important spiritual and culture values (Henning, 1998; Sheil and Wunder, 2002). Many human communities have lived in or around natural forests for many thousands of years: the livelihood and wellbeing of these populations especially depend on natural forest resources that they have actively harvested and managed (Davis and Wali, 1994; Toledo et al., 2003).

Forests are tightly linked with the global carbon cycle, and thus have a crucial role in mitigating climate change (Mitchard, 2018). They act as a carbon sink by sequestering a large amount of atmospheric carbon through photosynthesis, but can also become a carbon source when they undergo degradation and deforestation due to logging, agricultural conversion and forms of land use change (Baccini et al., 2017; Bullock et al., 2020), when climate change induces environmental stress and alters tree species distribution and demography (growth, mortality and recruitment), or when climate change causes changes in patterns of disturbance events. Disturbances may be mild and frequent, or conversely major and rare, and the intensity and recurrence time of disturbance events control to a large extent forest carbon storage ability (Pugh et al., 2019): increases in the frequency and intensity of disturbances may cause substantial tree mortality, reduce forest productivity and reduce the forest's capacity to store carbon (Franklin et al., 2016).

Forests are complex in structure and diversity, varying over a wide range of spatial and temporal scales, and they encompass a large array of interactions among individual trees that are challenging to disentangle, between trees and the abiotic environment, and between trees and other organisms. Tropical forests are particularly well-known for their rich biodiversity - they alone harbor more than half of the total terrestrial biodiversity (Gardner et al., 2010) - and the great complexity in their spatial structure, biogeochemical cycle and functioning (Mensah et al., 2020; Townsend et al., 2008). This means that their responses to climate change and disturbances are likely highly heterogeneous and site-specific. In addition, tropical forests have been under particularly strong pressure of deforestation and forest degradation and other forms of human disturbance in recent decades, and are also facing increasing threat of climate change and changes in disturbance regimes (Edwards et al., 2019).

Disturbances in forests

The study of disturbances in ecosystems has long held a prominent place in ecology. In fact, some of the earliest ecological theories arose from the interest in better characterizing how plant communities go through ecological succession after experiencing disturbance

(Clements, 1916; Gleason, 1926). Disturbances are important drivers of change in forest structure and dynamics (Ding et al., 2012; Kurz et al., 2008; Uriarte et al., 2009). As anthropogenic impacts on forests around the world have intensified in recent decades, it has become increasingly vital to assess how disturbance regimes will change due to anthropogenic effects, and how these changes will impact forest biodiversity and functioning (Newman, 2019; Seidl et al., 2017). Indeed, this information could aid plan appropriate conservation and management strategies (Charron and Hermanutz, 2016).

One definitions of disturbance came from Grime (1977), which defined it as the "partial or total destruction of the plant biomass", referring to environmental factors that determined plant growth strategy. Pickett and White (1985) offered a more general definition with an ecosystemic view: "any relatively discrete event that disrupts the structure of an ecosystem, community, or population, and changes resource availability or the physical environment." Disturbances can take the form of extreme climatic conditions, such as heatwave, drought, frost, heavy precipitation or high wind speed; exogenous events causing a sudden and drastic change in the environment, such as lightning, storm or volcanic eruption; or events involving an endogenous biotic component of the ecosystem, such as forest fires (which requires the accumulation of flammable plant biomass), or outbreaks of pests or pathogens (Reichstein et al., 2013; Turner, 2010). A distinction should be made between single disturbance events and the disturbance regime, which refers to the overall spatiotemporal pattern of disturbance events over a longer time period. A disturbance event can be characterized by its size (spatial extent of influence), duration, intensity (energy released by the disturbance), and severity (ecological effect of the disturbance), whereas a disturbance regime can be characterized by its spatial distribution, return frequency, intensity, and seasonality (Turner 2010, Newman 2019).

Each disturbance type has complex effects on forests, and different types of disturbances interact with each other in complex ways: Figure 2 provides an overview of the various disturbance types and their effects on various physiological processes in a forest ecosystem, as well as the interaction between different disturbances and processes.

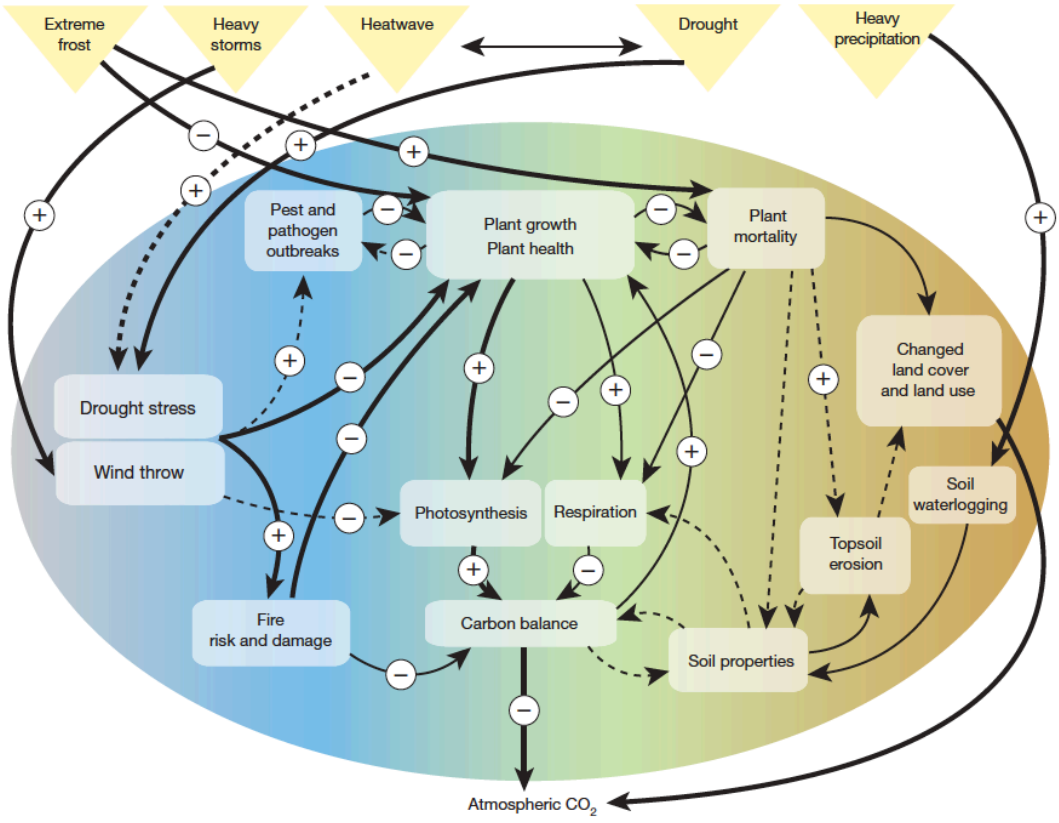

Figure 2. Schematic diagram illustrating the impacts, interactions and feedbacks between extreme climate events and forest processes. Solid arrows show direct impacts; dashed arrows show indirect impacts. The relative importance of the impact relationship is shown by arrow width. Reproduced from Reichstein *et al.* (2013).

Mild disturbance events may cause non-lethal structure damages to trees, such as loss of leaves and branches, and can alter physiological processes such as photosynthesis, respiration and growth, resulting in changes in the forest's carbon balance. Other changes, such as increased levels of volatile organic compounds, could directly affect global biochemical cycle (Guenther et al., 1995). More intense disturbances trigger immediate responses such as tree mortality and destruction of live biomass (McDowell et al., 2020; Reichstein et al., 2013).

Disturbances may affect different species to a different degree. Species-specific response to disturbance could lead to changes in relative species abundance and community composition, triggering successional dynamics or altering the successional trajectory (Pulsford et al., 2016), and could also create selective pressures that shape long-term adaptation and evolutionary dynamics (Jentsch and White, 2019).

At the landscape scale, disturbances cause spatial and temporal heterogeneity due to their sporadic occurrence and spatial location: recurrent forest fires and wind blowdowns, for example, create a mosaic of forest patches in different successional stages, and promote species diversity at the landscape scale (Magnabosco Marra et al., 2014; Turner, 2010). Although this thesis focuses on tree assemblages, it is important to keep in mind that

disturbance also have significant impact over other organisms in a forest, such as lianas and herbaceous plants, animals, microorganisms, as well as abiotic components such as soil nutrients.

Wind disturbances and tropical cyclones

Wind is an important disturbance agent with immediate and long-term effects on forests (Mitchell, 2013). Chronic low-intensity winds can cause plastic physiological responses in trees, such as the formation of flexure wood, which alter tree allometry and stature (Telewski, 1995). Stronger winds can cause partial damage to trees through branch snapping or defoliation; winds above a certain intensity can exceed the tree's resistance, causing windthrows (stem breakage, uprooting; see Figure 3) (Quine et al., 2021). Although windthrows often lead to tree mortality, although re-sprouting capacity or multi-stemming can increase the probability of survival after windthrow (Su et al., 2020).

Wind-driven disturbances come in a variety of forms. In tropical forests near the Equator, downburst winds can result in large areas of forest damage (Garstang et al., 1998). Storms are another common type of wind disturbance: tropical cyclones frequently affect forests in coastal regions of the subtropics, bringing strong wind and heavy precipitation (Lin et al., 2020). Figure 4 shows the global pattern of tropical cyclone occurrences, illustrating major regions where tropical cyclones often make landfall: the Western North and South Pacific, North Atlantic and the Indian Ocean.

Figure 3. Spruce trees suffering from stem breakage (left) and uprooting (right) in Harz National Park, Germany. Photography by E-Ping Rau.

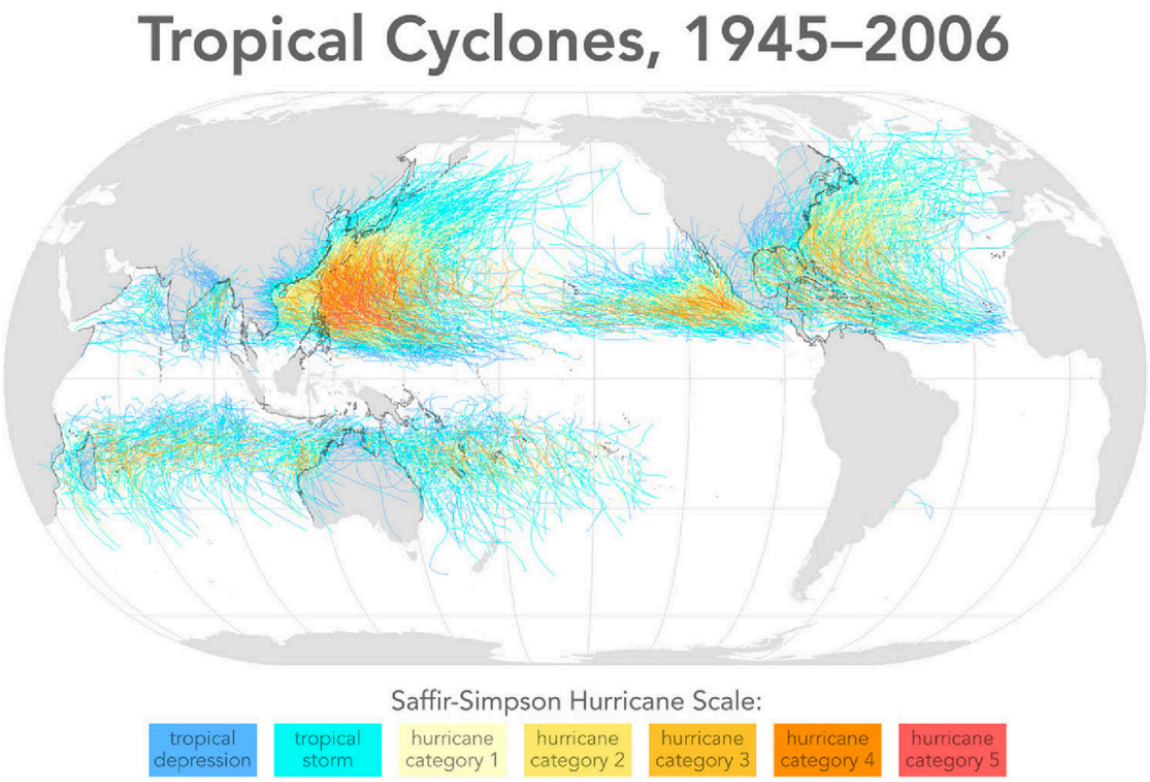

Figure 4. Record tracks of tropical cyclones from 1945 to 2006, with data from the Joint Typhoon Warning Center (JTWC) and the U.S. National Oceanography and Atmospheric Administration (NOAA). Reproduced from Xi (2015).

The formation and intensity of tropical cyclones are controlled by climate in complex ways. Factors predictive of tropical cyclone formation and intensity include vertical wind shear (change in wind speed and/or wind direction with altitude) or sea surface temperature, although a general theory on tropical cyclone formation is currently lacking (Walsh et al., 2016).

Studies have shown that tropical cyclone regime have been affected by climate change in recent decades, and have predicted that changes will continue in the near future: globally, tropical cyclone frequency is projected to decrease under climate change in most models, while tropical cyclone intensity is commonly projected to increase (Cha et al., 2020; Knutson et al., 2020). The decrease in tropical cyclone frequency is partly attributable to greater warming in the mid- and upper troposphere relative to the lower troposphere, which leads to a greater static stability of the atmosphere and reduced vertical mixing and upward mass flux, a phenomenon linked to tropical cyclone formation (Yoshimura et al., 2006). The increase in tropical cyclone frequency can be primarily attributed to the increase in sea surface temperature (Emanuel and Sobel, 2013). However, these predictions are debated, and there is considerable uncertainty and variability across basins and across models (Walsh et al., 2016). For example, Park *et al.* (2017) predicted a future increase in tropical cyclone frequency in the North Atlantic basin but increasing tropical cyclone frequency in the Northwest Pacific

basin. Increases in precipitation and storm surge risk (coastal flooding due to rising seawater caused by cyclonic wind) are generally predicted (Cha et al., 2020; Knutson et al., 2020). Some studies have predicted that dominant trajectories of TC may also change as a result of climate change, which could alter landfall probability (the probability that the center of a tropical cyclone reaches land), regions affected by tropical cyclones and the extent of their impact. For example, Murakami *et al.* (2013) predicted an increase in tropical cylone occurrence around the Hawaiian islands, and Nakamura *et al.* (2017) predicted a poleward and eastward shift in tropical cyclone tracks in the Northwest Pacific basin. In light of these predicted changes, it is important to have a detailed understanding of how tropical cyclone disturbances alter forest structure, dynamics and functioning, particularly through the process of tree mortality induced by extreme winds (McDowell et al., 2018).

Global comparative studies have shown that tropical cyclone occurrence is significantly correlated with forest structure and dynamics. Hogan *et al.* (2018) found that forest plots with intermediate cyclone storm frequency had higher variability in demographic rates (recruitment, growth and mortality) and functional trait divergence, compared to those with low or high storm frequency. Ibanez *et al.* (2019) found that higher tropical cyclone frequency and intensity correlated with shorter canopy stature and higher stem density. Ibanez *et al.* (2020) also found that tropical cyclone intensity was associated with the form of the species abundance distribution. However, in general, understanding of the long-term effects of tropical cyclones on forest composition, diversity and succession remains scarce, in large part due to lack of available data that include pre- and post-cyclone observations (Xi, 2015).

At the stand level, intense winds can cause extreme damage to trees by snapping their stem (stem breakage) or causing their root anchors to break (uprooting) (Everham and Brokaw, 1996; Quine et al., 2021). Numerous studies have attempted to characterize the abiotic and biotic factors associated with windthrow risk by observing the proportion of trees that experienced windthrow at forests sites after a recent cyclone. Table 1 presents a selection of those studies and their main findings. Properties generally associated with a higher proportion of windthrow were tree size (height, diameter), allometry (height-to-diameter ratio), crown dimension (crown width, crown width-diameter ratio), and wood strength (wood density). Overall, taller, larger trees with smaller wood density were more often observed to be more often damaged by wind (Everham and Brokaw, 1996; Webb et al., 2014).

Table 1. Summary of observed predictors of cyclone-related tree damage from a selection of past studies.

Study	Site	Cyclone	Predictors of uprooting risk	Predictors of stem breakage risk
Lugo et al. 1983	Dominica	Hurricane David, August 1979	Diameter: positive	Diameter: negative
Bellingham et al. 1991	Jamaica	Hurricane Gilbert, September 1988	Diameter: not predictive	Diameter: not predictive
Walker et al. 1992	Luquillo, Puerto Rico	Hurricane Hugo, September 1989	Diameter: not predictive	Diameter: not predictive Wood density: negative (only at Bisley)
Bellingham et al. 1996	Yakushima, Japan	Typhoon No. 13, September 1993	Diameter: not predictive	Diameter: not predictive
Ostertag et al. 2005	Luquillo, Puerto Rico	Hurricane Georges, September 1998	Growth rate: positive Size: positive Wood density: not predictive	Growth rate: positive Size: positive Wood density: not predictive
Curran et al. 2008	Queensland, Australia	Cyclone Larry, March 2006	Tree size: not predictive Buttress presence: not predictive	Tree size: not predictive Buttress presence: not predictive Wood density: negative
Lewis & Bannar-Martin 2011	Kirindy Mitea, Madagascar	Cyclone Fanele, January 2009	Diameter: positive	Diameter: positive
Lin et al. 2011	Fushan, Taiwan	Typhoon Haitang	Height: positive	Height: positive
Vandecar et al. 2011	southern Yucatán, Mexico	Hurricane Dean, August 2007	Diameter: positive Height: positive Wood density: negative (only when wind speed exceeds a threshold)	Diameter: positive Height: positive Wood density: negative (only when wind speed exceeds a threshold)
Webb et al. 2014	Ta'u, American Samoa	Cyclone Olaf , February 2005	Wood density: negative Diameter: positive	Wood density: positive Height: positive Diameter: negative Crown width/diameter ratio: positive

However, none of the relationships between structural properties and windthrow probability can be universally observed in all studies. The presence, strength and direction of the relationship often exhibit considerable variability for different types of damage and for different species, and depend on a number of abiotic factors such distance from the cyclone, site-specific disturbance or land use legacy, and topography (orientation, slope, elevation) (Everham and Brokaw, 1996; Mitchell, 2013).

In addition, although windthrow typically results in immediate tree death, it is possible for broken or even uprooted trees to survive and regenerate by re-sprouting (Su et al., 2020; Walker, 1995); conversely, a tree that has not experienced windthrow and has suffered only partial damage (e.g. branch snapping, defoliation) may nonetheless suffer delayed mortality, being more prone to resource depletion, disadvantaged in competition for light, water and other nutrients, or more vulnerable to disease and herbivory (Walker, 1995). This means that estimates of tree mortality depend on the time of observation after the cyclone event. Finally, other methodological differences exist between studies, such as the spatial extent of the areas sampled and tree properties that were observed and recorded.

The complex interactions among the abovementioned factors mean that making generalized predictions on the long-term effects of wind disturbance on forest ecosystems remains a significant challenge. Two strategies can be envisioned to overcome this challenge: one is to adopt a mechanistic approach to investigate generalizable mechanisms that control how wind causes tree mortality, which in turn shapes forest stand-level properties (Lin et al., 2020; Xi, 2015); the other is to collect comprehensive large-scale observational data which are representative of different situations. In the following sections, I will develop how I attempted to contribute to a more general understanding on long-term consequences of wind disturbance on forests by employing both strategies in this thesis.

Modeling forest ecosystems

Forest models are an indispensable tool that helps researchers unravel the enormous complexity of forest ecosystems, and discover how observed forest patterns are linked to the myriad of interacting abiotic and biotic processes, including wind disturbance and wind-induced mortality (Shifley et al., 2017; Shugart, 1984). They formally describe multiple physiological and demographic processes within forest ecosystems: simulations can be performed using the models to produce predictions on forest structure, dynamics and functioning, which can then be compared against observed data in order to test hypotheses (Botkin et al., 1972; Bugmann, 2001; Maréchaux et al., 2021; Porté and Bartelink, 2002). Model simulations also allow for virtual experiments on a large spatial and temporal scale, for example regarding forest response to environmental changes such as increasing temperature or CO_2 level (Feng et al., 2018; Holm et al., 2020), or the sensitivity and resilience of forest to various types of disturbances (Seidl et al., 2011b). All models are simplifications of reality, but a good forest model should contain a representation of the forest that is sufficiently realistic and robust in a wide range of conditions, so that the model can reliably approximate reality and provide answers to the research question (Prentice et al., 2015; Vanclay and Skovsgaard, 1997).

Dynamic global vegetation models

Dynamic global vegetation models (DGVMs) aim to model the global distribution of vegetation types, and are often embedded as a component of earth system models (ESMs), which model the interactive feedbacks between the biosphere and climate change. DGVMs represent the interface of vegetation and biogeochemical cycles, integrating climate, biogeochemistry and biophysics (carbon and nutrient cycle, energy and water vapor exchange), plant physiology (carbon and nutrient uptake), vegetation dynamics (tree

establishment, growth and mortality), as well as human-related land use changes (Prentice et al., 2007). Figure 5 illustrates the structure of a typical DGVM and its main modules. As models built with a top-down approach, DGVMs usually describe vegetation with a small number of plant functional types (PFTs), and include a simplified representation of vegetation structure and dynamics. This provides greater computational efficiency, facilitating coupling in ESMs for global-scale simulations, but also means that the representation of vegetation dynamics and structure can be simplistic and does not capture many of the important biological processes in the forest, such as gap dynamics, light competition, and notably recovery from disturbance (Fisher *et al.* 2018; but see Moorcroft, Hurtt, and Pacala 2001). Although newer-generation DGVMs have started to integrate individual-level interactions and physiological processes (Sato et al., 2007; Scheiter et al., 2013) and include a trait-based representation of vegetation to better account for functional diversity (Koven et al., 2020; Pavlick et al., 2013; Sakschewski et al., 2015), substantial challenges remain in adequately representing demographic processes. Tree mortality, in particular, is one of the most uncertain processes, resulting in uncertainties and low realism in model projections (Bugmann et al., 2019; Johnson et al., 2016). This underscores the need to develop bottom-up models that include a detailed description of forest size structure and functional composition, as well as mechanistic models of stem mortality.

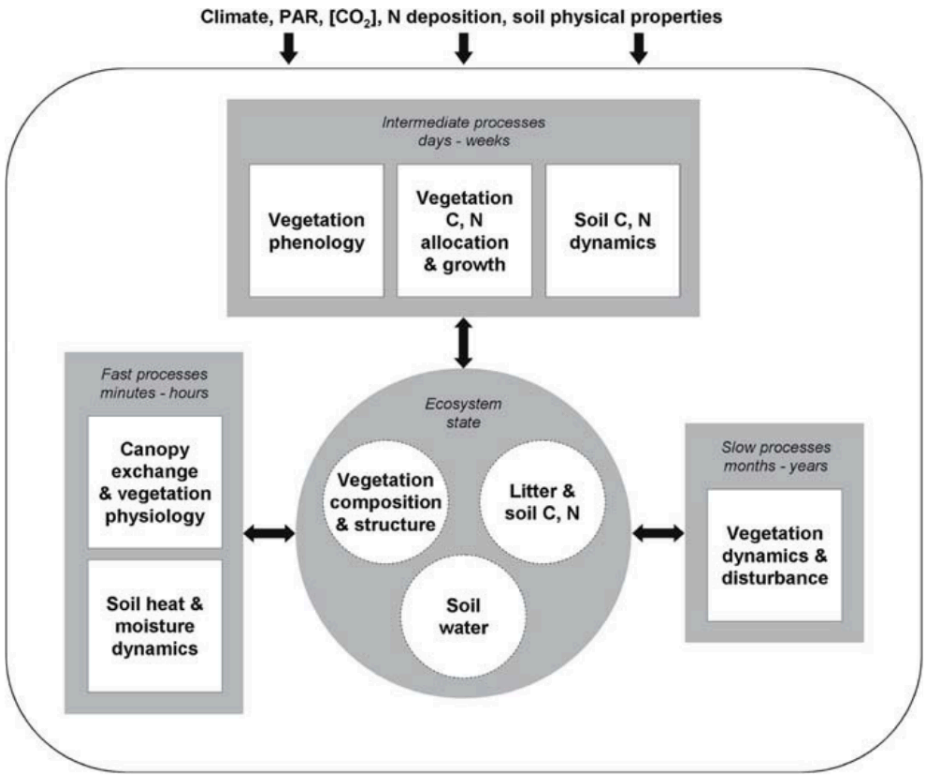

Figure 5. Typical structure of a DGVM, showing main driving variables, process modules and state variables. (Prentice et al., 2007)

Gap models and individual-based models

Individual-based models (IBMs) represent a forest with a bottom-up approach and formally describe key physiological (e.g. photosynthesis, respiration and carbon allocation) and demographic (growth, recruitment, mortality) processes that occur at the level of individual trees, including light competition that depends on the vertical canopy structure (Bugmann, 2001; Pacala et al., 1996). The user supplies the model with observed data on abiotic and biotic conditions such as climatic forcing, species composition and characteristics. As a model output, patterns of forest structure, dynamics and functioning are simulated as emergent properties from dynamic interactions among individual trees and between individuals and the environment. Because of their stochastic nature, the primary use of forest IBMs is not to compare a single simulated forest to field measurements and expect a perfect match: instead, because ecological processes are explicitly represented, it is possible to control and alter one or more processes separately to study how they drive observed forest patterns, and to conduct virtual experiments to test hypotheses on how changes in abiotic and biotic conditions affect forests (DeAngelis and Grimm, 2014; Schmitt et al., 2020). Knowledge gained from these model explorations can further be used to guide the design of field experiments or protocols (Medlyn et al., 2016).

Development of IBMs in forestry began around 60 years ago in response to the need to predict how changes in environmental conditions or forestry practice alter forest growth and timber yield (Shugart et al., 2018). Early forestry models used empirical observations to derive the relationship between the growth of a "standard tree" as a function of age, tree density and other site conditions. This relationship could then be scaled up to stand-level characteristics and forest yield, in the form of a "yield table" (Burkhart, 1990). This approach assumed that all the trees in a stand are identical and can be represented by the standard tree, which was appropriate for plantation forests, but less adapted for mixed-sized and mixed-aged natural forests. Later, models started to incorporate the process of size-dependent tree competition and mortality to follow growth and thinning of even-aged forests (Kohyama, 1993, 1992), marking a first step toward modeling the dynamics of forest mosaics and emphasizing the growth and interaction of individual trees. Subsequent development of IBMs has benefited considerably from the increase in computing power over the past few decades, which has reduced constraints on model complexity and allowed for the inclusion of more detailed process representation.

One particular subset of IBMs is called "gap models", including JABOWA (Botkin *et al.* 1972) or FORMIND (Fischer et al., 2016; Köhler and Huth, 1998). They apply the concept of

patch dynamics (Pickett and White, 1985), and represent forests as a mosaic of many small patches, of the size comparable to large trees in the forest (100 - 1000 m^2), each having a different age and successional status and in general independent of each other. The patches were assumed to be horizontally homogeneous, meaning that tree position was not considered within each patch, and that only competition in the vertical dimension was explicitly considered (Bugmann, 2001; Shugart and Woodward, 2001). Figure 6 illustrates the structural simplifications adopted by a typical gap model.

Other IBMs are spatially explicit, including the earliest forestry models and later-generation IBMs such as ZELIG (Weishampel et al., 1992), SORTIE (Pacala et al., 1996; Uriarte et al., 2009) and TROLL (Chave, 1999; Maréchaux and Chave, 2017). In these models, the spatial location of each tree individual is explicitly defined: this allows for more realistic simulation of individual-level interactions, such as light competition and secondary treefalls (caused when the trunk and crown of falling trees smash into neighboring trees). Figure 7 exemplifies a spatially explicit tree representation in the individual-based model TROLL.

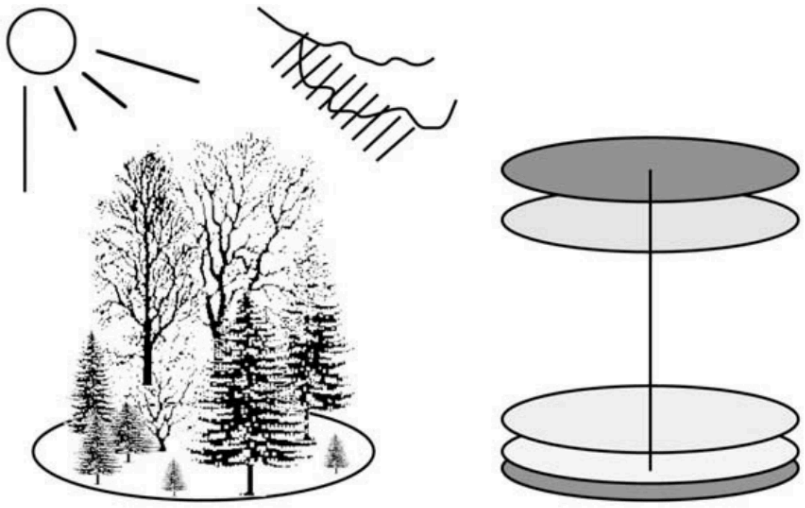

Figure 6. Illustration of a forest patch (on the left) and its simplified representation in a typical gap model (on the right) (Bugmann, 2001).

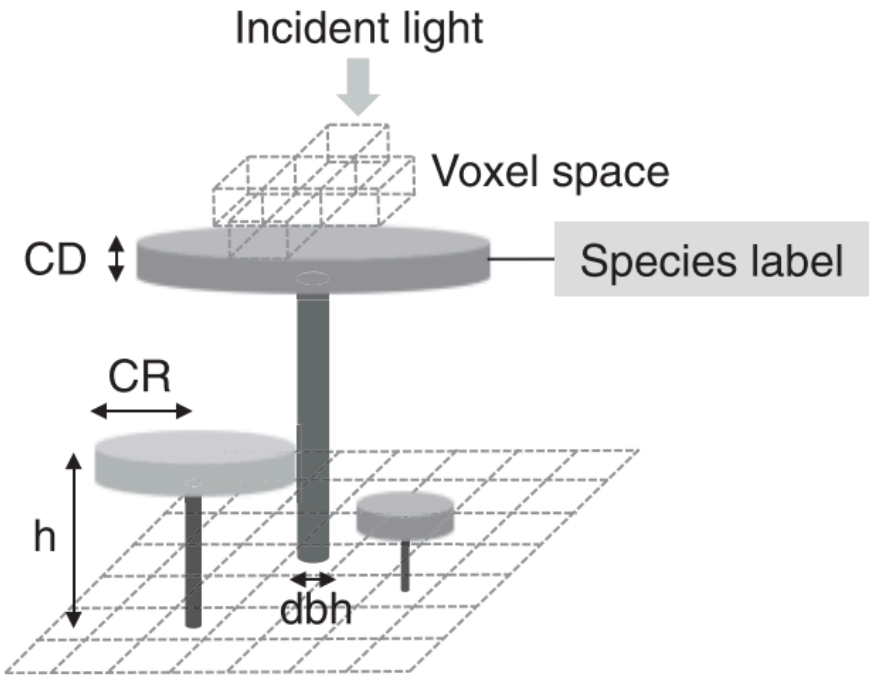

Figure 7. Representation of individual trees in a spatially explicit grid in TROLL. The 3D space of the forest stand is divided into 1-m^3 "voxels", and light diffusion is computed explicitly at each timestep within each voxel. Dimensions of each individual tree (CR: crown radius; CD: crown depth; h: height; dbh: diameter at breast height) are updated at each timestep based on the amount of net assimilated carbon allocated to growth and allometric relationships. (Maréchaux and Chave, 2017).

Upscaling of individual-based models: the question of transferability

Due to the cost of execution (amount of data necessary for model parameterization and demand on computational power), IBMs are usually applied at the forest stand level. However, in recent years, they are increasingly being implemented at larger spatial scales (Shugart et al., 2018). One approach involves the development of cohort-based models, which group tree individuals according to their size, age, functional type, or micro-environmental conditions (e.g., in gap or in understory) (Longo et al., 2019; Moorcroft et al., 2001). Another approach involves embedding IBMs as a component in earth system models (ESMs) to complement the shortcomings of DGVMs. The inclusion of individual-based processes in ESMs allows the prediction of vegetation structure and distribution from climate and plant trait input alone, without a priori constraint, and also provides opportunities of data-model integration at finer scale (Fisher et al., 2018). These models often present a number of simplifications themselves, such as the cohort-based approach where tree individuals with similar properties (size, age, functional type) are grouped together, as well as the grouping of highly diverse tree species into several "plant functional types". These simplifications reduce

the computational burden, but also raise the issue of model realism because they underrepresent the importance of demographic stochasticity, tradeoffs among traits and functional diversity (Fisher et al., 2018; Koven et al., 2020).

Whether run independently or embedded within a global-scale model, the application a forest IBM at many sites over a larger scale poses several challenges. Apart from the tradeoff between computational burden and model realism, the issue of model transferability inevitably arises (Wenger and Olden, 2012; Yates et al., 2018), which can be summarized with this question: once a model has been calibrated at one site, how well does it perform at another site? In theory, all biological processes in a model (e.g. photosynthesis, water uptake or carbon allocation) could be described as mechanistic functions, which are universally valid and only depend on directly measurable input data with clear biological meaning, such as climate forcing and plant traits. This would make the model site-independent, and applicable to any forest site in the world by only changing the environment and trait input without affecting model performance. In reality, however, site-specific data are still often used for the formulation and calibration of many mechanistic functions, which means that their genericity has not been fully explored. This leads to risk of overfitting, and hinders the transferability of models. In addition, current knowledge for some biological processes is insufficient to provide a completely mechanistic representation (e.g. tree mortality) (Bugmann et al., 2019; Johnson et al., 2016): they therefore have to be described with empirical and statistical relationships, which implies that their site-specificity is partially included in "free" parameters that are not directly measurable.

In order to improve the transferability of the models and to facilitate IBM upscaling, the parameterization and process representation must be made more general and less site-dependent. Homogeneous observational data with large spatial coverage, such as global climate reanalysis or satellite data, can provide better model initialization than local datasets derived from field observations or meteorological stations. In addition, when a forest IBM is applied at locations other than the original calibration site, recalibration will be required for some parameters. This is usually done by model inversion, which involves observing how well the simulation results fit certain observed metrics of forest structure, dynamics or functioning, while varying the parameter values (Hartig et al., 2014). Model inversion could also be a sensitivity analysis exercise to identify processes and parameters to which the model is most sensitive, in order to ease the burden of calibration and prioritize efforts to improve their mechanistic representation and model transferability (Huber et al., 2020). Figure 8 illustrates a general framework for scaling IBMs to regional or global DGVMs and land surface models (LSMs).

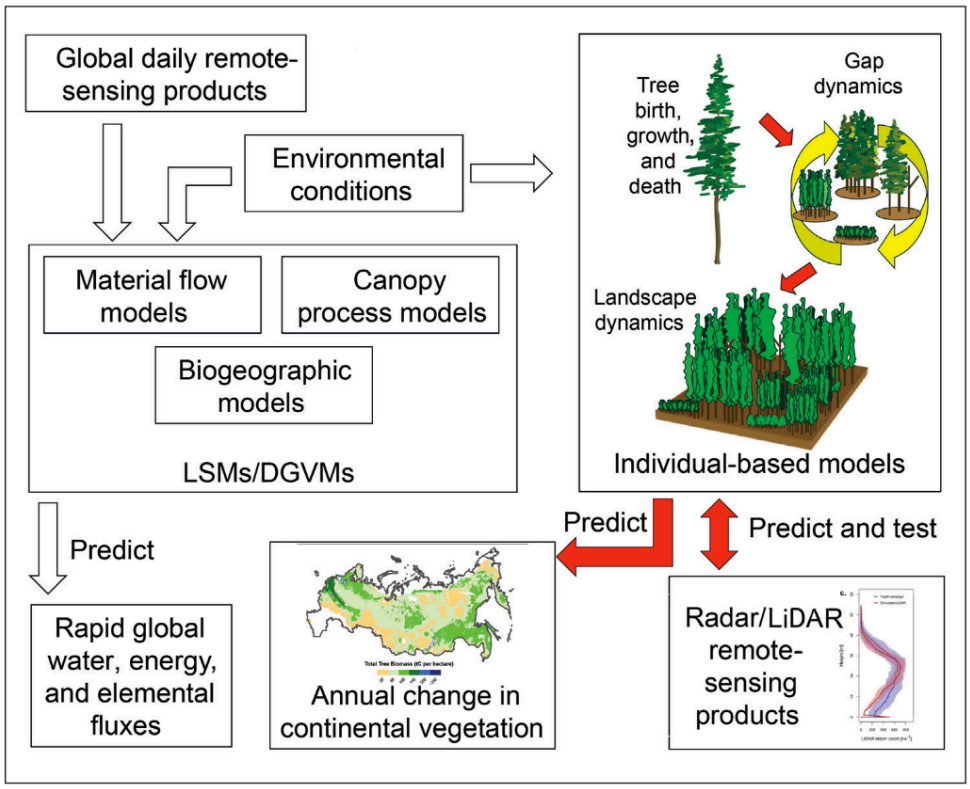

Figure 8. General features of land-surface models (LSMs), dynamic global vegetation models (DGVMs), and individual-based models (IBMs) of forests as used in global climate-change studies. Reproduced from Shugart *et al.* (2015).

Some studies have explored the issues of transferability and recalibration of forest IBM: Lagarrigues *et al.* (2015) evaluated the recalibration process of a forest IBM that simulates demographic processes using statistical equations with species-specific parameters (leading to a large number of demographic parameters to be calibrated), applied to a temperate forest with a small number of tree species. Fauset *et al.* (2019) examined whether an individual-based model performs reasonably well on two Amazonian forest sites with different climate and plant traits, but only used the overall trait distribution as input, without species-specific parameterizations. To our knowledge, currently there are still few studies that examine model transferability across tropical forests, and also employ a forest IBM with mechanistic, species-independent representation of biological processes, using species-specific plant traits as input for parameterization. The first research topic of this thesis thus involves **evaluating the transferability of an individual-based model** with a trait-based species parameterization and mechanistic representation of individual-level processes.

Individual-based models and wind disturbance

As noted above, in forest dynamic models, tree mortality has been identified as one of the least constrained biological processes in forest dynamics (Bugmann et al., 2019; Fauset et al., 2019; Johnson et al., 2016). This poses a problem for the predictive ability of forest models in general, and represents a particularly serious challenge for our understanding of the effects of natural disturbances on forests: increased tree mortality is one of the most important direct consequences of disturbances, but knowledge about the exact extent and pattern of their contribution to tree mortality is vastly incomplete (Allen et al., 2010; McDowell et al., 2018). It is therefore of crucial importance to include a mechanistic representation of how tree mortality and other processes in forest models are driven by various disturbance agents, and in particular by wind disturbances (Mitchell, 2013; Seidl et al., 2011a).

From a mechanical standpoint, wind drag induces an oscillating turning movement on the tree through its interaction with the tree crown and the trunk: when the turning moment (torque) exceeds a certain threshold, the tree suffers from major structural failure due to root anchoring failure (leading to uprooting), or due to the stem yielding to the bending stress (leading stem breakage). Numerous experimental studies have either investigated the dynamic interactions between wind drag and tree components with wind tunnel experiments (Gardiner et al., 2016), or have measured static tree resistance to uprooting through tree-pulling experiments (Nicoll et al., 2006). In recent years, a number of studies have used detailed biomechanical models to explore fine-scale wind-tree interaction. Some used time series of tree motion data collected in the field to relate tree motion in the wind, especially its fundamental sway frequency to its architectural properties (Jackson et al., 2021, 2019b). Others combined terrestrial laser scanning (TLS) data and the approach of finite-element analysis, which subdivides a complex structure into components with simpler parts, to model the dynamic response of trees when exposed to wind drag (Jackson et al., 2019c). These studies provide important insights on how tree structure is related to wind-tree interaction. However, this approach requires a large amount of fine-scale data and substantial computation effort, and is therefore generally impractical for stand-level application.

Another approach involves mechanistic wind damage risk models, which model trees as objects with a simpler geometry, and calculate the critical wind speed (CWS) required for a tree to be blown down based on biomechanical principles as a function of more easily measurable stand-level properties, such as tree spacing and canopy height, and individual-level properties, such as height, diameter and wood strength (Gardiner et al., 2008; Pivato et al., 2014). These models were originally developed to assess the likelihood and extent of wind damage in forest plantations, and thus were primarily applied to even-sized temperate forests. In mixed-sized natural forests, however, several difficulties are encountered: stand-level

properties (tree spacing and canopy height, etc.) are expected to vary both spatially and temporally, and the effect of sheltering from neighboring trees on the risk of wind damage can be important. In principle, unsheltered emergent trees are expected to be at a higher risk of wind damage than understory trees, even given the same size. This means that the spatial heterogeneity of tree size and architecture needs to be accounted for when modeling the impacts of wind disturbance, especially for subtropical and tropical forests (Duperat et al., 2021; Hale et al., 2012; Seidl et al., 2014): spatially explicit individual-based models (IBMs) of forest dynamics are therefore an appropriate modeling framework that addresses this need. By integrating forest IBMs with wind damage models that provide an estimate of critical wind speed , it is possible to explicitly represent a portion of tree mortality as the response to wind disturbance and to model the effect of sheltering from nearby trees, in order to understand how wind disturbances alter tree mortality and impact forests in the long run.

Several studies have integrated a wind-induced tree mortality module in a forest IBM: they provide promising results that confirm the relationship between wind damage and tree height and diameter (Ancelin et al., 2004; Schelhaas et al., 2007), and indicate the importance of within-stand heterogeneity (Ancelin et al., 2004; Seidl et al., 2014) and the role of acclimation (Kamimura et al., 2019). Another study also incorporated the wind damage module into a land surface model to model the effects of past storm events on forests at a regional scale (Chen et al., 2018).

However, these studies have mostly focused on temperate forests, with relatively homogeneous stand structure and low species diversity compared to subtropical and tropical forests, and most simulations were run over a relatively short time period (from one single storm event to several decades). Few studies have used forest IBMs with a wind-induced tree mortality module to investigate long-term effects of wind disturbance on the structure, dynamics and functioning of species-rich tropical forests. The second research topic of this thesis thus involves **using individual-based modeling to study the effects of wind disturbance on forests** with a heterogeneous structure and high species diversity.

Monitoring forest ecosystems

Long-term forest plots

In order to meet the enormous challenge of disentangling each abiotic and biotic process in forest ecosystems, including wind disturbance and wind-induced tree mortality, it is essential to collect and maintain standardized long-term field data over multiple spatial scales and levels of organization (from the molecular to the ecosystem levels) worldwide. Analyses of

extensive field data from multiple regions, including multiple continents, allows for better detection of both general trends and inter-regional differences (Sullivan et al., 2020).

One example of international collaboration with the goal of facilitating data collection and exchange in forestry research is the establishment of ForestGEO, a global network of long-term forest dynamics plots (FDPs) with a standardized data collection protocol, and scientists working across a wide variety of disciplines. The ForestGEO sites are established since as early as 1980, are located on all continents, and cover a wide range of environmental conditions (soil fertility, topography, rainfall pattern and disturbance regimes) (Figure 9). Over 7 million trees of around 12,000 species have been recorded in the ForestGEO network to date, representing about 20% of the known global tree diversity and including 59% of all plant families and 35% of all woody plant genera (Davies et al., 2021). This wealth of information provides invaluable resources for the study of the spatial and temporal variability of forest structure and dynamics.

Under the ForestGEO protocol, all tree individuals with a diameter ≥ 1 cm at 1.3 m above the ground (diameter at breast height, DBH), or above buttresses or other trunk deformities, are mapped, measured and identified, in gridded plots of typically 16-50 ha in size, and repeated censuses are carried out at approximately five-year intervals to track their recruitment, growth, and death. This protocol is labor- and time-intensive, and the identification of the diverse tree species, especially for small stems, is particularly difficult; however, it presents several advantages. Repeated sampling of a relatively large contiguous patch of forest allows for better monitoring of infrequent demographic events, such as tree mortality, and reduces the risk of undersampling uncommon species. In addition, a considerable portion of tree diversity and dynamics is found at diameters < 10 cm, and sampling small stems sheds a new light on tree demography. Last but not least, large mapped plots present an opportunity to monitor patterns of many types of natural disturbances in tropical forests that occur at the spatial scale of one to several hectares (e.g., treefalls, landslides, lightning strikes, etc.) (Davies et al., 2021; Gora et al., 2020).

Figure 9. Global map of 71 ForestGEO Forest Dynamics Plots. (Davies et al., 2021)

Remote sensing

In addition to field inventory data, advances in remote sensing in recent years have also generated forest observations with substantially enhanced spatial and temporal resolution and extent (Lechner et al., 2020). Major advances include the use of light detection and ranging (LiDAR) technology, and the collection of improved global-scale satellite data.

Also called 3D laser scanning, LiDAR uses a principle similar to radar and sonar, and measures the distance between the sensor and the target object or surface by emitting laser pulses, and measuring the elapsed time between emission and reception of the laser reflection by the sensor's receiver: this generates point cloud data that can be processed by various algorithms to reconstruct the 3D structure of the target object (Lefsky et al., 2002). Airborne LiDAR scanning (ALS) systems, mounted on aircrafts or satellites, scan the forest canopy and can be used to map forest canopy height at the regional scale; LiDAR instruments onboard satellites have even been used on a global scale (Simard et al., 2011), with new advances such as the GEDI project underway (Coyle et al., 2015). Figure 10 illustrates the basic principle of ALS data acquisition and processing. Canopy height information can then be used to estimate other forest attributes such as aboveground carbon stocks or primary productivity, either through calibration with ground measurements (Asner et al., 2012), or by linking canopy height to other forest attributes through model predictions (Rödig et al., 2018, 2017). From the vertical canopy structure in the ALS data, it is also possible to extract individual-level information on tree size and allometry, which can help constrain allometric relationships in forest modeling (Ferraz et al., 2016; Fischer et al., 2020, 2019; Jucker et al., 2017). Terrestrial LiDAR scanning (TLS), a ground-based counterpart to ALS remote sensing, involves LiDAR scans from the ground in the forest understory, and can generate plot-scale data on tree

architecture and diameter with extremely high precision and accuracy (Disney, 2018). Tree position and diameter information can facilitate tree mapping and forest plot surveys and reduce time and cost (Newnham et al., 2015). The reconstruction of 3D whole-tree structure from TLS data provides unprecedented information that can be used to study tree allometry and architecture, as well to give more accurate estimate of aboveground biomass (Disney, 2018; Disney et al., 2018; Malhi et al., 2018). In the context of studying wind disturbance, airborne LiDAR can be used to assess patterns of wind damage after a tropical cyclone (Coomes et al., 2018; Hayashi et al., 2015), and terrestrial LiDAR scanning data have been used to constrain biomechanical models of individual-level wind-tree interactions (Jackson et al., 2019b, 2019c).

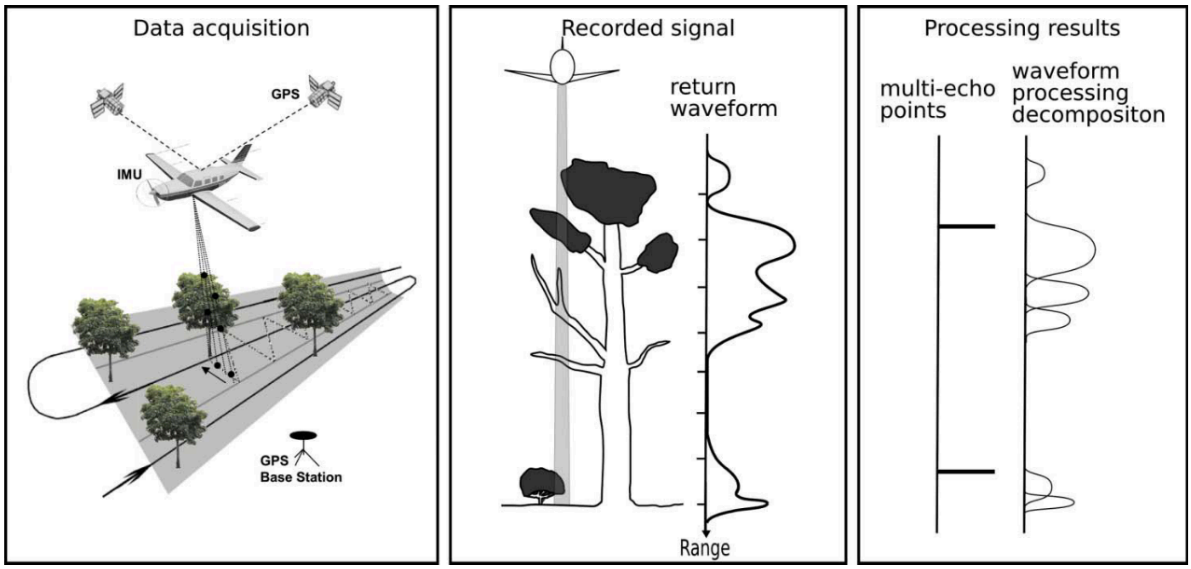

Figure 10. Principle of airborne lidar acquisition and data process. (Chauve et al., 2009)

In addition to Lidar, other types of spaceborne remote sensing use satellite-mounted sensors that detect electromagnetic radiation in various wavelength ranges, such as visible light, infrared, microwave or radio waves. They can provide temporally continuous records on forest structure and dynamics with broad spatial coverage, which can be used for model calibration or validation (Knapp et al., 2018; Shugart et al., 2015) and for monitoring of forest status change and natural or human disturbance dynamics.

Multispectral optical sensors in the visible light and infrared wavelengths, such as those on the Landsat satellites, MODIS sensor on board the Terra and Aqua satellites, and those on the Sentinel-2 satellites, produce optical images useful for monitoring land cover and vegetation change. In particular, the Landsat mission has provided uninterrupted optical imagery over the entire globe since 1972: with a high spatial resolution of 30 m and a return frequency of 16 days, this high-resolution dataset has proven invaluable for long-term

monitoring of land cover and spatial heterogeneity (Hansen et al., 2013; Vancutsem et al., 2021). In contrast, the relatively coarse spatial resolution (ranging from 250 m to 1 km) but high temporal resolution (return frequency of 1 to 2 days) of the MODIS sensor makes it useful for monitoring land, ocean and atmospheric processes occurring over a small time scale, including atmospheric water vapor, aerosol particles and cloud properties (King et al., 1992).

Microwave radiometry involves passive sensors that measure energy emitted at the microwave wavelength (from 1 mm to 1 m) from the Earth surface. It has been used to collect precipitation data (e.g., Tropical Rainfall Measuring Mission, TRMM) (Olson et al., 2006; Yang et al., 2006) and soil moisture data (e.g., Soil Moisture and Ocean Salinity, SMOS; Soil Moisture Active Passive, SMAP) (Barré et al., 2008; Brown et al., 2013; Ma et al., 2019; Oliva et al., 2020), and has also seen other uses such as for hurricane monitoring or measurement of Arctic snow thickness (Maaß et al., 2013; Reul et al., 2012).

Synthetic aperture radar (SAR) instruments create reconstruction of landscapes and forest canopy by emitting radio wave pulses from a moving platform (satellite) onto the target region (landscapes or forest cover), recording the backscattered echoes of these pulses, and processing the echoes recorded at different times, and thus at different positions, to reconstruct the surface shape of the target region (Kirscht and Rinke, 1998) (Figure 11). This method produces images with high spatial resolution, and has the advantage over optical imaging in that they are operational under all weather conditions. It has been useful for measuring topography (e.g. Shuttle Radar Topography Mission, SRTM) (Farr et al., 2007), as well as for estimating tree size and biomass, forest cover and forest loss (e.g. ALOS, PALSAR, Sentinel-1) (Balzter, 2001; Reiche et al., 2016).

Hyperspectral imaging instruments (also known as imaging spectroscopy), such as Hyperion on board of the EO-1 satellite, detect and record the reflected radiation reflected from the Earth's surface over many wavelength bands, producing a "spectrum" for each pixel scanned. A currently active research direction is to utilize these spectra to identify tree species, chemical compositions or functional traits over a large spatial scale, often combined with machine learning process (Féret and Asner, 2014, 2011; Goodenough et al., 2004).

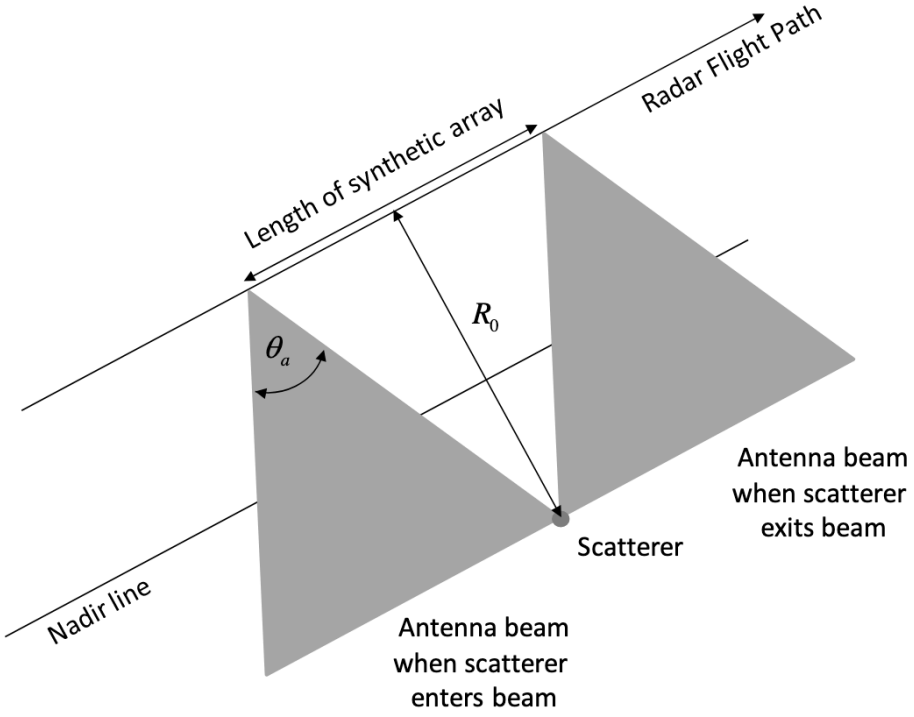

Figure 11. Principle of synthetic aperture radar remote sensing. The sensor detects the scatterer (target) by integrating all signals acquired during the period (length of the synthetic array) when the scatterer falls within the antenna beam (van Zyl and Kim, 2011).

Using satellite remote sensing to monitor forest disturbance

Satellite imagery has been instrumental in monitoring changes in forest condition and cover due to natural or human disturbances and deforestation dynamics, particularly in old-growth forested areas that are difficult to access (Bullock et al., 2020; Keenan et al., 2015). For example, satellite data have been used to estimate tree mortality rate in tropical rainforests (Clark et al., 2004), and to detect windthrow and disturbance patterns in forests after tropical cyclone passage (Kislov and Korznikov, 2020; Negrón-Juárez et al., 2014).

Due to the relative short time frame within which natural disturbance events occur (often in a matter of days), in order to characterize fine-scale natural disturbance dynamics, there is a need to detect forest disturbance events with short time intervals. This can be achieved by using data from near-real time (NRT) forest disturbance monitoring programs, which allow management programs to respond to new deforestation events in a timely manner (Hansen et al., 2016),. Forest disturbance monitoring has traditionally relied on optical remote sensing, although a major shortcoming of optical imagery is that data availability is limited by frequent cloud cover in the tropics, particularly during the wet season. Synthetic aperture radar (SAR) data are not subject to these meteorological constraints, and could be a powerful tool for detecting and mapping forest disturbances. Recently, a new methodology has been

developed to provide NRT deforestation detection using SAR data collected from the Sentinel-1 satellite, by taking advantage of the availability of Sentinel-1 acquisitions in both ascending and descending orbits (Ballère et al., 2021; Bouvet et al., 2018). With a revisit period of 6 to 12 days and a spatial resolution of 10 m, this new methodology can serve as an accurate tool for monitoring human deforestation, but also opens up the possibility of studying fine-scale temporal and spatial dynamics of natural disturbances in Amazonian forests, where wind could be an important disturbance agent (Magnabosco Marra et al., 2018; Peterson et al., 2019). The third research question of this thesis thus involves **the exploratiuon of natural disturbance dynamics in tropical forests using satellite imaging data.**

Summary

In summary, our understanding of how wind disturbance shapes forests has advanced greatly through the development of individual-based forest dynamics models, but the transferability of individual-based models in general needs to be better assessed, and the process of wind-induced tree mortality needs to be included, both to improve representation of mortality in models in general, and to study the long-term effects of wind disturbance on tropical forests in particular. Furthermore, in light of the great potential for remote sensing technology and satellite data, further explorations should be made to harness the potential of satellite remote sensing to provide near-real time, large-scale monitoring of the dynamics of wind disturbance impacts. The main objective of this thesis is thus to contribute to three previously formulated research topics:

1. **Evaluation of the transferability of an individual-based model**

2. **Investigation of the effects of wind disturbance on forests using individual-based modeling**

3. **Exploration of natural disturbance dynamics in tropical forests using satellite imaging data**

GENERAL METHODS

Individual-based forest dynamics model: TROLL

Model overview

The TROLL model, used for this PhD study, belongs to the family of spatially explicit individual-based models along with models such as SORTIE (Pacala et al., 1996; Uriarte et al., 2009) and FORMIND (Fischer et al., 2016; Köhler and Huth, 1998), and simulates the demography processes (recruitment, growth, seed production, and death) of all individual trees (self-standing stems) ≥ 1 cm in trunk diameter at breast height (DBH) in a forest stand (Chave, 1999; Maréchaux and Chave, 2017).

In TROLL, the aboveground space of the forest stand is divided into 3D cells of size 1 m^3 (voxels), and no more than one tree can establish in each 1 × 1 m pixel at any given time. Each modeled tree is a 3D object defined by a set of state variables (age, DBH, height, crown radius, crown depth, and total leaf surface area), and is assigned a species label inherited from the progenitor tree. Each species label is associated with seven species-specific traits: leaf mass per area (LMA), leaf nitrogen and phosphorus content (N_{mass} and P_{mass}), wood density, threshold DBH beyond which growth efficiency declines, asymptotic height, and a parameter of the DBH–height allometry (a_h). These traits control photosynthesis, growth and other physiological and processes.

For each voxel, the cumulated leaf area index (LAI, $m^2 \cdot m^{-2}$) is calculated as the vertical sum of leaf area density (LAD, $m^2 \cdot m^{-3}$) of all the voxels situated above it. Light intensity (photosynthetic photon flux density, PPFD, in µmol photons$\cdot m^{-2} \cdot s^{-1}$) within the voxel i is then computed as the fraction of solar irradiance (canopy-top PPFD) transmitted, based on the Beer-Lambert extinction law:

$$PPFD_i = PPFD_{canopytop} \times e^{-k \times LAI_i} \quad (1)$$

We considered only vertical light diffusion in this model, instead of employing more complex light interception models or radiative transfer models (Van der Zande et al., 2011; Widlowski et al., 2013). As such, although the light extinction rate k varies in reality with zenith angle and species-specific leaf inclination angle (Kitajima et al., 2005; Rich et al., 1993; Wang et al., 2007), it is assumed to be constant in the model. Temperature (T, °C) and vapor pressure deficit (VPD, kPa) within the canopy are also assumed to decrease with forest canopy depth (distance from canopy top).

In each monthly time step, photosynthesis is calculated over half-hourly periods of a representative day per month based on the Farquhar-von Caemmerer-Berry model of C_3 photosynthesis (Farquhar et al., 1980). Atmospheric CO_2 concentration is assumed to be

constant, and light intensity (PPFD, μmol photons·m^{-2}·s^{-1}), temperature (T, °C) and vapor pressure deficit (VPD, kPa) values for each half-hourly period are computed from the monthly mean and a representative daily course of variation. Under the FCB photosynthesis model, in light-limited conditions, carbon assimilation depends on the parameter of quantum carbon yield per quantum photon (φ, mol C·mol $photons^{-1}$): this corresponds to the initial slope of the photosynthetic carbon assimilation plotted against irradiance, and has been shown to be an important source of uncertainties in vegetation models (Rogers et al., 2017; Zaehle et al., 2005). In CO_2-limited conditions, carbon assimilation mainly depends on three parameters: stomatal conductance (g_s), maximum rate of carboxylation (V_{cmax}, μmol CO_2·m^{-2}·s^{-1}) and the maximal electron transport capacity (J_{max}, μmol electrons·m^{-2}·s^{-1}). Stomatal conductance is modeled following Medlyn et al. (2011). V_{cmax} and J_{max} are related to species-specific traits leaf mass per area (LMA), leaf nitrogen and phosphorus content (N_{mass} and P_{mass}), using the relationship found in Domingues *et al.* (2010).

Autotrophic respiration includes carbon uptake that are metabolized by plants for maintenance or growth, and also represents a large source of uncertainty in vegetation models (Thornley and Cannell, 2000). In the absence of a precise understanding of mechanistic causes of variation in respiration rate, empirical relationships are used in the TROLL model. Leaf maintenance respiration is modeled as a function of species-specific traits (LMA, N_{mass} and P_{mass}) and positively dependent on temperature (Atkin et al., 2015); daytime leaf respiration is assumed to be 40 % of night time respiration (Atkin et al., 2000). Stem maintenance respiration is assumed to be proportional to sapwood volume and positively dependent on temperature (Ryan et al., 1995), assuming that sapwood thickness increases with diameter at breast height (DBH) until reaching a maximum of 0.04 m. Fine root maintenance respiration is assumed to be 50% of leaf maintenance respiration. Coarse root and branch maintenance respirations are assumed to be 50% of stem respiration. Growth respiration is assumed to be 25% of gross carbon assimilation minus the maintenance respiration (Thornley and Cannell, 2000). These assumptions are reasonable first-step approximations that are commonly made in the literature: nevertheless, it would be necessary to provide more precise, mechanistic model representations for respiration in the future.

The net carbon uptake (gross assimilated carbon minus respiration) is allocated into tree growth and leaf production, which then modifies the leaf density and the light environment in the next timestep. Allocation of net carbon assimilates into the growth of aboveground woody mass (stem and branches) and tree crown (including leaves, fruits and twigs) are controlled by two empirically derived, species-independent parameters respectively (Aragão et al., 2009; Malhi et al., 2015, 2011). Leaf dynamics is modeled by partitioning species-specific leaf lifespan (calculated from plant traits) into the residence times in three distinct leaf age classes

(young, mature and old): newly produced leaves enter the young leaf class, and old leaves leave the old leaf class and turn into litterfall.

Carbon allocated to aboveground woody growth is converted into an increase in stem volume, which is then converted into increases in diameter and tree height (*H*) and diameter (DBH) following a height-DBH allometric relationship that is described by a Michael-Menten equation:

$$H = \frac{h_{lim} \times DBH}{DBH + a_h} \quad (2)$$

with species-specific h_{lim} and a_h parameters estimated from local measurements of tree heights and diameters.

The allometric relationship between crown radius (CR) and diameter DBH follows an empirical non-linear relationship:

$$CR = e^{(CR_a + CR_b \times \ln DBH)} \quad (3)$$

where CR_a and CR_b are general parameters that were estimated based on measurements in French Guiana (Chave et al., 2005). Identical values of CR_a and CR_b are prescribed for all species due to the paucity of species-specific data, even though it has been demonstrated that crown size allometry can vary within species, across species and across sites (Jucker et al., 2017; Loubota Panzou et al., 2021).

The recruitment process is modeled through a "seed" bank (representing seeds and seedlings < 1 cm DBH) defined for each 1 × 1 m pixel. The seed bank is emptied at the end of each timestep, and replenished by (1) seeds produced and dispersed from neighboring pixels and (2) a seed rain external to the forest stand. The current version of the model assumes that a large old-growth forest surrounds the simulated forest, and that there is no recruitment limitation due to the external seed rain.

In the standard version of the TROLL model, tree mortality is modeled by the following four processes. (i) The background stochastic tree mortality rate (*m*) is assumed to be negatively dependent on species-specific wood density (WD) (Wright et al., 2010):

$$m = m_{max} \times (1 - WD) \quad (4)$$

where m_{max} is the maximum value of the background mortality rate. (ii) Carbon starvation happens when net assimilated carbon is negative over a consecutive period exceeding leaf lifespan, and that old leaves have all died while no new leaves could be produced, assuming no mobilizable internal carbon storage. (iii) Stochastic treefalls are modeled through a stochastic tree height threshold Θ, calculated for each individual tree:

$$\Theta = h_{max} \times (1 - v_T \times |\zeta|) \quad (5)$$

where h_{max} is the species-specific maximum tree height, v_T is a variance parameter, and ζ is a standard normal random variable: if tree height *h* exceeds Θ, the tree falls with a probability of 1 - Θ/*h*. (iv) Secondary treefall happens when a tree is located on the trajectory of the

crown and stem of a falling neighboring tree. These mortality processes are not mechanistically linked to natural disturbance regimes such as cyclonic wind: the implementation of wind-induced tree mortality is thus an important aspect that is explored in this thesis.

Herbaceous plants and lianas are not included in the model. Ongoing model developments include complete modules of water balance, soil nutrient dynamics, and effect of species-specific dispersal limitation. Topography, in particular its effects on wind-induced tree mortality, will be explored in this thesis.

Study sites and species-specific parameterization

Two forest sites are explored in this thesis: Nouragues, French Guiana in South America, and Fushan, Taiwan in Southeast Asia. These two sites are chosen because of their markedly different climatic conditions and minimal floristic overlap (no tree species occur in both sites).

Within the Nouragues Ecological Research Station, there is a 12-hectare (400 m × 300 m) plot in a moist lowland tropical forest in the center of French Guiana: it is geologically located in the Guiana Shield, and is part of the Amazonian biome. The Nouragues site experiences two months of dry season per year, with mean annual precipitation around 3000 mm, mean annual temperature around 26°C, and a mean relative humidity around 99% (Bongers et al., 2001). Since plot establishment in 1994, tree censuses were regular conducted (once every 5~6 years), where all self-standing stems with DBH ≥ 10 cm were identified, measured, tagged and mapped: to date, 622 tree species have been recorded at the Nouragues site (Chave et al., 2008; Maréchaux and Chave, 2017).

The Fushan Forest Dynamics Plot (FDP) is a 25-hectare (500 m × 500 m) plot in a moist broadleaf subtropical forest in the northeastern region of Taiwan (Su et al., 2007). It is a part of the ForestGEO network (Forest Global Earth Observatory; Anderson-Teixeira et al., 2015; Condit, 1998). The Fushan site is under influence of northeasterly monsoon in winter, and frequent typhoon visits in summer and autumn, with mean annual precipitation around 4200 mm, mean annual temperature around 18°C, and a mean relative humidity around 95%. Plot elevation ranges from 600 m to 733 m (Su et al., 2007). Since plot establishment in 2004, censuses were completed every five years, where all self-standing stems with a DBH ≥ 1 cm were identified, measured, tagged and mapped: to date, 110 tree species have been recorded at the Fushan site (Su et al., 2007).

Species-specific trait data required for TROLL include leaf mass per area (LMA, $g \cdot m^{-2}$), nitrogen and phosphorus content per mass (N_{mass}, P_{mass} $g \cdot g^{-1}$), wood density (WD, $g \cdot cm^{-3}$), a

threshold DBH beyond which tree growth declines (d_{max}, cm), the two Michaelis-Menten parameters describing DBH-height allometry (h_{lim}, a_h), and regional relative abundance. At Nouragues, a complete set of measured trait values were available for 163 species occurring at the site: for the other species, a combination of species-specific values and genus means or abundance-weighted community means were assigned (Maréchaux and Chave, 2017). At Fushan, a full set of traits was available for 94 species, representing around 90% of the tree individuals. The measurement and collection of functional trait data follow the standardized protocol (Pérez-Harguindeguy et al., 2013).

Global parameter parameterization

Apart from In addition to species-specific parameters, TROLL includes a set of 41 species-independent parameters (or "global" parameters). For the majority of these parameters, values with high confidence from local measurement (at Nouragues, Fushan or in the Amazon area) or from past literature are available. There remain a handful of parameters for which it is difficult to obtain field estimates, and that are previously mentioned as generating high uncertainty and sensitivity in the model outputs. These parameters include φ (apparent quantum yield), v_T (variance term in stochastic treefall process), m_{max} (maximum value of background mortality rate), CR_a and CR_b (species-independent crown radius-diameter allometric relationship), and f_{wood} and f_{canopy} (proportion of net assimilated carbon allocated to woody growth and to tree crown growth, respectively), and are the primary target of the parameter calibration test.

We performed 500 TROLL simulations for both sites, while varying the value of these parameters simultaneous ("all-at-a-time" approach) across uniform prior distributions bounded within the reported value ranges. Since CR_a and CR_b exhibit strong correlation, correlated standard normal distributions were used as the prior. We used the principle of model inversion to examine which parameter combinations generated model outputs that are closest to field observations in four summary metrics of forest structure and functioning: stem density (DBH ≥ 10 cm; N_{10}, trees·ha^{-1}), large stem density (DBH ≥ 30 cm; N_{30}, trees·ha^{-1}), aboveground biomass (AGB, Mg·ha^{-1}), and gross primary productivity (GPP, MgC·ha^{-1}·yr^{-1}). We also examined whether model inversion resulted in a large reduction of uncertainty in the parameter values: i.e., how "informative" was the calibration test. This test aims to answer **Research Question 2**, and the results are presented in **Chapter 1**.

Climate forcing

Input data required for the TROLL model include: 1) climate forcing, 2) species-specific functional traits, and 3) species-independent general parameters. The TROLL model requires the following climate forcing variables: monthly mean values of daytime and nighttime mean temperature, cumulated rainfall, mean wind speed, and daytime mean irradiance, daytime mean vapor pressure deficit (VPD), and average normalized daily variation of temperature, irradiance and VPD.

In order to provide the model with a standardized, globally homogeneous climate forcing that allows cross-site comparison across sites, we used the CRU-NCEP reanalysis data set (version 8; version 7 archived at https://rda.ucar.edu/datasets/ds314.3/) (Viovy, 2018), a global gridded (0.5° × 0.5°) sub-daily (6-hourly) climate product resulting from the combination of observation-based CRU TS 3.2 data (Harris et al., 2014) and model-based NCEP-NCAR data (Kalnay et al., 1996). The CRU-NCEP data set spans the 1901-2016 period, we selected data in the time range of 1980-2016, for which the most observations are available, in order to ensure higher accuracy (Kistler et al., 2001). The CRU-NCEP data set contains seven climatic variables: temperature, precipitation, wind, downward longwave and shortwave radiations, air specific humidity, and atmospheric pressure. From them, the climatic variables necessary for TROLL input is calculated and extracted for all data grid points.

We performed a virtual experiment to explore model response to climate forcing, more precisely to values of temperature, irradiance and VPD. For this, we randomly sampled a subset of the CRU-NCEP data points that correspond to lowland non-water-limited rainforest biome within the 35°N – 35°S latitude range. Lowland was defined as points with elevation < 1000 m, and was evaluated using elevation data from the SRTM product, accessible at http://www.earthenv.org/topography (Amatulli et al., 2018). A forest was considered to be not water-limited when its annual precipitation is larger than 2000 mm (Guan et al., 2015; Wagner et al., 2016), and was evaluated using CRU-NCEP precipitation data. Rainforest biome was defined as points that fall into classes 50, 60, 70, 80, and 90 in the ESA C3S Global Land Cover product for 2018, accessible at https://maps.elie.ucl.ac.be/CCI/viewer/download.php (ESA, 2017). From the set of 3753 "reference climate" pixels which fit the criteria, we sampled 500 data points and used their CRU-NCEP climatic variables to perform TROLL simulations at both study sites (Nouragues and Fushan), each time using the previously calibrated general parameter values.

To evaluate model sensitivity, we calculated the mean steady-state values (values over the last 100 years of the simulation) of four summary metrics of forest structure and functioning: stem density (DBH ≥ 10 cm; N_{10}, trees·ha^{-1}), large stem density (DBH ≥ 30 cm;

N_{30}, trees·ha^{-1}), aboveground biomass (AGB, Mg·ha^{-1}), and gross primary productivity (GPP, MgC·ha^{-1}·yr^{-1}). We described the trends of model outcome and model sensitivity to each variable, and fitted linear models with climatic variables as independent terms and the summary metrics as dependent terms, and reported semi-partial coefficients as effect size. This experiment also aims to answer **Research Question 2**, and the results are presented in **Chapter 1**.

Modeling wind-induced tree mortality: ForestGALES

Due to the considerable economic costs associated with wind-induced failure of stems or root anchoring, forest managers have developed tools to predict the occurrence risk of windthrow events (including both stem breakage or uprooting) over the last decades, in order to conceive adapted forest management strategy that minimizes this type of tree damage. Apart from qualitative assessment or statistical models, mechanistic models characterize the physical processes involved in windthrows and describe the causal links between tree parameters and susceptibility to wind damage. This provides opportunities to test hypotheses on specific process and make predictions about consequences of changing environmental conditions (Gardiner et al., 2008).

Mechanistic wind damage models work by calculating the critical wind speed (CWS) needed for trees to undergo windthrow, based on a set of properties easily measurable at the stand level (e.g. tree spacing and canopy height) or at the individual level (tree height, diameter and wood strength): this critical wind speed is then compared with local observed or simulated wind speed patterns to assess the probability that a windthrow event occurs. Based on physical principles, the critical wind speed is calculated by estimating the force that are exerted by the wind on an individual tree (represented as an anchored vertical object), the bending moment this creates, and the mechanical resistance of the root anchorage and stem to the bending moment. The force that a tree experiences naturally depends on the local wind speed, which in turn is conditioned by the tree's position in the canopy and the density and height of neighboring trees in its vicinity. The bending moment created by the force depends on tree dimension and allometry, notably the tree crown's size, shape, distribution along the stem length and streamlining, which influence air drag and the effective "lever arm" length of the represented tree object. The mechanical resistance of a tree depends on its stem characteristics (e.g. diameter and wood strength), root morphology and depth, and soil properties of its anchorage location. Ideally, these factors could all be derived by a set of measurable plant traits based on physical principles. In reality, some empirical relations have to be employed, and models predicting the CWS should best be described as a hybrid of

empirical and mechanistic approaches. For example, as understanding of how root architecture and soil property influences root anchoring remains relatively limited (Fourcaud et al., 2008; Stubbs et al., 2019), modeling of uprooting risk is often done by tree-pulling experiments, which have shown that stem mass is a good empirical predictor of resistance to uprooting (Nicoll et al., 2006; Peterson and Claassen, 2013). Likewise, the streamlining of tree crowns under wind loading is modeled using measurements in wind tunnel experiments (Rudnicki et al., 2004; Vollsinger et al., 2005).

In this thesis, we chose to use ForestGALES, one such wind damage risk model that has seen wide application in both the forestry and the ecology research communities. As wind damage risk models were originally developed to evaluate wind damage in even-aged plantation forests, stand-level properties (e.g., tree spacing and canopy height) are often used to parameterize the model. However, in mixed-sized natural forests, stand-level properties often vary dynamically, and spatial heterogeneity in the forest stand means that the effect of neighbor sheltering can differ for each individual tree, on wind damage risk can be important. We used an updated version of ForestGALES that allows parameterization based on individual-level properties, and made further adjustments and simplifcations to implement it in the TROLL model, in order to explore the long-term effects of wind disturbance on the structure, dynamics and functioning of a mixed-sized natural forests. This work aims to answer **Research Questions 1 and 2**, and the results are presented in **Chapter 2**.

Model overview

In technical terms, wind flow over the forest canopy can be thought of as a horizontal fluid flow above a boundary layer: wind speed decreases as one approaches the canopy top. In ForestGALES, horizontal wind speed (u, $m \cdot s^{-1}$) is modelled by the aerodynamic momentum transfer model above a vegetation canopy (Monteith and Unsworth, 2008, p310), and represented with a logarithmic profile (Gardiner et al., 2008, 2000):

$$u(z) = \frac{u_*}{k} \ln(\frac{z-d}{z_0}) \quad (6)$$

where z (m) is the height above ground, k is Von Kármán's constant (≈ 0.4), z_0 (m) is the aerodynamic roughness of the boundary layer, d (m) is the zero-plane displacement, and u_* ($m \cdot s^{-1}$) is the friction velocity, which is related to the shear stress on the canopy surface (τ, $N \cdot m^{-2}$, or $kg \cdot m^{-1} \cdot s^{-2}$) through the following equation:

$$\tau = -\rho {u_*}^2 \quad (7)$$

where ρ ($kg \cdot m^{-3}$) is the air density. Assuming a regular tree spacing of D (m), and that this shear stress is applied uniformly on each tree, the average wind drag force received by each tree can be represented by τD^2 (N). Thom (1971) showed that this is can be considered as

exerting on the tree at the height of the zero-plane displacement (d). The mean bending moment (BM_{mean}, N·m) can therefore be represented as $(d - z) \times \tau D^2$. A gust factor (G, dimensionless), empirically estimated from wind tunnel experiments (Gardiner et al., 1997), is used to convert the mean bending moment to the maximum bending moment (BM_{max}, N·m), critical for evaluating tree resistance to wind. Based on the above equations, the maximum bending moment at any point on the stem can therefore be expressed as:

$$BM_{max}(z) = f_{CW} f_{edge} (d - z) \rho G \left(\frac{D u_h k}{\ln\left(\frac{h-d}{z_0}\right)} \right)^2 \quad (8)$$

where u_h (m·s) is wind speed at canopy-top tree height (h, m). Two dimensionless coefficients are added to account for different factors that influence the actual bending moment. f_{CW} accounts for the additional moment provided by the overhanging mass of tree crown that is displaced by wind. f_{edge} accounts for the proximity of the tree position to newly created forest edges, which increase its wind loading and damage risk. Trees near established edges (edges that are created a long time ago) are assumed not to increasing wind damage risk, due to trees acclimating to the increased wind exposure by adaptive growth.

Resistance to stem breakage is modeled with the assumption that tree stem is completely homogeneous, and that wind-induced stress is constantly distributed at all points between the crown base and stem base (Morgan and Cannell, 1994). The stress is then calculated at breast height (z = 1.3 m), and the stem is assumed to break when the stress exceeds the modulus of rupture (MOR, Pa). The critical bending moment for stem breakage ($M_{crit,\ break}$, N·m) is expressed by the following equation (Jones, 2013):

$$M_{crit,break} = \frac{\pi}{32} f_{knot} \times MOR \times DBH^3 \quad (9)$$

where f_{knot} (dimensionless) is a factor that accounts for weakening of the stem due to presence of knots.

Resistance to uprooting is modeled empirically based on the results tree-pulling experiments. A linear regression between the maximum recorded bending moment and stem weight (SW, kg) was found to provide the best fit to the data. The critical bending moment for uprooting ($M_{crit,\ uproot}$, N·m) is thus expressed by the following equation:

$$M_{crit,uproot} = C_{reg} \times SW \quad (10)$$

where C_{reg} (N·m·kg^{-1}, or m^2·s^{-2}) is the coefficient of the linear regression forced through zero (with the reasoning that as stem weight approaches zero, so should the bending moment required to uproot it). C_{reg} values for conifers and broadleaf species have been measured through tree-pulling experiments under different soil properties (Locatelli et al., 2016; Nicoll et al., 2006; Peltola et al., 2000; Peterson and Claassen, 2013), and its range in general was found to range from 110 to 185.

By combining equations (9) and (10) with equation (8), the critical wind speed (CWS, $m \cdot s^{-1}$), at which the bending moment reaches the critical value for either stem breakage or uprooting, can be expressed as:

$$CWS_{break} = \frac{1}{kD}\left[\frac{\pi MOR \times DBH^3}{32G(d-1.3)}\right]^{\frac{1}{2}}\left[\frac{f_{knot}}{f_{edge}f_{CW}}\right]^{\frac{1}{2}}\ln(\frac{h-d}{z_0}) \quad (11)$$

$$CWS_{uproot} = \frac{1}{kD}\left[\frac{C_{reg} \times SW}{\rho G d}\right]^{\frac{1}{2}}\left[\frac{1}{f_{edge}f_{CW}}\right]^{\frac{1}{2}}\ln(\frac{h-d}{z_0}) \quad (12)$$

The value of the aerodynamics parameters (d, z_0) depends on multiple forest canopy properties, including tree height, tree spacing, crown depth and crown width. The latter two depend on the crown frontal area, which in turn depends on wind speed due to the streamlining effect: consequently, equations (11) and (12) could not be directly solved. In the original implementation, an iterative approach was used to find an approximation of the critical wind speed (Gardiner et al., 2000).

One major empirical element in the above model is the gust factor (G), which relates the mean bending moment, calculated based on mean wind speed, to the maximum bending moment. Its parameterization at the individual level is difficult, and yet model output is very sensitive to its value. Another approach is to directly quantify the relationship between the maximum turning moment and the mean wind speed, thus eliminating the need for the gust factor and allowing the wind damage model to be more easily applied to mix-sized natural forests (Hale et al., 2015, 2012). Based on field measurements conducted at several temperate forest sites, the hourly maximum bending moment (M_{max}, N·m) was shown to be related to the hourly mean canopy-top wind speed (u, $m \cdot s^{-1}$) through the following relationship:

$$M_{max} = T_C \times u^2 \quad (13)$$

T_C ($N \cdot m^{-1} \cdot s^2$, or kg), the turning moment coefficient (TMC; turning moment is an alternative terminology for bending moment), represents the ratio between the square of the mean wind speed and the maximum bending moment, and was found to be related to tree characteristics as follows (Hale et al., 2012):

$$T_C = \tau \times DBH^2 \times H \quad (14)$$

where the constant τ ($kg \cdot m^{-3}$) = 111.7 (Hale et al., 2015). A higher T_C value represents larger turning moment for a given wind speed. By combining equations (13) and (14), which describe the maximum bending moment through tree properties and mean wind speed, and equations (9) and (10), which describe the critical bending moment that induces stem breakage or uprooting, we can reformulate the equations for critical wind speed as the following:

$$CWS_{break} = \left[\frac{\pi \times MOR \times {D_0}^3}{32 \times \tau \times DBH^2 \times H}\right]^{\frac{1}{2}} \left[\frac{f_{knot}}{f_{edge} f_{CW}}\right]^{\frac{1}{2}} \left[\frac{1}{TMC_{ratio}}\right]^{\frac{1}{2}} \quad (15)$$

$$CWS_{uproot} = \left[\frac{C_{reg} \times SW}{\tau \times DBH^2 \times H}\right]^{\frac{1}{2}} \left[\frac{1}{f_{edge} f_{CW}}\right]^{\frac{1}{2}} \left[\frac{1}{TMC_{ratio}}\right]^{\frac{1}{2}} \quad (16)$$

where TMC_{ratio} (dimensionless) is a factor that accounts for increase of wind loading after a recent thinning event, and is expected to tend towards 1 through time, as trees acclimate to the increased wind exposure by adaptive growth. Note that for Equation (15), diameter at stem base (D_0) is used rather than diameter at breast height (DBH) because with the TMC approach, only the bending moment at the tree base can be calculated (Hale et al., 2015).

Finally, in order for the estimated canopy-top critical wind speed to be compared with meteorological data, which conventionally measure wind speed at 10 m above the zero-plane displacement, a wind speed conversion using the logarithmic profile is used:

$$CWS_{d+10} = CWS_h \times \ln(\tfrac{10}{z_0}) / \ln(\tfrac{h-d}{z_0}) \quad (17)$$

Implementation of ForestGALES in TROLL

In this thesis, ForestGALES was implemented as a sub-model of wind-induced tree mortality in the TROLL model. At each time step, when there is an extreme wind event (see section **Wind simulation in TROLL**), each tree is evaluated to decide if it experiences windthrow, in which case it falls and dies. In keeping with the original TROLL module, secondary treefall is modeled by assuming that when a tree dies, it falls in a random direction, and increases the death rate of trees in the impacted pixels. In order to introduce stochasticity, we assumed that the probability of windthrow of each individual tree is positively related to the difference between the observed wind speed u(h) that it experiences and its critical wind speed (CWS) for damage: the higher $u(h)$ is relative to CWS, the more likely the tree is to fall and die. A logistic model was used to describe the relationship between wind-induced tree death probability (p) and the difference between $u(h)$ and CWS (Hale et al., 2015; Valinger and Fridman, 1999):

$$p = 1/(1 + e^{-(u(h) - CWS)}) \quad (18)$$

A crucial departure of the TROLL implementation of wind damage risk sub-model and the original ForestGALES model is their approach to account for the effect of neighborhood sheltering in a mixed-sized forest. The original ForestGALES model estimates canopy-top CWS for all tree individuals regardless of its relative position in the canopy, and converts them to atmospheric CWS for comparison with the observed atmospheric wind speed. To account for the sheltering at the sub-canopy level, the CWS calculation can be modulated by a competition index, which is a function of the tree height relative to neighboring tree heights,

so that sub-canopy and understory trees would have reduced wind loading and wind damage risk compared to top-canopy and emergent trees (Duperat et al., 2021; Hale et al., 2012; Quine et al., 2021). The TROLL implementation does not modify CWS with competition index, but instead of canopy-top CWS, it calculates individual tree-top CWS, which is then compared with the observed tree-top wind speed. During the conversion of observed atmospheric wind speed to the tree-top level, the neighborhood sheltering effect is taken into account by assuming that wind speed continues to decrease with diminishing height within the canopy. For canopy-level or emergent trees, where tree height (z, m) $\geq H$, the same logarithmic wind speed profile as in Equations (6) and (17) is used for the conversion: $u(z) = u_{d+10} \times \ln(\frac{z-d}{z_0}) / \ln(\frac{10}{z_0})$. For sub-canopy or understory trees, where $z < H$, the logarithmic profile is not applicable, and the within-canopy wind profile is represented with the following equation (Inoue 1963):

$$u(z) = u(H) \times e^{-\alpha(1-z/H)} \quad (19)$$

where $\alpha = H/L_s \approx 3$: empirical values of L_s are reported in Table I of Raupach *et al.* (1996). With this parameterization, horizontal wind speed $u(z)$ within the canopy at $H/2$ is 22% of $u(H)$: to reduce computational burden, we assumed that trees $z < H/2$ are not directly affected by wind, meaning that $u(z) = 0$. In order to account for horizontal canopy heterogeneity, average top canopy height (H, m) is calculated for every 20 × 20 m quadrat of the simulated forest stand, by taking the arithmetic mean of the top leaf-containing voxel layer of each pixel within the quadrat.

In addition, in this thesis, we assumed that the aerodynamic parameters d and z_0 only depended on average canopy height (H, m). The variation of both parameters over forest vegetation has been explored both from theoretical angles (Dorman and Sellers, 1989; Sellers et al., 1996; Shaw and Pereira, 1982) and through field measurements (Raupach et al., 1991; Shuttleworth et al., 1989), which showed that the overall values of d and z_0 range from 0.7 H to 0.9 H and from 0.04 H to 0.08 H, respectively. We therefore used the parameterization of $d = 0.8\ H$ and $z_0 = 0.06\ H$, choosing an intermediate value of the reported range. It is to be noted that z_0 value is expected to vary seasonally as plant area index (leaves plus woody components) fluctuates, although here it is assumed to be constant. Based on the above formulation, Figure 12 illustrates an example of horizontal wind speed above and within forest canopy.

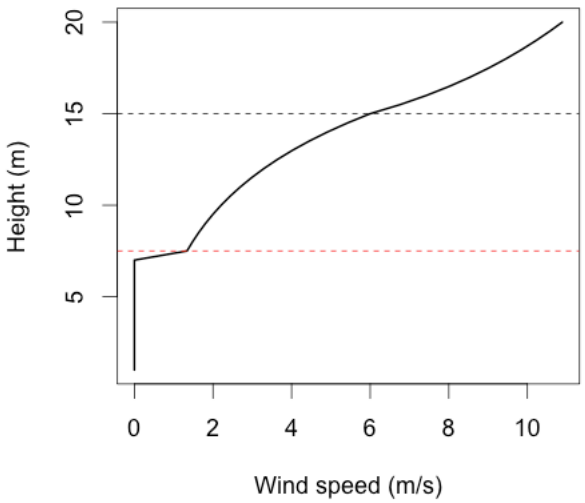

Figure 12. Horizontal wind speed profile above and within forest canopy simulated in TROLL, provided H = 15 m and u_{d+10} = 12 m·s^{-1}.

In Equations (15) and (16), besides DBH (diameter at breast height) and H (tree height), several other variables were parameterized by individual tree characteristics calculated in the TROLL model. MOR (fresh-wood modulus of rupture; Pa, or kg·m^{-1}·s^{-2}) was estimated from oven-dry wood density (WD_b, g·cm^{-3}) using the species-specific wood trait values reported in Green *et al.* (1999). We used hardwood species for which fresh-wood modulus of rupture was measured, and converted the reported wood density at 12% moisture (WD_{12}) into oven-dry wood density using the formula $WD_b = 0.828 \times WD_{12}$ (Vieilledent et al., 2018). The relationship between oven-dry wood density and fresh-wood MOR was then fit with an exponential function:

$$MOR = 17.2 \times e^{(2.51 \times WD_b)} \times 10^6 \quad (20)$$

D_0 (diameter at trunk base) was estimated using DBH with a linear corrective factor: $D_0 = \beta \times DBH$. SW (kg) represents fresh stem weight, and was estimated using aboveground biomass (AGB) with a linear corrective factor: $SW = \alpha \times AGB$.

This simplified model thus still contained numerous empirical factors: α (estimating SW from AGB), β (estimating D_0 from DBH), τ (estimating the turning moment coefficient from tree size), f_{knot} (accounting for the effect of stem knots), f_{edge} (accounting for the effect of newly created forest edge), f_{CW} (accounting for the effect of overhanging crown weight when the tree is bent under wind), and TMC_{ratio} (accounting for recent thinning events). Since it is not the objective of this thesis to explore in detail the role of each of these factors, we decided to further simplify the model by combining these factors and other constants into a single "wind damage parameter", P. Equations (15) and (16), calculating critical wind speed for each type of damage, could therefore be rewritten as follows:

$$CWS_{break} = P_{break} \times \left(\frac{MOR \times DBH^3}{DBH^2 \times H}\right)^{\frac{1}{2}} \quad (21)$$

$$CWS_{uproot} = P_{uproot} \times \left(\frac{AGB}{DBH^2 \times H}\right)^{\frac{1}{2}} \quad (22)$$

where P_{break} (dimensionless) and and P_{uproot} ($m \cdot s^{-1}$) are free parameters that encapsulate the following factors, respectively:

$$P_{break} = [(\pi \times \beta^3 \times f_{knot})/(\tau \times 32 \times f_{edge} \times f_{CW} \times TMC_{ratio})]^{1/2} \quad (23)$$

$$P_{uproot} = [(C_{reg} \times \alpha)/(\tau \times f_{edge} \times f_{CW} \times TMC_{ratio})]^{1/2} \quad (24)$$

The *P* parameters represent the overall susceptibility of a forest stand to wind-induced tree mortality: the smaller the *P* value of a damage type is, the lower the critical wind speed is for the same individual tree, meaning that the forest is overall more susceptible to wind-induced death due to that type of damage. Since these two parameters are empirical, and no observation-based parameterization is possible, we performed a sensitivity analysis to investigate model responses to these two parameters.

We first ran 500 TROLL simulations, each time randomly drawing one value for each parameter from a uniform prior range ([0.01, 1] for P_{break} and [0, 40] for P_{uproot}). The simulations were run for a forest stand of 4 hectares over 500 years (6000 time steps) from bare ground, and the wind-induced tree mortality sub-model was activated after a burn-in period of 100 years (1200 time steps). We used the principle of model inversion to examine which parameter combinations generated aboveground biomass (AGB) values that are closest to field-estimated values. As the best-fit simulations (25 simulations with the 5% smallest deviation between simulated and field AGB) did not converge to a narrower parameter value range, we decided to evaluate the relative contribution of each wind disturbance process to tree mortality: we calculated the average proportion of treefalls due to each type of damage in all timesteps in the last 100 years of the simulation where an extreme wind event happened. The results showed that the proportion of treefalls due to tree uprooting was low compared to those due to stem breakage. As field observations from annual mortality survey at the Fushan site also indicate that the proportion of tree uprooting is low compared to that of stem breakage, we decided to focus on wind-induced stem breakage.

A second sensitivity analysis and model calibration were thus performed, this time including only Equation 21 as the wind-induced tree mortality sub-model and a single free parameter *P*. We ran 1000 TROLL simulations, each time varying the *P* value by a step of 0.005 across the range of (0, 1], with five replicates for each parameter value. The simulations were run with the same stand size (4 hectares), duration (500 years, i.e. 6000 time steps), initial condition (from bare ground) and activation time of the wind-induced tree mortality sub-model (after a burn-in period of 100 years, i.e. 1200 time steps).

We calculated the mean steady-state values (values over the last 100 years of the simulation) of three forest structure metrics: stem density (DBH > 10 cm; N_{10}, trees·ha^{-1}), Lorey's height (basal area-weighted mean tree height, m) (Pourrahmati et al., 2018), and aboveground biomass (AGB, Mg·ha^{-1}). We also calculated two mortality statistics for trees with DBH > 10 cm: mean annual mortality and fraction of mortality due to treefalls ($\%M_{treefall}$). These mortality statistics were calculated at the onset of wind disturbance (first 100 years after wind submodule activation, i.e. year 101–200) and at the steady state (last 100 years of simulation, i.e. year 401–500). We qualitatively described trends and sensitivity of these statistics in response to variation of parameter value, and calculated the fit of simulated to field observed values of aboveground biomass.

Wind simulation in TROLL

Extreme wind events are simulated in TROLL in a two-step process: first, at each time step, it randomly determines if an extreme wind event happens based on past cyclone occurrence frequency; then, a wind speed is randomly drawn from the on-site cyclonic wind speed distribution. This assumes that one extreme wind event at most can occur per time step.

For a given site, we calculated the monthly average frequency of cyclones that have occurred within a sufficiently close distance to the study site, using the IBTrACS data set (International Best Track Archive for Climate Stewardship database; v04r00, archived at https://www.ncdc.noaa.gov/ibtracs/index.php?name=ib-v4-access). This data set contains best-track records of global tropical cyclones occurring since 1945 (Knapp et al., 2010).

A common measure of the spatial extent of tropical cyclones is the mean radius of gale-force winds (R_{17}, km) : gale-force wind is by convention defined as 17.5 m·s^{-1}. Based on the reported value ranges in the literature, we assumed R_{17} to be 150 km (Chan and Chan, 2012; Lu et al., 2017; Weber et al., 2014). We therefore calculated the monthly mean frequency of recorded tropical cyclones occurring within a 150-km distance from the Fushan site over the period of 1987-2020, where cyclone records were the most complete for the Northwest Pacific basin.

We calculated on-site cyclonic wind speed (V_{site}, m·s^{-1}) using the wind speed records of the selected cyclones, and based on the empirical function that relates it to the distance between the site and the cyclone center (d, km) (Anthes 1982, Hsu & Babin 2005): $V_{site} = 17.5 \times \sqrt{R_{17}/d}$ (since $d < R_{17}$ by definition, it follows that $V_{site} > 17.5$ m·s^{-1}). For each month, we then fitted the V_{site} values to a Weibull distribution using the R function *fitdistr* in the package *MASS* (Venables and Ripley, 2002), and used the scale and shape parameters as input climate forcing variables.

Exploration of effects of wind frequency and intensity

In order to examine how extreme wind pattern influences forest structure, dynamics and functioning, we performed two series of simulations varying cyclone frequency and wind intensity. In the first series, we varied cyclone occurrence frequency from 0.1 to 2 times the empirical frequency at the Fushan site, with a varying step of 0.1, while maintaining wind intensity. In the second series, we varied the scale parameter of the wind speed distribution, which controls the mean and median of the wind speed distribution, from 0.1 to 10 times the empirical value at the Fushan site, with a varying step of 0.1, while maintaining empirical frequency. Five replicates were performed for each condition (in total, 100 simulations for frequency and 500 simulations for intensity). Based on the results of the sensitivity analysis, we set $P = 0.7$, a value where simulation results are close to field observations and not near the forest tipping point ($P < 0.3$). The simulations were run with the same stand size (4 hectares), duration (500 years, i.e. 6000 time steps), initial condition (from bare ground) and activation time of the wind-induced tree mortality sub-model (after a burn-in period of 100 years, i.e. 1200 time steps).

As in the previous step, we calculated the mean steady-state values (values over the last 100 years of the simulation) of three forest structure metrics: stem density (DBH > 10 cm; N_{10}, trees·ha^{-1}), Lorey's height (basal area-weighted mean tree height, m) (Pourrahmati et al., 2018), and aboveground biomass (AGB, Mg·ha^{-1}). We also calculated two mortality statistics for trees with DBH > 10 cm: mean annual mortality and fraction of mortality due to treefalls ($\%M_{treefall}$). These mortality statistics were calculated at the onset of wind disturbance (first 100 years after wind submodule activation, i.e. year 101–200) and at the steady state (last 100 years of simulation, i.e. year 401–500). We qualitatively described trends and sensitivity of these statistics in response to variation of parameter value.

Exploration of effects of topography

Given that wind speed is altered over an uneven topography, we implemented quadrat-scale wind speed correction factors in the model to account for this topographical effect. For this, we used the Global Wind Atlas (GWA) data produced through downscaling with the WAsP program (Badger et al., 2015; Mortensen et al., 2001). We acquired 250 × 250 m GWA pixels that fall in the area covered by the 1° × 1° CRU-NCEP pixel where the Fushan site is located: this represents a grid of 200 × 200 GWA pixels. We normalized the GWA wind speed values of the selected pixels, so that the mean GWA wind speed is equal to the mean CRU-NCEP

wind speed. We then resampled the GWA pixels to the 20 × 20 m quadrat scale using bilinear interpolation with the *resample* function in the *raster* package (Hijmans, 2020), and selected the resampled pixels falling within the Fushan plot area: this represents a grid of 25 × 25 = 625 resampled pixels. We used the GWA wind speed values of these resampled pixels, normalized by their plot-wide mean, as the wind speed correction factor for each quadrat. The wind speed correction factor ranged from 0.27 to 1.96, and was used as a proxy for topographic heterogeneity: when topographic effect is activated, the wind speed experienced at each quadrat is the plot-wide wind speed (randomly drawn from the input wind speed distribution) multiplied by this correction factor: a value above 1 means that the wind speed at that quadrat is considered to speed up (due to exposed terrain), and vice versa when the value is below 1.

We then performed simulations with and without topographical effect at the Fushan site. The simulations were run for a forest stand size of 25 hectares, but with the same duration (500 years, i.e. 6000 time steps), initial condition (from bare ground) and activation time of the wind-induced tree mortality sub-model (after a burn-in period of 100 years, i.e. 1200 time steps) as before. As in previous steps, we calculated the mean steady-state values (values over the last 100 years of the simulation) of three forest structure metrics: stem density (DBH > 10 cm; N_{10}, trees·ha^{-1}), Lorey's height (basal area-weighted mean tree height, m) (Pourrahmati et al., 2018), and aboveground biomass (AGB, Mg·ha^{-1}). We performed linear regressions for each statistics to quantify the effect of wind speed correction factor on these quadrat-level metrics values.

Exploration of natural disturbances in tropical forests using satellite data

In order to develop near real-time (NRT) monitoring of natural disturbances in tropical forests, and to characterize fine-scale spatial pattern and temporal dynamics of forest gaps caused by natural disturbances, I analyzed Sentinel-1 synthetic aperture radar (SAR) data that has been processed to detect forest disturbance events in French Guiana from 2016 to 2019. I used field-derived synthesis data of land use in French Guiana in 2015, as well as Landsat-derived optical data product that provides detailed characterization of long-term tropical moist forest cover change to separate anthropogenic from natural disturbance events. I compared the spatial pattern of natural forest gaps detected by the Sentinel-1 data product and by the Landsat-derived data product to ascertain their congruency. Finally, I quantified the topographic association of forest gaps and the monthly dynamics of natural disturbance events detected by Sentinel-1 satellite data. This work aims to answer **Research Question 3**, and the results are presented in **Chapter 3**.

Study site: French Guiana

French Guiana, an overseas territory of France, is situated in equatorial South America, adjacent to Suriname and Brazil. 95% of its surface area is covered by old-growth tropical rainforests (Beck et al., 2018; Keenan et al., 2015), and inselberg features (isolated rock hills rising above the surrounding forest-covered lowlands) are common due to its geographical location within the Guiana Shield. Forests in French Guiana typically experience a long wet season from December to June (monthly precipitation 250–550 mm) and a dry season from July to November (monthly precipitation 100–180 mm). A minor dry season (monthly precipitation 170–370 mm) sometimes occurs around March for approximately one and a half months, with considerable interannual variability (Bonal et al., 2008).

Anthropogenic deforestation in French Guiana is mainly due to smallholder agriculture, forest exploitation (e.g. selective logging, road building), and notably gold mining (alluvial or in steep valleys) (Alvarez-Berríos and Mitchell Aide, 2015; Rahm et al., 2017). Although French Guiana is not affected by tropical cyclones, strong wind events caused by downburst storms have been suggested to be an important disturbance agent and ecological driver in the northwestern and central Amazon (Magnabosco Marra et al., 2018; Negrón-Juárez et al., 2018; Peterson et al., 2019). However, the influence of this disturbance factor in northeastern Amazonian forests in the Guiana Shield region remains to be elucidated.

Sentinel-1 SAR data

Sentinel-1 is a satellite constellation comprised of Sentinel-1A and Sentinel-1B, launched in 2014 and 2016 respectively by the European Space Agency (ESA). The global coverage, short revisit period (6 to 12 days) and fine resolution (10 m) of Setinel-1 satellites make them an ideal option for NRT forest monitoring. Sentinel-1 satellites are equipped with C-band (wavelength 7.5 - 3.75 cm) SAR sensors, which work by emitting radio wave pulses from the satellite onto the land surface and recording the backscatters of the pulse waves. The three-dimensional structure of the detected can then be reconstructed by processing the backscatters recorded at different moments (and therefore at different positions) (Kirscht and Rinke, 1998). Figure 11 provides an overview of the principle of SAR remote sensing system.

The wavelength of C-band radio wave allows it to partially penetrate into the forest canopy: its backscatter is thus affected by multiple factors of the ground and canopy components, such as canopy structure, canopy or soil moisture content, surface roughness and topography (Askne et al., 1999; Pulliainen et al., 1999). As a result, disturbed areas are not necessarily characterized by a sharp change of backscatter intensity. A new method of deforestation detection has been developed by Bouvet *et al.* (2018). This method bypasses the problem of variability in absolute backscatter intensity, and instead detects SAR shadowing, which occur due to the side-looking geometry of SAR sensor systems: as the radar pulses arrive the surface at an angle, some areas do not receive any radar pulse due to nearby obstacles, which include trees at the border between forest and non-forest areas. The shadow signals that appear (or disappear) following deforestation events are characterized by a sharp decrease in the backscatter in the time series. As this signal arises from a purely geometrical effect, it is expected to be less temporally variable than the absolute backscatter intensity, and can thus be used as an indicator of forest loss. Figure 13 provides an illustration of the principle of the shadow detection method. This method has been successfully tested and validated in Peru (Bouvet et al., 2018) and in French Guiana (Ballère et al., 2021) for anthropogenic deforestation detection.

In this study, we acquired Sentinel-1 SAR time series that has previously been processed using the shadow method, in the form of a raster data product that contains all disturbed pixels that has been detected in French Guiana from January 1st, 2016 to December 31st, 2019 (henceforth the Sentinel-1 dataset). The pixel values are the time of disturbance, originally in number of days since April 3rd 2014, (date of the Sentinel-1A satellite launch), adjusted to the number of days since January 1st, 2016 in this study for simplicity. I used the *clump* function in the *raster* R package (Hijmans, 2020) to cluster contiguous disturbed pixels into patches, and converted the raster layer into a vector layer containing polygons that each represent a disturbance patch in QGIS (QGIS.org, 2021).

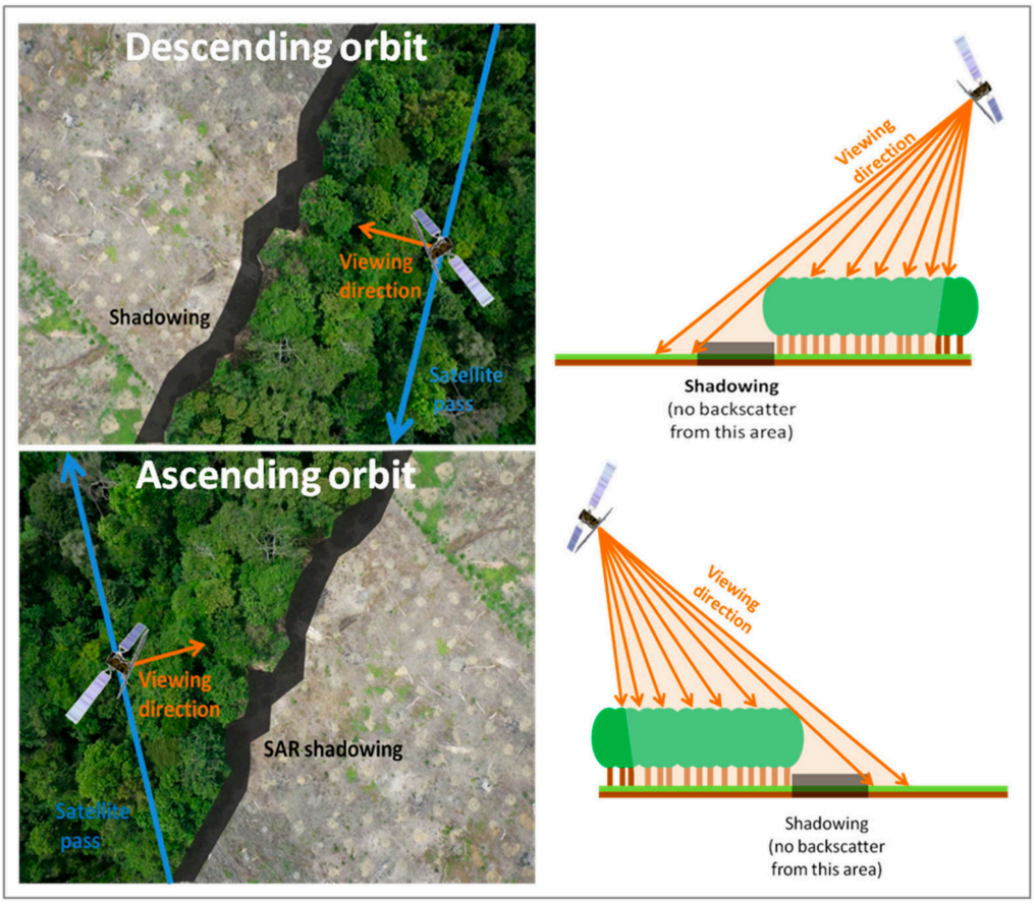

Figure 13. The principle of the shadow detection method for SAR satellite data. Reproduced from (Bouvet et al., 2018).

Landsat-derived tropical moist forest cover data

The Landsat satellite mission, led by NASA and USGS, consists of a series of satellites that have generated continuous optical imagery of the entire globe at a spatial resolution of 30 m since 1972 (Woodcock et al., 2008). A recent study, conducted by the Joint Research Center (JRC) of the European Commission, reprocessed the full Landsat archives to produce a dataset that characterizes land cover change and disturbance status of tropical moist forests (TMF) from 1982 to 2020 (Vancutsem et al., 2021). Three data layers of this data product (henceforth the JRC-TMF dataset) were used in this study. The "Transition map" layers summarize the overall forest cover change of each TMF pixel at the end of the observation period, classifying pixels into categories including undisturbed forests, forest degradation (short-term disturbances due to either natural or anthropogenic causes), deforestation (long-term conversion of forest to non-forest cover) and non-forest cover (permanent or seasonal water body, non-forest vegetation or non-vegetation cover such as road or buildings); the

"Degradation year" and "Deforestation year" layers show the year a pixel has been degraded or deforested for the first time, respectively.

In this study, we acquired the JRC-TMF dataset for the entire extent of French Guiana. I created a raster layer that included all disturbed pixels (the union of pixels classified as "degradation" and "deforestation" in the transition map), and used the *clump* function in the *raster* R package (Hijmans, 2020) to cluster contiguous disturbed pixels into patches, and converted the raster layer into a vector layer containing polygons that each represent a disturbance patch in QGIS (QGIS.org, 2021).

Identifying and selecting forest gaps caused by natural disturbance

In order to compare the Sentinel-1 and the JRC-TMF dataset over the same time period, I retained only JRC-TMF patches that overlap only with pixels of degradation year from 2016 to 2019, and that do not cover deforested pixels (pixels with a defined deforestation year). Our reasoning for excluding deforestation events is that it is defined in the JRC-TMF dataset as pixels that have undergone a complete and permanent conversion from forest to non-forest cover (such as agriculture or water surface), and therefore should not be considered as natural disturbance-induced forest gaps.

In order to delimit a study zone with minimal level of anthropogenic disturbances, where most detected forest gaps are likely due to natural disturbance, I acquired the summary data of land use in French Guiana in 2015, and added a 5-km buffer around the areas of anthropogenic disturbance activities in the summary data. Through visual observation, I identified and manually drew two zones that are far from the majority of anthropogenic disturbances, one in the north and one in the south (Figure 14). I then excluded the Sentinel-1 and TMF disturbance patches outside of the study zone.

I further excluded patches with size < 0.2 ha, based on the reasoning that the smallest patches are more likely to be misidentifications or artifacts (false positives). The minimum size threshold of 0.2 ha was chosen based on the reported minimum detected surface area for disturbance patches for the Sentinel-1 dataset in Ballère et al. (2021).

I also excluded a small proportion of irregular-shaped, large-sized patches situated near or within topographical features (e.g., hills or inselbergs), with the assumptions that these are either artifacts or disturbance events occurring at the edge between forests and the non-forests, and thus represent a different pattern than disturbance-driven gap dynamics. For this, I created a "non-forest cover" mask that included all the non-forest pixels in the transition map layer of the JRC-TMF dataset plus a 300-m buffer (corresponding to five JRC-TMF pixels), and excluded all disturbance patches overlapping with the non-forest mask.

Characterization of natural forest gap patterns and dynamics

In order to verify that the Sentinel-1 dataset detects forest gaps with higher precision and sensitivity, and that the overall gap pattern is consistent with the JRC-data product, I quantified and compared the total number of gaps, total disturbed areas, and the gap size-frequency distribution for both datasets. I also visually examined and compared the spatial patterns of the forest gaps in both datasets, and quantified the proportion of geographical match between the two datasets, both for all gaps and for large gaps (size $\geq$ 0.5 ha).

I then characterized the spatial distribution and temporal dynamics of the forest gaps detected in the Sentinel-1 dataset. Specifically, I calculated the ratio of disturbed area to total area for each elevation class in 50-meter bins, to see if the level of disturbance is correlated with topographical factors. I also compared the monthly dynamics of total disturbed areas with the monthly dynamics of precipitation and water deficit to see if there are seasonal variations in the level of disturbance.

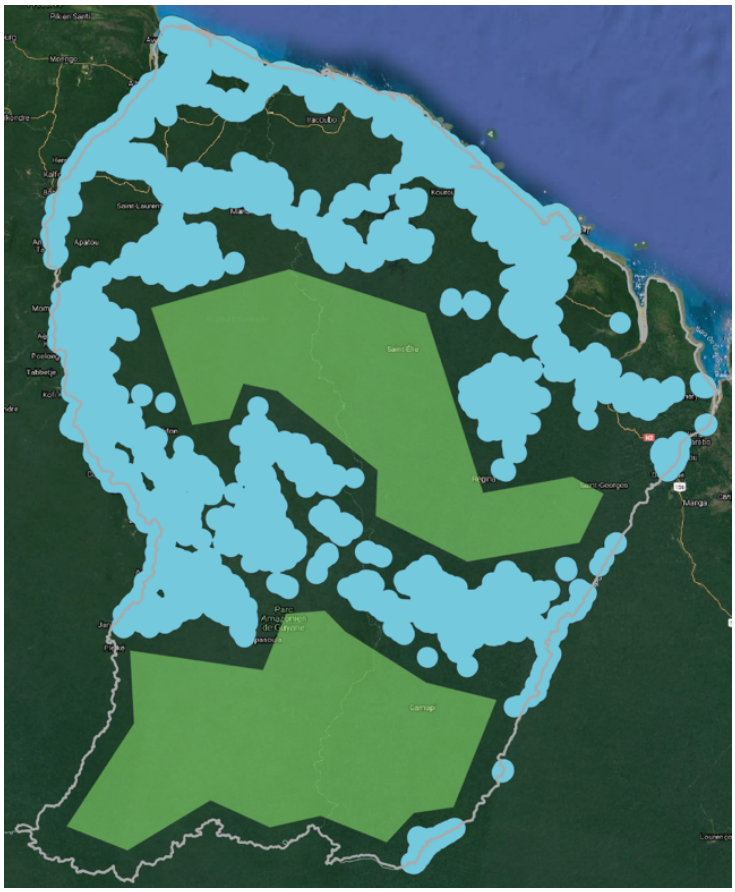

Figure 14. The entire extent of French Guiana (gray line), the region of frequent anthropogenic disturbance activities (blue) and the study zone (green). Underlying layer: Google Satellite Hybrid.

CHAPTER 1: Transferability of an individual- and trait-based forest dynamics model: a test case across the tropics

Accepted in *Ecological Modelling*.

This paper explores the transferability of a spatially explicit individual-based forest dynamics model, TROLL, by applying it at two forest sites with contrasting climatic condition and floristic composition. We tested the sensitivity of empirical parameters considered to control key processes, calibrated parameter values using field data based on the principle of model inversion, and explored model response to a wide range of realistic climatic variation. This work contributes to answer **Question 2**.

Authors: E-Ping Rau[a], Fabian Fischer[a], Émilie Joetzjer[b], Isabelle Maréchaux[c], I Fang Sun[d], Jérôme Chave[a*]

[a]Laboratoire Évolution et Diversité Biologique (UMR5174) Bâtiment 4R1, 118 route de Narbonne, 31062 Toulouse cedex 9, France

[b]INRAE, Universite de Lorraine, AgroParisTech, UMR Silva, Nancy, France

[c]AMAP Lab, University of Montpellier, INRAE, CIRAD, CNRS, IRD, F-34000 Montpellier, France

[d]Department of Natural Resources and Environmental Studies, National Dong Hwa University, Hualien, Taiwan

[*]Corresponding author

Keywords: TROLL, forest simulations, model calibration, climate forcing, Taiwan, Amazonia

1.1 Abstract

Individual-based forest models (IBMs) are useful to investigate the effect of environment on forest structure and dynamics, but they are often restricted to site-specific applications. To build confidence for spatially distributed simulations, model transferability, i.e. the ability of the same model to provide reliable predictions at contrasting sites, has to be thoroughly tested. We tested the transferability of a spatially explicit forest IBM, TROLL, with a trait-based species parameterization and global gridded climate forcing, by applying it to two sites with sharply contrasting climate and floristic compositions across the tropics, one in South America and one in Southeast Asia. We identified which parameters are most influential for model calibration and assessed the model sensitivity to climatic conditions for a given calibration. TROLL produced realistic predictions of forest structure and dynamics at both sites and this necessitates the recalibration of only three parameters, namely photosynthesis efficiency, crown allometry and mortality rate. All three relate to key processes that constrain model transferability and warrant further model development and data acquisition, with mortality being a particular priority of improvement for the current generation of vegetation models. Varying the climatic conditions at both sites demonstrate similar, and expected, model responses: GPP increased with temperature and irradiance, while stem density and aboveground biomass declined as temperature increased. The climate dependence of productivity and biomass was mediated by plant respiration, carbon allocation and mortality, which has implications both on model development and on forecasting of future carbon dynamics. Our detailed examination of forest IBM transferability unveils key processes that need to improve in genericity before reliable large-scale implementations can be envisioned.

1.2 Introduction

Forests harbor more than half of the total terrestrial biodiversity (Gardner et al., 2010) and contribute to climate change mitigation (Ellison et al., 2017; Mitchard, 2018). However, forest disturbances are important drivers of canopy cover change and they will likely impact tropical forest structure, diversity, and functioning in the future (Feng et al., 2018; Malhi et al., 2009; Zemp et al., 2017). These projections depend on a detailed understanding of the processes that link the abiotic environment and forest dynamics, as can be achieved through integration into simulation models (Fisher et al., 2018; Shugart et al., 2018). Confronting the robustness, reliability and realism of such models is crucial to gain confidence in their predictions (Prentice et al., 2015).

Dynamic global vegetation models (DGVMs) adopt a coarse representation of the coupling between vegetation and biogeochemical cycles. Their simplified description of vegetation dynamics assume a limited set of vegetation structure and summarize plant diversity with a few plant functional types (PFTs). Modern DGVMs simulate demographic processes and trait variability (Fisher et al., 2010; Koven et al., 2020; Sakschewski et al., 2015; Sato et al., 2007; Scheiter et al., 2013). However, difficulties remain in representing plant recruitment and mortality, translating into uncertainties in model projections of forest dynamics (Fisher et al., 2018).

Unlike DGVMs, individual-based forest models (IBMs) explicitly simulate tree establishment, growth, competition, and mortality, simulating forest structure and dynamics at the stand scale (Bugmann, 2001; DeAngelis and Grimm, 2014; Fischer et al., 2016; Shugart, 1984). Forest IBMs adopt a fine-grained representation of the diversity and structure of tree assemblages, which facilitates the exploration of mixed-species forest responses to climate variability (Maréchaux et al., 2021). One drawback is that the calibration of forest IBMs is data demanding, and requires data at a fine spatial and temporal scale. For this reason, IBMs have traditionally been restricted to stand-scale application, and even if their extension to regional or global scale is technically possible (Shugart et al., 2018, 2015), one fundamental challenge is to explore the model validity across space.

At the heart of model upscaling is the question of model transferability (Wenger and Olden, 2012; Yates et al., 2018): when a model has been calibrated at one site, how well does it simulate the vegetation dynamics at another site? Model transferability hinges upon how well the model is able to capture forest processes at any given site, and on whether the same biogeochemical and biophysical processes hold across sites (Fyllas et al., 2017; Sullivan et al., 2020). For instance, process-based models couple forest processes to environmental drivers in a generic way, through mechanistic modules, such as photosynthesis, water uptake, allocation. These processes are parameterized locally through measurable traits with

consistent biological and ecological meaning (e.g. functional traits). This means that, in theory, a completely process-based model should be transferable to any site, provided that measurements of the environmental drivers (e.g., climatic variables) and relevant traits of all locally present tree species are available.

However, for some processes, current knowledge is insufficient to develop generic functions, and a simplified representation is necessary to encapsulate finer processes mediated by environmental, biogeographic or evolutionary factors. As a result, part of the site-specificity is hidden in the model equations and parameters themselves. These site-specific parameters need to be re-calibrated from one site to the other to ensure reliable simulation outputs, which increases calibration efforts and hampers transferability (Lehmann and Huth, 2015; Maréchaux et al., 2021). Even generic equations have typically been formulated using input data from specific sites and under specific conditions, which will not always be consistent with the data provided for model initialization at other sites (Huber et al., 2018). This issue is especially important for tropical forests, which have high variability in composition, structure and functioning within and between sites, making model transferability and upscaling a greater challenge (Castanho et al., 2016; Johnson et al., 2016; Townsend et al., 2008).

Model transferability in part depends on the availability of standardized and spatially distributed data on forest structure and function. For example, site-specific information can be prescribed for a model through trait-based data on floristic diversity (Fyllas et al., 2014, Maréchaux and Chave, 2017) or remote sensing data (Fischer et al., 2019; Joetzjer et al., 2017; Shugart et al., 2015). Consistent climatic boundary conditions, derived from weather models and data assimilation systems, also increase model transferability (Bugmann and Fischlin, 1996; Fauset et al., 2019). This also facilitates the evaluation of how a model responds to changes in climate forcing conditions: for example, in light-limited tropical rainforests, we expect that GPP will exhibit weakly positive or even negative relationship with increasing temperature, due to increasing competition, mortality and faster turnover (Allen et al., 2010; Clark et al., 2010; McDowell et al., 2018).

Another way to improve model transferability is to convert modules that are implicitly site-specific into more generic formulations that encode site-specific conditions only through dependence on environmental and floristic composition. This can be facilitated by performing tests to identify model processes that are currently particularly site-specific: the improvement of the representation of those processes, through theoretical and empirical work across multiple sites, should then be prioritized. For instance, we expect that outputs of forest IBMs will be highly sensitive to parameters of mortality, and a more accurate mechanistic representation of mortality should improve the reliability of model projections under

conditions beyond the range of the original calibration data (Johnson et al., 2016; Bugmann et al., 2019). Although several studies have explored the issue of transferability of forest IBMs (Bugmann and Solomon, 1995; Lagarrigues et al., 2015; Ma et al., 2017; Shuman et al., 2015), they have so far been limited to temperate and boreal forests with low tree species diversity.

In this study, we explored the conditions of transferability of a forest IBM between two contrasting tropical forest sites chosen to maximize dissimilarity in geography, floristic composition and environmental conditions, evaluating separately the effect of parameter calibration and of climate forcing. We asked the following questions:

(1) How well does a locally calibrated forest IBM perform when transferred at another site? We expect a degradation of model performance with no fine-tuning at the contrasting site.

(2) What key parameters determine model performance during model transfer? We expect that, since most fundamental processes are captured by generic formulations in the model, only few parameters will be identified as in need of recalibration: these parameters point to limitations in model representation of the underlying processes.

(3) What are the expected responses to climatic conditions? In the absence of water limitation, as in light-limited rainforests, GPP should increase with temperature and irradiance, while biomass should depend less on temperature.

1.3 Materials and methods

1.3.1 Model description

The TROLL model is a spatially explicit individual-based model in which the aboveground space of a forest stand is divided into 3D cells of size 1 m^3 (hereafter called voxels; Chave, 1999; Maréchaux and Chave, 2017). Solar irradiance (photosynthetic photon flux density, PPFD) is computed inside each voxel as the irradiance fraction transmitted immediately above the focal voxel. We considered only vertical light transmittance in the canopy; for trees at the edge of the simulated plot, we simulate light interception only for the part of the crown that is inside the plot, and then scale total assimilation with crown radius. At most, one tree can establish in each 1 × 1 m pixel at any given time, and only self-standing stems ≥ 1 cm in trunk diameter at breast height (DBH) are explicitly modelled (herbaceous plants and lianas are not included). The effects of topography and water balance are not modeled. Seeds and seedlings < 1 cm DBH are indirectly modeled as part of a regeneration compartment, with inputs from an external seed rain and seed production within the simulated stand. Each modelled tree is a 3D object, characterized by DBH, height, crown radius, crown depth, total

leaf surface area, and age. Trees are assigned species-specific trait values, which influence processes such as photosynthesis, growth and mortality.

At each monthly timestep, the model simulates carbon assimilation (photosynthesis), respiration, carbon allocation and growth for each tree, and also simulates seed dispersal or tree death when conditions are met. Tree growth is the result of an explicit balance between carbon assimilation (photosynthesis) and respiration. Carbon assimilation is represented with the C3 photosynthesis model (Farquhar et al., 1980), which depends on temperature, irradiance, vapor pressure deficit (VPD), and atmospheric CO_2 concentration. During a monthly timestep, photosynthesis is calculated over half-hourly periods of a representative day (monthly mean values of temperature, irradiance and VPD); atmospheric CO_2 concentration is assumed constant. Stomatal conductance is modelled following Medlyn et al. (2011). We define the parameter φ (quantum carbon yield per quantum photon) as the initial slope of the photosynthetic carbon assimilation against irradiance curve; this parameter controls carbon uptake in light-limited conditions (Farquhar et al., 1980). The value of φ depends on environment and species, and it has been shown to be an important source of uncertainty in vegetation models (Domingues et al., 2014; Mercado et al., 2009).

After the gross assimilated carbon is calculated from the photosynthesis model, net assimilated carbon is calculated as the gross assimilated carbon minus respiration. Net assimilated carbon is then allocated into biomass in different organs based on parameters of fixed fractions, resulting in tree growth and leaf flush dynamics in the same timestep. The resulting changes in tree height, crown shape and position, and leaf density will then influence the calculation of the light environment and photosynthesis of each tree in the next timestep.

The allometric relationship relating tree height and DBH is assumed to be species-specific, while allometric functions relating DBH and crown size are assumed the same for all trees. Crown radius grows as a function of DBH, following a non-linear relationship: $CR = e^{(CR_a + CR_b \times \ln DBH)}$ where CR_a and CR_b are general parameters provided in input. Hence higher CR_a indicates larger crowns for trees of all sizes, whereas higher CR_b indicates that larger trees have disproportionately larger crowns than smaller trees. Identical values of CR_a and CR_b are prescribed for all species given the paucity of available data, even if it is acknowledged that crown size allometry can vary within species, across species and across sites (Jucker et al., 2017; Loubota Panzou et al., 2021).

In TROLL, tree mortality results from several processes: (i) stochastic mortality, modelled as function of a maximal background mortality rate m and a linearly decreasing relationship with species-specific wood density (WD), so that: $m_{eff} = m - \alpha \times WD$ (being positive, m is the maximal possible value of the mortality rate); (ii) carbon starvation if

net assimilated carbon is negative over a consecutive period exceeding leaf lifespan, so that old leaves have all died while no new leaves could be produced (assuming no internal carbon storage); and (iii) stochastic treefall events, assumed to depend on a tree height threshold, where the parameter *vC* represents the variability of this threshold. Both *m* and *vC* hence summarize complex processes that are not modeled mechanistically.

A schematic diagram, which illustrates the structures and processes controlling the individual- and community-level dynamics of a forest in the TROLL model, can be found in Maréchaux and Chave (2017) (Appendix S5, Figure S1). Necessary inputs for a run of TROLL include (i) climate forcing data for the simulated location, (ii) species-specific parameters of plant traits for the simulated forest, and (iii) species-independent parameters. The source code of TROLL (v2.5) is written in C++ and is available at https://github.com/troll-code/troll. On a computing cluster, each simulation of 200 × 200 m and 500 years uses around 15 min of CPU time.

1.3.2 Global climate forcing

The TROLL model requires the following climate forcing variables: monthly mean values of daytime and nighttime mean temperature, cumulated rainfall, mean wind speed, and daytime mean irradiance, daytime mean vapor pressure deficit (VPD), and average normalized daily variation of temperature, irradiance and VPD.

We used the CRU-NCEP reanalysis as a standardized climate forcing (version 8; version 7 archived at https://rda.ucar.edu/datasets/ds314.3/) (Viovy, 2018). The CRU-NCEP data set is a global gridded (0.5° × 0.5°) sub-daily (6-hourly) climate product spanning the 1901-2016 period. It provides seven climatic variables: temperature, precipitation, wind, downward longwave and shortwave radiations, air specific humidity, and atmospheric pressure, resulting from the combination of observation-based CRU TS 3.2 data (Harris et al., 2014) and model-based NCEP-NCAR data (Kalnay et al., 1996). We constructed reference monthly mean conditions based on the time range 1980-2016, a period for which the most observations are available, in order to ensure higher accuracy (Kistler et al., 2001), and calculated and extracted climatic variables necessary for TROLL input (Appendix A).

1.3.3 Study site and species parameterization

We parameterized the TROLL model for Nouragues, French Guiana, South America, and Fushan, Taiwan, Southeast Asia. Aside from the difference in climatic patterns, there is no floristic overlap between Nouragues and Fushan, and tree trait distribution at the two sites

differ widely: for example, there is no overlap in the interquartile range of leaf mass per area (LMA; $g.m^{-2}$) values (41.62 - 73.86 at Fushan, and 82.71 - 111.45 at Nouragues) and of wood density ($g.cm^{-3}$) values (0.464 - 0.524 at Fushan, and 0.600 - 0.727 at Nouragues).

The Nouragues Ecological Research Station includes a 12-hectare (400 m × 300 m) plot in a moist lowland tropical forest, part of the Amazonian biome. The Nouragues site experiences two months of dry season per year, with mean annual precipitation around 3000 mm, mean annual temperature around 26°C, and a mean relative humidity around 99% (Bongers et al., 2001). Since plot establishment in 1994, censuses were completed regularly (2001, 2007, 2012, 2017). All self-standing stems DBH ≥ 10 cm were identified, measured, tagged and mapped. The plot has 622 tree species (Chave et al., 2008; Maréchaux and Chave, 2017).

The Fushan Forest Dynamics Plot (FDP) is a 25-hectare (500 m × 500 m) plot in a moist broadleaf subtropical forest in the northeast of Taiwan (Su et al., 2007), and is a part of ForestGEO (Forest Global Earth Observatory; Anderson-Teixeira et al., 2015; Condit, 1998). The Fushan site is under influence of northeasterly monsoon in winter, and frequent typhoon visits in summer and autumn, with mean annual precipitation around 4200 mm, mean annual temperature around 18°C, and a mean relative humidity around 95%. Plot elevation ranges from 600 m to 733 m (Su et al., 2007). Since plot establishment in 2004, censuses were completed every five years, where all self-standing stems with a DBH ≥ 1 cm were identified, measured, tagged and mapped, with a total of 110 recorded tree species in the plot (Su et al., 2007).

Species-specific parameters of TROLL include leaf mass per area (LMA; $g \cdot m^{-2}$), nitrogen and phosphorus content per mass (N_{mass}, P_{mass} $g \cdot g^{-1}$), wood density ($g \cdot cm^{-3}$), maximum DBH (cm), DBH-height allometric parameters, and regional relative abundance. We implemented all 622 species in the model for the Nouragues site: a complete set of measured trait values were available for 163 species, and for the other species, a combination of species-specific values and genus means or abundance-weighted community means were assigned (Maréchaux and Chave, 2017). For the Fushan site, we implemented 94 species for which a complete set of measured trait values were available: this represents ca. 90% of the trees. The methodology of data collection is detailed in Appendix B.

Climatic data were extracted from the CRU-NCEP dataset at both sites. We also used local climate data, in order to force the model simulations. At Nouragues, semi-hourly meteorological data are available from 2013 to 2019, recorded 400 m away from the plot (4° 05' N, 52° 41' W). At Fushan, daily meteorological data are available from 1991 to 2012, with hourly data from 2013 to 2016, recorded at a meteorological station 3 km east of the forest

plot (24° 45′ N, 121° 35′ E). A comparison of the local versus gridded climatic conditions is provided in Appendix C.

For all simulations, we simulated forest regeneration from bare soil for a reference plot area of 4 hectares (200 m × 200 m) for a duration of 500 years (6000 monthly timesteps): based on trial simulation, after 500 years, the forest has reached a steady state.

1.3.4 Global parameter calibration

In addition to species-specific parameters, TROLL includes a set of 41 species-independent parameters (or 'global' parameters). The majority of these parameters can be measured empirically: initialization (plot size, initial size and leaf densities of trees etc.) and trait variability (intraspecific variation and covariance). Other parameters could vary across sites and they are the primary target of this study.

We first performed a preliminary sensitivity analysis on five parameters tested in a previous study (Maréchaux and Chave, 2017), which revealed that the model had a low sensitivity to the light extinction coefficient (*k)*, and to carbon allocation fractions: f_{wood} and f_{canopy}. We also found that stem density was not adequately estimated at Fushan (Appendix D): we hypothesized that asymmetric light competition and tree mortality may be factors shaping stem density. Thus, we focused on the calibration of five parameters (φ, *vC*, CR_a, CR_b, *m*; Table 1) for which it is difficult to obtain precise field estimates. We examined model responses by varying these parameters across a range of values, while using fixed values taken from literature for all other parameters, including *k*, f_{wood} and f_{canopy}.

For φ, *vC* and *m*, we generated uniform prior distributions, bounded within the reported value range. CR_a and CR_b, the slope and intercept of the log-transformed crown radius to DBH relationship are strongly correlated, so we generated correlated standard normal distributions using the Cholesky decomposition assuming a Pearson's r of 0.8, then transformed them to Beta prior distributions (of Beta(2, 2)), bounded within the empirically observed value ranges.

We performed 500 calibration runs for both study sites. For each simulation, three parameters (φ, *vC* and *m*) were randomly drawn from the uniform prior distribution, and the two crown allometry parameters (CR_a and CR_b) were drawn as a pair from the correlated Beta prior distributions. Goodness of fit was assessed using four summary metrics: stem density (DBH ≥ 10 cm; N_{10}, trees·ha^{-1}), large stem density (DBH ≥ 30 cm; N_{30}, trees·ha^{-1}), aboveground biomass (AGB, Mg·ha^{-1}), and gross primary productivity (GPP, MgC·ha^{-1}·yr^{-1}). These metrics summarize both forest structure and functioning and overall constrain the

model well. Empirical values for these metrics were obtained from census data for N_{10}, N_{30} and AGB, and from a global gridded database for GPP (Madani and Parazoo, 2020).

For each summary metric and each simulation, we calculated the steady-state value (defined as the mean over the last 100 years of simulation), and qualitatively described trends of model outcome and model sensitivity to each parameter using scatter plots of parameters against output metrics (Appendix E). Model goodness-of-fit was derived from individual summary statistics using an Euclidean distance between the simulated metrics and empirical values (centered and scaled), and we reported median and interquartile range of parameter values of the simulations with the 10% best overall fit (i.e., 50 best simulations out of 500).

We quantified parameter "informativeness", i.e. the degree to which the dispersion of the posterior parameter distribution is reduced compared to the prior distribution, using the ratio between the interquartile range (IQR) of the best-fit simulations to that of all simulations: a smaller ratio indicates higher parameter informativeness. Finally, we reported the temporal trends of the four summary metrics, and discussed their fit with field observation values.

Table 1. Parameters of the TROLL model calibrated at the two tropical forest sites.

	Description	Prior range
φ	quantum carbon yield per quantum photon	0.030-0.110 (Mercado *et al.* 2009)
vC	variability of the tree height-dependent stochastic treefall process	0.0-0.15
CR_a	intercept of the log-transformed CR-DBH allometry	1.5-2.8 (Fischer *et al.* 2020)
CR_b	slope of the log-transformed CR-DBH allometry	0.4-0.8 (Fischer *et al.* 2020)
m	maximal background mortality rate	0.005-0.045

1.3.5 Forest response to climatic conditions: a virtual experiment

To study the dependence of forest structure and dynamics on temperature, irradiance and VPD, we performed the following simulated experiment. In the CRU-NCEP dataset, we selected a subset of points corresponding to lowland light-limited rain forest within the 35°N – 35°S latitude range, based on elevation (< 1000 m), climate (annual precipitation > 2000 $mm \cdot yr^{-1}$; Guan et al., 2015; Wagner et al., 2016), and land cover (ESA 'forest' CCI Land Cover classes: 50, 60, 70, 80, and 90). At both study sites, we then performed 500 simulations, each time using the three climatic variables at a randomly sampled point within the selected subset, and using "optimal parameter values", the general parameter values of the one simulation that provided the best overall fit during calibration with the initial climatic condition (Table 2). The aim of this experiment is to explore the response of a forest stand as its climate forcing changes, with a range and correlation structure between the climatic

variables that are realistic for tropical forests, and to examine if this climate effect is consistent between sites.

To select the reference pixels, we used precipitation data from CRU-NCEP, the C3S Global Land Cover product for 2018 (accessible at https://maps.elie.ucl.ac.be/CCI/viewer/download.php; ESA, 2017), and elevation data from the SRTM product (accessible at http://www.earthenv.org/topography) (Amatulli et al., 2018). We used the *gdal_translate* utility to rescale the Land Cover data (300 m × 300 m) and elevation data (1 km × 1 km) to match the spatial scale of CRU-NCEP (0.5° × 0.5°). This resulted in a set of 3753 "reference climate" pixels, of which we randomly sampled 500, using the corresponding climatic variables to force simulations for both Fushan and Nouragues.

To evaluate model sensitivity, we used the same four summary metrics (N_{10}, N_{30}, AGB, GPP). For each metric, we calculated the steady-state value of each simulation (mean value of the last 100 simulated years), and described the trends of model outcome and model sensitivity to each variable using scatter plots of climatic variables against output metrics. In order to quantify the degree of influence of each climatic variable, we fitted linear models with climatic variables as independent terms and the summary metrics as dependent terms, and reported semi-partial coefficients as effect size. Assumptions for linear models were tested and confirmed; two sample points with temperature lower than 15°C were identified as high-leverage points, but their inclusion did not significantly deviate the statistical estimates (Appendix F).

Table 2. Optimal parameter values (parameter values of the simulation with best overall fit) at each site. Values in parentheses indicate the interquartile range of 50 best-fit simulations.

Parameter	Fushan	Nouragues
φ	0.071 (0.070 – 0.089)	0.074 (0.073 – 0.082)
vC	0.099 (0.022 – 0.070)	0.031 (0.029 – 0.111)
CR_a	1.93 (1.833 – 2.080)	2.10 (1.990 – 2.163)
CR_b	0.51 (0.510 – 0.610)	0.57 (0.523 – 0.618)
m	0.006 (0.005 – 0.017)	0.023 (0.017 – 0.032)

1.3.6 Data analysis

Data processing, statistical analysis and visualization were performed in R 3.3.0 (R Core Team, 2019). Apart from those already mentioned elsewhere, R packages *ggplot2*, *ggpubr*, *ncdf4*, *raster*, *data.table*, *geosphere*, *sp*, *tidyr*, *extRemes*, and *BIOMASS* were used for this study (Dowle and Srinivasan, 2020; Gilleland and Katz, 2016; Hijmans, 2020, 2019;

Kassambara, 2020; Pierce, 2019; Rejou-Mechain et al., 2017; Venables and Ripley, 2002; Wickham, 2020, 2016).

1.4 Results

Model outcomes were highly sensitive to φ, CR_a and m, and to a lesser extent to CR_b. Higher quantum yield (φ) led to higher large-stem density and AGB and a sharp increase in productivity. Higher overall crown size (larger CR_a values) led to lower stem density and AGB, and a slight increase in productivity; its relationship with large-stem density and AGB was non-linear at Fushan. Higher mortality rates (m) led to reduced large-stem density and AGB (Figure E1 & E2). The parameter values corresponding to the simulation maximizing the goodness of fit were similar between the two sites for φ and CR_b, but differed markedly for vC, CR_a and m (Table 2).

We used the IQR ratio as measure of parameter informativeness: lower IQR ratio signifies higher informativeness. The most informative parameter was found to be CR_a, informative at both sites (0.55 at Fushan and 0.38 at Nouragues). φ was informative at Nouragues (0.38) but less so at Fushan (0.78), and m was informative at Fushan (0.33) but less so at Nouragues (0.75). CR_b and vC were only moderately informative (values > 0.6 at both sites) (Figure 1).

Temporal change of all four summary statistics (N_{10}, N_{30}, AGB and GPP) were qualitatively similar at both sites, showing sigmoidal increase for stem densities (N_{10} and N_{30}). We observed , a gradual increase of AGB and rapid increase and stabilization of GPP at both sites, and an initial overshoot of N_{10} at Nouragues but not at Fushan (Table 3, Figure 2). At Nouragues, all steady-state estimated metric values showed a good fit to field values; at Fushan, N_{10} was underestimated (ca. 14%), GPP was overestimated (ca. 9%,), and N_{30} and AGB showed reasonably good fit to field values. Both climate forcings yielded similar model outputs, matching well field observations: N_{10} values were similar, N_{30} and AGB values were slightly lower when using ground-based climate forcing at Fushan, and GPP values were markedly lower when using ground-based climate forcing at both sites (Figure 2).

Median climate values across sampled pixels were: temperature = 26.25°C, irradiance = 207.6 $W \cdot m^{-2}$, VPD = 0.644 kPa. Temperature, irradiance and VPD all had significant effects on simulated forest structure and functioning, although effect sizes varied. Temperature effect on N_{10} was strongly negative at Fushan but non-significant at Nouragues; it had strong negative effects on N_{30} and AGB but a weak positive effect on GPP at both sites. Irradiance had a positive effect on all four metrics at both sites, and are especially strong for GPP. VPD had weakly negative effects on GPP at both sites; its effects on the other three metrics were weakly positive at Fushan and non-significant at Nouragues. Overall, effect sizes were weaker

at Nouragues than at Fushan (except for irradiance effects on N_{30} and AGB) (Figure 3, Table 4).

Table 3. Percentage difference between summary statistics of the optimal simulation (simulation with the best overall fit) and the mean empirical value. Values in parentheses indicate the interquartile range of percentage differences of the 50 best-fit simulations.

Metrics	Fushan	Nouragues
N_{10}	-14.4% (-18.1% – 0.8%)	-2.5% (-9.0% – 12.4%)
N_{30}	-5.9% (-14.9% – 5.3%)	0.1% (-8.4% – 4.2%)
AGB	-3.1% (-17.4% – 3.3%)	2.9% (-9.4% – 1.0%)
GPP	8.6% (5.6% – 28.5%)	-2.9% (-6.3% – 5.6%)

Table 4. Effect size of each climatic variable on the output metrics at both sites, expressed in semi-partial correlation coefficients. Effect sizes with absolute values larger than 0.3 are indicated in bold. Italic indicates non-significant effects ($p > 0.05$).

	Fushan				Nouragues			
	N_{10}	N_{30}	AGB	GPP	N_{10}	N_{30}	AGB	GPP
Temperature	**-0.341**	**-0.553**	**-0.489**	0.135	*-0.049*	**-0.385**	**-0.413**	0.032
Irradiance	0.251	0.296	**0.329**	**0.953**	0.142	**0.436**	**0.476**	**0.947**
VPD	0.228	0.230	0.183	-0.226	*0.061*	*0.039*	*0.027*	-0.202

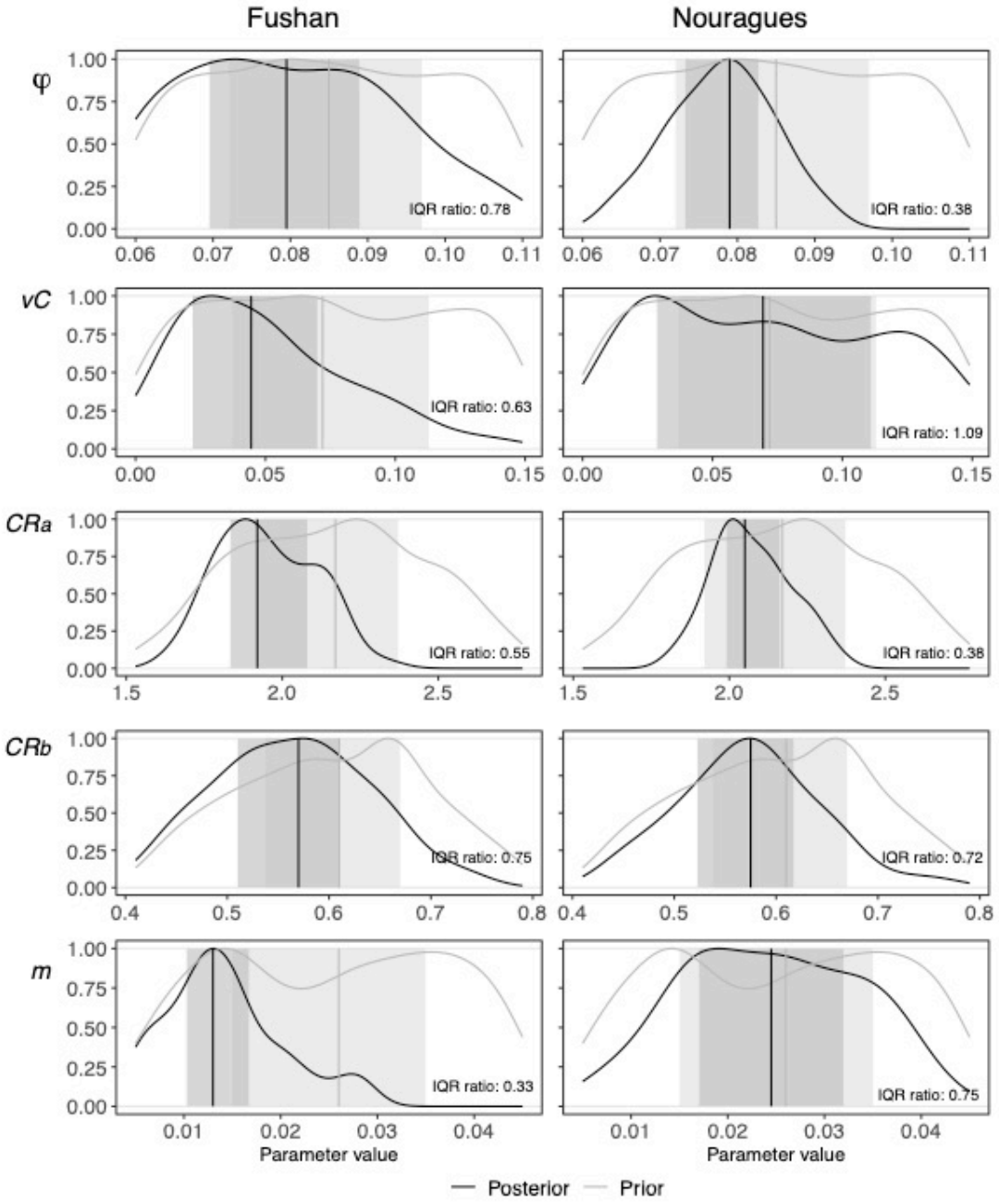

Figure 1. Prior (gray) and posterior (black) distributions for five parameters: φ (quantum yield), *vC* (treefall parameter), CR_a and CR_b (intercept and slope terms of the crown radius allometry), and *m* (background mortality). Results are reported for the Fushan site (Taiwan), and for the Nouragues site (French Guiana). Curves represent density functions, and vertical lines represent median value of the distributions. Shaded areas indicate interquartile range (IQR) of prior (light gray) and posterior (dark gray) distributions. IQR ratio is calculated as the posterior divided by prior IQR: lower IQR ratio is thus indicative of a higher parameter informativeness.

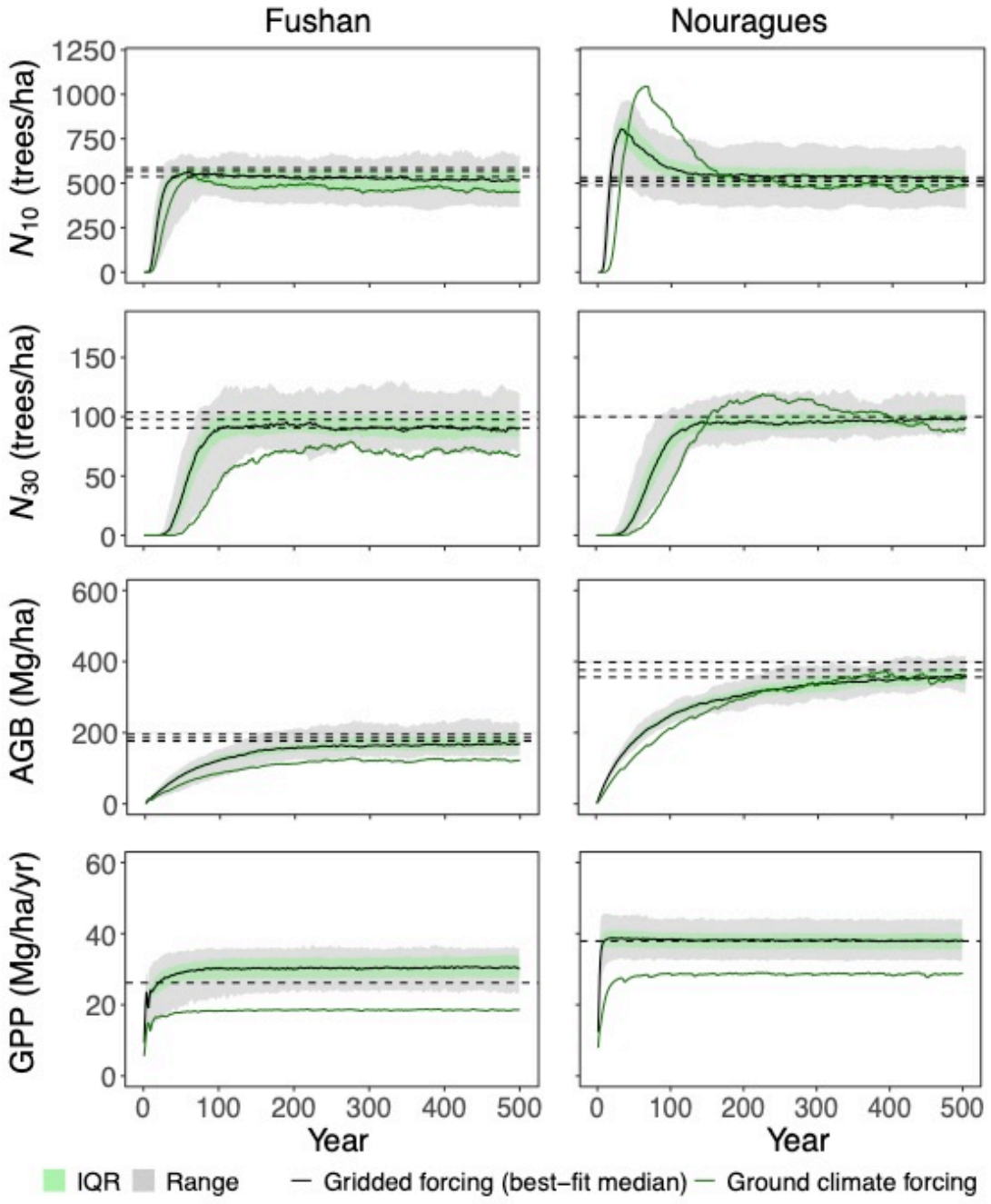

Figure 2. Successional dynamics of best-fit simulations at the Fushan and Nouragues sites, for four variables. Green shades represent the interquartile range, and gray shades represent the entire range of variation. Solid lines: median value of the best-fit simulations (black: gridded climate forcing; dark green: ground climate forcing); dashed lines: empirical values.

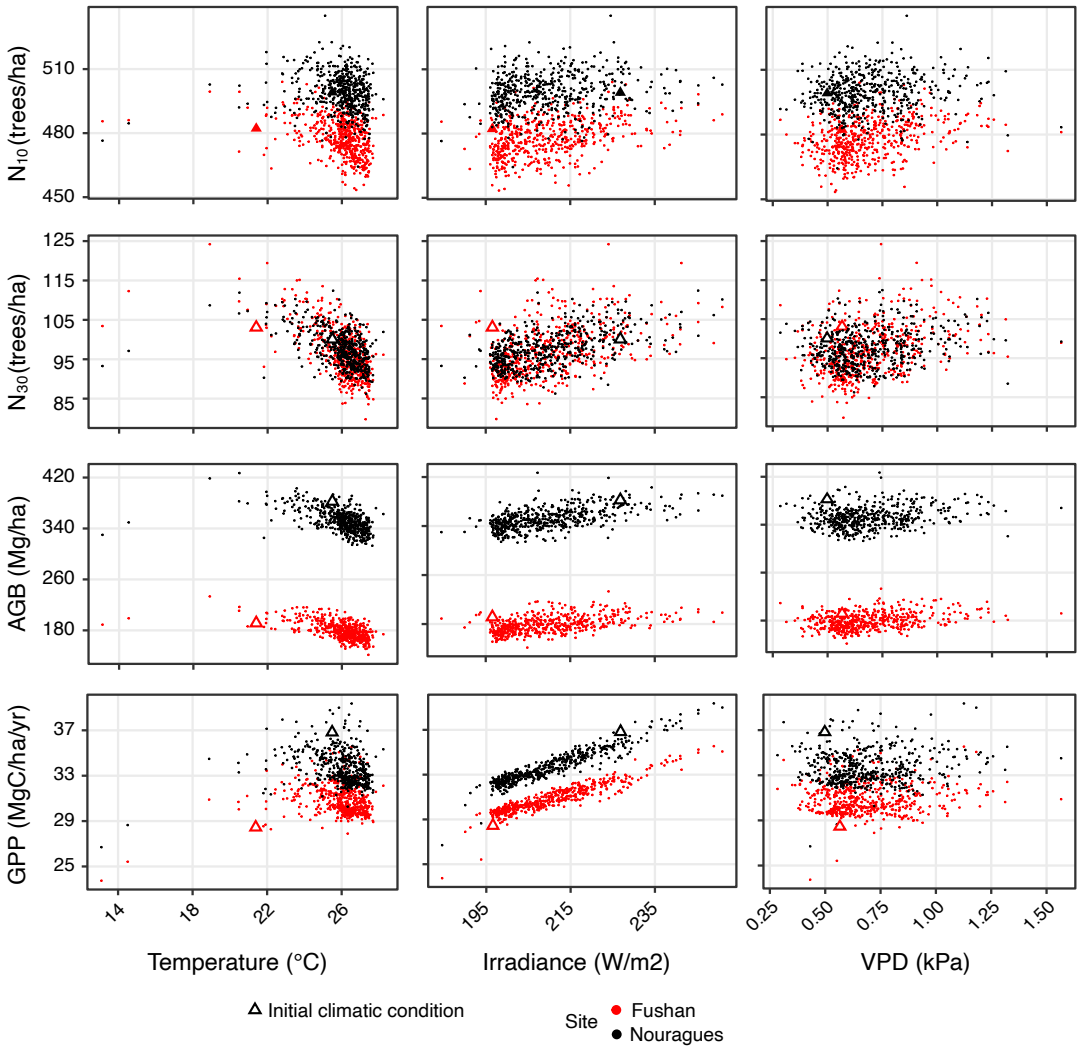

Figure 3. Effect of climatic conditions on forest structure and functioning at both sites (red: Fushan; black: Nouragues). Triangles indicate the simulations done under climatic condition of the original site.

1.5 Discussion

In this study, we tested the transferability of a forest IBM, and demonstrated that the model predicts forest structure and functioning with reasonable accuracy at two species-rich forest sites in different bioregions. Parameters controlling photosynthetic efficiency, crown allometry and background mortality were found to be key for model calibration. We showed that calibration could help identify influential processes in trait-based forest IBMs and suggests that there is potential of IBM upscaling with improved representation of influential processes and parameter estimation.

1.5.1 Transferability of an individual-based model

The TROLL model was designed to incorporate a detailed representation of forest diversity while remaining relatively easy to parameterize at a forest site, by prescribing each species using a set of commonly measured traits (Maréchaux and Chave, 2017). This approach alleviates the calibration burden of model transfer (DeAngelis and Grimm, 2014) and facilitates the implementation of large-scale testing of individual-based models. However, not all parameters used in the model are directly observable or easily measurable in the field: some are integrators of multiple processes not explicitly represented within the model. So the issue of model transferability still stands, and we here ask whether a calibrated parameter set for one site performs well elsewhere.

We estimated model parameters through model inversion, comparing model outputs against field observations (Hartig et al., 2012). This approach has been used for several DGVM parameterizations, usually by calibrating against eddy-covariance data (Ichii et al., 2010; Pappas et al., 2013; Restrepo-Coupe et al., 2017). Here, goodness-of-fit depends on four summary statistics of forest structure (stem density) and functioning (biomass and productivity) that are usually available in field inventory data or global gridded data. In the future, the approach could be improved by using the whole height or diameter distribution of the simulated forest, or by adopting a likelihood-based approach (Hartig et al., 2014, 2012).

We calibrated the model at two contrasted tropical forest sites. In spite of their marked differences in climatic conditions, species composition and functional diversity, the simulated forests matched field observations by calibrating a limited subset of parameters. This supports the view that forest models with trait-based parameterization are capable of capturing site-specific characteristics that underpin community dynamics and structure at a given forest site. We speculate that the use of trait-based species parameterization contributes to the reduced need for refitting (i.e., higher model genericity) (Christoffersen et al., 2016; Fisher et al., 2018; Fyllas et al., 2014; Pappas et al., 2016). Parameters that do differ across sites point to potential improvements in the model, a discussion we now turn to.

1.5.2 Parameter calibration

We performed calibrations for three parameters that influence predicted forest structure and functioning: photosynthetic efficiency (φ), crown allometry (CR_a), and tree mortality (m). As φ represents the actual quantum yield of photosynthesis (the amount of fixed carbon per light flux absorbed by the chloroplasts), higher φ value results in higher carbon assimilation (when light is limiting) and higher GPP. This parameter only leads to a moderate increase in large stem density (N_{30}) and AGB, and an even smaller effect on overall stem density (N_{10}),

indicating that forest demography and biomass accumulation are not solely conditioned by productivity, but also hinge on respiration, carbon allocation, and carbon residence time (Álvarez-Dávila et al., 2017; Johnson et al., 2016; Malhi et al., 2015).

Model calibration was not sensitive to TROLL's species-independent carbon allocation parameters (Appendix D), but it should be pointed out that carbon allocation does vary across and even within species (Malhi et al., 2015; Negrón-Juárez et al., 2015). Therefore, including a more mechanistic or trait-mediated representation of carbon allocation may unveil more heterogeneity in forest dynamics, and is an important objective in future model development (Merganičová et al., 2019; Negrón-Juárez et al., 2015; Schippers et al., 2015; Trugman et al., 2019).

In TROLL, crown allometry directly controls light use efficiency and tree competition. Higher CR_a values mean that trees have wider crowns at a given diameter, and achieve higher carbon assimilation rates due to increased light interception, leading to the observed pattern of increase in GPP with increased CR_a. Wider crowns also create more intense shading for smaller trees in the understory and cause higher tree turnover and mortality, leading to the observed pattern of decreasing stem density and AGB. Stand structure also strongly depends on the level of prescribed inter- and intraspecific variability of crown allometry, which determine how complementarity in crown architecture could increase light use efficiency and promote coexistence (Pretzsch, 2019; Vieilledent et al., 2010).

Mortality is an important calibration parameter in TROLL. Tree mortality is a complex process, and in current IBMs, it is often modeled empirically, and thus remains one of the main sources of model uncertainty (Bugmann et al., 2019). In the FORMIND model, the mortality rate is empirically correlated with environmental variables such as precipitation and soil property, which vary across space (Rödig et al., 2018, 2017). Such simplifications limit our ability to explore how different causes of tree mortality impact forest structure (McDowell et al., 2018).

Natural disturbance events such as fire, drought or wind are responsible for a significant proportion of tree mortality (Fischer et al., 2018; McDowell et al., 2018; Peterson et al., 2019), and they impact forest structure and functioning (Ibanez et al., 2019; Magnabosco Marra et al., 2018; Pugh et al., 2019). The two forest sites selected for this study depend on different wind disturbance regimes: notably, Fushan is influenced by frequent tropical cyclones (Dowdy et al., 2012; Lin et al., 2011), while Nouragues is not exposed to cyclones. At Nouragues, TROLL simulates an overshoot of stem density during early succession, indicating self-thinning, but not at Fushan. One hypothesis for this pattern is that cyclones shape a more open canopy at Fushan, resulting in a less intense self-thinning. This may also explain why the optimal value for the mortality rate (m) is lower at Fushan than at Nouragues.

It would be important to devise more mechanistic representations of disturbance events in TROLL.

1.5.3 Upscaling of individual-based models

Various efforts have been made to upscale IBMs to the regional or global scale. Individual-based approaches have been coupled to or developed within DGVMs (Fisher et al., 2018; Sakschewski et al., 2015; Sato et al., 2007) to represent cohort processes. Ma et al. (2017) prescribed environmental data for simulations of the FORCCHIN IBM model at several flux tower sites, and validated the simulated carbon flux against flux tower data. Rödig et al. (2018, 2017a) performed regionalization for the FORMIND model by calibrating the mortality parameter at a number of sites and correlating it with environmental variables (precipitation and soil properties), and performing simulations at sites over the entire Amazon using mortality parameters predicted from the environmental variables. Simulated temporal dynamics of canopy height were then compared with remote sensing data to determine the succession status of each site, which was then used to generate Amazon-wide estimation of other forest attributes such as biomass and productivity.

Yet, these studies assigned trees to a small number of plant functional types that relied on empirical parameterization. Our study, although smaller in scope, is a proof of concept demonstrating that trait-based IBM upscaling is achievable with minimal calibration and is therefore realistic in the tropics, provided that trait measurements exist and tree floristic composition is available at the focal site. Moreover, since model output contains detailed information about forest composition, TROLL could also help answer how plant diversity responds to environmental changes.

With every forest model, assumptions are made about which parameters are species-dependent and which are not. The model described here, TROLL, is designed with the aim to contain as much species-specific information that is currently available. For an individual-based model, this choice does not necessarily incur higher computational burden than the plant functional type approach, since in both cases every individual tree is simulated. However, supplying models with species-specific information requires considerably more parameterization effort. With the ongoing collection effort of plant traits in permanent plots around the world, the assembly of global trait databases (Anderson-Teixeira et al., 2015; Chave et al., 2009; Kattge et al., 2020) and development of techniques to measure new plant traits, we expect that it will be easier to generalize this approach to many sites. Here we show that of the species-independent parameters, only a few require site-specific calibration for realistic model output to be achieved, and identifying these parameters helps identifying

priorities for future theoretical and modeling development, as well as for field measurements (Medlyn et al., 2016).

1.5.4 Climate impact on forests using IBMs

Another important part of assessing transferability of forest IBMs consists in evaluating how the model responds to environmental forcing, an important step in understanding how forests respond to climate change (Shugart et al., 2018). We here examined the effect of climate forcing without the need of re-calibration (Fauset et al., 2019; Shugart et al., 2018). Many forest IBMs prescribe climatic conditions based on locally measured data (Ma et al., 2017; Shuman et al., 2015), yet it is important to provide a consistent climate forcing condition even at places where local measurements do not exist, and to ensure comparability among sites. The integration of the gridded CRU-NCEP climate dataset as model input fulfills this condition, and thus further simplifies large-scale implementation.

TROLL simulations at the Fushan and Nouragues sites with different climatic conditions demonstrate that the model reproduces a general pattern of climatic response that remain nearly identical upon model transfer, with only quantitative differences between sites. The simulated positive relationship of GPP with temperature and irradiance and the negative relationship with VPD are in agreement with expectations (Malhi et al., 2015; Reyer, 2015).Under the current model version, VPD constrains leaf stomatal conductance in the photosynthesis process, and we found a weak effect of VPD. As water availability is one of the key climatic factors that shape forest dynamics and functioning (Álvarez-Dávila et al., 2017; Feng et al., 2018; Galbraith et al., 2010; Poorter et al., 2017), further investigation of forest response to drought and soil water stress is necessary, and will be the focus of future model development.

At both sites, we observed a decoupling between the response of productivity and that of stem density and AGB. With increasing temperature, GPP increased while large tree density and AGB decreased. These observations are consistent with empirical studies that showed that productivity is a poor predictor of biomass in old-growth tropical forests (Johnson et al., 2016; Malhi et al., 2015). Biomass accumulation is controlled by numerous processes other than carbon assimilation, including mortality, functional composition, and size structure (Allen et al., 2010; Bugmann et al., 2019; Johnson et al., 2016).

The Fushan site responded more to variation in climatic conditions than Nouragues. One interpretation of this finding is that the native bioclimatic conditions of Nouragues were closer to the average condition of reference climatic conditions, whereas Fushan has a fringe

climatic condition (subtropical). Consequently, constraining the Fushan forest to average tropical forest climatic conditions had more effect than on the Nouragues forest.

1.5.5 Conclusion and perspectives

We have demonstrated that a detailed exploration of the calibration and transferability of trait-based forest IBMs offers an opportunity to assess the genericity of model assumptions. Even though our results are based on model simulations, they do pave the way towards a much more systematic exploration of model behavior across a wide range of sites that are representative of a variety of forest types.

We here identify two main priorities for future individual-based model development: 1) including more detailed and mechanistic representation of important physiological processes, such as disturbance-driven tree mortality (Seidl et al., 2014, 2011a; Uriarte et al., 2009), and 2) improving constraints of key parameters with detailed and spatially distributed data, such as informing crown allometry with remote sensing data (Calders et al., 2018; Fischer et al., 2020; Shugart et al., 2015). With the help of improvements in these two directions, we argue that upscaling of individual-based vegetation models with detailed, trait-based species description need not be associated with high calibration burden, and that they have great potential for large-scale implementation.

1.6 Acknowledgements and author contributions

Simulations were run on the OLYMPE cluster at CALMIP, Toulouse. We thank Dr. Shiang-Yue Lu and Hui-Hsueh Huang at TFRI (Taiwan Forestry Research Institute), Taiwan for providing us with the local climate data at the meteorological station. This work was supported by the “Investissement d’Avenir” grants managed by the Agence Nationale de la Recherche (CEBA, ref. ANR-10-LABX-25-01; TULIP, ref. ANR-10-LABX-0041; ANAEE-France: ANR-11-INBS-0001).

EPR and JC designed the research; EPR conducted the research; FF, IM and JC provided assistance in modeling and statistical analyses; EJ and IFS provided data used for analyses; all authors proofread and edited the paper.

1.7 Supplementary data

Appendix A: generation of monthly mean climatic variables for TROLL input

Automated global reanalysis climate data calculation and extraction

The CRU-NCEP data are stored in NetCDF format, and the following variables are available: *Tair* for air temperature (K), *rain* for precipitation (mm), *WindN* and *WindE* for each of the two horizontal directional components of wind speed ($m \cdot s^{-1}$), SW*down* for incoming short-wave radiation exposure ($J \cdot m^{-2}$), *Qair* for air specific humidity, and *PSurf* for surface atmospheric pressure (Pa). We retrieved data for the period from 1980 to 2016, a period when many direct observations complemented model-based inferences in CRU-NCEP.

We processed the CRU-NCEP data across the entire land surface on Earth using the Climate Data Operators (cdo) tool (Schulzweida, 2019) and stored the results in NetCDF files, with a total of 74 files (2 files for each year). For each year, one file contains the monthly mean values of the following climatic variables: mean, maximum and minimum daily temperature (°C), mean and maximum daily irradiance ($W \cdot m^{-2}$), mean and maximum daily VPD (vapor pressure deficit, kPa), as well as monthly total precipitation (mm); another file contains the 6-hourly average wind speed ($m \cdot s^{-1}$), calculated as the quadratic average of the two wind speed components. Irradiance was calculated as the short-wave radiant exposure, divided by the time length of each measurement interval (6 hours, i.e. 6 × 3600 = 21600 seconds). VPD was calculated from temperature (T, °C), air specific humidity (R, unitless), and surface atmospheric pressure (P, kPa) with the following equations (Buck, 1981; Monteith and Unsworth, 2008):

$$VP_{sat} = 0.61121 \times e^{(18.678 - \frac{T}{234.5}) \times (\frac{T}{257.14+T})} \quad \text{(A1)}$$

$$VPD = VP_{sat} - \frac{R \times P}{0.622 + 0.378 \times R} \quad \text{(A2)}$$

where VP_{sat} is the temperature-dependent saturated vapor pressure.

Subsequently, we used an R script to extract the monthly climatic variables from the files for a geographic coordinate, and generated a text file that is used as an input file for TROLL.

Appendix B: Data at Fushan FDP

At Fushan FDP, local meteorological data, daily from 1991 to 2012 and hourly from 2013 to 2016, was recorded at a meteorological station three kilometers east of Fushan FDP (24° 45′ N, 121° 35′ E). Temperature and humidity were measured by a Rotronic MP101A meteorological probe, precipitations by a tipping bucket rain gauge, irradiance by an E20 Silicon pyranometer (Homeray), and instantaneous wind speed by a Wind Monitor Model 05103 (Young).

In Fushan FDP, the sampling of functional traits was conducted in 2009, where 1 to 26 individuals per species were chosen randomly according to accessibility of tree canopy, and 1 to 3 intact and mature leaves or leaflets exposed to sunlight were collected for each individual. Collected leaves were sealed in Ziploc® bag with wet paper towels and kept in an insulated cooler box in order to prevent from water loss until transport back to the field station. There, the fresh weight of the leaves was measured to a precision of 0.1 mg, and they were scanned with a flatbed scanner within 12 hours. Leaf area (LA, cm^2) was quantified with the software ImageJ (Rasband, n.d.). The leaf samples were subsequently oven-dried at 80 °C for 72 - 96 hours, until constant dry weight. Leaf mass per area (LMA, $g \cdot m^{-2}$) were then calculated as dry weight divided by fresh leaf area (Pérez-Harguindeguy et al., 2013). Nitrogen and phosphorus content (N_{mass} and P_{mass}, $g \cdot g^{-1}$) were determined by the microplate method (Huang et al., 2011; Iida et al., 2014).

Wood density (WD, $g \cdot cm^{-3}$) was measured following the ForestGEO wood density measurement protocol (Condit, 2008; Iida et al., 2014), by taking wood core samples of randomly chosen individuals outside the plot, measuring fresh volume by water displacement method and dry weight after oven-drying at 80 °C. Wood density was calculated as dry weight divided by fresh volume.

The allometric relationship between DBH and tree height (H) in the TROLL model was assumed to follow a Michaelis-Menten function with two parameters, asymptotic height (h_{max}) and the Michaelis constant (a_h), numerically equal to the diameter at which the tree height is half of h_{max}:

$$H = \frac{h_{max} \times DBH}{a_h + DBH} \tag{B1}$$

Although DBH values for all individuals were available, tree heights were only measured for 1 to 18 individuals for each species, depending on the accessibility of tree individuals. Due to the scarcity of available height data, a hierarchical Bayesian model was used to estimate model parameters: the model assumed that the species-specific Michaelis-Menten parameters $h_{max,\,i}$ and $a_{h,\,i}$ for species i are distributed normally around common hyperparameters h_{max} and a_h (Molto et al., 2014). Parameters are close to the hyperparameters

when data points are scarce for a particular species, while the species parameters dominate when data points are numerous for the species. Calculations were carried out with the software STAN and the R package *RStan* (Stan Development Team, 2016a, 2016b).

Appendix C: comparisons of different climate forcing sources.

The comparison between three climatic variables (temperature, precipitation, irradiance) extracted from CRU-NCEP data and ground station data showed that apart from minor differences, the climatic variables were largely congruent between CRU-NCEP and ground measures for the two ground study sites, the main difference being that seasonal variability for irradiance and precipitation was noticeably larger in ground data than in CRU-NCEP data at Fushan (Figure C1-2).

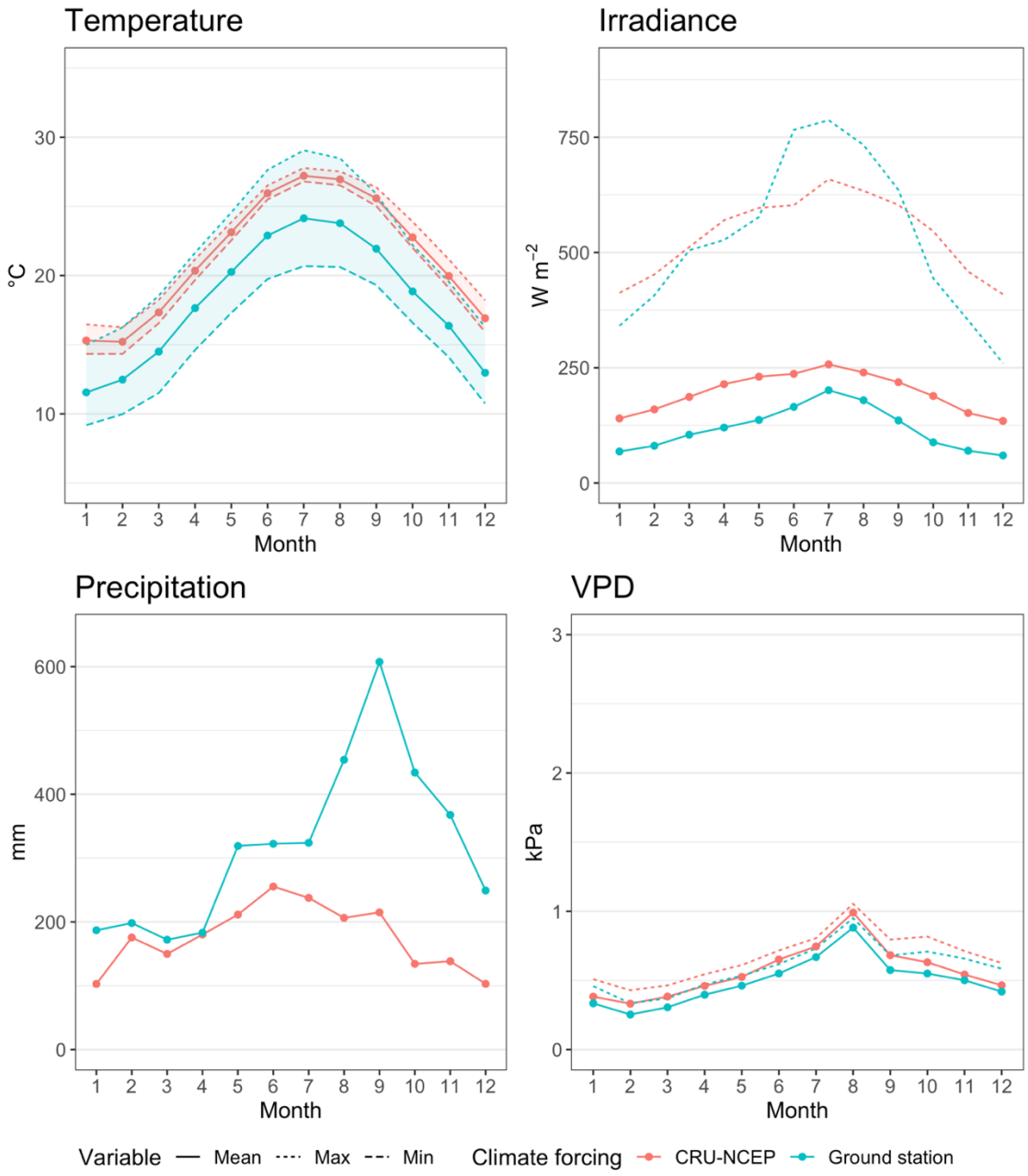

Figure C1. Comparison of climatic variables from CRU-NCEP gridded data or ground-based data at Nouragues.

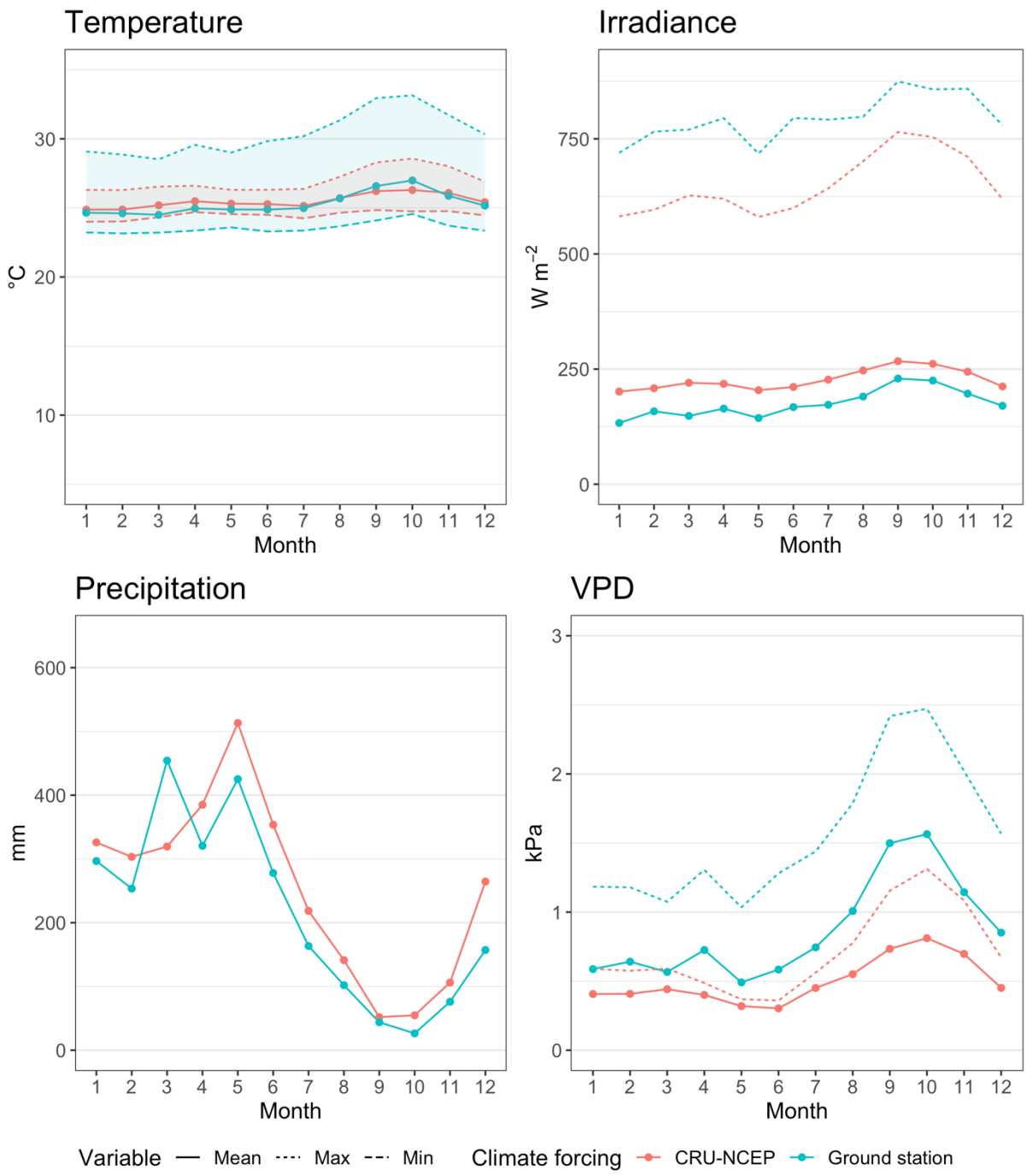

Figure C2. Comparison of climatic variables from CRU-NCEP gridded data or ground-based data at Nouragues.

Appendix D: preliminary parameter calibration

In the preliminary calibration tests, three other parameters were calibrated besides the parameters φ and *m*: *k*, the light extinction coefficient, describes the proportion of light extinction by each canopy layer; f_{wood} represents the fraction of assimilated carbon allocated to aboveground wood (branches and stem), and f_{canopy} represents the fraction allocated to canopy (twigs, leaves, and reproductive organs) (Table D1). We conducted the calibration tests following the same procedure as described in the main text, performing 500 simulations and selecting simulations with the 10% best overall fit (i.e., 50 simulations). The results indicated that model output was weakly sensitive to *k*; model sensitivity to f_{wood} and f_{canopy}, was non-negligible, but the overall model output did not deviate clearly from the observed value range no matter what their calibrated values were (Fig. D1 & D2). As a result, in all subsequent simulations we set a constant value for these three parameters. For *k*, we chose the lower bound value of 0.5 since reported values for forest ecosystems in Zhang *et al.* (2014) are primarily cluster around 0.5. For the allocation parameters, an intermediate value within the reported range was chosen (f_{wood} = 0.35, f_{canopy} = 0.25).

k	light extinction coefficient	0.50-0.95 (Cournac *et al.* 2002, Zhang *et al.* 2014)
φ	quantum carbon yield per quantum photon	0.030-0.110 (Mercado *et al.* 2009)
f_{wood}	fraction of NPP allocated to aboveground wood	0.20-0.45 (Aragão *et al.* 2009, Malhi *et al.* 2011)
f_{canopy}	fraction of NPP allocated to canopy	0.20-0.45 (Aragão *et al.* 2009, Malhi *et al.* 2011)
m	maximal background mortality rate	0.005-0.045

Table D1. Parameters of the TROLL model calibrated at the two tropical forest sites in preliminary tests.

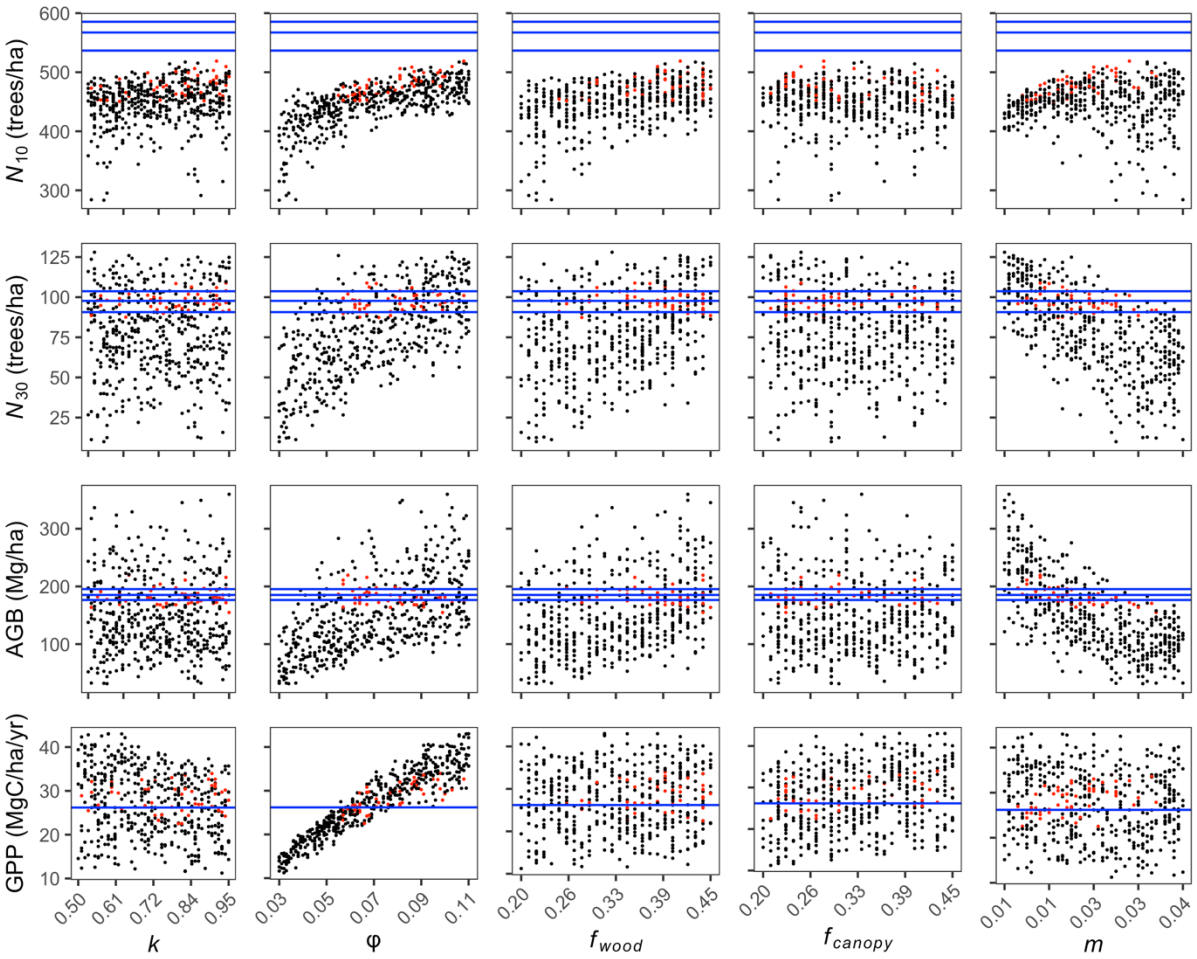

Figure D1. Calibration of TROLL general parameters for Fushan (*k*: light extinction coefficient; φ: quantum yield; f_{wood} and f_{canopy}: carbon allocation to different plant organs; *m*: background mortality). Horizontal blue lines are observed values from field censuses. Each point represents one simulation, and red points are best-fit simulations.

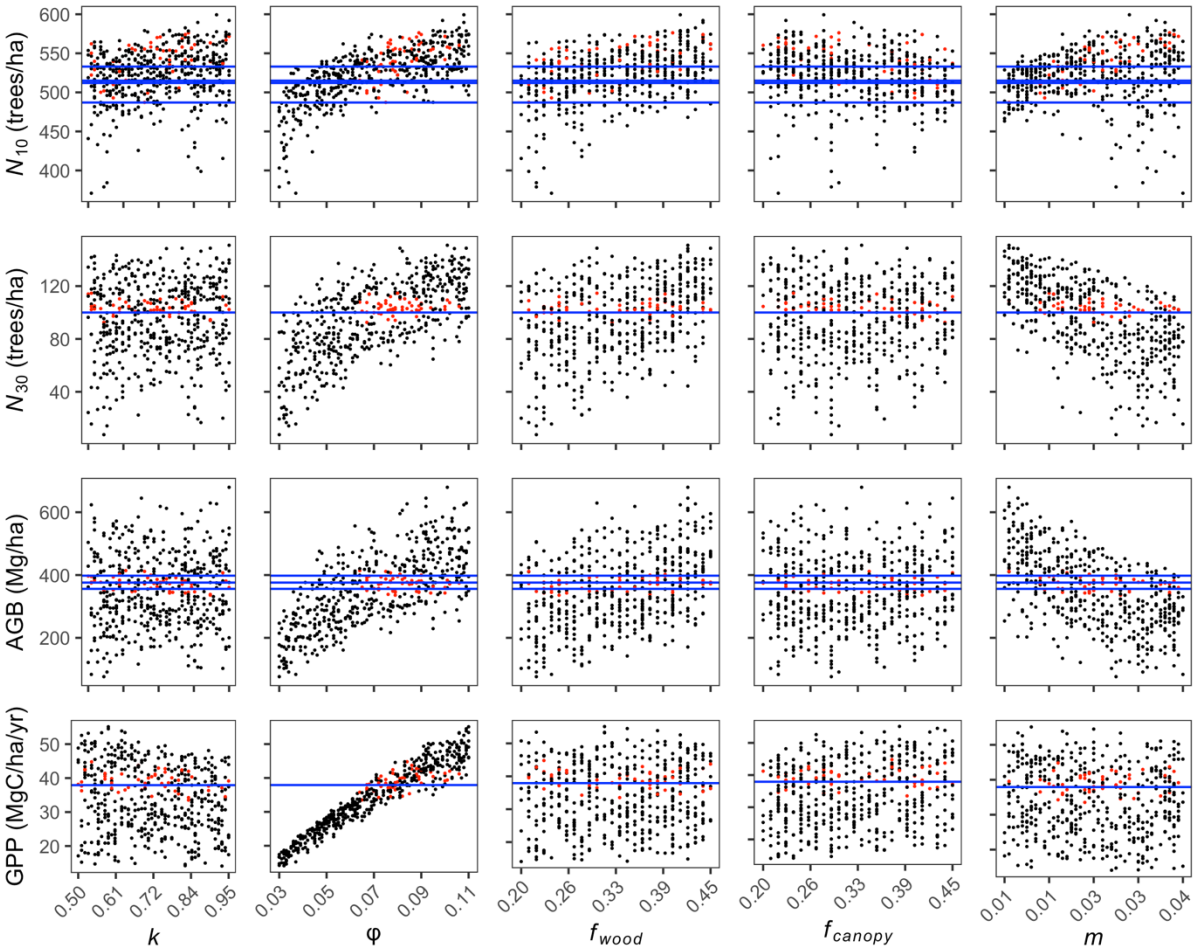

Figure D2. Calibration of TROLL general parameters for Nouragues (*k*: light extinction coefficient; φ: quantum yield; f_{wood} and f_{canopy}: carbon allocation to different plant organs; *m*: background mortality). Horizontal blue lines are observed values from field censuses. Each point represents one simulation, and red points are best-fit simulations.

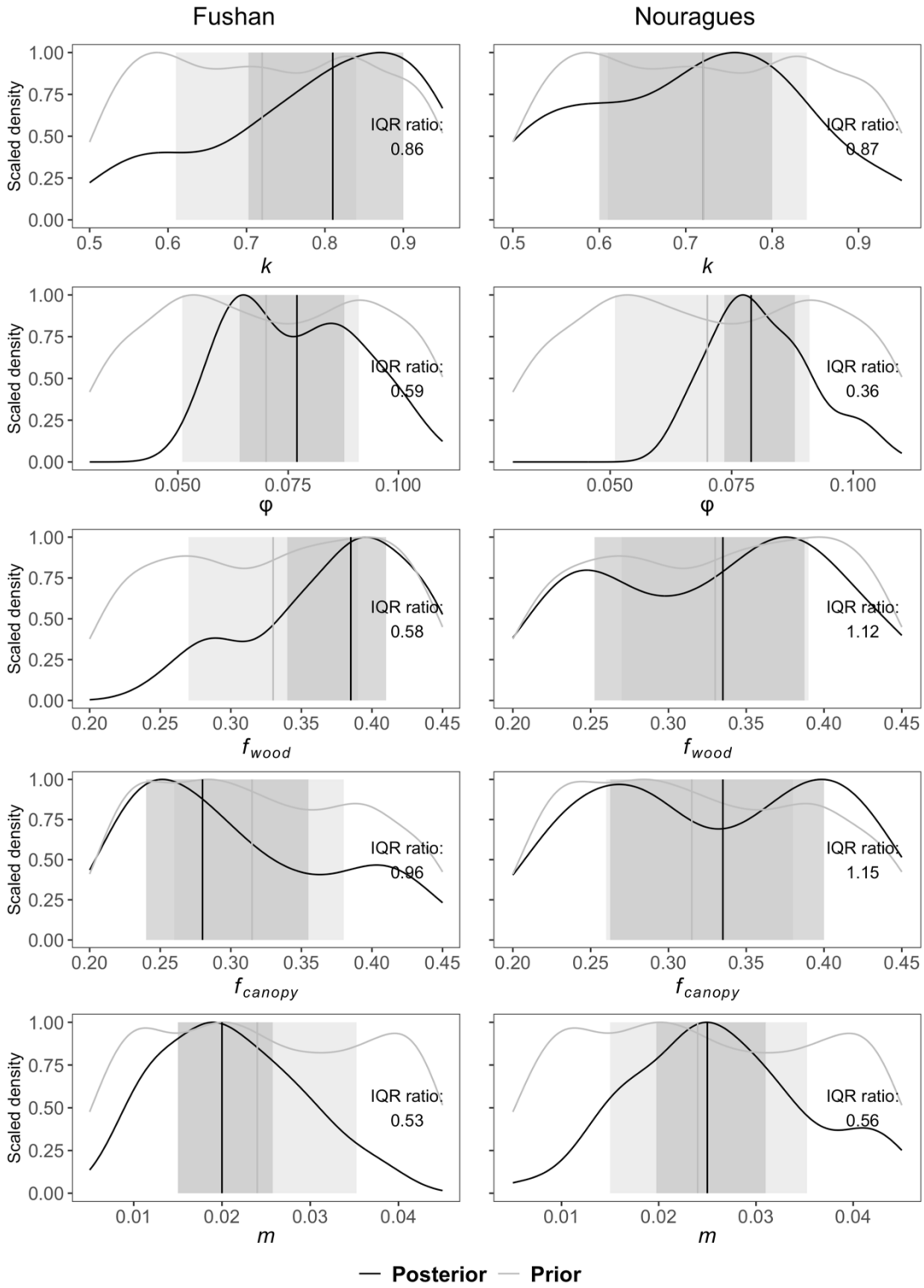

Figure D3. Prior (grey) and posterior (black) density distributions for parameter values (*k*: light extinction coefficient; φ: quantum yield; f_{wood} and f_{canopy}: carbon allocation to different plant organs; *m*: background mortality). Solid vertical lines indicate median and dashed vertical lines indicate interquartile range (IQR). Parameter informativeness is calculated as the ratio between IQR of best-fit simulations and that of all simulations.

Appendix E: parameter calibration

We conducted calibration tests on five parameters: φ (quantum carbon yield per quantum photon), *vC* (variability of the tree height-dependent stochastic treefall process) CR_a, CR_b (intercept and slope terms of the log-transformed CR-DBH allometry), and *m* (maximal background mortality rate), following the procedure as described in the main text, performing 500 simulations and selecting simulations with the 10% best overall fit (i.e., 50 simulations). The results showed that model output was strongly sensitive to φ, CR_a and *m*, and to a lesser exten to CR_b.

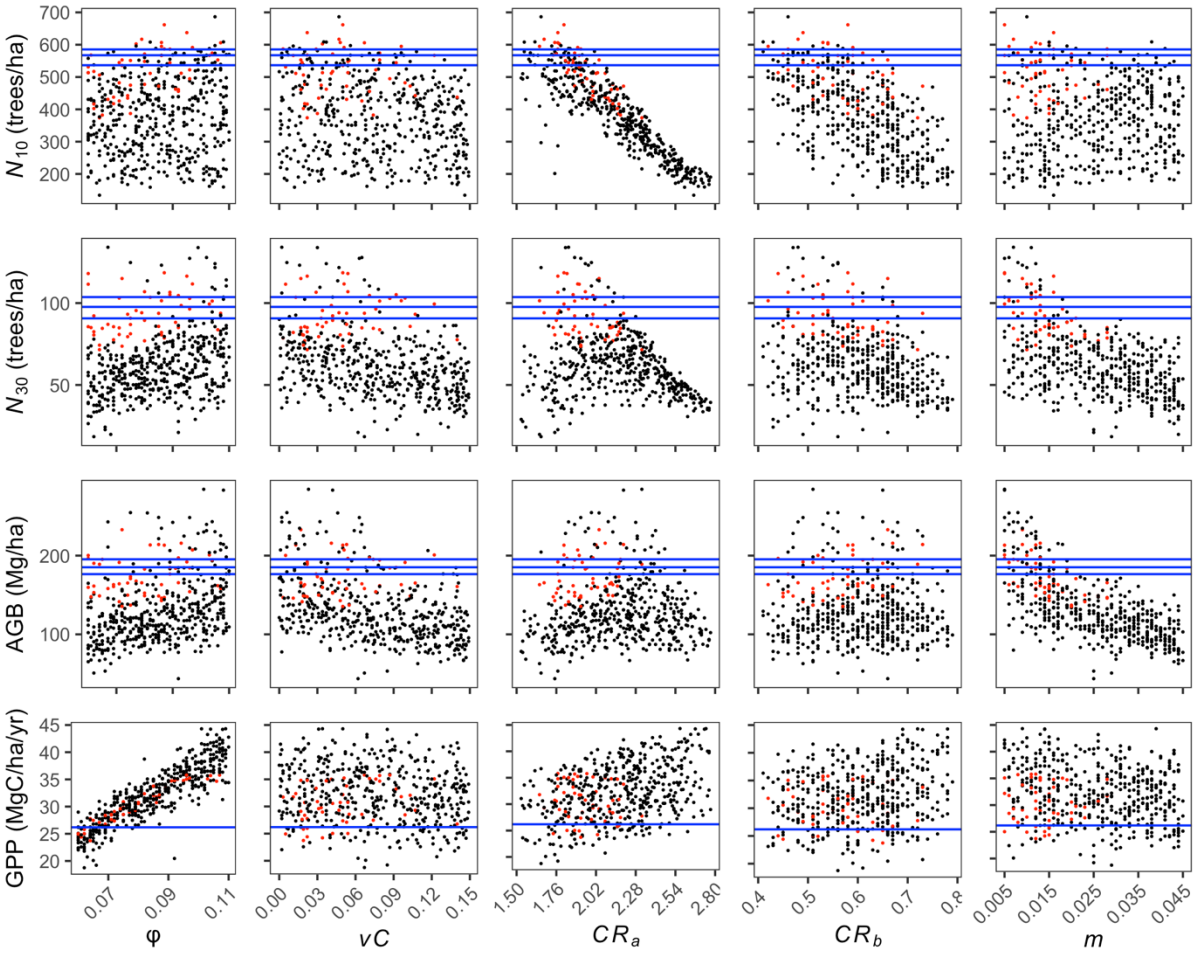

Figure E1. Calibration of TROLL general parameters (φ: quantum yield; *vC*: treefall parameter; CR_a and CR_b: intercept and slope terms of the crown radius allometry; *m*: background mortality) for Fushan. Horizontal blue lines are observed values from field censuses. Each point represents one simulation, and red points are the best-fit simulations (10% best simulations).

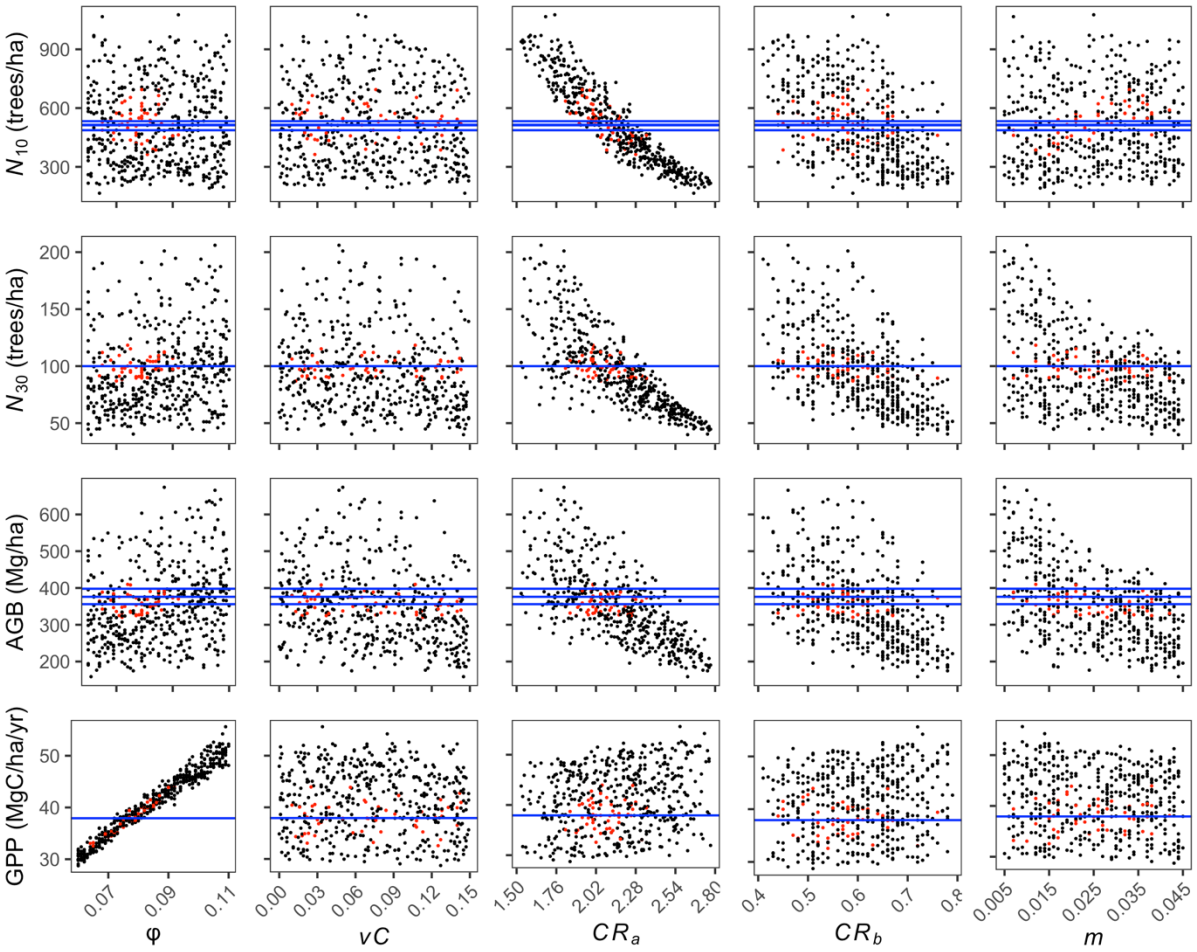

Figure E2. Calibration of TROLL general parameters (φ: quantum yield; *vC*: treefall parameter; CR_a and CR_b: intercept and slope terms of the crown radius allometry; *m*: background mortality) for Nouragues. Horizontal blue lines are observed values from field censuses. Each point represents one simulation, and red points are the best-fit simulations (10% best simulations).

Appendix F: verification of assumptions for linear model for the sampled climate experiment

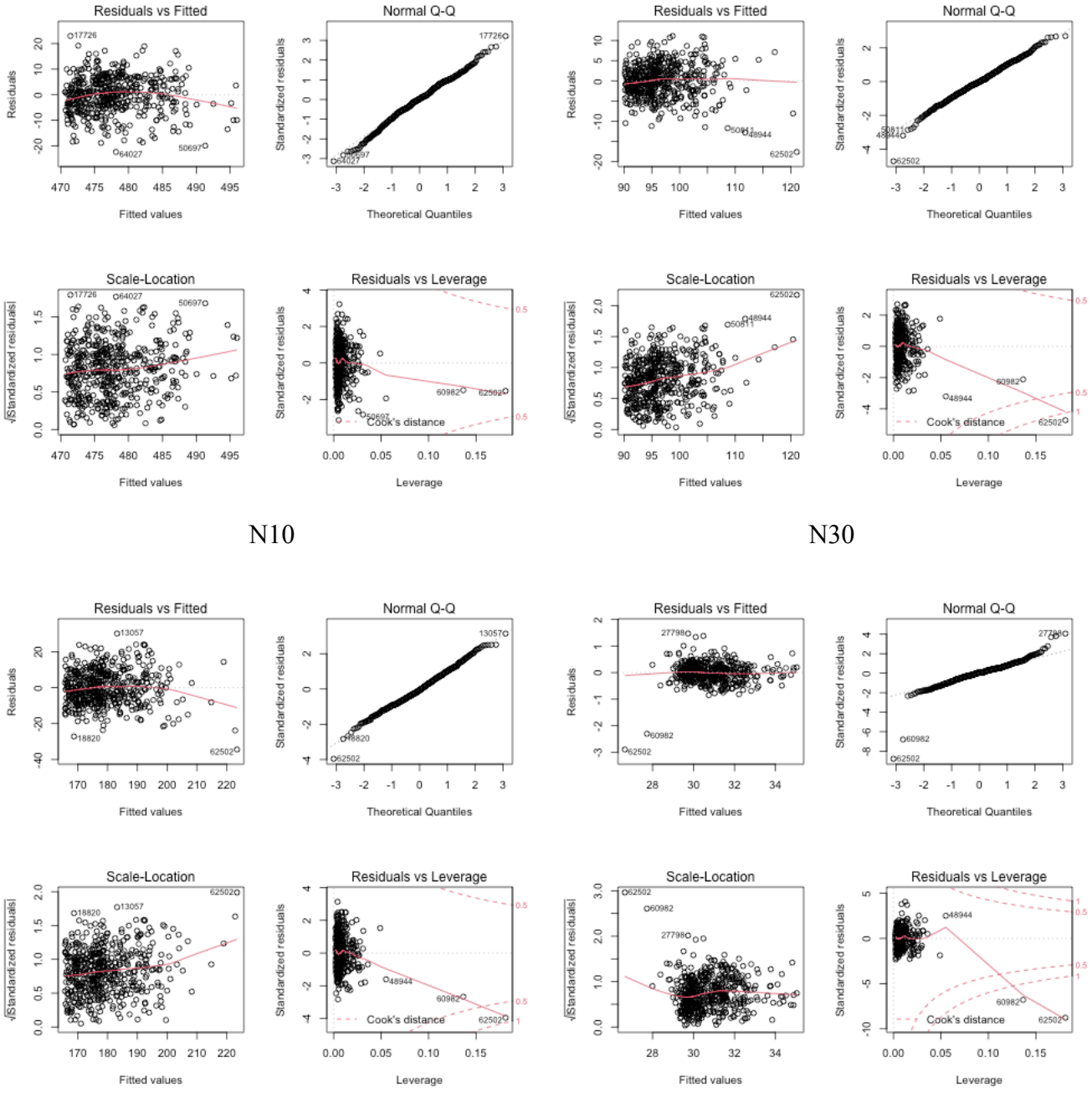

Figure F1. Diagnostic plots of linear model for the sampled climate experiment at Fushan, with each summary statistics as dependent variables and the three climatic variables (temperature, irradiance and VPD) as independent variables. The four graphs represent respectively residual linearity, residual normality, residual homoscedasticity, and presence or absence of leverage points (influential points).

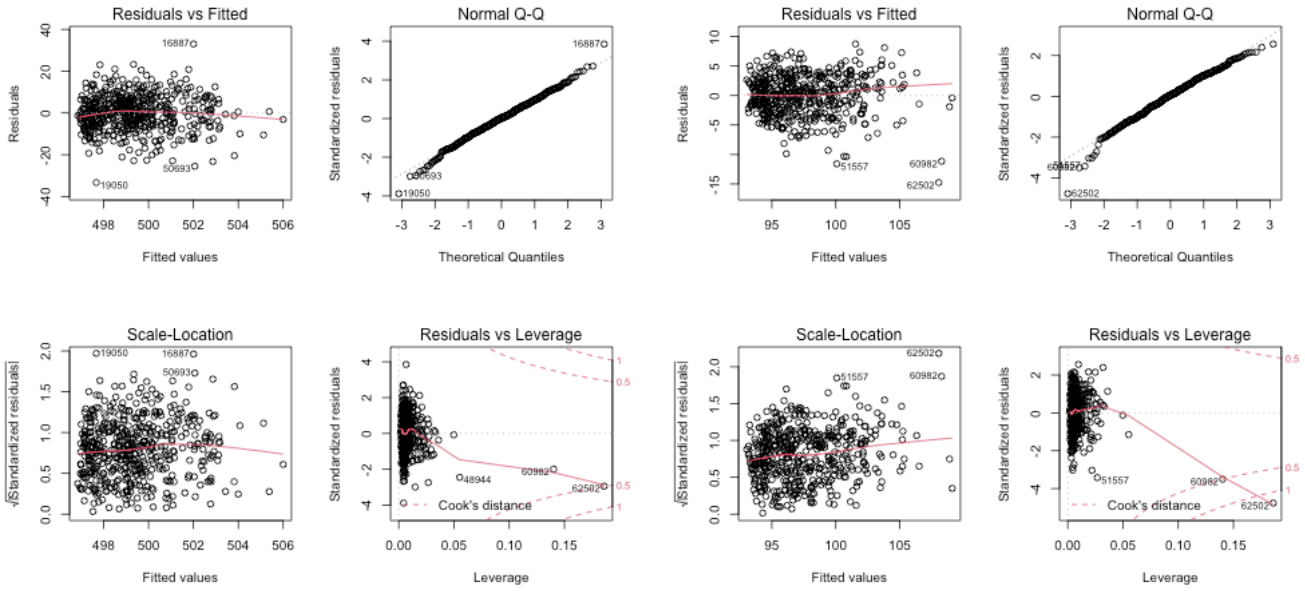

N10 N30

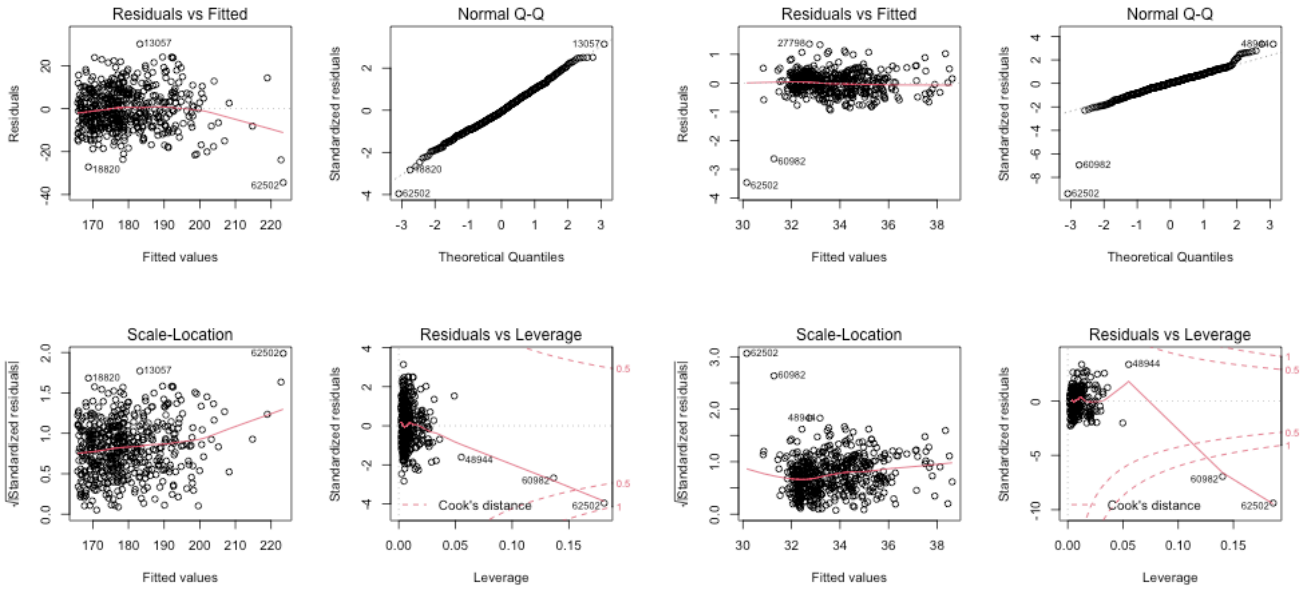

AGB GPP

Figure F2. Diagnostic plots of linear model for the sampled climate experiment at Nouragues, with each summary statistics as dependent variables and the three climatic variables (temperature, irradiance and VPD) as independent variables. The four graphs represent, respectively, residual linearity, residual normality, residual homoscedasticity, and presence or absence of leverage points (influential points).

CHAPTER 2: Wind speed controls forest structure in subtropical forests exposed to cyclones: a case study using an individual-based model

Submitted to *Frontiers in Forest and Global Change*.

This paper implements the mechanistic wind damage model ForestGALES in the individual-based based model TROLL, examines model sensitivity and response to the process of wind-induced tree mortality, investigated the effects of factors such as varying frequency and intensity of extreme winds on forest structure and dynamics, and explores a simple implementation of topographic heterogeneity. This work contributes to answer **Questions 1 and 2**.

Authors: E-Ping Rau[1], Barry Gardiner[23], Fabian Fischer[1], Isabelle Maréchaux[4], Emilie Joetzjer[5], I Fang Sun[6], Jérôme Chave[1*]

[1] Laboratoire Evolution et Diversité Biologique (EDB, UMR 5174) CNRS, Université Toulouse 3, IRD, Bâtiment 4R1, 118 route de Narbonne, 31062 Toulouse cedex 9, France

[2] Laboratoire Interactions Sol Plante Atmosphère (UMR 1391 ISPA), Bâtiment C2, INRAE Centre de Bordeaux-Aquitaine, 71 avenue Edouard Bourleaux, CS 20032, 33882 Villenave d'Ornon cedex, France

[3] Institut Européen De La Forêt Cultivée, 33610 Cestas, France

[4] AMAP, Univ Montpellier, CIRAD, CNRS, INRAE, IRD, 34000 Montpellier, France

[5] UMR SILVA INRAE, Universite de Lorraine, AgroParisTech, UMR Silva, Nancy, France

[6] Department of Natural Resources and Environmental Studies, National Dong Hwa University, Hualien, Taiwan

[*]Corresponding author

Keywords: disturbance regime, windthrow, tree mortality, topography, forest recovery, acclimation, ecosystem resilience

2.1 Abstract

Extreme wind blowdown events can significantly modify the structure and composition of forests, and the predicted shift in tropical cyclone regimes due to climate change could strongly impact forests across the tropics. In this study, we coupled an individual-based and spatially-explicit forest dynamics model (TROLL) with a mechanistic model estimating wind damage as a function of tree size, traits, and allometry (ForestGALES). We assimilated floristic trait data and climate data from a subtropical forest site in Taiwan to explore the effect of wind regimes on forest properties. We found that the average canopy height and biomass stocks decreased as wind disturbance strength increased, but biomass stocks showed a nonlinear response. Above a wind intensity threshold, both canopy height and biomass drastically decreased to near-zero, exhibiting a transition to a non-forest state. Wind intensity strongly regulated wind impact, but varying wind frequency did not cause discernible effects. The implementation of within-stand topographic heterogeneity led to weak effects on within-stand forest structure heterogeneity at the study site. In conclusion, the intensity of wind disturbances can greatly impact forest structure by modifying mortality. Individual-based modeling provides a framework in which to investigate the impact of wind regimes on mortality, other factors influencing wind-induced tree mortality, as well as interaction between wind and other forms of forest disturbances and human land use legacy.

2.2 Introduction

Natural disturbances shape forest structure, composition and dynamics, and play a substantial role in controlling the global carbon cycle (Pugh et al., 2019; Reichstein et al., 2013). Wind is a major source of natural disturbances and an important driver of tree mortality (Locatelli et al., 2016; Mitchell, 2013): while wind can cause partial tree damages such as branch snapping and defoliation, extreme wind events can lead to tree death, mainly through as stem breakage and tree uprooting. In particular, extreme wind disturbances generated by tropical cyclones in regions such as the Caribbean (Lugo et al., 2000) and the northwestern Pacific (Lin et al., 2011) have been shown to control forest structure at a global scale (Hogan et al., 2018; Ibanez et al., 2020), with one notable effect being the reduction of canopy height with increased cyclone frequency and intensity (Ibanez et al., 2019). Cyclone regimes are projected to change in the future (Lin et al., 2020), with a general increase in cyclone intensity and interregional differences in the trend of cyclone frequency (Knutson et al., 2020). In order to anticipate how such changes will affect community- and ecosystem-scale properties, it is essential to deepen our understanding of the mechanisms through which cyclonic winds regulate tree mortality, which remains one of the demographic processes that are less well constrained in forest ecosystems (Bugmann et al., 2019; Koch et al., 2021).

However, it remains intrinsically difficult to reach general conclusions on factors driving wind-induced tree mortality based on empirical studies: these studies rely on observations of forest damage after individual cyclone events, which are both limited in their temporal extent, and driven by contingent factors such as cyclone trajectory and force (Lugo, 2008) and human land use legacy (Kulakowski et al., 2011; Schwartz et al., 2017). In various studies, a higher probability and level of damage has been found to be correlated to tree characteristics such as larger diameter (Halder et al., 2021; Ostertag et al., 2005), larger height (Dunham and Cameron, 2000; Vandecar et al., 2011), or lower wood density (Curran et al., 2008; Webb et al., 2014). However, the size dependence of damage can vary with tree species (Xi, 2015) and damage type (Everham and Brokaw, 1996), and some studies even did not observe any size effect on tree damage (Bellingham et al., 1996). In addition, wind impact on trees can vary at fine scales within a given forest and for a given species, as wind speed interacts in complex ways with terrain topography, often accelerating at hilltops and mountain ridges, and decelerating in leeward valleys (Belcher et al., 2011; Ruel et al., 1998). As a result, windward, exposed terrains can experience heavier wind damage than leeward regions and valleys (McEwan et al., 2011; Yap et al., 2016) (but see de Toledo *et al.* 2012).

Recently, a number of studies have contributed to a more mechanistic understanding of wind-tree interactions at a finer scale. To do so, they modelled the response of trees or tree-like structures when exposed to wind drag using the finite-element method (Jackson et al.,

2019b, 2019c; Moore and Maguire, 2008), and used continuously collected field data to relate tree motion to architectural properties (Jackson et al., 2021, 2019a). These studies provide important insights into the mechanisms underlying wind-tree interaction. However, the response of trees to wind depends not only on individual characteristics, but also on the tree neighborhood, and more specifically on the presence and the relative size of neighboring trees, which influences wind sheltering: as an illustration, wind typically has a disproportionate impact on emergent, unsheltered trees (Duperat et al., 2021; Hale et al., 2012; Seidl et al., 2014). Hence, the impact of wind on a forest stand is more than the sum of the impacts on single trees: the heterogeneity of forest structure and composition must be accounted for when modeling the impacts of wind, especially for mixed sized forests.

In light of these challenges, dynamic forest models that are both spatially-explicit and individual-based could be useful since they link external environmental conditions to community- and ecosystem-scale properties, through individual-level processes such as mortality, while explicitly accounting for spatiotemporal heterogeneity of forests (Fischer et al., 2016; Seidl et al., 2014). By including extreme wind disturbances in the climate forcing of these models, it is possible to represent mortality in a more mechanistic fashion, and generate stand-level predictions about forest response to wind disturbances, which could then be compared with forest inventory or remote sensing data. Several individual-based models (Ancelin et al., 2004; Kamimura et al., 2019; Schelhaas et al., 2007; Seidl et al., 2014; Uriarte et al., 2009) and land surface models (Chen et al., 2018), have incorporated windthrow or storm damage models. However, these models are mainly limited to temperate forests with relatively homogeneous stand structure. To the best of our knowledge, there is currently no forest dynamics model that implements cyclonic extreme wind forcing and simulates its effects on individual-level mortality processes for subtropical and tropical forests, even though tropical cyclones cause substantial impacts on these ecosystems with high biodiversity and carbon stocks.

In this study, we explore the community-wide consequences of wind disturbances, using a model-based approach. We coupled a wind disturbance module to an individual-based forest model, and created forcing conditions from tropical cyclone records and wind speed data. We parameterized this model for the Fushan forest in Taiwan, located in a cyclone-prone region, and explored how extreme wind events impact tree mortality and forest structure and dynamics. Specifically, we addressed the following questions:

(1) How do wind-induced tree mortality impact forest structure and dynamics? We expect that the presence of wind-induced tree mortality would cause a reduction in average canopy height due to higher vulnerability of tall trees to wind damage. This could in turn increase light availability in the understory and facilitate tree establishment, leading to an

increase in stem density. We also expect that total mortality as well as the fraction of mortality due to treefalls would increase.

(2) How do changes in frequency and intensity of extreme wind events lead to shifts in forest dynamics and structure? We expect that higher wind frequency and intensity would result in more wind-induced mortality for large trees, which in turn would increase the extent of canopy height reduction and stem density increase.

(3) How does topographical heterogeneity within a forest stand influence wind damage patterns? We expect that the inclusion of topography would lead to a higher heterogeneity in forest structure, with lower canopy height and higher stem density on more exposed terrains.

2.3 Material and methods

2.3.1 Description of the TROLL model

The TROLL model is a spatially explicit individual-based model that divides the aboveground space of a forest stand into 3D cells of size 1 m^3 (voxels). Solar irradiance inside each voxel is computed as the irradiance fraction transmitted from immediately above the focal voxel (Chave, 1999; Maréchaux and Chave, 2017). No more than one individual tree can establish in each 1 × 1 m pixel at any given time, and only self-standing stems ≥ 1 cm in DBH (diameter at breast height, measured at 1.3 m above ground, or 20 cm above deformities or buttresses if present) are explicitly modelled (herbaceous plants and lianas are not included). Seeds and seedlings < 1 cm in DBH are not directly modeled, but represented as part of a seed/seedling pool. Each modelled tree is characterized by its DBH, height, crown size (radius and depth), total leaf surface area, and age. Trees are assigned species-specific traits, which control photosynthesis, growth as well as other physiological and demographic processes. At each monthly time step, trees grow depending on the balance between carbon acquisition based on a C3 photosynthesis model (Farquhar et al., 1980) and respiration, with assimilated carbon allocated into wood or leaf production. Height-DBH allometric relations are prescribed at the species level, while the DBH-crown size allometry is assumed to be species-independent. Tree mortality in TROLL is represented by several processes: (i) stochastic tree death, here assumed to be negatively dependent on species-specific wood density (WD) (Wright et al., 2010): $m_{eff} = m - \alpha \times WD$, ($\alpha$ is positive, so m is the maximal possible value of the mortality rate), (ii) carbon starvation, when net assimilated carbon is negative over a consecutive period exceeding leaf lifespan, so that old leaves have all died while no new leaves could be produced, (iii) stochastic treefall, dependent on a species-specific tree height threshold related to maximum realized tree height, and (iv) secondary treefall, when a tree is affected by a falling neighboring tree. To more explicitly link tree

mortality to exogenous factors such as wind disturbance, we updated the treefall module for this study to simulate treefall more mechanistically (cf. below).

Inputs for a typical run of TROLL (v3.0) include 1) monthly mean climate forcing data for the simulated location, 2) average trajectory of daily climatic variation, 3) species-specific plant traits for the simulated forest, and 4) species-independent general parameters, including those related to the stochastic tree death and treefall. The source code of TROLL (v3.0) is written in C++ and is available on https://github.com/troll-code/troll. On a computing cluster, each simulation of 200 × 200 m and 500 years uses around 15 minutes of computer processing unit (CPU) time.

2.3.2 Modeling tree-top wind speeds in a mixed-sized forest

Horizontal wind speed decreases as one approaches the canopy top from above the canopy. This is modelled by the aerodynamic momentum transfer model above a vegetation canopy (Monteith and Unsworth, 2008, p310). The horizontal wind speed profile with height is represented with the following equation:

$$u(z) = \frac{u_*}{k}\ln\left(\frac{z-d}{z_0}\right) \quad \text{if } z \geq H \tag{1a}$$

where $u(z)$ (m·s^{-1}) is the horizontal wind speed at height z (m) above ground or a displacement surface, $k = 0.41$ is the von Kármán constant, and u_* (m·s^{-1}) is the friction velocity. Parameter d is called the zero-plane displacement height, and z_0 the aerodynamic roughness. Both d and z_0 are dependent on canopy height H (m), and much research has explored the variation in both parameters d and z_0 over forest vegetation (Dorman and Sellers, 1989; Raupach et al., 1991; Shaw and Pereira, 1982; Shuttleworth et al., 1989). In general, d ranges from 0.7 H to 0.9 H, and z_0 from 0.04 H to 0.08 H for tropical forests. For this study, we chose the intermediate values of $d = 0.8$ H and $z_0 = 0.06$ H. These values are consistent with dense and tall evergreen forest vegetation as simulated in the SiB2 model (Sellers et al., 1996).

The aerodynamic momentum transfer model (1a) is only applicable above the canopy. In this study, we decided to apply an additional model to represent wind (Inoue 1963):

$$u(z) = u(H)\exp\left(-\alpha(1 - z/H)\right) \quad \text{if } z < H \tag{1b}$$

where $\alpha = H/L_s \approx 3$; empirical values of L_s are reported in Table I of Raupach *et al.* (1996). With this parameterization, horizontal wind speed $u(z)$ at a height of $d + z_0 = 0.86H$ and within the canopy at H/2 is 66% and 22% of u(H), respectively. To reduce computational burden, we assumed that trees whose height is lower than H/2 were not directly affected by wind. To account for canopy height heterogeneity and neighbor tree sheltering, we calculated

canopy height H for every 20 × 20 m quadrat by taking the arithmetic mean of the top leaf-containing voxel layer of each pixel within the quadrat.

From the CRU-NCEP reanalysis dataset, we obtained empirical atmospheric wind speed values (cf. the "Climate forcing" section below), which are conventionally measured at 10 m above ground or above a displacement surface. In order to obtain the horizontal wind speed experienced by each tree, we applied the following equation, derived from equation (1a), to convert horizontal atmospheric wind speed at $d + 10$, $u(d + 10)$, into top-canopy wind speed $u(\mathrm{H})$ within each 20 × 20 m quadrat:

$$u(H) = u(d+10) \times \frac{\ln\left(\frac{H-d}{z_0}\right)}{\ln\left(\frac{10}{z_0}\right)} = u(d+10) \times \frac{1.204}{5.116 - \ln(H)} \quad (2)$$

Finally, for each tree with height $h > H/2$, we computed $u(h)$ using either Equations (1a) or (1b).

2.3.3 Modeling wind-induced tree death: critical wind speed

To simulate the impact of extreme wind disturbance, we assumed that wind-induced treefall is a stochastic process whose probability depends on the difference between the tree-top wind speed $u(h)$ exerted on a tree of height h (m), and a tree-specific critical wind speed (CWS). The higher $u(h)$ is relative to CWS, the more likely the tree is to fall and die. In this study, we used a logistic model to relate the wind-induced tree death probability to ($u(h)$ – CWS) (Hale et al., 2015; Valinger and Fridman, 1999):

$$p = 1/(1 + e^{-(u(h) - CWS)}) \quad (3)$$

For the estimation of CWS, we followed the approach of ForestGALES, a wind damage risk model originally developed for even-sized and even-spaced plantation forests (Gardiner et al., 2008, 2000) but then adapted for use with individual trees in more complex forest structures (Duperat et al., 2021; Hale et al., 2015, 2012; Quine et al., 2021). ForestGALES explores the biomechanical conditions under which the tree, simplified as an anchored vertical object, will break (causing stem breakage) or lose root anchorage (causing uprooting) when subject to a turning moment caused by wind loading.

Importantly, the formulation of Equation (3) departs from that of ForestGALES, where the control of wind speed on mortality is defined to be u(H), the top-canopy wind speed. To account for the reduced impact of wind within forest canopies, the CWS in ForestGALES can be modulated by a competition index, so that trees within the canopy are less exposed to wind damage than top-canopy trees (Duperat et al., 2021; Hale et al., 2012; Quine et al., 2021). In the present formulation, CWS does not depend on the tree neighborhood, but the probability

of wind-induced tree death depends on wind speed at tree height, as computed from Equations (1a) and (1b).

At our study site, field observations indicate that the proportion of tree uprooting is low compared to that of stem breakage (Appendix A). We therefore focused on wind-induced stem breakage. The critical wind speed (CWS, $m \cdot s^{-1}$) inducing stem breakage and treefall is calculated by the following equation (Hale et al., 2015):

$$CWS = P \times \left(\frac{MOR \times DBH^3}{T_C}\right)^{\frac{1}{2}} \quad (4)$$

where DBH (m) is the tree diameter at breast height, and MOR (Pa, $kg \cdot m^{-1} \cdot s^{-2}$) is the fresh-wood modulus of rupture. We estimated MOR from oven-dry wood density (WD, $g\ cm^{-3}$) through the following exponential relationship (Green *et al.* 1999, see Appendix B):

$$MOR = 17.2 \times e^{(2.51 \times WD)} \times 10^6 \quad (5)$$

T_C is the turning moment coefficient (kg), which relates the square of mean wind speed ($m^2 \cdot s^{-2}$) to the maximum turning moment ($kg \cdot m^2 \cdot s^{-2}$) experienced by an individual tree. We used the following empirical equation for T_C (Hale et al., 2012):

$$T_C = \tau \times DBH^2 \times h \quad (6)$$

where the constant τ ($kg \cdot m^{-3}$) = 111.7 (Hale et al., 2015). A higher T_C value means larger turning moment for a given wind speed.

The wind damage parameter P (unitless) is stand-specific and determines the overall susceptibility of a forest stand to wind-induced tree death: the smaller P value is, the lower the critical wind speed is for any given tree under the same condition, meaning that the forest is overall more susceptible to wind-induced tree death. It encapsulates multiple constants and corrective factors, as well as factors in the original equation (see Hale *et al.* 2015, Equations 11 and 12; also see Appendix C) that are difficult to estimate, and whose interpretation is beyond the scope of this study. The value of P was thus tuned here by means of a sensitivity analysis (see below).

2.3.4 Climatic forcing

The TROLL model requires the following monthly mean climatic variables: daytime and nighttime mean temperature, daytime mean irradiance, and daytime mean vapor pressure deficit (VPD). We used the CRU-NCEP dataset to provide the monthly climate forcing, a global gridded (0.5° × 0.5°) sub-daily (6-hourly) climate product spanning the 1901-2016 period (version 8; version 7 archived at https://rda.ucar.edu/datasets/ds314.3/) (Viovy, 2018). It was constructed by combining observation-based CRU TS 3.2 data (Harris et al., 2014) and

model-based NCEP-NCAR data (Kalnay et al., 1996). We used CRU-NCEP variables for the 1980-2016 period, for which the most observations are available (Kistler et al., 2001).

We estimated the monthly average frequency of cyclones occurring within a sufficiently close distance to the study site. For this, we used the IBTrACS dataset (International Best Track Archive for Climate Stewardship database; v04r00, archived at https://www.ncdc.noaa.gov/ibtracs/index.php?name=ib-v4-access), which contains records of global tropical cyclones occurring since 1945 (Knapp et al., 2010). A common measure of the spatial extent of tropical cyclones is the mean radius of gale-force winds, by convention defined as 17.5 $m \cdot s^{-1}$. Based on the range of reported values in the literature, we assumed the mean radius of gale-force winds (R_{17}, km) to be 150 km (Chan and Chan, 2012; Lu et al., 2017; Weber et al., 2014). Thus, for a given site, we calculated the monthly mean frequency of recorded tropical cyclones occurring within a 150-km distance from the site over the period of 1987-2020. At Fushan, cyclone occurrence frequency was highest from July to September (~ 0.5 cyclones per month); on average, total annual cyclone frequency was around 1.84 cyclones per year.

For the selected tropical cyclone records, we calculated on-site cyclonic wind speed (V_{site}, $m \cdot s^{-1}$) using the empirical function that relates the radial variation of the tangential wind speed beyond the radius of maximum sustained wind in mature tropical cyclones (Anthes 1982, Hsu & Babin 2005): $V_{site} = 17.5 \times \sqrt{R_{17}/d}$, where d (km) is the distance between the site and the cyclone center. Since $d < R_{17}$ by definition, it follows that $V_{site} > 17.5$ $m \cdot s^{-1}$. We then fitted the on-site cyclonic wind speed values of each month to a Weibull distribution, using the function *fitdistr* in the R package *MASS* (Venables and Ripley, 2002), and used the scale and shape parameters as input climate forcing variables. At Fushan, the year-round V_{site} distribution is right-skewed, with 1st quartile = 18.85 $m \cdot s^{-1}$, median = 20.60 $m \cdot s^{-1}$, and 3rd quartile = 25.18 $m \cdot s^{-1}$.

The coupling of TROLL to wind disturbances was performed as follows. At each time step, the occurrence of an extreme wind event was drawn from a cyclone occurrence probability, assuming that one extreme wind event at most can occur per time step. If an extreme wind event occurred, we drew a random wind speed value from the input wind speed distribution. We accounted for canopy heterogeneity and neighbor tree sheltering by only considering trees with height > H/2 as being exposed to wind disturbance, where H represents quadrat-wide average top canopy height, calculated by the mean value of the top leaf-containing voxel height of each pixel within the quadrat. For each exposed tree, we converted atmospheric wind speed, $u(d + 10)$, to its tree-top wind speed, $u(h)$ (Equation 2, 1a and 1b), and calculated its critical wind speed (Equation 4). We then compared the two wind speed values, and determined if wind-induced tree death happens through a stochastic process,

dependent on a logistic function of the difference between the two wind speeds (Equation 3). Secondary treefall was modeled by assuming that when each tree dies, it falls in a random direction and increases the death rate in the impacted pixels.

2.3.5 Study site and parameterization

We parameterized the TROLL model with wind-induced tree mortality for a forest site of Taiwan. The Fushan Forest Dynamics Plot (FDP) is a 25-hectare (500 m × 500 m) plot in a moist broadleaf forest in the northeastern region of Taiwan (Su *et al.* 2007), part of ForestGEO (Forest Global Earth Observatory) (Anderson-Teixeira et al., 2015; Condit, 1998). Fushan is under strong influence of the northeasterly monsoon in winter and frequent typhoon visits in summer and autumn, with mean annual precipitation around 4200 mm, mean annual temperature around 18°C, and a mean relative humidity around 95%. Plot elevation ranges from 600 m to 733 m (Su et al., 2007). It was established in 2004 and censused every five years since then: all self-standing stems with a DBH ≥ 1 cm were identified, measured, tagged and mapped, with a total of 110 recorded tree species in the plot (Su et al., 2007).

Species-specific plant functional traits that TROLL requires as input parameters include leaf mass per area (LMA, $g \cdot m^{-2}$), nitrogen and phosphorus content (N_{mass} and P_{mass}, $g \cdot g^{-1}$), wood density (WD, $g \cdot cm^{-3}$), maximum DBH (cm), DBH-height allometric parameters and regional relative abundance. These traits were measured at Fushan according to ForestGEO protocol (Iida et al., 2014) for 94 species, covering ca. 90% of the censused trees. Climatic variables were extracted from the CRU-NCEP dataset at the geographic coordinates closest to Fushan FDP (24° 45' N, 121° 32' E).

Stem density and aboveground biomass (AGB) estimations were available at Fushan from census data. In order to estimate on-site tree mortality, we used data from the annual tree mortality survey, which has been conducted at Fushan following ForestGEO protocol since 2017. The mortality survey records the number of tree deaths and cause of death (standing, uprooted, or broken) of a subset of censused trees (Arellano et al., 2021). Using the mortality data at Fushan spanning 2017 to 2020, we calculated the mean annual mortality rate for all trees DBH > 10 cm, as well as the proportion of mortality attributed to treefall. For the detailed protocol of attribution of mortality factors, see Appendix A.

Unless otherwise specified, for all simulations, we simulated forest regeneration from bare soil for a reference plot area of 4 hectares (200 m × 200 m) for a duration of 500 years with a monthly timestep. Since we aimed to examine the effects of extreme wind on mature forest, the wind-induced tree mortality sub-model was activated after a 100-year spin up phase.

2.3.6 Sensitivity analysis

The wind-induced tree mortality sub-model includes a single parameter P (unitless). To investigate model responses to its value, we conducted a sensitivity analysis by varying the value of P across a range of (0, 1], with a varying step of 0.005: for each value, we performed five replicates of TROLL simulations (a total of 1000 simulations).

We calculated the steady-state values (mean over the last 100 years of the simulation) of three structure metrics: stem density (DBH > 10 cm; N_{10}, trees·ha^{-1}), Lorey's height (basal area-weighted mean tree height, m) (Pourrahmati et al., 2018), and aboveground biomass (AGB, Mg·ha^{-1}). For trees with DBH > 10 cm, we also calculated two mortality statistics: mean annual mortality and fraction of mortality due to treefalls ($\%M_{treefall}$). We reported mortality statistics at the onset of wind disturbance (year 101 - 200, i.e. first 100 years after wind submodule activation) and after reaching the steady state (year 401· - 500, i.e. last 100 years of simulation). We qualitatively described trends and sensitivity of these statistics in response to variation of parameter value.

2.3.7 Effects of wind frequency and intensity

To examine how the frequency and intensity of extreme wind events influence forests, we performed two series of simulations: 1) we varied cyclone occurrence frequency from 0.1 to 2 times the empirical frequency (obtained from cyclone best-track data), with a varying step of 0.1, while maintaining wind intensity; 2) we varied the scale parameter of the wind speed distribution (parameter controlling mean and median of the Weibull distribution), from 0.1 to 10 times the empirical values (estimated from the cyclone best-track wind speed distribution), with a varying step of 0.1, while maintaining empirical frequency. Five replicates were performed for each condition (in total, 100 simulations for frequency and 500 simulations for intensity were performed). We set $P = 0.7$ based on the results of the sensitivity analysis, where simulation results are close to field observations and not near the forest tipping point ($P < 0.3$). As in previous steps, we calculated the steady-state values (mean over the last 100 years of the simulation) of stem density (DBH > 10 cm) (trees·ha^{-1}), Lorey's height (m), aboveground biomass (AGB, Mg·ha^{-1}), as well as mean annual mortality and fraction of mortality due to treefalls ($\%M_{treefall}$) for trees with DBH > 10 cm. We qualitatively described trends and sensitivity of these statistics in response to variation of wind frequency and intensity.

2.3.8 Effects of topography on wind disturbances

In the original TROLL and ForestGALES model, the effect of topography was not taken into account. Based on the knowledge that wind speed is altered over an uneven topography, we implemented quadrat-scale wind speed correction factors in the model that account for these topographical effects. For this, we used the Global Wind Atlas (GWA) data, which are produced through downscaling using the WAsP program (Mortensen *et al.* 2001), incorporating surface elevation and aerodynamic roughness lengths (Badger *et al.* 2015). We obtained 250 × 250 m GWA pixels that fall in the area covered by the 1° × 1° CRU-NCEP pixel where the Fushan site is located: this represents a grid of 200 × 200 GWA pixels. We normalized the GWA wind speed values of the selected pixels so that the mean GWA wind speed is equal to the mean CRU-NCEP wind speed. We then resampled the GWA pixels to the 20m × 20m quadrat scale using bilinear interpolation with the *resample* function in the *raster* package (Hijmans, 2020), and selected the resampled pixels falling within the area of the Fushan plot: this represents a grid of 25 × 25 = 625 resampled pixels. We used the GWA wind speed values of these resampled pixels, normalized by the plot-wide mean, as the wind speed correction factor for each quadrat.

The wind speed correction factor ranged from 0.27 to 1.96, and was used as a proxy for topographic heterogeneity: if topographic effect is implemented, the wind speed experienced at each quadrat is the plot-wide wind speed (randomly drawn from the input wind speed distribution) multiplied by this correction factor: a value above 1 means that the wind speed at that quadrat is considered to speed up (due to exposed terrain), and vice versa when the value is below 1.

We performed simulations with and without topographical effect at the Fushan site for a plot area of 25 hectares (500 × 500 m), and examined the relationship between quadrat-level steady-state values (mean over the last 100 years of the simulation) of stem density (DBH > 10 cm) (trees·ha^{-1}), Lorey's height (m), aboveground biomass (AGB, Mg·ha^{-1}) and the topographic effect by performing linear regressions for each statistics as a function of quadrat-level wind speed correction factor. As comparison, we also calculated the observed relationship between forest structural heterogeneity topographic heterogeneity, based on census data at the Fushan FDP (Appendix D).

2.3.9 Data analysis

Data processing, statistical analysis and visualization were performed in R 3.3.0 (R Core Team, 2019). Apart from those already mentioned elsewhere, R packages *ggplot2*, *cowplot*, *ncdf4*, *BIOMASS*, *geosphere*, *sp*, and *tidyr* were used for this study (Dowle and Srinivasan,

2020; Hijmans, 2019; Jackson et al., 2019b; Pierce, 2019; Rejou-Mechain et al., 2017; Wickham, 2020, 2016; Wilke, 2020).

2.4 Results

2.4.1 Sensitivity analysis

As the *P* parameter value decreased (stronger wind-induced tree mortality), both average canopy height (Lorey's height) and aboveground biomass (AGB) decreased, although AGB showed a hump-shaped pattern (Figure 1): at low *P* values ($P < 0.3$), canopy height and biomass decreased to extremely low levels, suggesting a transition from forest to non-forest state. Stem density (N_{10}) only slightly decreased, but showed an abrupt increase around the transition point of $P = 0.15$ before decreasing again at lower *P* values.

Mean annual mortality and fraction of mortality due to treefalls ($\%M_{treefall}$) increased as *P* decreased, although $\%M_{treefall}$ exhibited an erratic nonlinear response. Both statistics were markedly lower at the end of the simulation (after the steady state has been reached) than immediately after the onset of wind forcing (Figure 2).

2.4.2 Effects of wind frequency and intensity

None of the forest structure and mortality statistics showed significant change with varying wind frequency. On the other hand, as wind intensity increased, stem density (N_{10}), average canopy height (Lorey's height) and aboveground biomass (AGB) all decreased (with a hump-shaped response for aboveground biomass), and mean mortality and the fraction of mortality due to treefalls ($\%M_{treefall}$) increased, especially at higher wind intensity, where the near-zero level canopy height and biomass suggested a transition from forest to non-forest state as observed during the sensitivity test (Figure 3).

2.4.3 Effects of topography on wind disturbances

Implementing the topographic effect, we found weak but significant relationships between topographic wind speed correction and forest structure. Results of linear regressions showed that stem density (DBH > 10 cm, N_{10}) was not significantly related to wind speed correction ($p = 0.09$), but average canopy height (Lorey's height) decreased and aboveground biomass (AGB) increased significantly at quadrats with higher wind speed correction factors (signifying more exposed terrain) (Figure 4, Table 1).

Table 1. Slope estimates of linear models of each quadrat-level forest structure metrics to the wind speed correction factor, with p-values in parentheses. N.S.: non-significant ($p > 0.05$). N_{10}: stem density (DBH > 10 cm). Lorey's height: basal area-weighted mean tree height. AGB: aboveground biomass.

	Without topography	With topography
N_{10} (trees·ha^{-1})	10.76 (N.S.)	-8.13 (N.S.)
Lorey's height (m)	-0.02 (N.S.)	-0.52 (< 0.01)
AGB (Mg·ha^{-1})	-5.78 (N.S.)	92.00 (< 0.01)

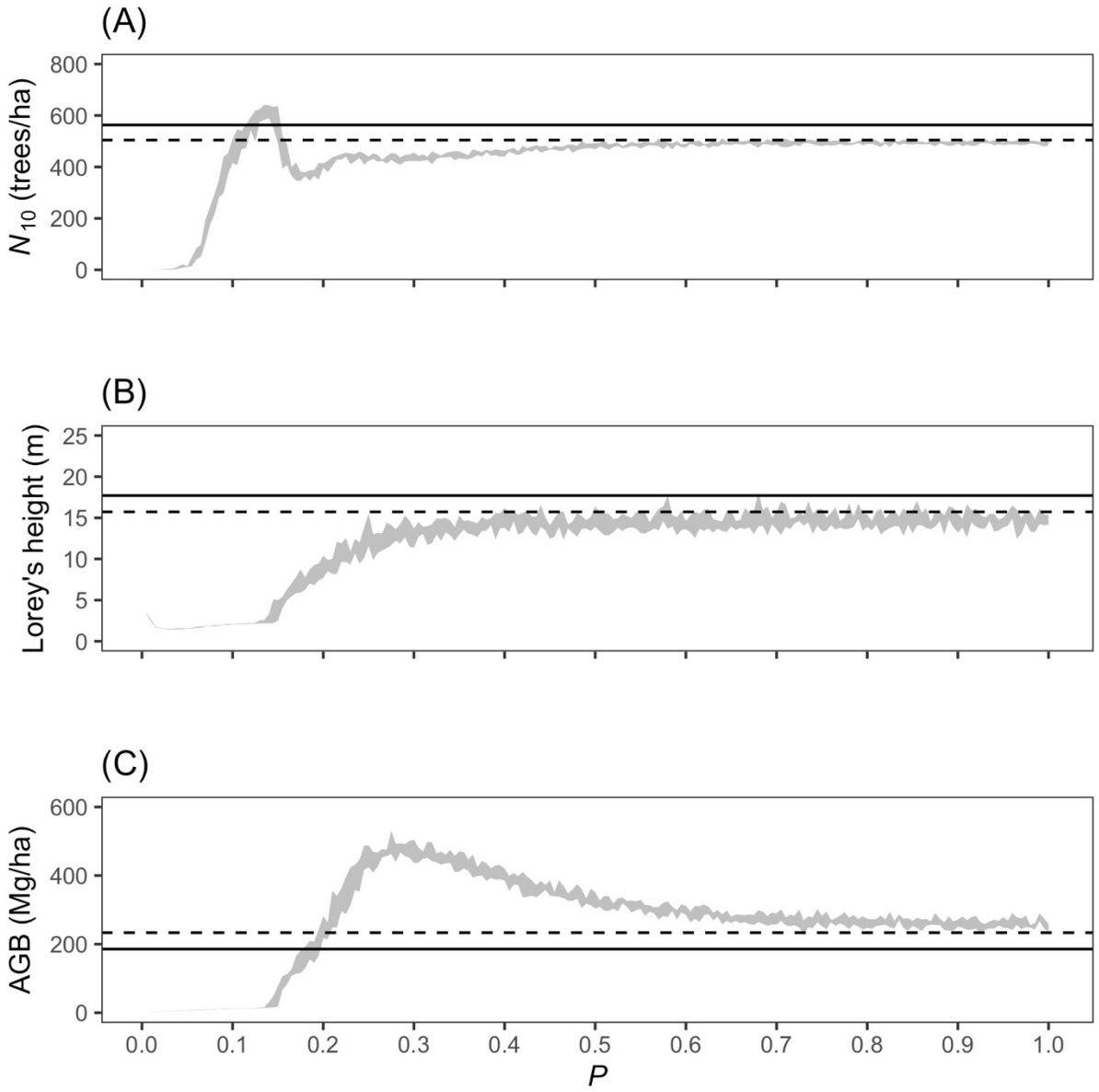

Figure 1. Summary statistics of the simulated forests, in relation to the critical wind speed parameter *P* (smaller *P* means stronger effect): **(A)** N_{10}, density of stems with DBH > 10 cm (trees·ha^{-1}); **(B)** Lorey's height, basal area-weighted mean tree height (m); **(C)** AGB, aboveground biomass (Mg·ha^{-1}). Shaded areas represent the value range of five replicates for each simulation condition. Dashed lines represent simulation value with no wind disturbance, and Solid lines represent field observations.

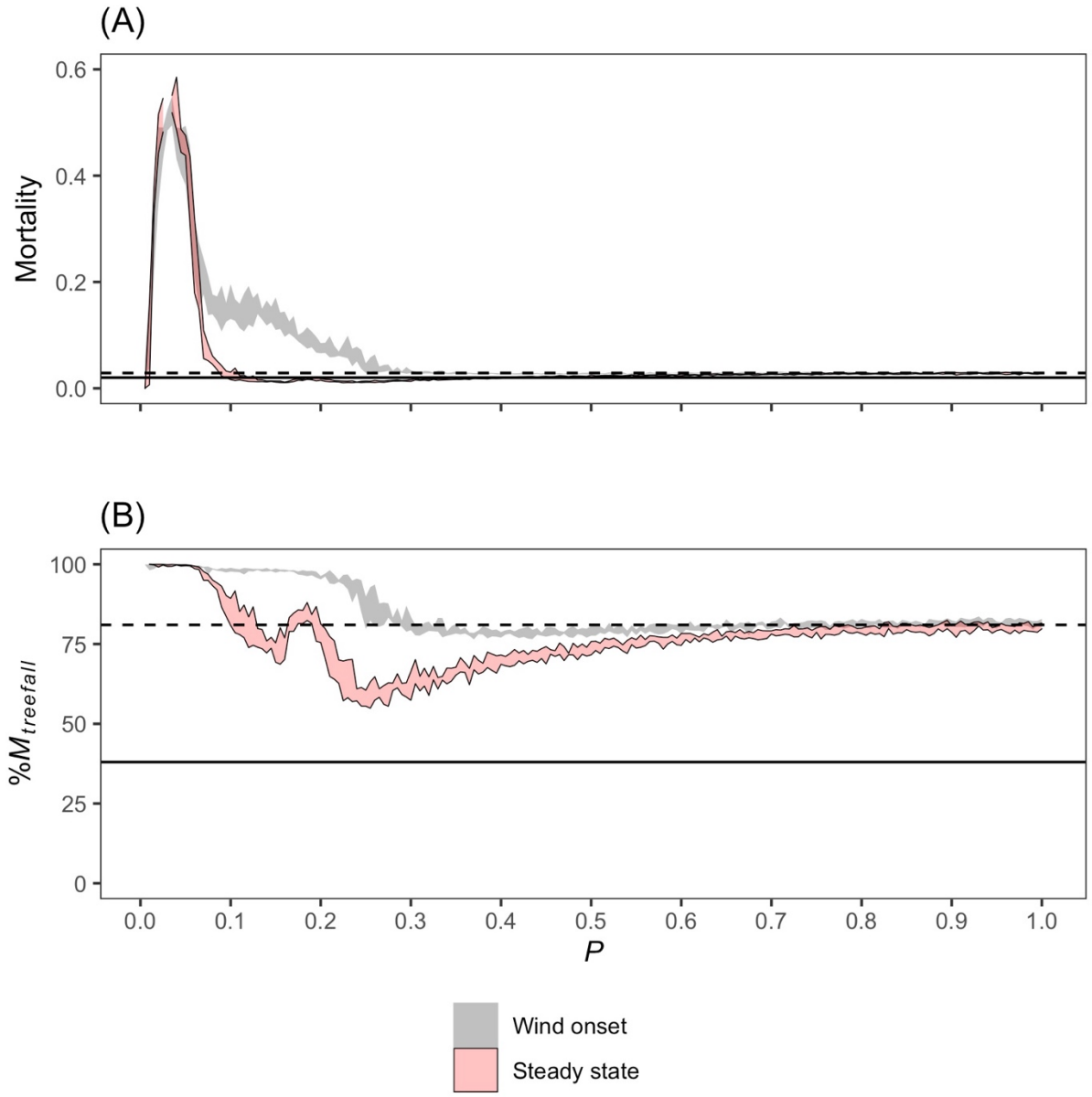

Figure 2. **(A)** Mean annual mortality rate and **(B)** fraction of mortality attributed to treefalls (%$M_{treefall}$) for trees with DBH > 10 cm, in relation to the critical wind speed parameter *P* (smaller P means stronger effect). Shaded areas represent the value range of five replicates for each simulation condition. Black without border: mean values of the first 100 years after wind onset (year 101-200). Red with border: mean values of the last 100 years of simulation (year 401-500). Dashed lines represent simulation value with no wind disturbance, and solid lines represent field observations.

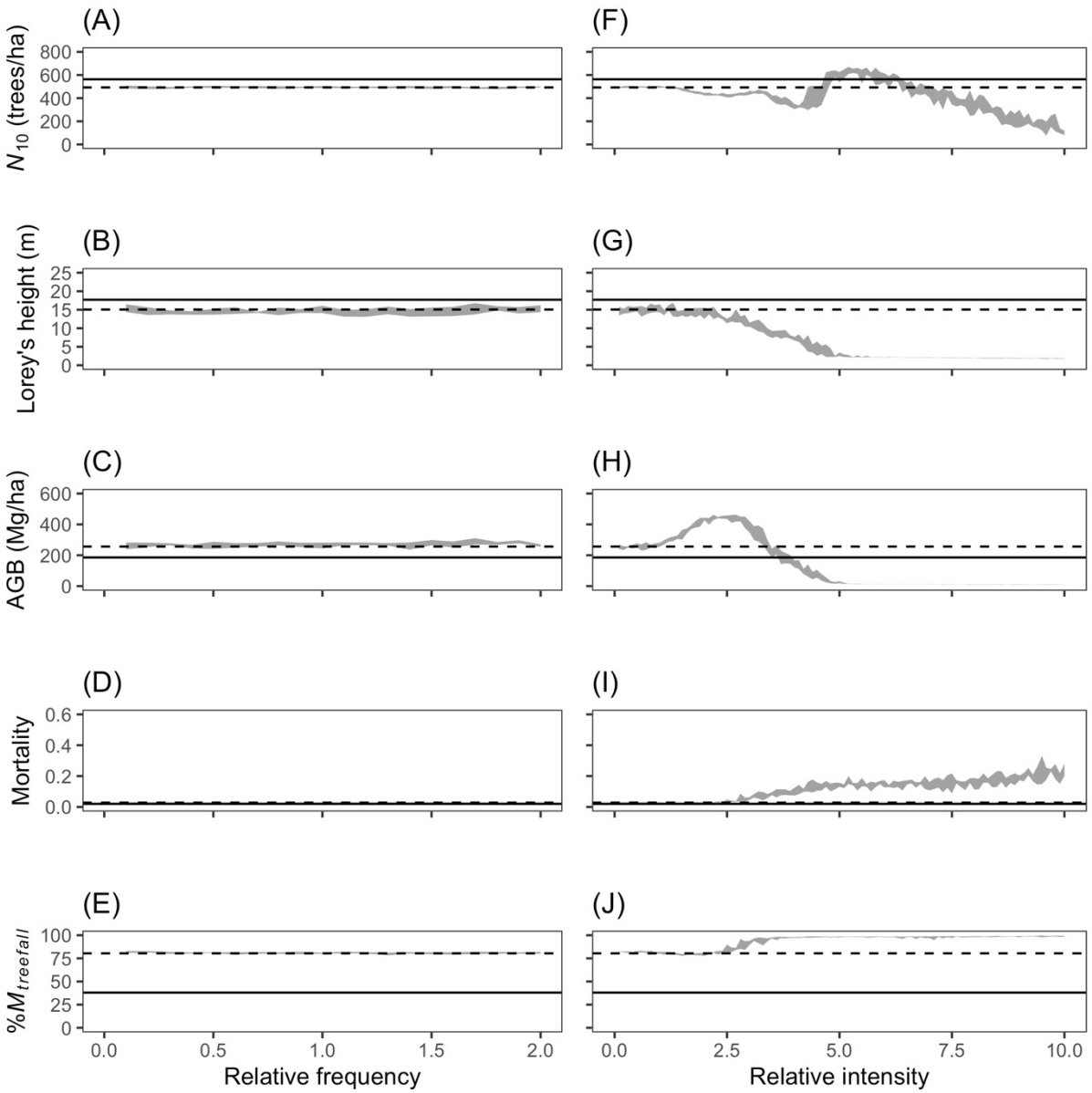

Figure 3. Simulated forest structure in relation to extreme wind frequency **(A - E)** and intensity **(F - J)**, relative to empirical values from cyclone best-track data. For simulations with varying frequency, empirical wind intensity were used, and vice versa. Shaded areas represent the value ranges of five replicates for each simulation condition. **(A, F)** N_{10}, density of stems with DBH > 10 cm (trees·ha^{-1}). **(B, G)** Lorey's height, basal area-weighted mean tree height (m). **(C, H)** AGB, aboveground biomass (Mg·ha^{-1}). **(D, I)** mean annual mortality rate. **(E, J)** $\%M_{treefall}$, fraction of mortality due to treefalls. Dashed lines represent simulation value with no wind disturbance, and solid lines represent field observations.

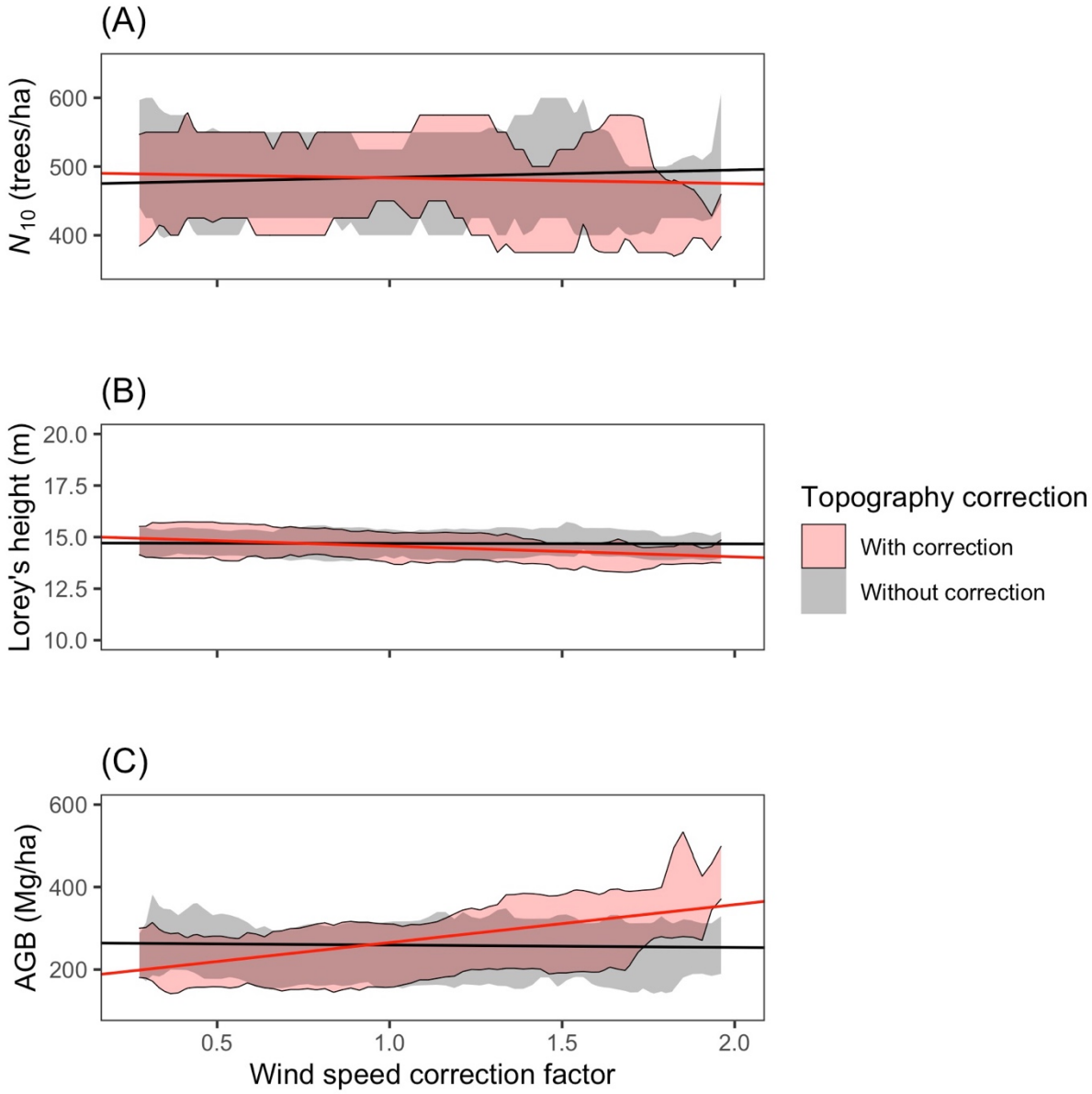

Figure 4. Simulated quadrat-level forest structure statistics as a function of the topography-related wind speed correction factor of each quadrat. A correction factor > 1 means that the quadrat-level wind speed is accelerated, , and a correction factor < 1 means that the quadrat-level wind speed is decelerated. Shaded areas represent interquartile ranges (IQR), calculated within a moving window frame (0.025) across the whole x-axis value range and then linearly interpolated to the x-axis value at each quadrat. Black without border: without topography correction. Red with border: with topography correction. Solid lines represent the linear regression curve. **(A)** N_{10}, density of stems with DBH > 10 cm (trees·ha^{-1}). **(B)** Lorey's height, basal area-weighted mean tree height (m). **(C)** AGB, aboveground biomass (Mg·ha^{-1}). For all structure statistics, the quadrat-wide values are converted to the corresponding hectare-wide values.

2.5 Discussion

In this study, we included a model of wind-induced tree mortality in a forest individual-based model, and simulated how wind-induced tree mortality affects the structure and dynamics of a subtropical forest. We found that wind-induced tree mortality had a large negative impact on canopy height and a more complex influence on stem density and biomass. The comparison of tree mortality at the onset of wind disturbance and at the steady state reveals forest acclimation and adaptation to repeated wind disturbances. Wind intensity was found to exert a strong control on wind impact, while wind frequency did not. Implementation of topographic heterogeneity showed a weak but significant effect on within-stand canopy height and biomass at the Fushan site: this implementation could serve as a basis to incorporate more complex wind-terrain interactions in individual-based models.

2.5.1 Effects of wind-induced tree death

In response to increasing susceptibility to wind-induced tree death, canopy height was found to decrease sharply. According to the wind damage model, T_C is proportional to $DBH^2 \times H$ (Eq. 6), and $CWS_{stembreak}$ is proportional to $(\mathrm{DBH}^3 / T_C)^{1/2}$ (Eq. 4): it thus follows that $CWS_{stembreak}$ is proportional to $(\mathrm{DBH} / H)^{1/2}$. Hence, wind damage risk is higher for trees with a smaller diameter-to-height ratio, and the observed reduction of canopy height may be caused by the fact that taller trees are in general more exposed and less protected by the sheltering of neighboring trees, meaning that they experience higher tree-top wind speed and higher wind damage risk (Duperat et al., 2021; Hale et al., 2012). A corollary of this hypothesis is that tree height in the canopy may become more homogenous as the effect of wind-induced tree mortality strengthens (Chi et al., 2015; Van Bloem et al., 2007). The hump-shaped response of biomass, although unexpected, could be attributed to the joint effect of the selection of trees with denser wood and the reduction of larger trees, which contribute the most to total forest biomass.

A transition from forest to non-forest state around $P = 0.3$ was apparent, where stem density increased abruptly as canopy height and biomass decreased to near-zero. This increase in stem density likely reflects a light condition that favors more smaller trees to establish as the forest canopy opens up. As the effect of wind disturbances grew even stronger, even these small-height trees started to be affected due to the absence of sheltering from taller trees, causing stem density to decrease as well.

Total mortality increased with disturbance intensity, but only starting from around the transition point, and the steady-state fraction of mortality due to treefalls decreased as disturbance intensity increased; in addition, both mortality statistics were markedly lower at

the end of the simulation than at the onset of wind disturbance. These observations suggest that long-term exposure to wind disturbances results in plastic acclimation as well as adaptation through the selection of more resistant species. Forest acclimation and adaptation could account for the low immediate mortality after a cyclone passage observed in some empirical studies (Bellingham et al., 1992; Walker, 1991), and a model simulation study also showed that acclimation could regulate forest response to wind disturbances, especially at the forest edge (Kamimura et al., 2019). In this study, the selection of trees with allometric traits of larger diameter-to-height ratio and higher wood density could cause adaptation, but plastic acclimation was not taken into account as the model did not allow traits to vary plastically over the lifetime of an individual, and trait variations were not inheritable. In the future, it would be highly interesting to explore the eco-evolutionary dynamics that results from temporally plastic trait variability and the inheritance of more wind-resistant traits.

2.5.2 Effects of wind frequency and intensity

Increasing wind intensity negatively affects forest stature and biomass stocks, consistent with results of global-scale studies that showed a clear empirical relationship between higher cyclone intensity and lower overall forest stature (Ibanez et al., 2019); however, varying wind frequency did not cause any effect on forest structure. Forest response to disturbance must be considered by placing the return period of the disturbance events in perspective with the life span of the affected organism (Turner and Dale, 1998): as trees can live for decades or even centuries in a forest, they can be exposed to centennial disturbance events. Therefore, a forest could be capable of acclimating and adapting to frequent cyclone visits without suffering catastrophic loss, as long as their intensity is within the tolerance range of the forest. On the other hand, extremely intense cyclones, even when occurring on a centennial basis, could be sufficient to cause severe consequences on forest structure and potentially even threaten the very persistence of the forest ecosystem. In light of predictions on future increase in tropical cyclone intensity (Knutson et al., 2020), this result suggests that forest ecosystems in cyclone-prone area may risk undergoing profound structural modifications or even state shifts, and more intensive and preemptive monitoring would be needed to anticipate the consequences (Newman, 2019). Modeling scenarios of simultaneous modifications of wind frequency and intensity, as well as gradual changes of the wind regime over the course of the simulation (non-stationary extreme winds) should also be explored, in order to improve the realism of disturbance forcing.

2.5.3 Effect of topography

Topography alters the impact of extreme wind on forests in complex ways, even though many studies have found that exposed locations tended to be subject to more severe wind damage than sheltered locations (Magnabosco Marra et al., 2014; Ruel et al., 1998). In this study, we introduced a simple correction factor to model the effect of quadrat-wide topographic heterogeneity, based on the assumption that wind speed accelerates locally on exposed terrain such as hilltop and mountain ridges, and decelerates locally in sheltered terrain such as valleys (Belcher et al., 2011; Mitchell, 2013). The results showed a weak but significant effect of topographic heterogeneity on canopy height and biomass stocks within the forest plot at Fushan: average canopy height was higher at more exposed quadrats, and the increase of aboveground biomass at more exposed quadrats was consistent with the hump-shaped response of biomass as wind disturbance strength increased (Figure 1). The weak effect size could reflect the fact that trees at Fushan, even those at exposed terrains, are well adapted to the simulated wind level. Nevertheless, the observed relationship between quadrat-scale forest structure statistics and elevation at the Fushan site was stronger and exhibited a different pattern, with higher stem density and lower average canopy height at more exposed quadrats, but no variations in biomass (Appendix D). This suggests that it is highly probable that our preliminary implementation did not fully capture the effects of the topography. In the future, it is crucial to refine the model representation of topographic effects by considering how wind interacts with finer-scale features such as top-canopy topography, and factors such as wind direction. Parameterization for topography currently comes from a data set at 250-m resolution, and employing more fine-scale data could also improve topographic representation. Nevertheless, this preliminary exploration could serve as a framework under which to further investigate how topography mediates the effect of wind disturbances in an individual-based model.

2.5.4 Challenges of model representation of wind-induced tree mortality

The first and foremost challenge when simulating wind disturbance in a mixed-sized forest is the description of the wind profile: since the individual-based model TROLL does not prescribe fixed stand-level characteristics (notably top canopy height), many factors that control wind profile dynamically change across time and space. Wind speeds above the tree canopy are commonly modeled by a logarithmic profile (Raupach et al., 1991), which is the approach taken in the ForestGALES model. The aerodynamic parameters used in the logarithmic profile have been shown to depend on the plant area index, and as such, they are expected to vary seasonally. A detailed parameterization has recently been proposed based on

remote-sensing LAI and canopy height products, which could help account for this variability and enhance realism of wind profile modeling (Liu et al., 2021).

In this study, we further assumed that the wind speed experienced by trees within the canopy follows an exponentially decreasing profile (Inoue, 1963), and that trees well below the displacement height in effect do not experience wind disturbance; other equations have been derived to describe the decreasing wind speed profile within canopy (Ancelin et al., 2004; Raupach and Thom, 1981), and measurements have also been made (Raupach et al. 1996). Significant variations in wind profile could exist due to the heterogeneity of forest structural characteristics, such as leaf area index, stem density and spacing (De Santana et al., 2017; Lalic et al., 2003; Moon et al., 2016). In addition, the interaction of horizontal winds with the canopy structure creates turbulent eddy structures, whose effects have not yet been explored in the current model (de Langre, 2008a; Raupach et al., 1996).

The original ForestGALES model estimated critical wind speed for both types of wind-induced damage, tree uprooting and stem breakage. In a preliminary test, we simulated both processes, but found that few tree uprooting occurred compared to stem breakage (Appendix C). This is consistent with the empirical mortality survey at Fushan, where many more dead trees exhibit stem breakage than uprooting (Appendix C). This has motivated our decision to simplify model representation and focus on stem breakage. One further motivation for ignoring tree uprooting is that it is largely controlled by root anchoring, which is currently still difficult to represent mechanistically and to parameterize for all tree species, due to our limited understanding on root traits and the physics underlying root-soil interaction. In the future, efforts should be made to devote more attention to the process of root anchoring.

Lastly, although we parameterized species-specific wind susceptibility using plant traits to the extent possible, and assumed that the free parameter P was identical for all the trees in a forest stand, *P* may in reality still be species-specific due to factors such as wood deformities, stem tapering, relative allocation of total biomass to stem weight, as well as the capacity for defoliation that reduces wind loading. These factors could all contribute to model uncertainty, and further investigation is needed to better constrain them in future model developments.

2.5.5 Field mortality survey data

In this study, we retrieved data from the annual mortality surveys conducted in ForestGEO sites, in the hope of calibrating the model using empirical mortality data as a complement to inventory data. The survey data could inform us on the number of tree deaths and treefalls that occur within the forest plot, and simulated mortality rates showed good correspondence with observed values calculated from the survey data, but inferring the cause of tree death

from the observed damage modes of the dead trees has proven to be difficult. A tree may experience multiple damages successively or simultaneously, which would all contribute to causing treefall, or it may experience damage after its death: these different scenarios could not be distinguished by *post hoc* records of observed damage on dead trees. In addition, a large proportion of stem breakage and uprooting in the understory are likely to be caused secondarily by treefall events of neighboring trees, and not directly by wind.

As a consequence, it is possible that the field observed numbers of tree deaths with uprooting or stem breakage were an overestimation of the wind-induced uprooting or stem breakage events in reality. However, the observed fraction of tree deaths due to treefalls were considerably lower than the simulated values, suggesting that there might be additional acclimation and adaptation phenomena limiting treefalls, which were not accounted for in the current model. Nevertheless, the annual mortality survey data still contain the most detailed fine-scale records on tree mortality in species-rich natural forests available to date, and the observed patterns of damage modes, while not sufficient to calibrate the model, still served as a heuristic basis that inform on patterns of tree death.

2.5.6 Perspectives

In a mixed-sized natural forest, natural thinning and gap dynamics frequently modify tree density and local stand height, causing changes in the level of physical sheltering from neighboring trees: the wind loading and damage risk of a tree may change considerably as its sheltering status changes even when its size does not (Quine and Gardiner, 1995; Schelhaas et al., 2007; Seidl et al., 2014). In the current implementation of the wind damage model, local sheltering is accounted for by considering a tree's height with respect to local canopy top height, simulating within-canopy wind attenuation, and assigning a height threshold under which a tree is not considered to experience wind disturbances. A finer representation of the effect of local sheltering could be achieved by including a "competition index", calculated based on a tree's relative size to neighboring trees, in the formulation of the tree's turning moment (T_C), so that local sheltering is represented as a continuous variation and not as a cutoff point (Duperat et al., 2021; Hale et al., 2012), even though the choice of competition index is not trivial and requires careful consideration. In addition, the T_C equation is currently empirically fitted at a limited number of temperate plantation forest sites, and its transferability to the tropics and to mixed-sized natural forests needs to be examined in more detail: recent works of fine-scale measurement of tree movement in response to wind in natural forests represent the first step to overcome this challenge (Jackson et al., 2020, 2019c, 2019b).

The current model could be further refined by including other aspects of wind impact on trees, such as successive damages that do not immediately cause death but increases delayed mortality (Tanner et al., 2014; Walker, 1995), coping mechanisms such as defoliation (reduction of wind drag at the cost of temporary lower productivity) and re-sprouting (allowing survival even after stem breakage). Other factors influencing tree mortality, such as preexisting stem rotting or deformities, interactions with other forms of disturbance such as insect attacks, fire and drought (Newman, 2019; Reichstein et al., 2013; Seidl et al., 2011a), as well as human land use legacy and fragmentation (Laurance and Curran, 2008; Schwartz et al., 2017; Uriarte et al., 2009), could also be considered conjointly with the wind disturbance model. Parameter calibration and model validation could also be improved with the help of high-resolution satellite data that monitor wind gap formation and dynamics (Ballère et al., 2021; Hayashi et al., 2015; Kislov and Korznikov, 2020).

Finally, although the current study focuses on the impacts of wind on a cyclone-prone forest, the model we developed could also be applied to explore wind vulnerability of forests that are less accustomed to wind disturbances, as well as the effects of localized wind blowdown events, which are thought to shape the structure and dynamics of Amazonian forest (Magnabosco Marra et al., 2018; Negrón-Juárez et al., 2018; Peterson et al., 2019). The exploration of more forest settings and wind regimes could help us go beyond single forest plots and take into account landscape- and regional-level heterogeneity in the model (Peereman et al., 2020; Seidl et al., 2014), in order to explore the consequences of wind disturbance at a landscape or even regional level.

2.5.7 Conclusion

In this study, we explored the effects of wind-induced tree mortality and long-term consequences of wind disturbances at a subtropical forest, and the results indicate that wind disturbances could have strong negative effects on forest structure when intensity is strong, which has strong implications given the projected increase in tropical cyclone intensity. This modeling framework of wind-induced tree mortality, including the preliminary implementation of topographic effects, could serve as the basis for improving representation of the mortality processes in vegetation models, deepen our mechanistic understanding of how wind disturbances act on forest over a larger spatial scale in conjunction with other types of disturbance, as well as generate predictions on the future of natural forests in response to the changing wind regime.

2.6 Acknowledgments and author contributions

Simulations were run on the OLYMPE cluster at CALMIP, Toulouse. We thank Dr. Chia-Hao Chang-Yang at National Sun Yat-Sen University for helping to provide us with the mortality survey data at Fushan FDP. Fushan FDP is supported by the Taiwan Forestry Bureau, the Taiwan Forestry Research Institute and the Ministry of Science and Technology of Taiwan. We would like to express our gratitude to all field technicians and students who helped with the implementation and censuses of Fushan Forest Dynamics plots. We also thank the staff at Fushan Research Center for providing logistic support. This work was supported by the "Investissement d'Avenir" grants managed by the Agence Nationale de la Recherche (CEBA, ref. ANR-10-LABX-25-01; TULIP, ref. ANR-10-LABX-0041; ANAEE-France: ANR-11-INBS-0001).

EPR and JC designed the research; EPR conducted the research; FF, BG, IM and JC provided assistance in modeling and statistical analyses; EJ and IFS provided data used for analyses; all authors proofread and edited the paper.

2.7 Supplementary data

Appendix A: estimation of on-site mortality values

The dataset used to calculate mortality rate and proportion of mortality attributed to each cause were four years of annual mortality survey data, conducted from 2017 to 2020 for a subset of the censused trees selected following ForestGEO protocol (Arellano et al., 2021). For each survey, each surveyed tree was assigned a label for its survival status (OK: "alive with no damage", A: "alive with damage", D: "dead", NF: "not found", X: "dead stem in living individual"), and a label for its damage mode (S: "standing (with canopy damage)", B: "broken stem", U: "uprooting (with root bole exposure)", BU: "both broken stem and uprooting"). After extracting tree tag, DBH, status and mode labels from each survey data, we simplified the data structure by grouping status "OK", "X" and "A" as alive tree individuals, and grouping status "NF" and "D" as dead tree individuals, and merged the data from the four different years.

In Fushan, the survey reported a high incidence of "zombie trees", which are trees that were recorded as dead in one year, but found to be actually alive in the next year, due to the re-sprouting of basal shoots. In order to exclude these entries to the best of our ability, we considered only trees that were alive in 2017 and ended up dead in 2020 to be a "real" death event, and calculated mortality rate by the proportion of death events to the number of all alive trees in 2017. This number will still be an overestimation, due to the fact that a proportion of trees recorded as dead since 2019 or 2020 may not actually be dead yet, and may still possess the ability to re-sprout in subsequent years. The mortality rate over three years (m_3, 2017 - 2020) was converted to annual mean mortality (m_{ann}) by the following equation:

$$m_{ann} = 1 - (1 - m_3)^{1/3} \quad \text{(A1)}$$

These values were compared with estimates calculated from census data with five-year intervals, and were found to be of similar range (Table A1).

Table A1. Mean annual mortality rate in different diameter classes.

	From mortality survey	From census
DBH ≥ 1 cm	0.0517	0.0461
DBH > 10 cm	0.0201	0.0289
DBH > 30 cm	0.0172	0.0101

To determine the most likely cause of mortality, we referred back to the mode label that indicates the type of damage in the year that a tree is last recorded dead. Damage mode labels

"U" and "B" indicate tree uprooting (root bole exposure) and stem breakage respectively, and were treated as such. "BU" indicates that both uprooting and stem breakage were observed: we divided trees in this category into two parts, and attributed them equally to stem breakage and uprooting. Finally, we calculated the fraction of dead trees observed with stem breakage ($\%M_{break}$) or uprooting ($\%M_{uproot}$), as well as the total fraction of tree deaths due to treefalls ($\%M_{treefall}$; labeled with "U", "B" or "BU") and the fraction of tree deaths due to other causes ($\%M_{other}$; labeled with "S") (Table A2).

Table A2. Proportion of tree mortality attributed to different causes per diameter classes ($\%M_{treefall} = \%M_{break} + \%M_{uproot}$).

	$\%M_{break}$	$\%M_{uproot}$	$\%M_{treefall}$	$\%M_{other}$
DBH ≥ 1 cm	44%	4%	48%	52%
DBH > 10 cm	51%	8%	57%	42%
DBH > 30 cm	45%	12%	59%	41%

Appendix B. Relation between wood density and green modulus of rupture for hardwoods

The table for species-specific wood traits reproduced below is taken from Green *et al.* (1999), including only hardwood species for which green modulus of rupture was measured. Wood density at 12% moisture (D_{12}) was converted into oven-dry wood density (D_b) using the formula $D_b = 0.828\ D_{12}$ (Vieilledent et al., 2018). The relationship between oven-dry wood density and green modulus of rupture was then fit to an exponential function (Equation 5).

Table B1. Wood traits for a selection of hardwood species.

Common species name	Oven-dry wood density (g cm^{-3})	Green modulus of rupture (MPa)
African mahogany	0.38	51
afrormosia	0.56	102
andiroba	0.49	71
angelique	0.55	78.6
azobe	0.80	116.5
banak	0.38	38.6
Brazilian rosewood	0.73	97.2
bulletwood	0.78	119.3
cativo	0.37	40.7
ceiba	0.23	15.2
courbaril	0.65	88.9
cuangare	0.28	26.7
dark red meranti	0.42	64.8
degame	0.61	98.6
determa	0.48	53.8
goncalo alves	0.77	83.4
greenhart	0.73	133.1
hura	0.35	43.4
ilomba	0.37	37.9
Indian rosewood	0.69	63.4
ipe	0.84	155.8
iroko	0.49	70.3
jarrah	0.61	68.3
jelutong	0.33	38.6
kaneelhart	0.88	153.8
kapur	0.59	88.3
karri	0.75	77.2
kempas	0.65	100
kruing	0.63	82
light red meranti	0.31	45.5

limba	0.35	41.4
macawood	0.86	153.8
manbarklak	0.80	117.9
manni	0.53	77.2
marishballi	0.80	117.9
merbau	0.59	88.9
mesaw	0.48	55.2
mora	0.71	86.9
obeche	0.27	35.2
opepe	0.58	93.8
para-angelim	0.58	100.7
pau marfim	0.67	99.3
peroba rosa	0.60	75.2
pilon	0.59	73.8
piquia	0.66	85.5
primavera	0.37	49.6
ramin	0.48	67.6
robe	0.48	74.5
sande	0.45	58.6
santa maria	0.48	72.4
sapele	0.50	70.3
sepetir	0.51	77.2
shorea baulau group	0.62	80.7
spanish cedar	0.37	51.7
sucupira	0.68	118.6
sucupira bowdichia	0.71	120
teak	0.50	80
tomillo	0.41	57.9
true mahogany	0.41	62.1
wallaba	0.71	98.6
white meranti	0.50	67.6
yellow meranti	0.42	55.2
Aerican beech	0.53	59
American basswood	0.31	34
American chestnut	0.36	39
American elm	0.41	50
American sycamore	0.41	45
balsam poplar cottonwood	0.28	27
bigleaf maple	0.40	51
bigtooth aspen	0.32	37
bitternut pecan hickory	0.55	71
black ash	0.41	41
black cherry	0.41	55

black cottonwood	0.29	34
black locust	0.57	95
black maple	0.47	54
black red oak	0.51	57
black tupelo	0.41	48
black walnt	0.46	66
black willow	0.32	33
blue ash	0.48	66
bur white oak	0.53	50
butternut	0.31	37
cherrybark red oak	0.56	74
chestnut white oak	0.55	55
cucumber tree magnolia	0.40	51
Eastern cottonwood	0.33	37
green ash	0.46	66
Hackberry	0.44	45
honeylocust	0.55	70
laurel red oak	0.52	54
live white oak	0.73	82
mockernut tree hickory	0.60	77
northern red oak	0.52	57
nutmeg hickory	0.50	63
oregon ash	0.46	52
overcup white oak	0.52	55
paper birch	0.46	44
pecan hickory	0.55	68
pignut hickory	0.62	81
pin red oak	0.52	57
post white oak	0.55	56
quaking aspen	0.31	35
red alder	0.34	45
red maple	0.45	53
Rock elm	0.52	66
sassafras	0.38	41
scarlet red oak	0.55	72
shagbark hickory	0.60	76
shellbark hickory	0.57	72
silver maple	0.39	40
Slippery elm	0.44	55
southern magnolia	0.41	47
southern red oak	0.49	48
sugar maple	0.52	65
swamp chestnut white oak	0.55	59

swamp white oak	0.60	68
sweet birch	0.54	65
sweetgum	0.43	49
tanoak	0.53	72
water hickory	0.51	74
water red oak	0.52	61
water tupelo	0.41	50
white ash	0.50	66
white oak	0.56	57
willow red oak	0.57	51
yellow birch	0.51	57
yellow poplar	0.35	41

Appendix C: description of the original ForestGALES model

In the original ForestGALES model, critical wind speed (CWS) is calculated for two types of tree damage: stem breakage and tree uprooting. Based on the T_C approach, which relates maximum turning moment to mean wind speed, the critical wind speed for the two types of tree damage follows the following relation (Hale et al., 2015, 2012):

$$CWS_{stembreak} = \left[\left(\frac{\pi \times MOR \times {d_0}^3}{32 \times T_C}\right)\left(\frac{f_{knot}}{f_{edge} \times f_{CW} \times TMC_{ratio}}\right)\right]^{1/2} \quad \text{(C1)}$$

$$CWS_{uprooting} = \left[\left(\frac{C_{reg} \times SW}{T_C}\right)\left(\frac{1}{f_{edge} \times f_{CW} \times TMC_{ratio}}\right)\right]^{1/2} \quad \text{(C2)}$$

MOR, the modulus of rupture (Pa, $kg \cdot m^{-1} \cdot s^{-2}$), is related to wood density and was estimated using Equation (5). T_C , the turning moment coefficient (kg), relates the square of mean wind speed to the maximum turning moment, in a relationship described in Equation (6). d_0 (diameter at trunk base, 0 m) was converted from DBH (diameter at breast height, 1.3 m) by a linear corrective factor: $d_0 = \beta \times DBH$.

C_{reg} ($m^2 \cdot s^{-2}$) is an empirical parameter which depends on soil and rooting depth. C_{reg} values have been measured through tree-pulling experiments for conifers and broadleaf species (Locatelli et al., 2016; Nicoll et al., 2006; Peltola et al., 2000; Peterson and Claassen, 2013), and were found to range from 110 to 185. *SW* (kg) represents fresh stem weight, and is related to total aboveground biomass (AGB) through a linear proportional factor: $SW = \alpha \times AGB$.

Several other corrective factors were present in this model: f_{knot} accounts for the presence of knots reducing wood strength; f_{edge} accounts for the position of the tree relative to a newly created forest edge; f_{CW} accounts for overhanging crown weight when the tree is bent; TMC_{ratio} accounts for the increasing wind loading after thinning due to reduced neighbor tree sheltering. By combining these factors, as well as other corrective factors into a single wind damage parameter *P*, the equations was simplified and rewritten as:

$$CWS_{stembreak} = P_{stembreak} \times \left(\frac{MOR \times DBH^3}{T_C}\right)^{\frac{1}{2}} \quad \text{(C3)}$$

$$CWS_{uprooting} = P_{uprooting} \times \left(\frac{AGB}{T_C}\right)^{1/2} \quad \text{(C4)}$$

where $P_{stembreak}$ is unitless and $P_{uprooting}$ has the unit of $m \cdot s^{-1}$. They encapsulate the following factors respectively:

$$P_{stembreak} = [(\pi \times \beta^3 \times f_{knot})/(32 \times f_{edge} \times f_{CW} \times TMC_{ratio})]^{1/2} \quad \text{(C5)}$$

$$P_{uprooting} = [(C_{reg} \times \alpha)/(f_{edge} \times f_{CW} \times TMC_{ratio})]^{1/2} \quad \text{(C6)}$$

As stated in the main text, the *P* parameters determine the overall susceptibility of a forest stand to wind-induced tree mortality: the smaller a *P* value for a damage type is, the lower the critical wind speed is for any given tree in a forest stand, meaning that the forest is overall more susceptible to wind-induced damage and death of that type.

We performed a preliminary sensitivity analysis to investigate model responses to the two free parameters, $P_{stembreak}$ (unitless) and $P_{uprooting}$ ($m \cdot s^{-1}$). We chose [0.01, 1] for the value range of $P_{stembreak}$ and (0, 40] for the value range of $P_{uprooting}$, and randomly drew 500 values from within each value range for use in TROLL simulations. We calculated the steady-state values (mean over the last 100 years of the simulation) of three structure metrics: stem density (DBH > 10 cm; N_{10}, $trees \cdot ha^{-1}$), Lorey's height (basal area-weighted mean tree height, m) (Pourrahmati et al., 2018), and aboveground biomass (AGB, $Mg \cdot ha^{-1}$) (Figure C1). We then performed model calibration based on aboveground biomass, by calculating the absolute difference between simulation and field observation values, scaled by the standard deviation of the simulation values. We selected the simulations having the 5% best fit (25 out of 500 simulations).

As the parameter values of the best-fit simulations were scattered and did not converge to a narrower value range (Figure C1), we turned to evaluate the relative contribution of each wind disturbance process to tree mortality, in the goal of simplifying the model. For each best-fit simulations, we calculated the proportion of treefalls due to each wind disturbance process, averaged over all timesteps where an extreme wind event happened in the last 100 years of the simulation. The results showed that the proportion of treefalls due to tree uprooting was lower compared to the proportion of treefalls due to stem breakage (Figure C2). Based on these preliminary results, we decided to focus on the process of wind-induced stem breakage for this study.

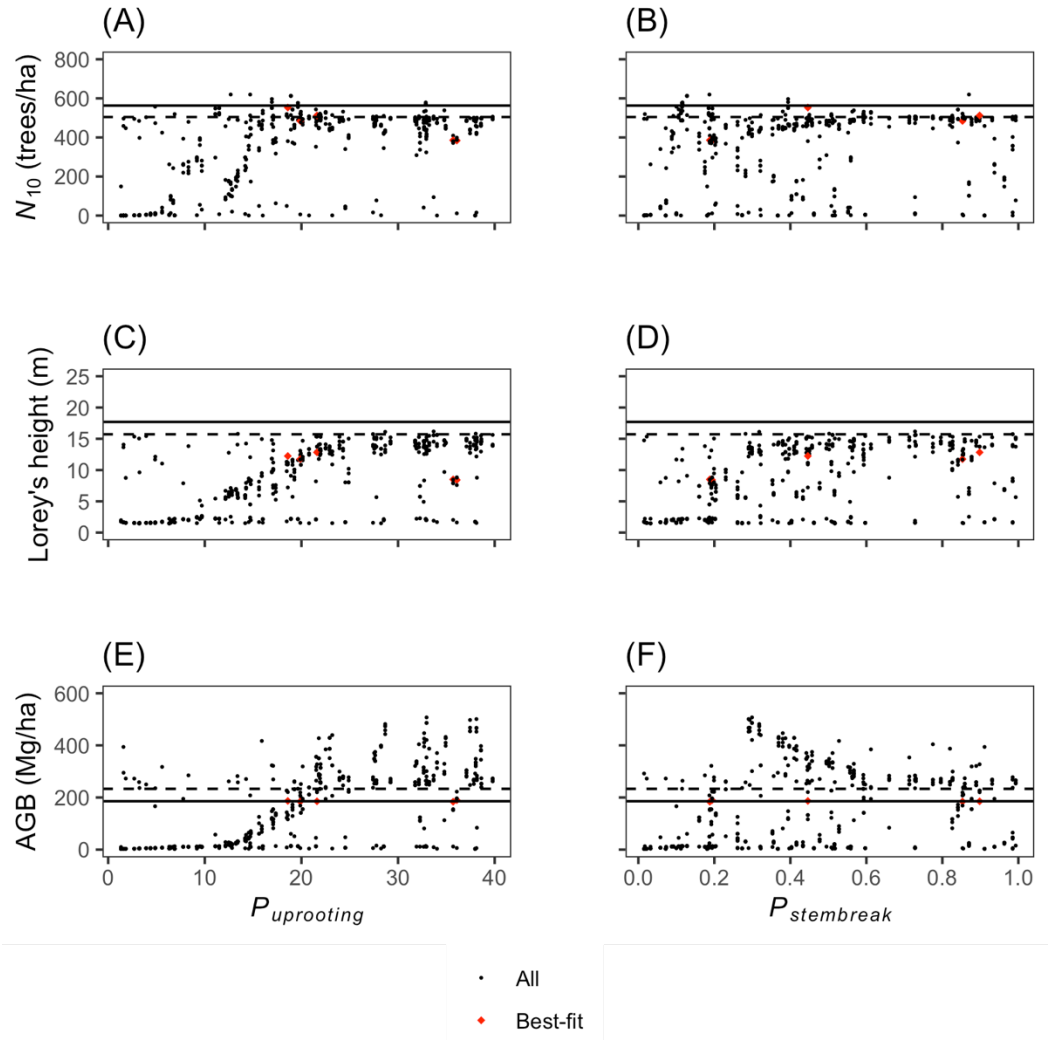

Figure C1. Summary statistics of the simulated forests, in relation to the critical wind speed parameters $P_{uprooting}$ and $P_{stembreak}$ (smaller value means stronger effect). N_{10}: density of stems with DBH > 10 cm. Lorey's height: basal area-weighted mean tree height. AGB: aboveground biomass. Dashed lines represent simulation value with no wind disturbance, and Solid lines represent field observations. Red diamond-shaped points: simulations having the 5% best fit.

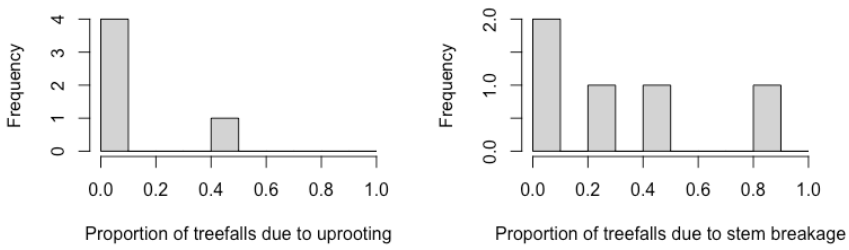

Figure C2. Histogram of the proportion of treefalls due to each of the two wind disturbance processes for the 25 best-fit simulations in the preliminary calibration test.

Appendix D. Observed structural heterogeneity at the Fushan FDP in relation to topographic heterogeneity

Quadrat-level mean elevation at the Fushan forest plot ranges from 616 to 730 m. The linear regression results based on field census data showed that stem density (N_{10}) increased with elevation, average canopy height (Lorey's height) decreased with elevation, while aboveground biomass (AGB) did not vary significantly in relation to elevation (Figure D1, Table D1).

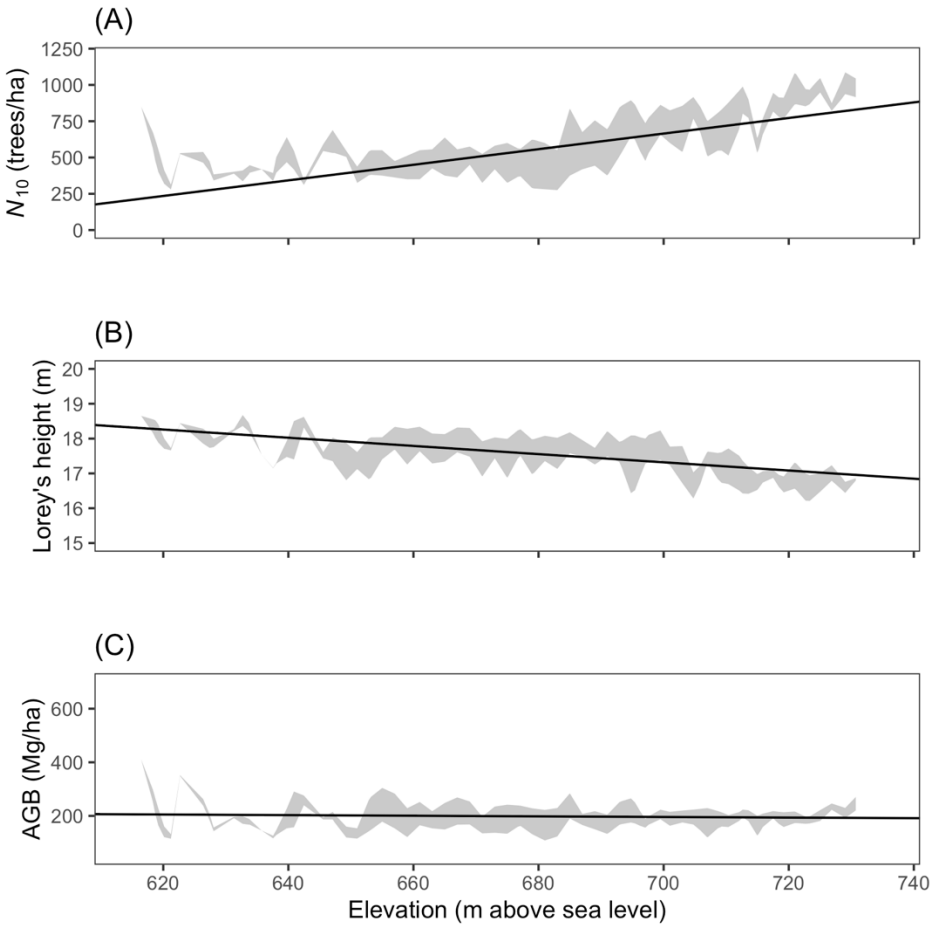

Figure D1. Quadrat-wide (20 m × 20 m) forest summary statistics at the Fushan site, as a function of the quadrat elevation above sea level. Shaded areas represent interquartile ranges (IQR), calculated within a moving window frame (2 m) across the whole x-axis value range and then linearly interpolated to the x-axis value at each quadrat. Solid lines represent the linear regression curve. **(A)** N_{10}, density of stems with DBH > 10 cm (trees·ha^{-1}). **(B)** Lorey's height, basal area-weighted mean tree height (m). **(C)** AGB, aboveground biomass (Mg·ha^{-1}). The quadrat-wide values were converted to corresponding hectare-wide values.

Table D1. Slope estimates of linear models of each quadrat-level forest structure metrics to the wind speed correction factor, with p-values in parentheses. N.S.: non-significant ($p > 0.05$). N_{10}: stem density (DBH > 10 cm). Lorey's height: basal area-weighted mean tree height. AGB: aboveground biomass.

N_{10} (trees·ha^{-1})	5.37 (< 0.001)
Lorey's height (m)	-0.012 (< 0.001)
AGB (Mg·ha^{-1})	-0.12 (N. S.)

CHAPTER 3: Detecting Natural Disturbances in Tropical Forests Using Sentinel-1 SAR Data: a Test in French Guiana

In preparation, to be submitted to *Remote Sensing of Environment*.

This paper describes the synthetic aperture radar (SAR) data set, collected by Sentinel-1 satellite, with high temporal and spatial coverage, and previously treated with an algorithm based on the shadowing effect of SAR data to detect deforestation patches (Bouvet et al., 2018). In this paper, we present a protocol to further process this data set using GIS tools, in order to select a subset of disturbance events that are considered to be due to natural causes and not human activities, and describe the spatial pattern and temporal dynamics of natural deforestation patches in French Guiana from 2016 to 2019. This work contributes to answer **Question 3**.

Authors: E-Ping Rau[a], Nicolas Labrière[a], Marie Ballère[b], Alexandre Bouvet[b], Thierry Koleck[bc], Pierre Joubert[d], Jérôme Chave[a*]

[a] Laboratoire Évolution et Diversité Biologique (UMR5174) Bâtiment 4R1, 118 route de Narbonne, 31062 Toulouse cedex 9, France

[b] Centre d'Études Spatiales de la Biosphère, Rond-Point du Professeur Francis Cambou, 31400 Toulouse, France

[c] Centre National d'Études Spatiales - Centre Spatiale de Toulouse, 18 avenue Édouard Belin, 31401 Toulouse cedex 9, France

[d] ONF, Direction Régionale de Guyane, F-97300 Cayenne, France

[*]Corresponding author

Keywords: gap dynamics, precipitation, water deficit, remote sensing, near real-time monitoring

3.1 Abstract

Natural disturbances create forest gaps in a heterogeneous manner, and drive gap dynamics which shapes forest structure, diversity and functioning. Near real-time monitoring of the extent and pattern of natural disturbance in tropical forests is necessary for a better understanding of how they shape tropical forests, over different spatial and temporal scales. especially in light of ongoing changes in natural disturbance regimes due to climate change. Satellite remote sensing provide long-term forest monitoring, but optical images are limited in availability by frequent cloud cover in the tropics. In this study, we used radar data from Sentinel-1 satellites, which have been successfully used for the detection of anthropogenic disturbances, and examined if they could also reliably detect natural disturbance events in French Guiana, in a zone with low level of anthropogenic disturbances delimited using land use data. Compared to Landsat-derived optical data, Sentinel-1 data detected around three times as many natural forest gaps, and both datasets exhibited consistent spatial pattern and size-frequency distribution, even though level of colocation is low between the two datasets. Disturbance level was not found to vary with elevation. Disturbance level was higher in dry seasons, but which could be due to the lagged effects of the wet seasons because of the increase in disturbance level before climatic water deficit rises. In conclusion, this study demonstrated the capacity of Sentinel-1 radar data to detect and characterize fine-scale pattern and dynamics of forest gaps due to natural disturbances, and that this information could enhance our knowledge on large-scale variations in environmental factors control gap dynamics. Future directions include examining the influence of other topographical variables, exploring the possibility of expanding natural disturbance monitoring to the regional level, and using for calibration and validation of vegetation models that simulate the effects of disturbance events.

3.2 Introduction

Tropical forests harbor a high level of biodiversity, and play an essential role in the global biosphere and biogeochemical cycles (Gardner et al., 2010; Mitchard, 2018; Pan et al., 2013). Tropical forests are threatened by deforestation and degradation (Baccini et al., 2017; Bullock et al., 2020), but also by changes in natural disturbance pattern (Franklin et al., 2016; Pugh et al., 2019). While much research concerns the quantification of anthropogenic disturbances in tropical forests, natural disturbances are also important because canopy gaps control both forest structure and composition (Hunter et al., 2015; Shugart, 1984).

Natural canopy openings span a wide range of sizes: individual treefalls can create small gap openings in the forest canopy, while larger forest gaps can be triggered by disturbance events such as storms, tornadoes or landslides. The size and nature of the gaps caused by

natural disturbances are also influenced by topography, soil types and soil moisture content (Belcher et al., 2011; Dupuy et al., 2005; Nicoll et al., 2006; Ruel et al., 1998).

Forest gaps locally create environmental heterogeneity and contrasting opportunities for regeneration, for both light-demanding and share-tolerant species (Chazdon et al., 1996; Van Der Meer et al., 1998). The disturbance dynamics that create a mosaic of forest patches, within which plant recruitment occurs, promotes species coexistence (Jentsch and White, 2019; Kohyama, 1993), and has been advanced as an important factor of why tropical forest tree diversity is high (Connell, 1978; Wright, 2002).

The systematic characterization of the impact of natural disturbances on forests is a notoriously difficult challenge. In the field, it is nearly impossible to monitor the falling of trees over large areas and in near real-time (NRT), that is, with a minimal time lag between the occurrence of disturbance events and their detection. Such a rapid monitoring system, in addition to its practical values for timely adequate management of anthropogenic deforestation and degradation, is also an important tool for detecting more precisely the impact of natural disturbances.

Earth observing satellite imagery has already made a major contribution to forest monitoring. It has been used to monitor patterns and dynamics of natural and anthropogenic disturbance over large areas and at global scale (see e.g. Achard et al., 2010; Bullock et al., 2020; Keenan et al., 2015). With its medium spatial resolution and revisit period (30 m and 16 days, respectively) as well as extensive timespan (optical data continuously collected since 1972), the Landsat program has been pivotal to the development of a continuous monitoring system of forest cover change (Hansen et al., 2016, 2013; Woodcock et al., 2008).

In a recent study conducted by the Joint Research Center (JRC) of the European Commission, the full Landsat archives were reprocessed to produce a detailed characterization of disturbance-related tropical moist forest (TMF) cover change over the last three decades (from 1982 to 2020) (Vancutsem et al., 2021). This data product (henceforth referred to as JRC-TMF) describes the annual transition status of each forest pixel, and provides a valuable context for large degradation and deforestation events. There exist other data products with a sub-monthly temporal resolution, based on optical satellites, but since tropical forests are frequently occluded by clouds and haze, NRT monitoring cannot be achieved with optical-based satellite data. Non-optical satellites, such as synthetic aperture radar (SAR), offer a promising alternative.

SAR transmits microwave-length radar pulses and receives the backscattered radiation signal (Kirscht and Rinke, 1998). This technology is operational under all meteorological conditions (Balzter, 2001), and has been used to detect and map forest disturbance events at a large scale (Reiche et al., 2016). The application of SAR data in NRT forest disturbance

monitoring has thus far been limited, due to the difficulty of radar data processing and interpretation, as well as the incomplete spatial or temporal coverage of past SAR missions (Bouvet et al., 2018; Reiche et al., 2016).

The deployment of the two Sentinel-1 satellites by the European Space Agency (ESA) since 2014 is a new opportunity for NRT forest monitoring. Sentinel-1 satellites are equipped with C-band (wavelength 7.5 - 3.75 cm) SAR instruments, have global coverage, shorter revisit period than Landsat (6 to 12 days), and high spatial resolution (10 m). C-band backscatter from the disturbed area is composed of multiple components, including the ground backscatter attenuated by the canopy layer, and the backscatter from the canopy, which are affected by multiple factors of the surface conditions, such as 3D vegetation structure, canopy or soil moisture content, surface roughness, and topography (Askne et al., 1999; Pulliainen et al., 1999). Thus, Sentinel-1 is a good candidate to NRT monitoring of tropical deforestation (Reiche et al., 2021). However, deforested or degraded areas are not necessarily characterized by a step change of backscatter.

Recently, a new gap detection algorithm has been developed using Sentinel-1 data (Ballère et al., 2021; Bouvet et al., 2018). This method does not rely on absolute backscatter intensity to detect gap formation, but is based on the detection of SAR shadowing. Shadowing occurs in SAR images due to the side-looking characteristics of SAR systems, which create areas that are blocked by higher objects and that cannot be reached by any radar pulse: these obstacles could be topographical features such as mountain peaks, but could also be edges between forest and non-forest areas. When a forest patch is deforested, shadows appear or disappear at some of its edges, and are characterized by a sharp decrease in the backscatter across the forest edge. As this signal reflects structural change, it is expected to be more persistent and less temporally variable than the level of backscatter within the deforested area, and can thus be used as an indicator of the anthropogenic or natural loss of forest cover. This method has been successfully tested and validated in Peru (Bouvet et al., 2018) and in French Guiana (Ballère et al., 2021) for anthropogenic deforestation detection.

In this study, we explore whether the Sentinel-1 SAR data product could be used to investigate fine-scale spatiotemporal patterns of forest gaps caused by natural disturbances in old-growth forests. We contrast the Sentinel-1 SAR product with the Landsat-derived JRC-TMF product. Specifically, we asked the following questions: 1) How well do the spatial patterns of natural forest gaps detected by Sentinel-1 match those of the JRC-TMF product? 2) What is the size distribution of natural forest gaps? 3) What is the temporal trend of natural forest gaps in the Sentinel-1 NRT analysis?

3.3 Methods

3.3.1 Study site

French Guiana is a French overseas territory situated in equatorial South America, adjacent to Suriname and Brazil. Its surface area totals 83,534 km^2, approximately 95% of which is covered by old-growth forest (Keenan et al., 2015). Inselberg features (isolated rock hills rising above the surrounding forest-covered lowlands) are common, due to its geographical location within the Guiana Shield. French Guiana is part of the Amazon biome, has a tropical rainforest climate (Beck et al., 2018), with a long wet season from December to June (rainfall from 250 to 550 mm per month) and a dry season from July to November (100 to 180 mm of rainfall per month). A minor dry season with reduced rainfall (170 to 370 mm per month) sometimes marks the period around March for approximately one and a half months, with considerable interannual variability (Bonal et al., 2008). The main causes of anthropogenic deforestation are smallholder agriculture, forest exploitation (e.g. selective logging, road building), and most notably gold mining (mostly alluvial or in steep valleys) (Alvarez-Berríos and Mitchell Aide, 2015; Rahm et al., 2017). Although tropical cyclones do not affect French Guiana, studies have shown that strong wind caused by events such as downburst storms is an important disturbance agent in the northwestern and central Amazon (Negrón-Juárez et al., 2018, 2017; Peterson et al., 2019), and could be an important driver of biomass, diversity and functional patterns of the Amazonian forest (Magnabosco Marra et al., 2018, 2014). However, the extent to which wind disturbance affects northeastern Amazonian forests in the Guiana Shield region remains unclear. Elevation data are available for the entire extent of French Guiana from the SRTM 1 Arc-Second Global data product (tiles of 2–5°N, 53–55°W), at a resolution of 1 arc-second (approximately 30 meters) (USGS, 2015).

3.3.2 Forest gaps detected by the Sentinel-1 SAR time series

Sentinel-1 SAR time series were processed as in Ballère et al. (2021) to produce a raster data of disturbance events for the entire French Guiana at a 10-m scale (hereafter referred to as the S1 dataset). The S1 dataset contains all pixels detected as having experienced disturbance from January 1st, 2016 to December 31st, 2019. The value of each pixel is its time of disturbance. Originally in number of days since April 3rd 2014, the date of the Sentinel-1A satellite launch, it was adjusted to the number of days since January 1st, 2016 in this study for clarity. The S1 dataset has already been used for the near real-time detection of anthropogenic disturbances in French Guiana, and showed high detection accuracy for deforestation events larger than 0.2 ha (i.e. 20 S1 pixels) during validation (Ballère et al., 2021).

We used the *clump* function in the *raster* R package (Hijmans, 2020) to create a raster layer of forest gaps for the S1 dataset, where contiguous S1 pixels were grouped into the same gap and assigned a unique number. We then converted the raster layer into a vector layer containing polygons that each represent a forest gap . For each gap, we calculated its area (m^2, converted to hectares), start date (earliest disturbance date in all pixels), finish date (latest disturbance date in all pixels), median date (median value of disturbance date in all pixels), and mean elevation (m).

3.3.3 Forest gaps detected by the Landsat-derived tropical moist forest cover data

For the Landsat-derived JRC-TMF data product (Vancutsem et al., 2021), tropical moist forest (TMF) is defined as all closed forests in the humid tropics with two main forest types, the tropical rain forest and the tropical moist deciduous forest (Grainger, 1993).

The JRC-TMF dataset contains raster layers that depict the spatial distribution and status of the TMFs, with three data layers important for the purpose of this study. The "Transition map" layers summarize the sequential forest cover change of each TMF pixel at the end of the latest observation period, including undisturbed forests, forest degradation (short-term disturbances due to either natural or anthropogenic causes), deforestation (long-term conversion of forest to non-forest cover) and non-forest cover (permanent or seasonal water body, non-forest vegetation or non-vegetation cover such as road or buildings). The "Degradation year" and "Deforestation year" layers show the year a pixel has been degraded or deforested for the first time, respectively. A more detailed description of the data layers in the JRC-TMF dataset can be found in Appendix A (see Supplementary information).

In this study, we acquired the JRC-TMF dataset for the 10° × 10° tile encompassing French Guiana (10 N, 60 W). To compare the JRC-TMF dataset and the S1 dataset over the same period, we retained only forest gaps that have been created due to disturbance during the 2016–2019 period. To this end, we first created a raster layer that included all disturbed pixels (the union of degraded and deforested pixels) in QGIS, and used the *clump* function in the *raster* R package (Hijmans, 2020) to create a raster layer of forest gaps for the JRC-TMF dataset, where contiguous JRC-TMF pixels were grouped into the same gap and assigned a unique patch number. We then converted the raster layer into a vector layer containing polygons that each represent a forest gap. Out of these gaps, we retained those that contained only forest degradation or deforestation pixels from 2016 to 2019. For each gap, we calculated its area (hectares), start year (earliest disturbance year in all pixels), finish year

(latest disturbance year in all pixels), median year (median value of disturbance year in all pixels), and mean elevation (m).

3.3.4 Criteria for retention of natural forest gaps

In order to retain only forest gaps caused by natural disturbances from those obtained in the S1 and the JRC-TMF dataset, we delimited a study zone using the land use summary data of French Guiana in 2015 (data and metadata available at: https://catalogue.geoguyane.fr/geonetwork/srv/fre/catalog.search#/metadata/3d681d4f-b8bd-48b2-80d2-04a215a8a099). The land use summary data depict areas with verified human activities, including such as agriculture, logging and gold mining. We added a 5-km buffer around all areas of human activities, assuming that human activities are spatially aggregated, and thus mainly occur near other existing human-disturbed areas. By visually observing this zone of frequent human activities, we identified and manually delineated two study zones that were deemed to be far from most anthropogenic disturbances, one in the north and the other in the south of the territory, and excluded the S1 and JRC-TMF gaps located outside of the study zone. The study zone has a total area of ca. 25,690 km^2 (12,100 km^2 in the north, 13,590 km^2 in the south), around one fourth of the total area of French Guiana (Figure 1).

We also excluded gaps smaller than 0.2 hectare, based on the reasoning that these smallest detected gaps run a higher risk of being misidentifications or artifacts (false positives). The choice of 0.2 hectare as a size threshold was based on the reported minimum detected surface area for disturbance patches for the S1 dataset (Ballère et al., 2021).

A preliminary visual inspection of the retained gaps in the study zone revealed that a small proportion of them have distinctly different morphology from the majority of the gaps. They have irregular shapes, with areas larger than 0.5 hectare, and situated near or within topographical features that correspond to non-vegetated surfaces such as hills, inselbergs or water bodies. In addition to representing the non-vegetated surfaces themselves, we theorized that these gaps could also be disturbances occurring in the transition zone between the forest and the non-vegetated surfaces, or artifacts when the shadowing method could not accurately detect forest edges within a primarily non-forest backdrop. Although the pattern and dynamics of these disturbance events are also interesting in their own right, they are likely distinct from the gap dynamics driven by natural disturbances in the interior of an intact forest. We therefore chose to exclude them from the analysis in the current study, by selecting all the “non-forest cover” pixels in the Transition map layer of the JRC-TMF product, and adding a 300-m buffer (distance of five JRC-TMF pixels) around the non-forest pixels to create a mask of “non-forest cover” regions, and excluded all gaps overlapping with the non-

forest mask. We expect that the majority of the retained forest gaps will be caused by natural disturbances. All data layers were projected to the WGS 84 / UTM zone 22N Coordinate Reference System (EPSG:32622) before processing in QGIS (QGIS.org, 2021). A detailed description of the forest gap selection procedure in QGIS and R can be found in Appendix B.

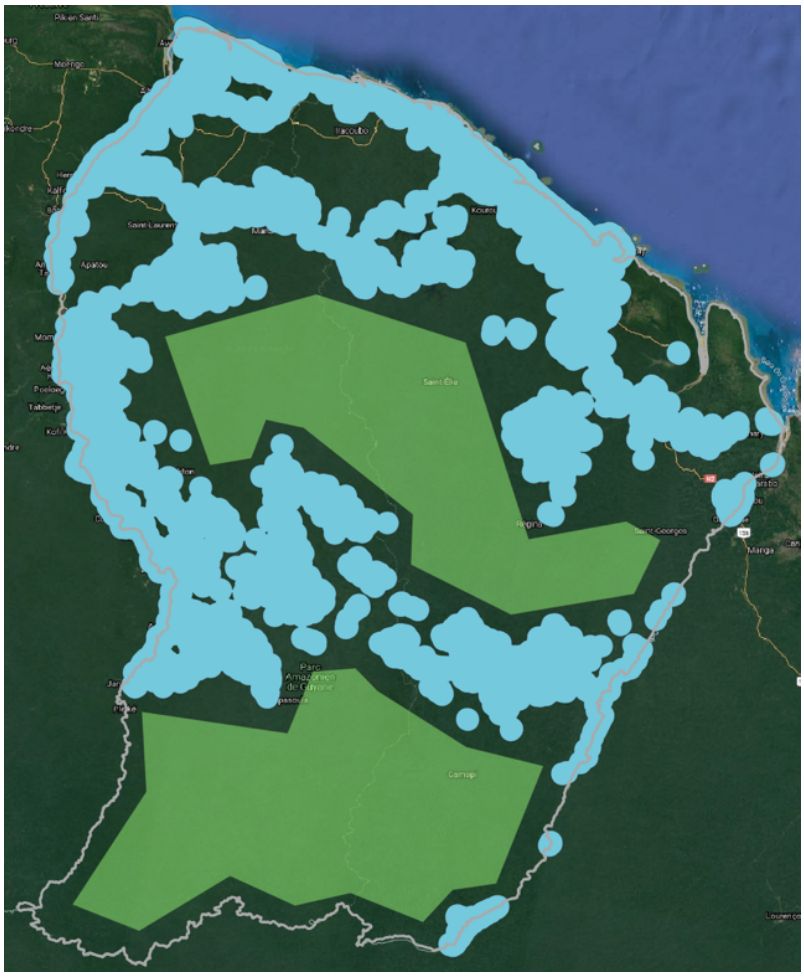

Figure 1. The entire extent of French Guiana (gray line), the region of frequent anthropogenic disturbance activities (blue) and the study zone (green). Underlying layer: Google Satellite Hybrid.

3.3.5 Comparison of natural forest gaps detected in S1 and JRC-TMF datasets

We visually examined and compared the spatial patterns of the retained forest gaps detected by the S1 and the JRC-TMF dataset, and quantified the proportion of total gaps and large gaps (size ≥ 0.5 ha) that overlap in the two datasets. For both datasets, we also quantified the size distribution of all gaps in log-log scales.

3.3.6 Influence of topography and temporal dynamics on natural forest gaps

For the natural forest gaps detected in the S1 dataset, we quantified the disturbed-to-total-area ratio by elevation classes in 50-m bins, and performed linear models to examine if there was a significant relationship between elevation (midpoint value of each elevation class) and disturbed-to-total-area ratio, for both study zones separately as well as combined.

We also quantified the monthly dynamics of total disturbed areas in relation to that of the following climatic variables: precipitation, climatic water deficit (CWD, mm), and mean hourly maximum wind speed ($m \cdot s^{-1}$). We retrieved precipitation data from the 3IMERG multi-satellite monthly time series, and surface maximum wind speed data from the MERRA-2 model-generated hourly time series (detailed description available in Appendix A). For both dataset, we extracted data for the 2014–2019 period, in order to be able to examine if lagged effect of climatic conditions from previous years could contribute to the temporal pattern of disturbance during the study period. We extracted values for the extent of both the north and the south study zone, and calculated an average monthly precipitation over the two study zones.

CWD results from the difference between evapotranspiration and precipitation: assuming monthly evapotranspiration level is around 100 mm, CWD = 0 when monthly precipitation > 100 mm, and becomes progressively negative as monthly precipitation decreases below that threshold. As such, we estimated CWD in this study as follows: supposing CWD_1 (CWD at January 1st) = 0 and equal-length months of 30 days, CWD_i (CWD at day i starting from January 1st) = $\text{Min}[0, CWD_{(i-1)} + (P_i - 100)/30]$, where P_i is the monthly precipitation of the month containing day i. We then converted daily CWD to mean monthly CWD by calculating its arithmetic mean. We hypothesized that higher soil water content during the wet season would weaken root anchorage, leading to higher probability of treefalls and consequently more number and total area of forest gaps (Hales and Miniat, 2017; Osman and Barakbah, 2006).

3.4 Results

3.4.1 Comparison of natural forest gaps detected by the S1 and JRC-TMF datasets

A total of 3,524 S1 (area: 1,019.2 ha, or 0.039% of the study zone) and 1,008 JRC-TMF gaps (area: 382.7 ha, or 0.015% of the study zone) were retained (Table 1). Thus, S1 detected about three times as many gaps as JRC-TMF, and the total disturbed area was also about three times higher. The South study zone contained both a higher density of gaps and a higher proportion of disturbed area to total area (Table 1). 172 large gaps (size ≥ 0.5 ha) were detected in the S1 dataset, representing 5% of total gap numbers and 12% of total gap area, while 141 large gaps were detected in the JRC-TMF dataset, representing 13% of total gap numbers and 27% of total gap area. The JRC-TMF dataset thus detected a higher proportion of large forest gaps than the S1 dataset.

Comparing S1 and JRC-TMF gap location, very few gaps were collocated: out of all 3,524 gaps in the S1 dataset, only 59 had an overlap with a JRC-TMF gap (ca. 2%). The percentage rose to ca. 16% for large gaps (size ≥ 0.5 ha): out of all 172 large gaps in the S1 dataset, 27 had an overlap with a JRC-TMF gap.

Most of the forest gaps exhibited a scattered distribution with no apparent aggregation (Figure 2). Two regions in the study zone showed noticeably different spatial patterns of the forest gaps between the two datasets (see Appendix C for further detail).

The median S1 gap size was 0.25 ha, versus 0.27 ha for JRC-TMF gaps. Gap size showed a power law distribution: the log-log gap size-frequency curve had a slope of ca. -2.8 (Figure 3). The shapefiles of the retained gaps in both datasets, the shapefile of the study zone, as well as the raster file of the non-forest mask are provided as Supplementary Material.

Table 1. Basic summary statistics of the study zone area and the number and total area of forest gaps in both datasets during the 2016–2019 period.

		Total	North	South
Study zone area (km^2)		25690	12100	13590
S1	Number of gaps	3,524 (0.14 per km^2)	1,445 (0.12 per km^2)	2,079 (0.15 per km^2)
	Total area (ha)	1,019.2 (0.039%)	425.4 (0.035%)	593.8 (0.046%)
JRC-TMF	Number of gaps	1,008 (0.04 per km^2)	259 (0.02 per km^2)	749 (0.06 per km^2)
	Total area (ha)	382.7 (0.015%)	98.8 (0.008%)	283.9 (0.021%)

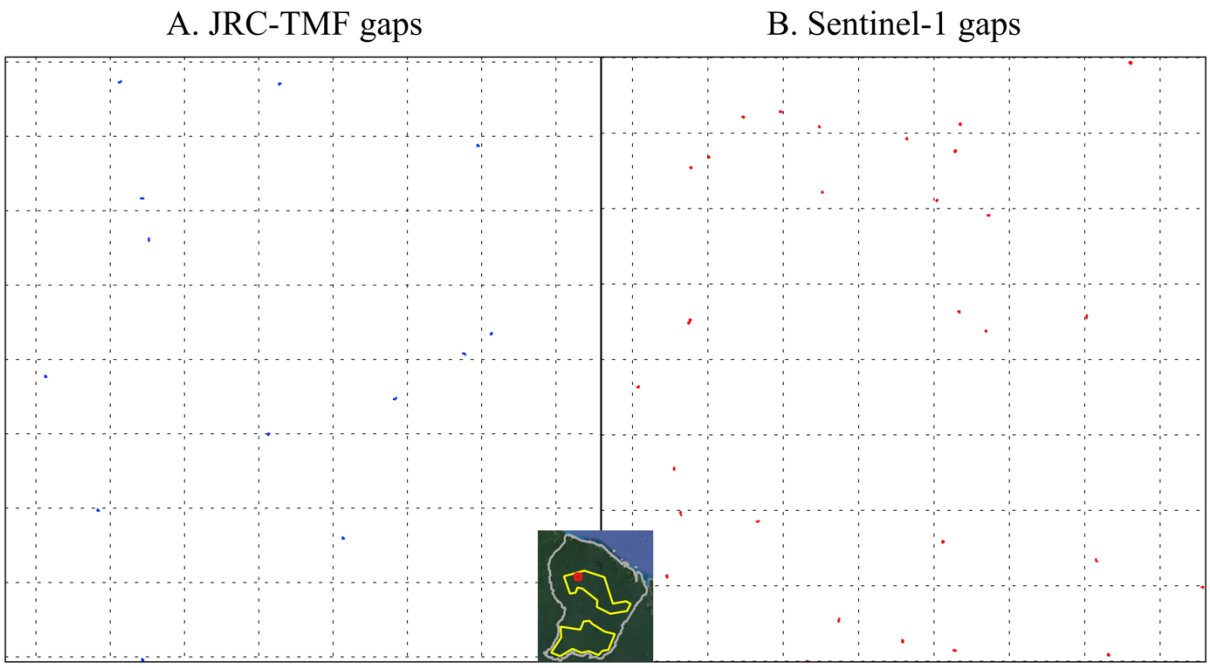

Figure 2. Example of scattered-distributed forest gaps in (A) JRC-TMF (left) and (B) Sentinel-1 (right) datasets. Gap colocation is low. Each dashed grid line is 2 km apart. The inset shows the extent of French Guiana (gray), study zone (yellow), and the extent of the example zone in the panels (ca. 16 km × 16 km).

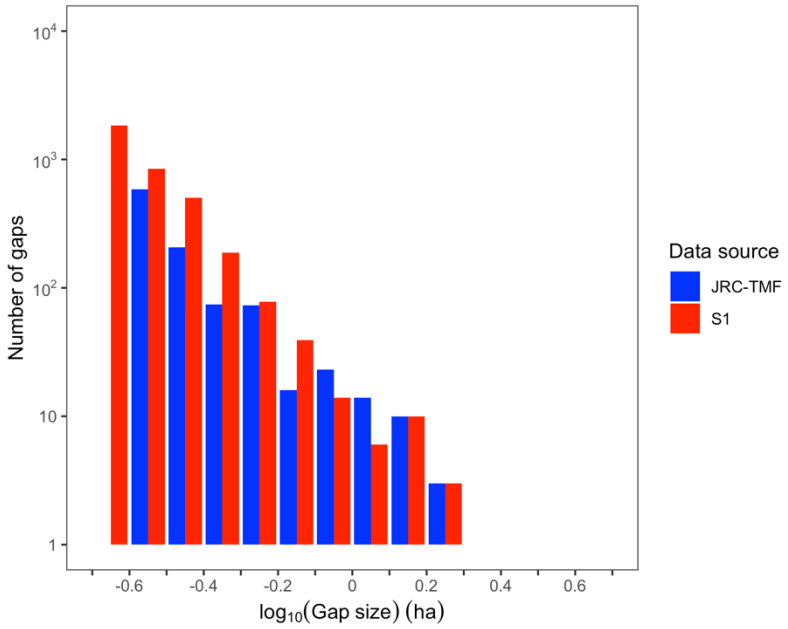

Figure 3. Size-frequency distribution of forest gaps in both datasets in log-log scale (bins of $10^{0.1}$ for gap size), over the study zone during the 2016–2019 period.

3.4.2 Influence of topography and temporal dynamics of natural forest gaps

The disturbed-to-total-area ratio did not show any clear trend with increasing elevation (Figure 4): linear models showed that the elevation effect was non-significant for the north study zone ($p = 0.15$), the south study zone ($p = 0.10$), and for both zones combined ($p = 0.25$). Over the 2016–2019 period, annual disturbed areas ranged from 185.6 to 380.7 hectares (254.8 ha on average) in the S1 dataset, and annual area fraction of new forest gaps ranged from 0.007% to 0.014%. The time series of the monthly total disturbed area showed that disturbances predominantly occurred in the second half of the year, during the dry season (Figure 5). The only exception was March to May in 2017, when disturbances peaked during the wet season, especially in the south zone. The monthly dynamics of climatic water deficit (CWD, mm) showed that at each disturbance peak, disturbance level started increasing before CWD started decreasing (Figure 6). The monthly dynamics of maximum wind speed was not observed to have clear trend with disturbance level (Figure 7).

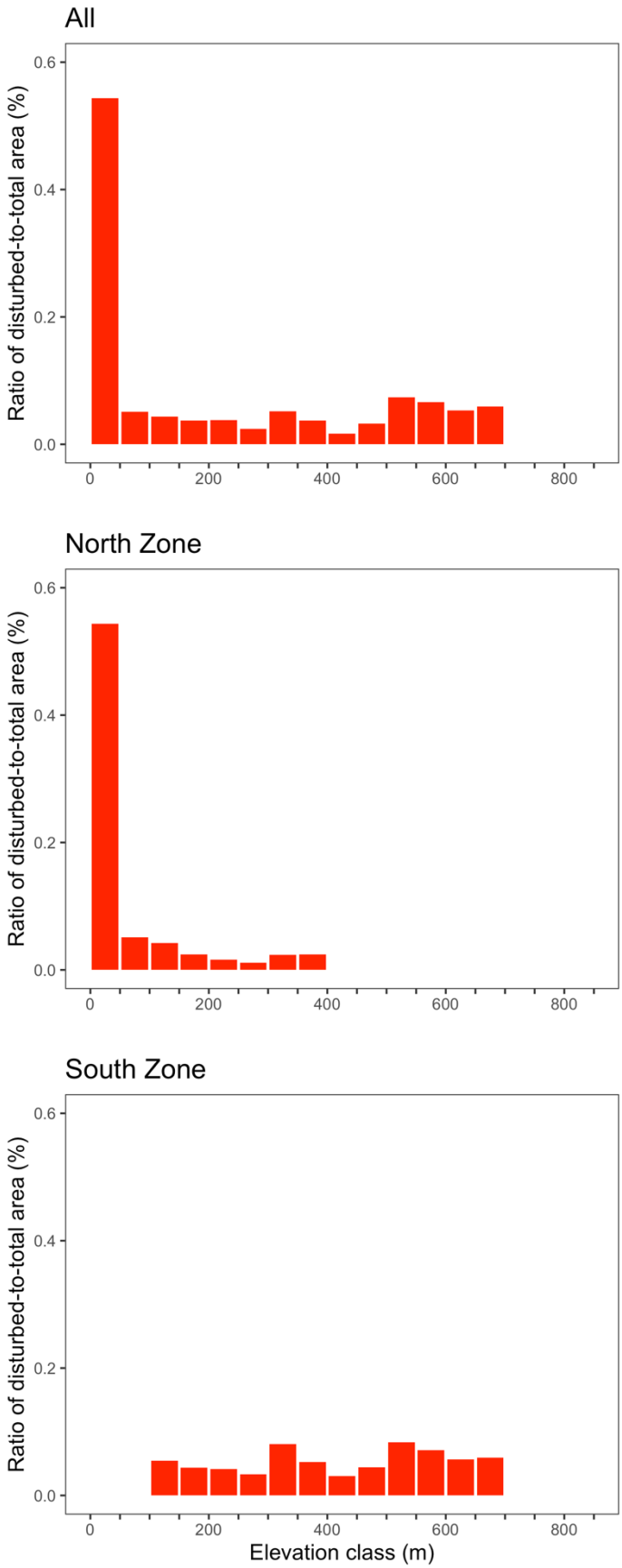

Figure 4. Disturbed-to-total-area ratio by elevation class (50-m bins) for gaps from the S1 dataset over the study zone during the 2016–2019 period.

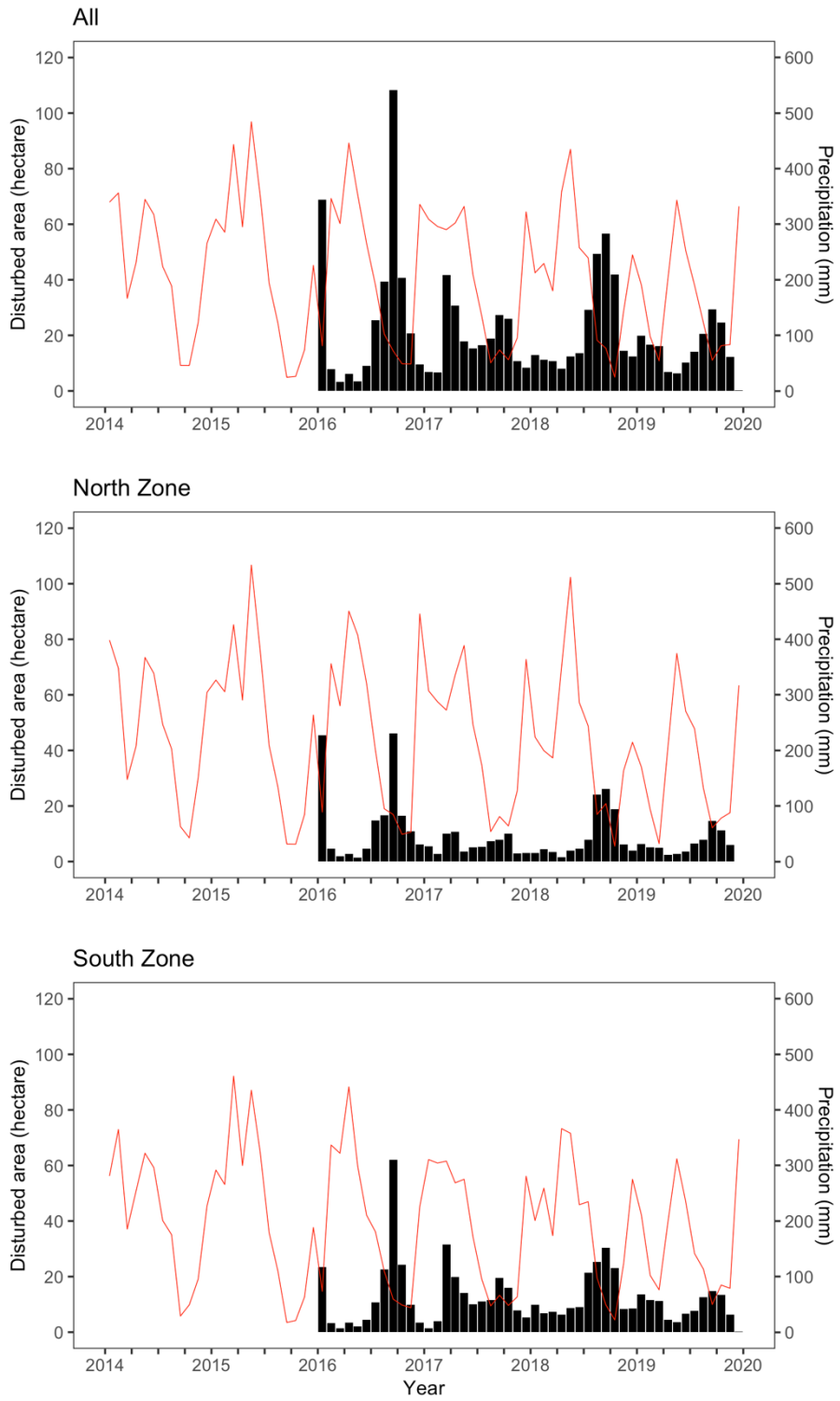

Figure 5. Monthly dynamics of precipitation (mm) and total disturbed area for gaps from the S1 dataset over the study zone during the 2016–2019 period. Each bar represents monthly total disturbed area, and the red curve represents monthly total precipitation.

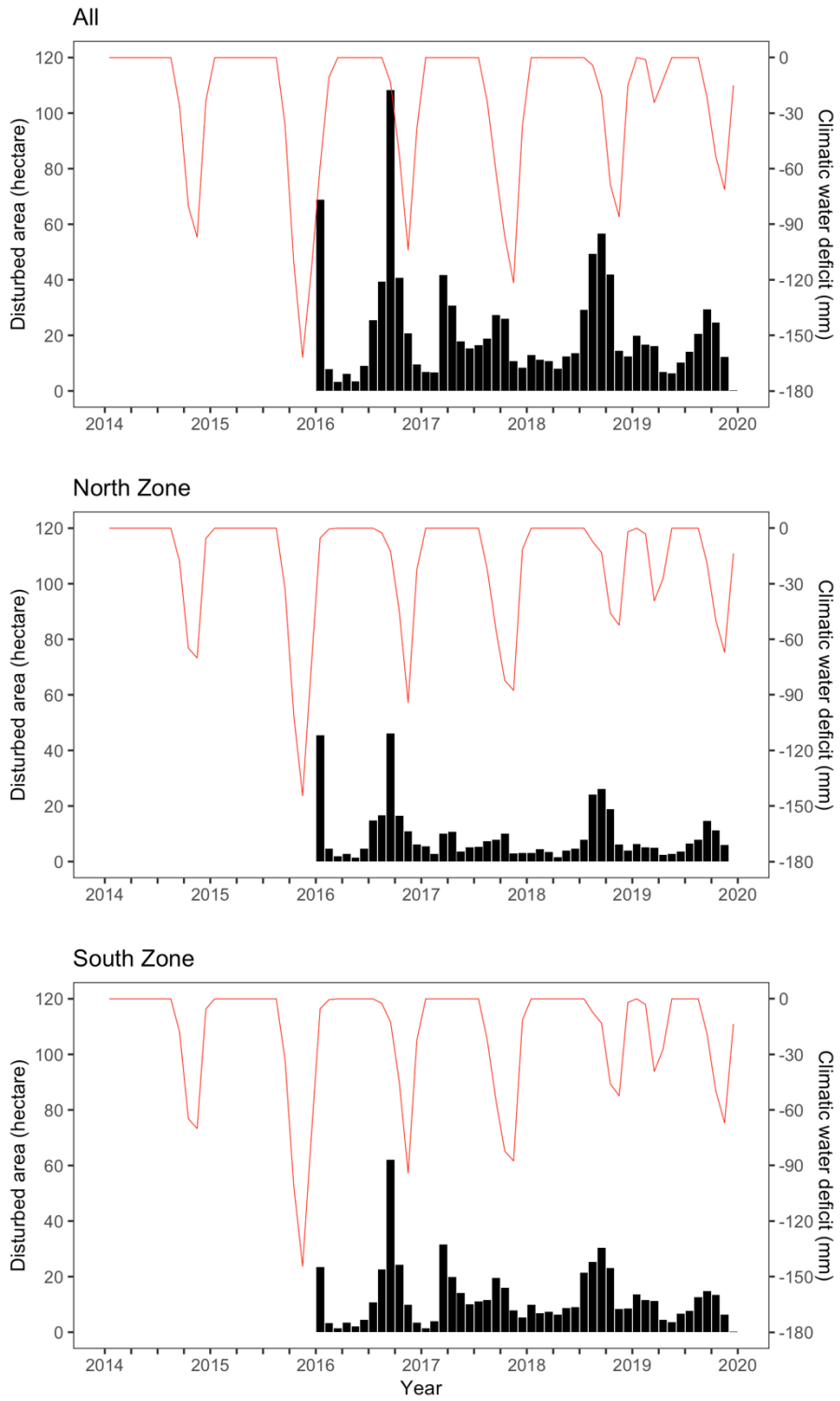

Figure 6. Monthly dynamics of climatic water deficit (mm) and total disturbed area for gaps from the S1 dataset over the study zone during the 2016–2019 period. Each bar represents monthly total disturbed area, and the red curve represents monthly total precipitation.

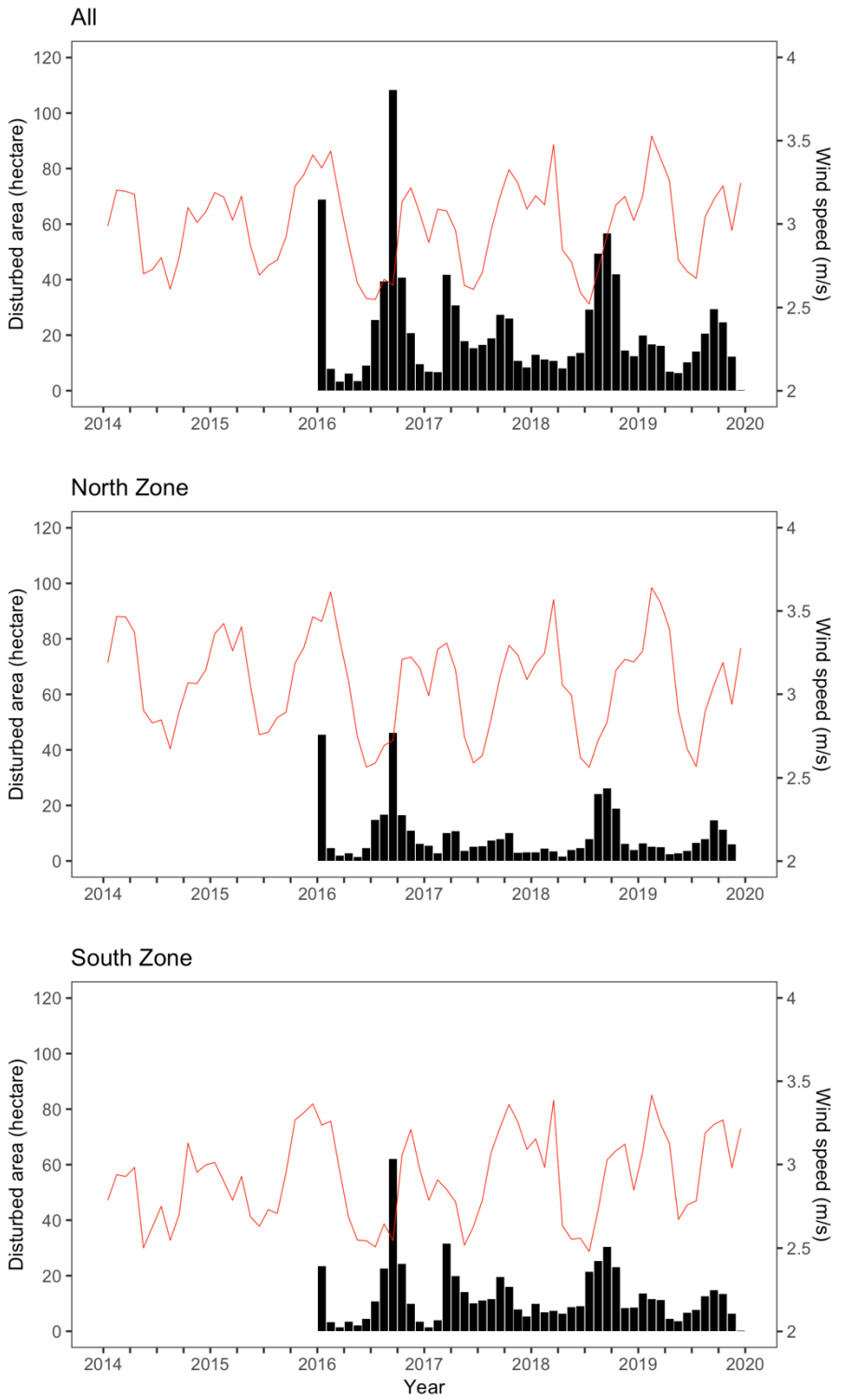

Figure 7. Monthly dynamics of average hourly maximum wind speed ($m \cdot s^{-1}$) and total disturbed area for gaps from the S1 dataset over the study zone during the 2016–2019 period. Each bar represents monthly total disturbed area, and the red curve represents monthly total precipitation.

3.5 Discussions

In this study, we explored the potential of Sentinel-1 for detection of forest gaps caused by natural disturbances. A product derived from Sentinel-1 SAR data and a recently published Landsat-derived tropical moist forest cover data product were processed along historical forest cover and land use data to obtain records of forest gaps likely to be natural in origin. We found that although gap colocation was very low between the two datasets, their respective gap size distribution followed a similar power law relationship for gaps above 0.2 hectare. Therefore, although the comparison of data products is not a real ground truthing exercise, it does bring confidence that the gap opening events detected with the new Sentinel-1 product are not artifacts caused by the "shadowing" algorithm. The disturbed-to-total-area ratio did not show significant trends with increasing altitude, but the temporal dynamics of natural forest gaps revealed a clear pattern of higher natural disturbance level during dry seasons: further examination of the timing of the increase in disturbance level suggested that it could be due to the delayed effect of the wet seasons, which weaken root anchorage and increase treefall risk, rather than the direct effect of the increased water stress during dry seasons.

3.5.1 Comparison of spatial patterns of natural forest gaps detected by the two datasets

Visually, the retained forest gaps in the two datasets exhibited globally similar spatial pattern, with low level of aggregation. Compared to the JRC-TMF dataset, the Sentinel-1 dataset detected three times as many natural forest gaps. This can partly be explained by the 0.2-ha size threshold, based on the threshold above which the shadowing method detected forest gaps with high confidence in Sentinel-1 data, which effectively excluded all the 1- and 2-pixel gaps (covering 0.09 and 0.18 ha, respectively) in the original JRC-TMF dataset. Since 3-pixel gaps are 0.27 hectare, gaps with a size between 0.2 and 0.26 hectare (above 2 pixels and below 3 pixels) size class cannot be quantified correctly by the JRC-TMF dataset. This demonstrates the advantage of the finer spatial resolution of the Sentinel-1 satellite data.

Although only around 2% of S1 gaps overall were collocated with JRC-TMF ones, for most of these pairs disturbances occurred during the same year (coarsest temporal resolution from the JRC-TMF annual dataset). Collocation was higher (ca. 15% of all the S1 gaps) for large gaps (size $\geq$ 0.5 ha): this lends confidence for the capability of the S1 to accurately detect large natural forest gaps.

The lack of highly-aggregated clusters of gaps or linearly-shaped gaps along rivers in the retained dataset, which would strongly suggest anthropogenic disturbances such as agriculture

or gold-mining, demonstrated that the exclusion mask based on past survey of human activities was a reliable basis on which to delimit regions with low levels of anthropogenic disturbance. The north-central part of the south zone contained an unusually high density of JRC-TMF patches (Appendix C, Figure C2): this anomaly warrants further inspection, but it is suspected that those areas are actually under the influence of anthropogenic disturbances as well, possibly due to proximity to the town of Maripasoula.

3.5.2 Gap size distribution of natural forest gaps

The gap size distribution of both datasets followed a similar power law relationship, meaning that log(number of gaps) and log(gap size) exhibited a linear relationship, with the slope estimated around -2.9. Past quantifications of forest gap size distribution in Amazonia using a combination of plot data, airborne Lidar data and Landsat satellite data reported a slope value of -2.5 (Espírito-Santo et al., 2014), while another study using airborne Lidar data at two Brazilian Amazonian sites reported slope values of the log-log linear relationship ranging from 1.88–2.16 to 2.86–3.26, depending on how gaps were defined (Hunter et al., 2015). The slope of the log-log gap size-frequency distribution obtained in this study is thus consistent with past reported values. This would support the hypothesis that the scaling component of forest gap size distribution is invariable across differing environmental and floristic conditions, and that gap scaling could reflect convergent filling rules of the three-dimensional space in forest canopy (Asner et al., 2013). Although few studies have attempted to explain the biological or ecological causes of the gap scaling relationship, they likely involve light limitation and asymmetrical light competition, as well as canopy responses to treefalls (for instance, how initial treefall propagates in the canopy and causes secondary treefall).

The detection of intermediate-sized natural forest gaps ($10^{-0.7}$–$10^{0.4}$ or ca. 0.2–2.5 ha) by Sentinel-1 satellites can be contrasted to the study by Espírito-Santo et al. (2014), where only Lidar data were used for the detection of intermediate gaps (10^{-1}–10^{1} ha), and where Landsat satellite data were used only for detection of large gaps caused by blowdown events (≥ 5 ha). This suggests that the Sentinel-1 satellite data could be used for forest gap detection over a wider range of spatial scales than Landsat-derived optical satellite data, and that they could be complementary to airborne Lidar data for the detection of intermediate-sized forest gaps, due to their larger spatial coverage and continuous temporal coverage.

The study of natural forest gaps was limited here to gaps larger than 0.2 hectare. Natural forest gaps can actually be much smaller, and airborne LiDAR-based studies are typically able to detect gaps down to 100 m^2 (0.01 ha) (Goulamoussène et al., 2017), while plot surveys

report gaps down to 10 m^2 (10^{-3} ha) (Espírito-Santo et al., 2014). The annual area fraction of new forest gaps reported in this study (0.007–0.014%) is several orders of magnitude smaller than most documented values (1% in Goulamoussène et al. (2017), 1.7–5.5% in Hunter et al. (2015), 1.5–11.18% in Dalagnol et al. (2021)). This is likely due to our inability to detect very small disturbance events (< 0.2 ha). Extrapolating the number of gaps to the 0.01–0.2 ha range (0.01 ha being the pixel size of Sentinel-1 data) using the slope of the modeled gap size distribution (ca. -2.8, using a log-log linear model), 1.8×10^7 additional forest gaps (covering an additional area of ca. 1.7×10^3 km^2) should be accounted for during the three-year period. Adding this extrapolated number to our first estimate, the annual total area of new forest gaps is estimated to be 568 km^2 on average. This would represent ca. 2.2% of the total study zone area, a value more in line with the literature (Hunter et al., 2015).

3.5.3 Temporal trend of natural forest gaps

Few studies in the literature explored the temporal and seasonal dimensions of forest gap dynamics in tropical forests (but see Dalagnol et al., 2021). Thanks to the fine temporal resolution of Sentinel-1 data, we were able to quantify monthly dynamics of natural forest gaps over a large spatial extent. Our results clearly showed that natural disturbances, both in terms of occurrences and spatial extent, were much higher during the dry season compared to the wet one, contrary to our original hypothesis that there would be higher disturbance level during wet season.

Many abiotic factors could contribute to the seasonality of tree mortality and gap formation. Higher level of precipitation brings higher soil water content, which could lead to weakened root anchorage and increased mortality risk due to tree overturning. In support of this, a study has observed that tree mortality in Central Amazonia was higher in wetter months, even in years with overall drought (Aleixo et al., 2019). On the other hand, higher water deficit in dry seasons could increase competition for water, and thereby also increase mortality due to heightened risk of hydraulic failure (McDowell et al., 2018). In support of this, a study using multiple airborne Lidar observations across the Amazon found that higher water deficit was related to higher gap fractions (Dalagnol et al., 2021). However, as our results demonstrated, snapshot observations of disturbance level could produce correlations that do not reflect actual causal relationship, and continuous observations of fine-scale timing of disturbance events is necessary to uncover the possible environmental factors driving the dynamics of natural disturbance level.

One important aspect to consider about seasonality of disturbance is that extreme environmental conditions and weather events do not always trigger immediate mortality, but

could cause delayed effects of increase in mortality (Aleixo et al., 2019): indeed, we observed that within the monthly dynamics, disturbance level started increasing before climatic water deficit increased, which would support the hypothesis that the higher disturbance level in dry seasons is caused by the wet seasons that precede them, rather by the environmental condition of the dry seasons themselves. This result highlighted that single-date remote sensing observations of disturbance could fail to reveal correlations that reflect actual causal link between environmental factors and natural disturbance dynamics, and continuous observations are necessary to capture the fine-scale disturbance dynamics in relation to environmental changes with higher confidence.

Wind is another important disturbance agent, and could often be the determining factor of the moment treefall and tree death actually occur for a tree, even when other underlying causes (e.g., water stress, disease, senescence) contribute to its death (Aleixo et al., 2019). However, in this study, disturbance level was not found to be related to monthly average of hourly maximum wind speed. This may be due to the long-term climatic data used in this study, which do not sufficiently capture locally wind speed maximum actually controlling treefall probability, and that more fine-scale estimation of wind speed will be necessary to uncover its relationship with large-scale disturbance level. Another possibility is that wind acts primarily on a spatial scale that is under the 0.2 ha size threshold used in this study, and therefore many gaps exhibiting seasonality due to wind speed dynamics were filtered out by the current method (see, e.g., Dalagnol et al., 2021).

The two disturbance peaks that did not follow the general pattern of higher disturbances during the dry season, one in January 2016 and the other one in March-April 2017 (especially in the south study zone), as well as the exceptionally high disturbance peak in September 2016 during the wet season, also deserves attention. One hypothesis is that these exceptional peaks could be caused by the drought effect of the 2015/16 El Niño, which could be directly responsible for the peaks in January 2016 peak and September 2016, and indirectly for the 2017 peak through delayed response to climatic events.

3.5.4 Perspectives

In this study, no significant relationship was found between the occurrence of natural forest gaps and elevation. Dalagnol et al. (2021) also found that topographic predictors did not explain regional-scale variation of gap occurrence in Amazonia: in contrast, soil and hydrological factors such as higher soil fertility, higher water deficit and higher level of flooding or waterlogging have been observed to be related to higher forest gap fractions at the site scale (Goulamoussène et al., 2017) or at the regional scale (Aleixo et al., 2019; Dalagnol

et al., 2021). They did not find significant link between mean wind speed and regional-scale gap fractions, even though wind is acknowledged to be an important disturbance agent in Amazonia (Magnabosco Marra et al., 2018; Negrón-Juárez et al., 2018; Peterson et al., 2019). In the future, one important research direction is thus to investigate how the temporal dynamics of environmental factors such as wind speed, water deficit and flooding/waterlogging correlates with the fine temporal dynamics of forest gaps provided by Sentinel-1 data. In addition, the interaction between multiple factors, such as between wind and topographical factors (e.g., windward vs. leeward slope), or between wind and soil water content, should also be explored as potential factors capable of explaining gap dynamics variability (Goulamoussène et al., 2017).

Information on natural forest gaps detected by Sentinel-1 satellites could also aid validation and development of vegetation models, through the comparison between spatial patterns of forest gaps detected by satellite data and produced by model simulations. In particular, spatial point-pattern analyses seek to explore hypotheses about the links between ecological processes and the patterns they produce (Getzin et al., 2014; Wiegand and Moloney, 2014), and could thus be used to examine if treefall or mortality processes represented in a model (disturbance-induced or otherwise) generate landscape-scale patterns of forest gaps that are consistent with satellite observations.

As a verification of the utility of Sentinel-1 data for natural forest gap detection, this study also provides a crucial first step in the endeavor of extending the gap detection method to an entire region, e.g. Amazonia. For this, the mapping of region-wide land use will be necessary to aid in determining the relevant study zone.

In conclusion, this study demonstrated the utility of Sentinel-1 SAR data to detect natural canopy openings in near real-time, and is therefore a benchmark for establishing a monitoring system for undisturbed tropical forests, potentially over a larger spatial extent. This information could also serve as a basis for future data-model fusion in the study of natural disturbances.

3.6 Acknowledgments and author contributions

This work was supported by the “Investissement d’Avenir” grants managed by the Agence Nationale de la Recherche (CEBA, ref. ANR-10-LABX-25-01; TULIP, ref. ANR-10-LABX-0041; ANAEE-France: ANR-11-INBS-0001).

EPR, JC and NL designed the research; EPR conducted the research; NL, JC, MB, AB and TK provided assistance and inputs in methodology; MB and PJ provided data used for analyses; all authors proofread and edited the paper.

3.7 Supplementary data

Appendix A: detailed dataset description

JRC-TMF dataset

The JRC-TMF dataset includes raster layers that depict the spatial distribution of the TMFs and show the land cover status change of each TMF pixel. The "Transition map - main Classes" and "Transition map - subtypes" layers provide a summary of the sequential forest transition at the end of the latest observation period, classified into general "main classes" and more detailed "subtypes" respectively. The main classes in the Transition Map layer include: 1) undisturbed forests (without any observed disturbance during the period of Landsat monitoring), 2) forest degradation (short-term disturbances, which may be of either natural or anthropogenic causes), 3) deforestation (long-term conversion of forest to non-forest cover), 4) forest regrowth (vegetative growth on a previously deforested pixel), 5) ongoing degradation/forestation (disturbance events initiated since 2018, for which it is not yet possible to determine whether it should be attributed to degradation or deforestation), 6) water body (permanent or seasonal), and 7) other land cover (including non-TMF vegetation such as savannah or shrubland, agriculture, or non-vegetation cover such as road or buildings).

The "Undisturbed and degraded TMF" layer is a simplification of the Transition Map layer, and shows the spatial extent of both undisturbed and degraded tropical moist forests. The "Annual change collection" layers depicts the extent and status of the TMF (degradation, deforestation or regrowth) for each year, with one layer for each year in the observation period. The "Degradation year" and "Deforestation year" layers show the year a pixel has been degraded or deforested for the first time, respectively. Other layers characterize the disturbance duration and intensity, as well as the number of observations. The dataset is freely available at https://forobs.jrc.ec.europa.eu/TMF/, with a user guide that contains detailed technical description of the dataset.

Monthly time series of climatic conditions

Data of monthly dynamics of precipitation (mm) were taken from a single multi-satellite precipitation product, which assimilates data from Global Precipitation Mission (GPM) constellation and other precipitation-relevant satellite passive microwave sensors. The data product was assimilated through version 6 of the Integrated Multi-satellitE Retrievals for GPM (IMERG) unified algorithm, gridded at 0.1° resolution (GPM_3IMERGM; Huffman et al., 2019);. Data of dynamics of monthly average of hourly maximum wind speed ($m \cdot s^{-1}$) were taken from a model-based MERRA-2 data product, which is a global atmospheric reanalysis produced by NASA Global Modeling and Assimilation Office (GMAO) using the Goddard Earth Observing System Model (GEOS) version 5.12.4.

For both climatic variables, we retrieved their time series for the north study zone (extent: 53.5474–52.6025° W, 4.025–4.7281° N) and south study zone (extent: 53.6792–53.1738° W, 2.7067–3.0582° N) separately, from January 1st, 2014 to December 31st, 2019. Data was processed and curated in the Giovanni online data system, which is developed and maintained by the NASA Goddard Earth Sciences Data and Information Services Center. Monthly dynamics time series of the entire study zone was calculated as the average of the time series of the two study zones.

Appendix B: selection procedure of disturbance patches

Preparation of general datasets

1. Set the project projection to WGS84 / UTM Zone 22N (EPSG: 32622) (the zone used for the majority of French Guiana)
2. Project all data layers (S1 disturbance map, JRC-TMF layers, French Guiana contour line, SRTM elevation data, 2015 French Guiana Land Use Summary data) to WGS84 / UTM Zone 22N
3. In R, crop the JRC-TMF layers (Degradation year, Deforestation year, Transition map) to the French Guiana contour

```
contour_guyane = sf::st_read(paste0(path, "contour_guyane_22N.shp"))
degradation_year = raster::raster(paste0(path,
"JRC_TMF_DegradationYear_v1_1982_2020_SAM_ID49_N10_W60_22N.tif"))
degradation_year_cropped = raster::crop(degradation_year, raster::extent(contour_guyane))
degradation_year_masked = raster::mask(degradation_year_cropped, contour _guyane)
raster::writeRaster(degrad_year_masked, paste0(path,
"JRC_TMF_DegradationYear_v1_1982_2020_guyane_22N.tif"), format = "GTiff", overwrite = T)
```

Creation of study zone

1. Create 5-km buffer around the human disturbance zones in the French Guiana Land Use Summary data with the Buffer tool

   [Distance: 5 kilometers]
2. Based on the human disturbance zones, manually draw two polygons for the north and south study zones

   [create columns for features:
   area: $area
   zone: “north” and “south”
   Save as: “study_zone”]

Preparation of the S1 dataset

1. Adjust the time of disturbance from days since April 3rd 2014, (the date of the Sentinel-1A satellite launch) to days since January 1st, 2016 (start of the study period) with Raster Calculator

   [expression: “distmap_guyane_2016_2019@1” - 637]
2. In R, use *clump* function from *raster* package to cluster pixels

```
s1_patch = raster::clump(s1_distmap, directions = 8)
raster::writeRaster(s1_patch, paste0(path, "s1_patch.tif"), format = "GTiff", overwrite = T)
```

3. Load s1_patch.tif
4. Create vector shapefile layer with Vectorize

   [input layer: s1_patch

name of the field to create: patch

Use 8-connectedness: yes]

5. Fix geometries of the polygons with Fix Geometry
6. Ensure that all polygons having the same patch number are merged into one polygon with Dissolve

   [Input layer: s1_patch

   Dissolve field(s): patch]
7. Calculate area of each patch with Field Calculator

   [Output field name: area

   Output field type: Decimal number (real)

   Expression: $area]
8. Calculate mean elevation of each patch with Zonal Statistics

   [Input layer: s1_patch

   Raster layer: SRTM_guyane_2016_2019_22N

   Output column prefix: elev_

   Statistics to calculate: Mean]
9. Calculate start date, finish date and median date of each patch with Zonal Statistics

   [Input layer: s1_patch

   Raster layer: distmap_guyane_2016_2019

   Output column prefix: time_

   Statistics to calculate: Minimum, Maximum, Median]
10. Select patches within the study zone with Select by Location

    [Select features from: s1_patch

    Where the features: are within

    By comparing to the features from: study_zone

    Modify current selection by: creating new selection

    Save to file: s1_patch_selected]
11. Add study zone labels ("north"/"south") with Intersection

    [Input layer: s1_patch_selected

    Overlay layer: study_zone

    Fields to keep from input layer: all

    Fields to keep from overlay layer: zone]
12. Select patches with area ≥ 0.2 ha (2000 m^2) with Select Features Using Expression

    [expression: area >= 2000

    Save to file: s1_patch_selected]

Preparation of the JRC-TMF dataset

1. Adjust the values in the Deforestation year and Degradation year layers to convert all pixel values smaller than 1982 (0 or 2, representing undisturbed pixels) to NULL with Raster Calculator

[expression: (("JRC_TMF_DeforestationYear_v1_1982_2020_guyane_22N@1" >= 1982) *
"JRC_TMF_DeforestationYear_v1_1982_2020_guyane_22N@1") /
("JRC_TMF_DeforestationYear_v1_1982_2020_guyane_22N@1" >= 1982)]

2. In R, combine the adjusted Deforestation year and Degradation year layers to create a mask representing all disturbed pixels by 1, and undisturbed pixels by 0

```
degradation_year_adj[which(degradation_year_adj [, ] > 0)] = 1
degradation_year_adj[which(is.na(degradation_year_adj[, ]))] = 0
deforestation_year_adj[which(deforestation_year_adj[, ] > 0)] = 1
deforestation_year_adj[which(is.na(deforestation_year_adj[, ]))] = 0
raster_disturbed = degradation_year_adj + deforestation_year_adj
raster_disturbed[which(raster_disturbed[, ] >= 1)] = 1
```

3. In R, use *clump* function from *raster* package to cluster pixels

```
tmf_patch = raster::clump(raster_disturbed, directions = 8)
raster::writeRaster(tmf_patch, paste0(path, "tmf_patch.tif"), format = "GTiff", overwrite = T)
```

4. Load tmf_patch.tif
5. Create vector shapefile layer with Vectorize

   [input layer: tmf_patch
   name of the field to create: patch
   Use 8-connectedness: yes]
6. Fix geometries of the polygons with Fix Geometry
7. Ensure that all polygons having the same patch number are merged into one polygon with Dissolve

   [Input layer: tmf_patch
   Dissolve field(s): patch]
8. Calculate area of each patch with Field Calculator

   [Output field name: area
   Output field type: Decimal number (real)
   Expression: $area]
9. Calculate mean elevation of each patch with Zonal Statistics

   [Input layer: tmf_patch
   Raster layer: SRTM_guyane_2016_2019_22N
   Output column prefix: elev_
   Statistics to calculate: Mean]
10. Calculate start year, finish year and median year of forest degradation of each patch with Zonal Statistics

    [Input layer: tmf_patch
    Raster layer: JRC_TMF_DegradationYear_v1_1982_2020_guyane_22N
    Output column prefix: degra_
    Statistics to calculate: Minimum, Maximum, Median]
11. Calculate start year, finish year and median year of deforestation of each patch with Zonal Statistics

[Input layer: tmf_patch
Raster layer: JRC_TMF_DeforestationYear_v1_1982_2020_guyane_22N
Output column prefix: defor_
Statistics to calculate: Minimum, Maximum, Median]

12. Select patches within the study zone with Select by Location

[Select features from: tmf_patch
Where the features: are within
By comparing to the features from: study_zone
Modify current selection by: creating new selection
Save to file: tmf_patch_study_zone]

13. Add study zone labels ("north"/"south") with Intersection

[Input layer: tmf_patch_study_zone
Overlay layer: study_zone
Fields to keep from input layer: all
Fields to keep from overlay layer: zone]

14. Select patches with degradation or deforestation pixels only during the period of 2016-2019 with Select Features Using Expression

[expression: ((degra_min > 2015) AND (degra_max < 2020) AND (defor_min IS NULL)) OR ((defor_min > 2015) AND (defor_max < 2020) AND (degra_min IS NULL)) OR ((degra_min > 2015) AND (degra_max < 2020) AND (defor_min > 2015) AND (defor_max < 2020))
Select Features]

15. Select patches with area ≥ 0.2 ha (2000 m^2) with Select Features Using Expression

[expression: area >= 2000
Filter Current Selection
Save to file: tmf_patch_selected]

Selection of natural forest gaps outside of non-forest areas

1. Create a raster layer of non-forest pixels (categories 41, 42, 43, 60, 70) with Raster Calculator

[expression:
("JRC_TMF_TransitionMap_MainClasses_v1_1982_2020_guyane_22N@1" = 41) OR
("JRC_TMF_TransitionMap_MainClasses_v1_1982_2020_guyane_22N@1" = 42) OR
("JRC_TMF_TransitionMap_MainClasses_v1_1982_2020_guyane_22N@1" = 43) OR
("JRC_TMF_TransitionMap_MainClasses_v1_1982_2020_guyane_22N@1" = 60) OR
("JRC_TMF_TransitionMap_MainClasses_v1_1982_2020_guyane_22N@1" = 70)
Output: Save to file > mask_non_forest]

2. Create 300-m buffer around the non-forest pixels with Proximity (Raster Distance)

[Input layer: mask_non_forest
A list of pixel values… to be considered target pixels: 1
Distance units: Georeference coordinates (meters)
Maximum distance to be generated: 300

Value to be applied to all pixels… within the -maxdist of target pixels: 1

Nodata value: 0

Save to file > “mask_non_forest_buffer”

3. Create a “non-forest” mask representing all non-forest pixels and buffer pixels by 1, and other pixels by 0 with Raster Calculator

   [expression: "mask_non_forest@1" + "mask_non_forest_buffer@1"

   Output: Save to file > mask_non_forest]

4. Calculate overlap between disturbance patches (for both S1 patches and JRC-TMF patches) with the non-forest mask with Zonal Statistics

   [Input layer: s1_patch_selected/tmf_patch_selected

   Raster layer: mask_non_forest

   Output column prefix: nf_

   Statistics to calculate: Maximum]

5. Select patches (for both S1 patches and JRC-TMF patches) not overlapping with non-forest mask with Select Features Using Expression

   [expression: nf_max < 1

   Select Features]

Appendix C: regions with particular different spatial patterns of disturbance patches

In the southwestern corner of the south study zone, there is an area of visibly higher density of Sentinel-1 patches but no higher density of JRC-TMF patches (Figure C1). On the other hand, in the central part of the north zone, there is an area with an especially high density of JRC-TMF patches, but no higher density of Sentinel-1 patches (Figure C2): these disturbed patches were often located near previously disturbed pixels, and were located at low elevation.

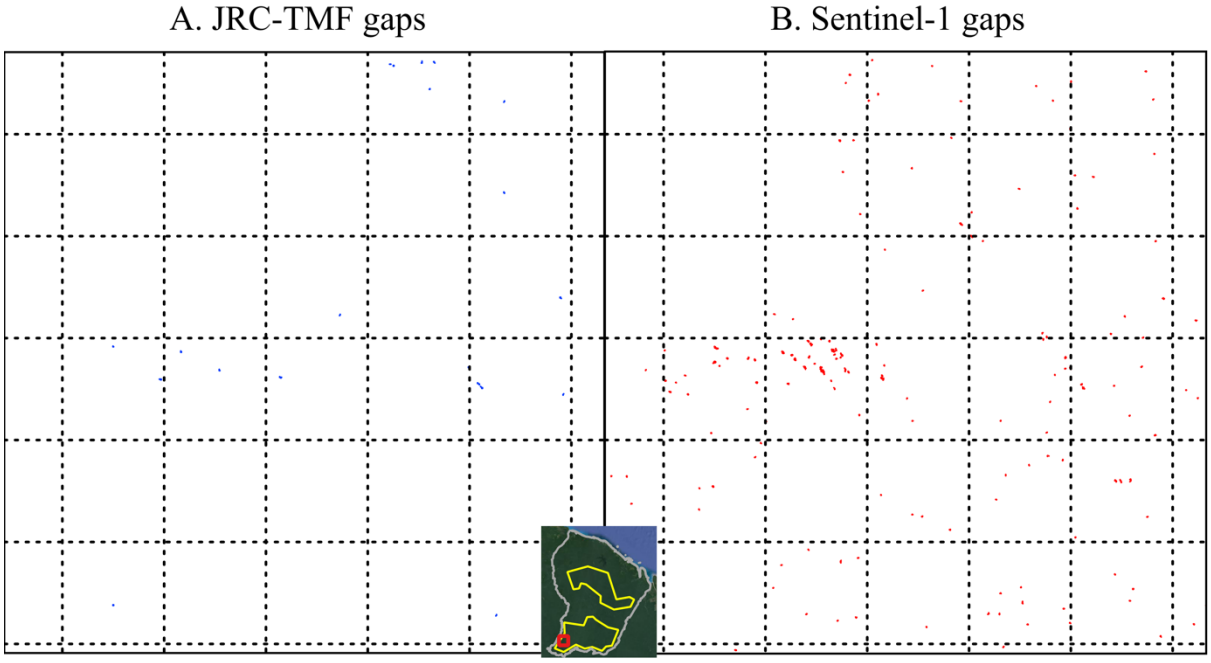

Figure C1. A zone where detected forest gaps are less dense in (A) JRC-TMF (left) than in (B) Sentinel-1 (right) datasets. Each dashed grid line is 5 km apart. The inset shows the extent of French Guiana (gray), study zone (yellow), and the extent of the example zone in the panels (ca. 30 km × 30 km).

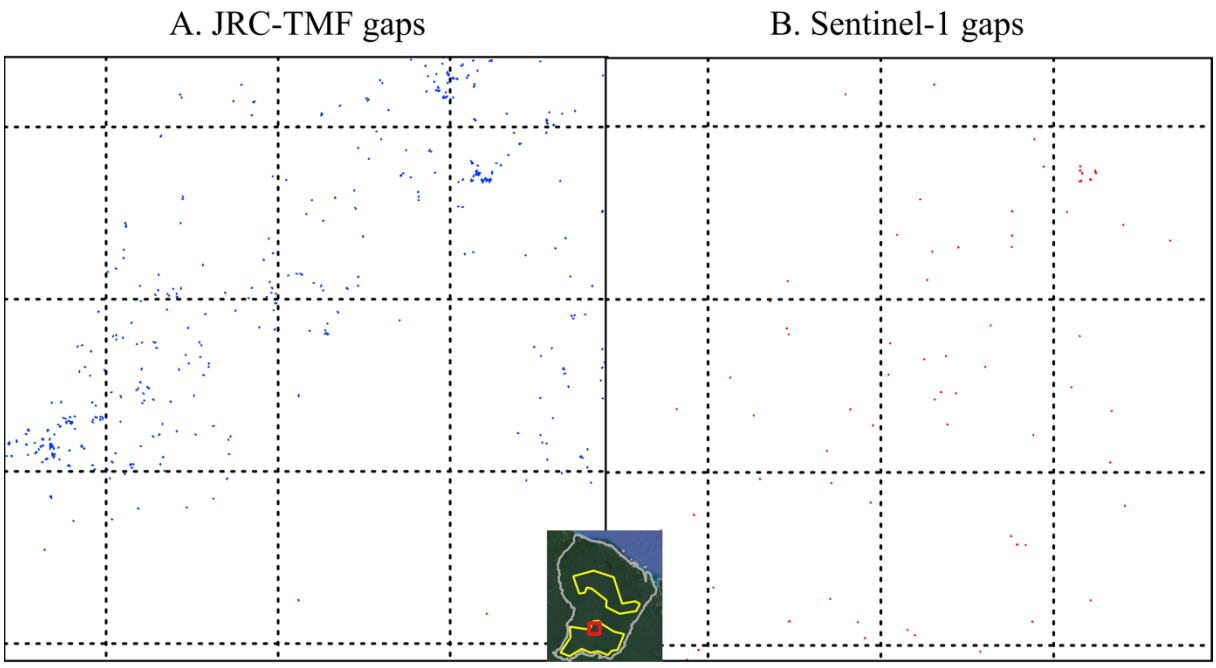

Figure C2. A zone where detected forest gaps are denser in (A) JRC-TMF (left) than in (B) Sentinel-1 (right) datasets. Each dashed grid line is 10 km apart. The inset shows the extent of French Guiana (gray), study zone (yellow), and the extent of the example zone in the panels (ca. 35 km × 35 km).

GENERAL DISCUSSION AND CONCLUSIONS

Natural disturbance in forests is an important study subject because it is an integral environmental process that shapes forest dynamics and functioning in complex ways, and its pattern has undergone profound shift due to both human activities and climate change all around the world, but especially in species-rich, complex tropical forests. Although many studies attempt to elucidate the impacts of natural disturbances on forest, knowledge on the mechanisms through which disturbance events directly modify biological processes in a forest ecosystem remains lacking. The main objective of this thesis was thus to provide new insights from a more mechanistic perspective on how the structure and functioning of tropical forests are affected by natural disturbance, in particular wind disturbance.

I used an individual-based forest dynamics model, TROLL to achieve this objective: I first evaluated if the TROLL model remained robust and realistic when applied across two contrasting forest sites, and examined how the model behavior and performance changes as a function of general parameter values and climatic variables. The two sites contrast notably in the presence or absence of tropical cyclone disturbances: therefore, after demonstrating the transferability of the TROLL model, I implemented a wind-induced tree mortality sub-model based on biomechanical principles in TROLL, and used it to explore the consequences of long-term wind disturbance on forest structure and functioning.

In addition to model development, I also explored the potential of satellite data to provide information on fine-scale dynamics of natural disturbance events. I focused in particular on synthetic radar aperture (SAR) time series from Sentinel-1 satellites, which have global forest coverage, with high return period (12 days) and high spatial resolution (10 m). A recently developed “shadow” method has allowed the detection of forest disturbance events from Sentinel-1 SAR time series (Ballère et al., 2021; Bouvet et al., 2018).

For the tropical moist forests of French Guiana, I retrieved records of disturbance patches detected either in a Landsat-derived forest cover dataset (Vancutsem et al., 2021) or in the Sentinel-1 disturbance dataset, and delimited a study zone based on past land use records to retain as much as possible only natural forest gaps in regions unimpacted by human activities. I characterized the spatial pattern, size distribution and temporal dynamics of these natural forest gaps, compared the results from the two datasets and against past studies on natural forest gap dynamics, and we investigated if natural forest gap dynamics is influenced by topographic or seasonal factors.

In the Discussion and Conclusions section, I first summarize the main findings and the novel contributions of this thesis within the context of research of wind disturbance in tropical forests. I then discuss some of the limitations and difficulties encountered in this study, and

propose future perspectives that could help advance our understanding on the way disturbance affects tropical forests.

Main contributions

Evaluation of the transferability of an individual-based model

Due to their detailed and often mechanistic representations of individual-level processes (e.g. establishment, growth, competition, and mortality), individual-based forest models are suitable for investigating how stand-scale forest patterns and dynamics are influenced by various abiotic and biotic factors, including disturbance patterns. However, higher model complexity also means a larger amount of site- and species-specific data is need to parameterize the model, and the question of model transferability, i.e., whether models calibrated at one site can be transferred to other sites and maintain performance, has rarely been tested (but see Shuman, Shugart, and Krankina 2014; Shuman et al. 2015). The study of Chapter 1 thus examined the transferability of a spatially explicit individual-based model, TROLL, which used species-specific traits that are easily measurable in the field to constrain many biological processes. Nevertheless, other biological processes needed to be represented by empirical relationships (e.g. carbon allocation, crown allometry, mortality), which calls model transferability into question.

The results showed that the TROLL model reasonably reproduced forest structure and functioning at two sites with contrasting climatic conditions and floristic compositions after calibrations of only five parameters, and that model response to gradual changes in climatic condition is consistent at both sites. This result supported the potential of trait-based, individual-based models to be applied over larger scales without overly extensive fine-tuning of a large number of parameters.

Calibration tests identified that photosynthetic efficiency, crown allometry and background mortality to be among the most influential factors on model output. The representation of photosynthetic efficiency and crown allometry could be improved by prescribing species-specific measurements. In addition, the constraining of crown allometry parameters could benefit from fusion with remote sensing techniques, such as using Lidar data that contained detailed information on crown structure in forests. The sensitivity of model output to mortality corroborated with previous studies which found the tree mortality process to be a major source of model uncertainty, and also highlights the potential importance of disturbance which modulates mortality. The decoupling observed between productivity and biomass, both in sensitivity analysis and in the virtual experiment of varying climatic conditions, hints at the importance of processes intervening between the step of

carbon assimilation and carbon storage, such as respiration, as well as factors influencing carbon storage and turnover time in forests, including disturbance and mortality.

Investigation of the effects of wind disturbance on forests using individual-based modeling

The results of Chapter 1 have revealed that the mortality process has an important role in influencing model output: since mortality is highly linked to disturbance, development of a more mechanistic and precise mortality module can go hand in hand with disturbance modeling. This was explored in Chapter 2, where I incorporated a module of wind-induced tree mortality in the model, and applying it at the typhoon-prone Fushan forest site in Taiwan. Many models have included disturbance processes in individual-based models (Kamimura et al., 2019; Seidl et al., 2014, 2011a), but few have done so to model long-term forest response, and few have been implemented in species-rich tropical forests. The study of the Chapter 2 is one of the first to provide a mechanistic representation of wind-induced tree mortality in an individual-based model, based on biomechanical principles, in order to explore long-term consequences of wind disturbance on a species-rich forest.

We found that average canopy height decreased as wind disturbance strength increased, confirming observations in global empirical studies (Ibanez et al., 2019). The nonlinear response of biomass as wind disturbance strength increased could be linked to shifts in distribution of community traits such as wood density, suggests that the response of carbon storage capacity to shifts of wind regime may be variable and site-specific, depending on previous wind disturbance level and floristic composition (notably inter- and intraspecific variability in tree allometry).

Decreased mortality rate at the end of the simulation, compared to the onset of wind disturbance, indicated that forest acclimation and adaptation could arise in individual-based models as a stand-level emergent property. Forest acclimation and adaptation to wind disturbance can involve modifications in species and functional composition of the forest community: as such, this provides an appropriate framework to investigate eco-evolutionary effects of wind disturbance on tropical forests (Ibanez et al., 2020; Lin et al., 2020).

Simulation results showed that wind intensity tightly controlled forest structure whereas wind frequency did not cause significant effects as long as the intensity remained low: this points to the important effect of rare, extreme events in controlling forest properties. Although empirical studies have observed that forest structure and composition were correlated to tropical cyclone frequency (Hogan et al., 2018; Ibanez et al., 2019), higher cyclone frequency does not only mean higher frequency of wind disturbance, but could also be associated with

higher maximally sustained wind speed. In addition, it is a possibility that the effect of changing frequency in wind disturbance events only appears at a larger spatial scale, such as at the landscape or regional level, where different forest stands experience disturbance at different timing and intervals, and an upscaling exercise of the present model could serve to examine this possibility.

The development of a representation of the horizontal wind profile above and within a dynamically changing mixed-sized canopy, was a challenging but important step that could serve as a basis on which more realistic wind-canopy interactions can be envisioned and tested. The exploration of the topographic effect, although rudimentary, represent a first step to incorporate wind-terrain interaction in forest models.

Exploration of natural disturbance dynamics in tropical forests using satellite imaging data

As uncertainties are still high concerning the consequences of forest cover change on global carbon cycle (Achard et al., 2010), near real-time (NRT) monitoring is necessary to better understand the extent and pattern of both anthropogenic and natural disturbance and forest loss. Natural disturbance, in particular, has received less attention compared to artificial deforestation (Bullock et al., 2020), despite it being an important component influencing forest structure and functioning (Reichstein et al., 2013). Although optical imagery has commonly been used for forest disturbance monitoring (Hansen et al., 2016; Vancutsem et al., 2021), frequent cloud cover in the tropics limits its usability. In the study of Chapter 3, I thus explored if non-optical synthetic aperture radar (SAR) data, acquired by Sentinel-1 satellites, could be used to detect forest gaps caused by natural disturbances, and thereby quantify spatial distribution and fine-scale temporal dynamics of natural forest gaps in old-growth tropical forests in French Guiana.

After using synthetic land use data in French Guiana to delineate a study zone of limited human activities, wherein the detected disturbance patches were likely to be natural forest gaps, I compared the gaps detected by the Sentinel-1 dataset with those detected by the Landsat-derived optical data. Sentinel-1 data detected almost twice as more forest gaps than the Landsat-derived optical data, but the two shared consistent spatial pattern, which brings confidence that the Sentinel-1 gaps are not algorithm artifacts. The size-frequency distribution of the detected forest gaps above 0.2 hectare followed a power law relationship, consistent with past findings (Espírito-Santo et al., 2014; Hunter et al., 2015). The monthly dynamics of cumulated gap area showed a clear pattern of higher level of disturbances during the dry season, which could be due to higher water stress, a hypothesis in accordance with previous

studies (Dalagnol et al., 2021; Goulamoussène et al., 2017). This work thus provides preliminary confirmation of the utility of SAR satellite data, aided by an innovative data processing method, to monitor and quantify fine-scale dynamics of natural disturbances over large spatial scales.

Perspectives

Evaluation of model transferability

Although individual-based forest model can achieve higher realism due to their detailed representation of biological processes, the higher model complexity also inevitably means that model parameterization and calibration are a difficult challenge (Huber et al., 2020; Yates et al., 2018). Striving for more mechanistic and generic representations of biological processes is evidently an important goal of model development. However, the findings of Huber *et al.* (2020) is a reminder that optimizing the model for a single process would often lead to models that are performant in one aspect but not the most performant overall. Therefore, for the evaluation of overall model performance and transferability, multiple applications and objectives should be considered, and multiple processes should be evaluated conjointly, over a wide range of site conditions.

As the study in Chapter 1 has indicated, trait-based models have the advantage of making process formulation more generic, reducing the need for empirical parameters and by consequence calibration burden (DeAngelis and Grimm, 2014; Pappas et al., 2016). As global plant trait information continues to accumulate (Chave et al., 2009; Kattge et al., 2020), large-scale implementation of trait-based models should become easier and easier. Nevertheless, there will conceivably always be empirical parameters in a model that need to be recalibrated between sites, where model outputs produced with various parameter values are compared against observations to find the parameter values providing the best fit . Sensitivity analysis can help characterize the contribution of each parameter to overall model output variability, and thus help prioritize efforts of parameter calibration (Pianosi et al., 2016). Various statistical tools, including notably approximate Bayesian computation (ABC), has been developed to facilitate parameter calibration (Hartig et al., 2014; Lagarrigues et al., 2015; Lehmann and Huth, 2015). When it comes to the choice of metrics used to compare model output and observations, although the study in Chapter 1 used only summary statistics of forest structure and functioning (stem density, biomass and productivity), whole distributions, such as functional trait or tree size distribution, could provide a more complete information on forest structure and composition, and allow for more accurate evaluation of model performance (Fischer et al., 2019; Koven et al., 2020).

In the context of improving model transferability, remote sensing data could be beneficial in one of two ways. Firstly, we could estimate the value of certain input parameters using remote sensing data, such as crown allometry parameters obtained from Lidar data (Calders et al., 2018; Fischer et al., 2020; Shugart et al., 2015). Secondly, we could extract statistics to be used for model calibration from remote sensing data. For example, the spatial pattern (e.g. aggregation level, size distribution) of natural forest gaps detected by Sentinel-1 satellite data in Chapter 3 could be compared against forest gaps that are predicted to appear in a forest dynamics model.

Modeling wind profile in a mixed-size forest

The main challenge of modeling wind damage risk in a mixed-size forest is the representation of the horizontal wind speed profile. Traditionally, horizontal wind above the canopy is modeled with a logarithmic function (Equation 6). The function includes a variable of the zero-plane displacement (d), which represents the vertical displacement of wind due to obstacles such as forest canopy: in ForestGALES, d is estimated from several canopy structure measurements, most importantly height of the canopy top (usually taken to be the average height of the tallest trees in the forest stand); in another wind damage risk model, HWIND, d is assumed to be zero (i.e., wind profile at the forest edge is used) (Gardiner et al., 2000). In both cases, a stand-level top canopy height (H) is calculated, and the critical wind speed (CWS) for tree damage is then estimated for each tree at H, regardless of individual tree height.

This approach is obviously not adapted for mixed-size forests, where any measure of canopy height should take into account spatial variability of the forest stand. Later versions of ForestGALES tackled the problem by introducing a competition index in CWS calculation, which takes into account a tree's relative height: various competition indices exist, some calculated at the stand level, and some calculated at the neighborhood level using a distance-based approach (Duperat et al., 2021; Hale et al., 2012).

In the study of Chapter 2, we made a conscious choice not to adopt this competition index-based approach that is used for the ForestGALES model, due to the design of the TROLL model that simulates competition in an explicitly mechanistic manner. Instead, for each tree, we calculated the top canopy height of its neighborhood (H), and the critical wind speed (CWS) for tree damage was then calculated at the height of the focal tree (h). Aside from the logarithmic wind profile above the canopy, sub-canopy wind speed was modeled with an exponential decay profile that is a function of difference between h and H (Equation 19) (Inoue 1963), although other approximations for wind profile within the canopy exist (De

Santana et al., 2017; Raupach and Thom, 1981; Thom, 1971). For the calculation of *H*, we divided the simulated forest into 20 m × 20 m quadrats, and the neighborhood of a tree is all the trees within the same quadrat as it. We decided not to adopt a distance-based approach or a radius-based approach (neighborhood being all trees within a radius *r* of the focal tree), due to the substantially higher computational burden.

Future research focuses involve providing a more realistic wind profile: this would rely on a more comprehensive understanding of the spatial and temporal variability of leaf area index (LAI) and stem spacing in the forest canopy, as well as wind-canopy interactions which create turbulent eddy structures (de Langre, 2008b; Lalic et al., 2003; Raupach et al., 1996).

Topography and wind disturbance

The topographic surface can alter local wind speed and direction, and have complex effects on wind-forest interaction and the level of wind damage. In general, wind speed is predicted to increase in higher altitudes and when wind is funneled through constricted terrain features. Therefore, within a given wind regime, windward slopes, ridgetops, and narrow valleys parallel to wind direction are locations where wind speed is expected to be higher, whereas leeward slopes are expected to have lower wind speed (Belcher et al., 2011; Mitchell, 2013). An empirical study that measured local wind speed in a complex terrain also observed higher wind speed at higher elevations and in valleys parallel to wind direction, and lower wind speed in valleys vertical to wind direction (Ruel et al., 1998).

Detailed numerical models could now realistically simulate terrain effects on wind speed and direction at a small spatial scale (e.g., the Global Wind Atlas: Badger et al., 2015), but due to their high computational burden and high demand of surface condition data for calibration, they are currently unsuitable for incorporation into individual-based forest models. Instead, simplified predictors of wind exposure have been used (e.g., Mikita and Klimánek, 2012). In Chapter 2, we implemented a simple wind exposure index based on 20 m × 20 m quadrat-level average elevations. The weak but statistically significant topographic effect was a promising sign that more precise formulations could help us more fully capture how topographic features influence local wind speed, and elucidate how they drive spatial variability of wind damage.

The empirical relationship between topography and cyclonic wind damage of trees reported in the literature is even less straightforward and consistent than the relationship between topography and wind speed (Everham and Brokaw, 1996). In some studies, no topographic effect was observed; in some other, less damage was observed on ridgetops than in valleys. One hypothesis to explain this is that trees on ridgetops have acclimated to the

chronically higher wind level, and consequently have developed lower wind susceptibility. In addition, leeward slopes have been observed variously to experience more or less damage than the overall. Several hypotheses have been proposed to explain cases of higher observed wind damage on leeward slopes, such as turbulent flow, differences in soil properties, and less acclimation to chronic wind. The above findings point to the need to take into account the phenomena of tree acclimation and adaptation: in this respect, individual-based models with species-level trait parameterization should provide an ideal framework to explore how wind disturbance shape inter- and intraspecific trait variability, and consequently tree acclimation and adaptation.

Moreover, topography can cause spatial heterogeneity in canopy height and species composition through other factors such as soil properties or water availability (Everham and Brokaw, 1996), which can affect tree susceptibility to wind disturbance, and which have been observed to be related to regional-scale gap fractions (Dalagnol et al., 2021; Goulamoussène et al., 2017). The inclusion of soil properties as site-specific input parameterization, as well as the formulation of a complete water cycle in the forest model, could allow a more comprehensive modeling of effects of topographic variability.

At the regional scale, observational studies on spatial variability of tree mortality and gap dynamics also showed variable results. For the region of Central Amazonia, tree mortality associated with wind disturbance was found to vary for different topographic zones (e.g., higher mortality on slopes) (de Toledo et al., 2012; Magnabosco Marra et al., 2014). Goulamoussène et al. (2017) also found the relative frequency of large gaps was significantly correlated to wind exposure and slope in French Guiana. In contrast, Dalagnol et al. (2021) did not find topographic predictors to explain variation of occurrence of gaps detected in the Amazon, and gap size-frequency distributions were found to be largely invariable in relation to topographic conditions in the Peruvian Amazon (Asner et al., 2013). A preliminary analysis performed in the study of Chapter 3 did not find level of disturbance detected by Sentinel-1 satellite data to be related to elevation either, although more thorough analyses are needed. Nevertheless, the different results observed suggest that there might be different factors that govern forest gap formation and dynamics at the landscape and regional scale, from factors controlling tree mortality at the stand scale. Upscaling of individual-based models may thus provide an opportunity to investigate how topography, as well as other environmental factors (e.g., edaphic or climatic conditions), shape tree mortality and gap dynamics at the two scales simultaneously.

Other aspects of forest disturbance

The study in Chapter 2 presents a relatively basic implementation of wind-induced tree mortality, which could be expanded in several aspects. Tree uprooting was not modeled, in part due to the low proportion of field observed tree death with tree uprooting compared to stem breakage, and in part due to our insufficient understanding of characterization and consequences of root anchoring. It is hoped that continuing theoretical and empirical studies on the root-soil interaction, notably with the aid of finite element modeling, will facilitate mechanistic modeling of wind-induced tree uprooting in the future (Stubbs et al., 2019; Yang et al., 2014).

Several empirical factors in the original ForestGALES model were assumed to be identical for all trees, and were combined into general "wind damage parameters". However, it is likely that this assumption does not hold true for several factors, such as wood deformities, stem tapering, and relative allocation of total biomass to stem weight. In the future, further investigation is needed to uncover interspecific or even intraspecific variations in these factors that can modulate tree response to wind disturbances.

In addition to tree mortality, wind disturbance and tropical cyclones bring about a myriad of changes at all levels of a forest ecosystem. At the individual level, defoliation is a common non-lethal effect of strong winds, which decrease sail area and risks of windthrow, but also limits productivity and growth, and could increase the risk of carbon starvation if re-occurring at high frequency (McDowell et al., 2018); in addition, defoliation also increases overall light availability in the understory, and may thus influence forest regeneration dynamics by reducing spatial heterogeneity of light availability (Yao et al., 2015). Branch or even stem breakage do not necessarily lead to death: tree species have been observed to have variable re-sprouting abilities, and the variability of this resistance trait can play an significant role in an eco-evolutionary dynamics, and shape forest adaptation and succession in response to wind disturbance. Conversely, wind damage on trees may not always cause immediate death, but can manifest as successive damages that increase long-term mortality (Tanner et al., 2014; Walker, 1995). At the ecosystem level, nutrient cycling can be modified by the intense rain that is a common feature of tropical cyclones (Lin et al., 2011), and defoliation, branch and stem breakage and windthrows all provide litter and necromass entering the litter dynamics. All of the above points can be investigated under the individual-based modeling framework.

Furthermore, as wind speed is the only environmental forcing needed for the module of wind-induced tree mortality, the model can be applied not only to tropical cyclones, but also to other wind disturbance regimes such as temperate storms (Xi and Peet, 2011) or scattered blowdown events in the Amazon (Magnabosco Marra et al., 2018; Peterson et al., 2019). This

also means that with model upscaling, it is possible to generate predictions of spatial and temporal patterns of disturbance events and forest gaps at the landscape or regional scale. The model predictions could then be validated by large-scale near real-time data series on natural forest gaps, such as those detected by Sentinel-1 satellites, providing a great potential for data-model fusion.

Application of the model at a larger scale could also allow to test how gap dynamics is related to environmental factors such as wind speed, water deficit and flooding/waterlogging. Curiously, several previous empirical studies did not find significant relationships between wind speed and regional-scale gap fractions (Dalagnol et al., 2021; Goulamoussène et al., 2017), although these studies were limited in the temporal extent of both wind speed data and forest gap data. The combination of long-term wind speed forcing for the ForestGALES-TROLL model and the fine-scale temporal dynamics of forest gaps detected by Sentinel-1 satellites could serve to overcome this limitation. Once a complete water cycle module is included in the model, it will be a possibility and a priority to test the hypothesis that the seasonal variability of disturbance level, observed in the study in Chapter 3, is linked to water availability.

Finally, the work in this thesis could serve as a general framework, based on which individual-based models could be further developed to include other natural disturbance processes such as fire, drought, insect or pathogen outbreaks (Brazhnik et al., 2017; Lucas et al., 2017; Seidl et al., 2011a; Shugart et al., 2018), as well as how anthropogenic land use change such as fragmentation or selective logging interact with natural disturbances and influence their effects (Laurance and Curran, 2008; McGroddy et al., 2013; Schwartz et al., 2017; Uriarte et al., 2009), in the hope of constructing a comprehensive view of how disturbance is expected to shape forests in the present and in the future.

REFERENCES

Achard, F., Stibig, H.J., Eva, H.D., Lindquist, E.J., Bouvet, A., Arino, O., Mayaux, P., 2010. Estimating tropical deforestation from Earth observation data. Carbon Manag. 1, 271–287. https://doi.org/10.4155/cmt.10.30

Aleixo, I., Norris, D., Hemerik, L., Barbosa, A., Prata, E., Costa, F., Poorter, L., 2019. Amazonian rainforest tree mortality driven by climate and functional traits. Nat. Clim. Chang. 9, 384–388. https://doi.org/10.1038/s41558-019-0458-0

Allen, C.D., Macalady, A.K., Chenchouni, H., Bachelet, D., McDowell, N., Vennetier, M., Kitzberger, T., Rigling, A., Breshears, D.D., Hogg, E.H. (Ted., Gonzalez, P., Fensham, R., Zhang, Z., Castro, J., Demidova, N., Lim, J.H., Allard, G., Running, S.W., Semerci, A., Cobb, N., 2010. A global overview of drought and heat-induced tree mortality reveals emerging climate change risks for forests. For. Ecol. Manage. 259, 660–684. https://doi.org/10.1016/j.foreco.2009.09.001

Alvarez-Berríos, N.L., Mitchell Aide, T., 2015. Erratum : Global demand for gold is another threat for tropical forests (Environmental Research Letters (2014) 10 (014006)). Environ. Res. Lett. 10. https://doi.org/10.1088/1748-9326/10/2/029501

Álvarez-Dávila, E., Cayuela, L., González-Caro, S., Aldana, A.M., Stevenson, P.R., Phillips, O., Cogollo, Á., Peñuela, M.C., Von Hildebrand, P., Jiménez, E., Melo, O., Londoño-Vega, A.C., Mendoza, I., Velásquez, O., Fernández, F., Serna, M., Velázquez-Rua, C., Benítez, D., Rey-Benayas, J.M., 2017. Forest biomass density across large climate gradients in northern South America is related to water availability but not with temperature. PLoS One 12, 1–16. https://doi.org/10.1371/journal.pone.0171072

Amatulli, G., Domisch, S., Tuanmu, M.N., Parmentier, B., Ranipeta, A., Malczyk, J., Jetz, W., 2018. Data Descriptor: A suite of global, cross-scale topographic variables for environmental and biodiversity modeling. Sci. Data 5, 1–15. https://doi.org/10.1038/sdata.2018.40

Ancelin, P., Courbaud, B., Fourcaud, T., 2004. Development of an individual tree-based mechanical model to predict wind damage within forest stands. For. Ecol. Manage. 203, 101–121. https://doi.org/10.1016/j.foreco.2004.07.067

Anderson-Teixeira, K.J., Davies, S.J., Bennett, A.C., Gonzalez-Akre, E.B., Muller-Landau, H.C., Joseph Wright, S., Abu Salim, K., Almeyda Zambrano, A.M., Alonso, A., Baltzer, J.L., Basset, Y., Bourg, N.A., Broadbent, E.N., Brockelman, W.Y., Bunyavejchewin, S., Burslem, D.F.R.P., Butt, N., Cao, M., Cardenas, D., Chuyong, G.B., Clay, K., Cordell, S., Dattaraja, H.S., Deng, X., Detto, M., Du, X., Duque, A., Erikson, D.L., Ewango, C.E.N., Fischer, G.A., Fletcher, C., Foster, R.B., Giardina, C.P., Gilbert, G.S., Gunatilleke, N., Gunatilleke, S., Hao, Z., Hargrove, W.W., Hart, T.B., Hau, B.C.H., He, F., Hoffman, F.M., Howe, R.W., Hubbell, S.P., Inman-Narahari, F.M., Jansen, P.A., Jiang, M., Johnson, D.J., Kanzaki, M., Kassim, A.R., Kenfack, D., Kibet, S., Kinnaird, M.F., Korte, L., Kral, K., Kumar, J., Larson, A.J., Li, Y., Li, X., Liu, S., Lum, S.K.Y., Lutz, J.A., Ma, K., Maddalena, D.M., Makana, J.-R., Malhi, Y., Marthews, T., Mat Serudin, R., Mcmahon, S.M., McShea, W.J., Memiaghe, H.R., Mi, X., Mizuno, T., Morecroft, M., Myers, J.A., Novotny, V., de Oliveira, A.A., Ong, P.S., Orwig, D.A., Ostertag, R., den Ouden, J., Parker, G.G., Phillips, R.P., Sack, L., Sainge, M.N., Sang, W., Sri-ngernyuang, K., Sukumar, R., Sun, I.-F., Sungpalee, W., Suresh, H.S., Tan, S., Thomas, S.C., Thomas, D.W., Thompson, J., Turner, B.L., Uriarte, M., Valencia, R., Vallejo, M.I., Vicentini, A., Vrška, T., Wang, Xihua, Wang, Xugao, Weiblen, G.D., Wolf, A., Xu, H., Yap, S., Zimmerman, J.K., 2015. CTFS-ForestGEO: A worldwide network monitoring forests in an era of global change. Glob. Chang. Biol. 21, 528–549. https://doi.org/10.1111/gcb.12712

Aragão, L.E.O.C., Malhi, Y., Metcalfe, D.B., Silva-Espejo, J.E., Jiménez, E., Navarrete, D., Almeida, S., Costa, A.C.L., Salinas, N., Phillips, O.L., Anderson, L.O., Alvarez, E., Baker, T.R., Goncalvez, P.H., Huamán-Ovalle, J., Mamani-Solórzano, M., Meir, P., Monteagudo, A., Patïo, S., Peñuela, M.C., Prieto, A., Quesada, C.A., Rozas-Dávila, A., Rudas, A., Silva, J.A., Vásquez, R., 2009. Above- and below-ground net primary productivity across ten Amazonian forests on contrasting soils. Biogeosciences 6, 2759–2778. https://doi.org/10.5194/bg-6-2759-2009

Arellano, G., Zuleta, D., Davies, S.J., 2021. Tree death and damage: A standardized protocol for frequent surveys in tropical forests. J. Veg. Sci. 32. https://doi.org/10.1111/jvs.12981

Askne, J.I.H., Dammert, P.B.G., Ulander, L.M.H., Smith, G., 1999. C-band repeat-pass interferometric SAR observations of the forest. Doktorsavhandlingar vid Chalmers Tek. Hogsk. 35, 25–35.

Asner, G.P., Kellner, J.R., Kennedy-Bowdoin, T., Knapp, D.E., Anderson, C., Martin, R.E., 2013. Forest Canopy Gap Distributions in the Southern Peruvian Amazon. PLoS One 8. https://doi.org/10.1371/journal.pone.0060875

Asner, G.P., Mascaro, J., Muller-Landau, H.C., Vieilledent, G., Vaudry, R., Rasamoelina, M., Hall, J.S., van Breugel, M., 2012. A universal airborne LiDAR approach for tropical forest carbon mapping. Oecologia 168, 1147–1160. https://doi.org/10.1007/s00442-011-2165-z

Atkin, O.K., Bloomfield, K.J., Reich, P.B., Tjoelker, M.G., Asner, G.P., Bonal, D., Bönisch, G., Bradford, M.G., Cernusak, L.A., Cosio, E.G., Creek, D., Crous, K.Y., Domingues, T.F., Dukes, J.S., Egerton, J.J.G., Evans, J.R., Farquhar, G.D., Fyllas, N.M., Gauthier, P.P.G., Gloor, E., Gimeno, T.E., Griffin, K.L., Guerrieri, R., Heskel, M.A., Huntingford, C., Ishida, F.Y., Kattge, J., Lambers, H., Liddell, M.J., Lloyd, J., Lusk, C.H., Martin, R.E., Maksimov, A.P., Maximov, T.C., Malhi, Y., Medlyn, B.E., Meir, P., Mercado, L.M., Mirotchnick, N., Ng, D., Niinemets, Ü., O'Sullivan, O.S., Phillips, O.L., Poorter, L., Poot, P., Prentice,

I.C., Salinas, N., Rowland, L.M., Ryan, M.G., Sitch, S., Slot, M., Smith, N.G., Turnbull, M.H., Vanderwel, M.C., Valladares, F., Veneklaas, E.J., Weerasinghe, L.K., Wirth, C., Wright, I.J., Wythers, K.R., Xiang, J., Xiang, S., Zaragoza-Castells, J., 2015. Global variability in leaf respiration in relation to climate, plant functional types and leaf traits. New Phytol. 206, 614–636. https://doi.org/10.1111/nph.13253

Atkin, O.K., Evans, J.R., Ball, M.C., Lambers, H., Pons, T.L., 2000. Leaf respiration of snow gum in the light and dark. Interactions between temperature and irradiance. Plant Physiol. 122, 915–923. https://doi.org/10.1104/pp.122.3.915

Baccini, A., Walker, W., Carvalho, L., Farina, M., Sulla-Menashe, D., Houghton, R.A., 2017. Tropical forests are a net carbon source based on aboveground measurements of gain and loss. Science (80-.). 358, 230–234. https://doi.org/10.1126/science.aam5962

Badger, J., Davis, N., Hahmann, A., Larsen, X.G., Kelly, M., Olsen, B.T., Mortensen, N.G., Hans, E., Troen, I., Petersen, E.L., Volker, P., Lange, J., Badger, J., Hahmann, A., Larsen, X.G., Badger, M., Davis, N., Olsen, B.T., Mortensen, N.G., 2015. The Global Wind Atlas - An EUDP project carried out by DTU Wind Energy. Final Report Project.

Ballère, M., Bouvet, A., Mermoz, S., Le Toan, T., Koleck, T., Bedeau, C., André, M., Forestier, E., Frison, P.L., Lardeux, C., 2021. SAR data for tropical forest disturbance alerts in French Guiana: Benefit over optical imagery. Remote Sens. Environ. 252. https://doi.org/10.1016/j.rse.2020.112159

Balzter, H., 2001. Forest mapping and monitoring with interferometric synthetic aperture radar (InSAR). Prog. Phys. Geogr. 25, 159–177. https://doi.org/10.1191/030913301666986397

Barré, H.M., Duesmann, B., Kerr, Y.H., 2008. SMOS: The mission and the system. IEEE Trans. Geosci. Remote Sens. 46, 587–593.

Beck, H.E., Zimmermann, N.E., McVicar, T.R., Vergopolan, N., Berg, A., Wood, E.F., 2018. Present and future köppen-geiger climate classification maps at 1-km resolution. Sci. Data 5, 1–12. https://doi.org/10.1038/sdata.2018.214

Belcher, S.E., Harman, I.N., Finnigan, J.J., 2011. The wind in the willows: Flows in forest canopies in complex terrain. Annu. Rev. Fluid Mech. 44, 479–504. https://doi.org/10.1146/annurev-fluid-120710-101036

Bellingham, P.J., Kapos, V., Varty, N., Healey, J.R., Tanner, E.V.J., Kelly, D.L., Dalling, J.W., Burns, L.S., Lee, D., Sidrak, G., 1992. Hurricanes need not causes high mortality: the effects of Hurricane Gilbert on forest in Jamaica. J. Trop. Ecol. 8, 217–223.

Bellingham, P.J., Kohyama, T.S., Aiba, S., 1996. The effects of a typhoon on Japanese warm temperate rainforests. Ecol. Res. 11, 229–247. https://doi.org/10.1007/BF02347781

Bonal, D., Bosc, A., Ponton, S., Goret, J.Y., Burban, B.T., Gross, P., Bonnefond, J.M., Elbers, J., Longdoz, B., Epron, D., Guehl, J.M., Granier, A., 2008. Impact of severe dry season on net ecosystem exchange in the Neotropical rainforest of French Guiana. Glob. Chang. Biol. 14, 1917–1933. https://doi.org/10.1111/j.1365-2486.2008.01610.x

Bongers, F., Charles-Dominique, P., Forget, P.-M., Théry, M., 2001. Nouragues: dynamics and plant-animal interactions in a neotropical rainforest.

Botkin, D.B., Janak, J.F., Wallis, J.R., 1972. Some Ecological Consequences of a Computer Model of Forest Growth. J. Ecol. 60, 849–872.

Bouvet, A., Mermoz, S., Ballère, M., Koleck, T., Le Toan, T., 2018. Use of the SAR shadowing effect for deforestation detection with Sentinel-1 time series. Remote Sens. 10, 1–19. https://doi.org/10.3390/rs10081250

Brandon, K., 2015. Ecosystem Services from Tropical Forests: Review of Current Science. SSRN Electron. J. https://doi.org/10.2139/ssrn.2622749

Brazhnik, K., Hanley, C., Shugart, H.H., 2017. Simulating changes in fires and ecology of the 21st century Eurasian boreal forests of Siberia. Forests 8. https://doi.org/10.3390/f8020049

Brown, M.E., Escobar, V., Moran, S., Entekhabi, D., O'Neill, P.E., Njoku, E.G., Doorn, B., Entin, J.K., 2013. NASA's soil moisture active passive (SMAP) mission and opportunities for applications users. Bull. Am. Meteorol. Soc. 94, 1125–1128. https://doi.org/10.1175/BAMS-D-11-00049.1

Buck, A.L., 1981. New equations for computing vapour pressure and enhancement factor. J. Appl. Meteorol. https://doi.org/10.1175/1520-0450(1981)0202.0.CO;2

Bugmann, H., 2001. A Review of forest gap models. Clim. Change 51, 259–305. https://doi.org/10.1017/S0022112088002617

Bugmann, H., Fischlin, A., 1996. Simulating forest dynamics in a complex topography using gridded climatic data. Clim. Change 34, 201–211. https://doi.org/10.1007/BF00224631

Bugmann, H., Seidl, R., Hartig, F., Bohn, F., Brůna, J., Cailleret, M., François, L., Heinke, J., Henrot, A.J., Hickler, T., Hülsmann, L., Huth, A., Jacquemin, I., Kollas, C., Lasch-Born, P., Lexer, M.J., Merganič, J., Merganičová, K., Mette, T., Miranda, B.R., Nadal-Sala, D., Rammer, W., Rammig, A., Reineking, B., Roedig, E., Sabaté, S., Steinkamp, J., Suckow, F., Vacchiano, G., Wild, J., Xu, C., Reyer, C.P.O., 2019. Tree mortality submodels drive simulated long-term forest dynamics: assessing 15 models from the stand to global scale. Ecosphere 10. https://doi.org/10.1002/ecs2.2616

Bugmann, H.K.M., Solomon, A.M., 1995. The use of a European forest model in North America: a study of ecosystem response to climate gradients. J. Biogeogr. 22, 477–484. https://doi.org/10.2307/2845944

Bullock, E.L., Woodcock, C.E., Souza, C., Olofsson, P., 2020. Satellite-based estimates reveal widespread forest degradation in the Amazon. Glob. Chang. Biol. 26, 2956–2969. https://doi.org/10.1111/gcb.15029

Burkhart, H.E., 1990. Status and future ofgrowth and yield models, in: Proceedings of a Symposium on State of the Art Methodology of Forest Inventory USDA Forest Service, General Technical ReportP NWGTR-263. pp. 409–414.
Calders, K., Origo, N., Burt, A., Disney, M., Nightingale, J., Raumonen, P., Åkerblom, M., Malhi, Y., Lewis, P., 2018. Realistic forest stand reconstruction from terrestrial LiDAR for radiative transfer modelling. Remote Sens. 10, 1–15. https://doi.org/10.3390/rs10060933
Castanho, A.D.A., Galbraith, D., Zhang, K., Coe, M.T., Costa, M.H., Moorcroft, P., 2016. Changing Amazon biomass and the role of atmospheric CO2 concentration, climate, and land use. Global Biogeochem. Cycles 30, 18–39. https://doi.org/10.1002/2015GB005135
Cha, E.J., Knutson, T.R., Lee, T.-C., Ying, M., Nakaegawa, T., 2020. Third assessment on impacts of climate change on tropical cyclones in the Typhoon Committee Region – Part II: Future projections. Trop. Cyclone Res. Rev. 9, 75–86. https://doi.org/10.1016/j.tcrr.2020.04.005
Chan, K.T.F., Chan, J.C.L., 2012. Size and strength of tropical cyclones as inferred from QuikSCAT data. Mon. Weather Rev. 140, 811–824. https://doi.org/10.1175/MWR-D-10-05062.1
Charron, L., Hermanutz, L., 2016. Prioritizing boreal forest restoration sites based on disturbance regime. For. Ecol. Manage. 361, 90–98. https://doi.org/10.1016/j.foreco.2015.11.003
Chauve, A., Vega, C., Durrieu, S., Bretar, F., Allouis, T., Deseilligny, M.P., Puech, W., 2009. Advanced full-waveform lidar data echo detection: Assessing quality of derived terrain and tree height models in an alpine coniferous forest. Int. J. Remote Sens. 30, 5211–5228. https://doi.org/10.1080/01431160903023009
Chave, J., 1999. Study of structural, successional and spatial patterns in tropical rain forests using TROLL, a spatially explicit forest model. Ecol. Modell. 124, 233–254. https://doi.org/10.1016/S0304-3800(99)00171-4
Chave, J., Andalo, C., Brown, S., Cairns, M.A., Chambers, J.Q., Eamus, D., Fölster, H., Fromard, F., Higuchi, N., Kira, T., Lescure, J.P., Nelson, B.W., Ogawa, H., Puig, H., Riéra, B., Yamakura, T., 2005. Tree allometry and improved estimation of carbon stocks and balance in tropical forests. Oecologia 145, 87–99. https://doi.org/10.1007/s00442-005-0100-x
Chave, J., Coomes, D.A., Jansen, S., Lewis, S.L., Swenson, N.G., Zanne, A.E., 2009. Towards a worldwide wood economics spectrum. Ecol. Lett. 12, 351–366. https://doi.org/10.1111/j.1461-0248.2009.01285.x
Chave, J., Olivier, J., Bongers, F., Châtelet, P., Forget, P.-M.M., van der Meer, P., Norden, N., Riéra, B., Charles-Dominique, P., Chatelet, P., Forget, P.-M.M., van der Meer, P., Norden, N., Riera, B., Charles-Dominique, P., 2008. Above-ground biomass and productivity in a rain forest of eastern South America. J. Trop. Ecol. 24, 355–366. https://doi.org/10.1017/S0266467408005075
Chazdon, R.L., Pearcy, R.W., Lee, D.W., Fetcher, N., 1996. Photosynthetic Responses of Tropical Forest Plants to Contrasting Light Environments. Trop. For. Plant Ecophysiol. 5–55. https://doi.org/10.1007/978-1-4613-1163-8_1
Chen, Y.Y., Gardiner, B.A., Pasztor, F., Blennow, K., Ryder, J., Valade, A., Naudts, K., Otto, J., McGrath, M.J., Planque, C., Luyssaert, S., 2018. Simulating damage for wind storms in the land surface model ORCHIDEE-CAN (revision 4262). Geosci. Model Dev. 11, 771–791. https://doi.org/10.5194/gmd-11-771-2018
Chi, C.H., McEwan, R.W., Chang, C. Te, Zheng, C., Yang, Z., Chiang, J.M., Lin, T.-C., 2015. Typhoon Disturbance Mediates Elevational Patterns of Forest Structure, but not Species Diversity, in Humid Monsoon Asia. Ecosystems 18, 1410–1423. https://doi.org/10.1007/s10021-015-9908-3
Christoffersen, B.O., Gloor, M., Fauset, S., Fyllas, N.M., Galbraith, D.R., Baker, T.R., Kruijt, B., Rowland, L., Fisher, R.A., Binks, O.J., Sevanto, S., Xu, C., Jansen, S., Choat, B., Mencuccini, M., McDowell, N.G., Meir, P., 2016. Linking hydraulic traits to tropical forest function in a size-structured and trait-driven model (TFS v.1-Hydro). Geosci. Model Dev. 9, 4227–4255. https://doi.org/10.5194/gmd-9-4227-2016
Clark, D.B., Castro, C.S., Alvarado, L.D.A., Read, J.M., 2004. Quantifying mortality of tropical rain forest trees using high-spatial-resolution satellite data. Ecol. Lett. 7, 52–59. https://doi.org/10.1046/j.1461-0248.2003.00547.x
Clark, D.B., Clark, D.A., Oberbauer, S.F., 2010. Annual wood production in a tropical rain forest in NE Costa Rica linked to climatic variation but not to increasing CO2. Glob. Chang. Biol. 16, 747–759. https://doi.org/10.1111/j.1365-2486.2009.02004.x
Clements, F.E., 1916. Plant succession: an analysis of the development of vegetation, Carnegie I. ed.
Cohn, A., 2017. Leveraging Climate Regulation by Ecosystems for Agriculture to Promote Ecosystem Stewardship. Trop. Conserv. Sci. 10, 1–7. https://doi.org/10.1177/1940082917720672
Condit, R., 2008. Methods for estimating aboveground biomass of forest and replacement vegetation in the tropics. Cent. Trop. For. Sci. Res. Man.
Condit, R.S., 1998. Tropical forest census plots. Springer Science & Business Media, Berlin/Heidelberg. https://doi.org/10.1007/978-3-662-03664-8
Connell, J.H., 1978. Diversity in Tropical Rain Forests and Coral Reefs. Science (80-.). 199, 1302–1310. https://doi.org/10.1126/science.199.4335.1302
Coomes, D.A., Šafka, D., Shepherd, J., Dalponte, M., Holdaway, R., 2018. Airborne laser scanning of natural forests in New Zealand reveals the influences of wind on forest carbon 1–14. https://doi.org/10.1186/s40663-017-0119-6
Coyle, D.B., Stysley, P.R., Poulios, D., Clarke, G.B., Kay, R.B., 2015. Laser transmitter development for

NASA's Global Ecosystem Dynamics Investigation (GEDI) lidar. Lidar Remote Sens. Environ. Monit. XV 9612, 961208. https://doi.org/10.1117/12.2191569
Curran, T.J., Brown, R.L., Edwards, E., Hopkins, K., Kelley, C., McCarthy, E., Pounds, E., Solan, R., Wolf, J., 2008. Plant functional traits explain interspecific differences in immediate cyclone damage to trees of an endangered rainforest community in north Queensland. Austral Ecol. 33, 451–461. https://doi.org/10.1111/j.1442-9993.2008.01900.x
Dalagnol, R., Wagner, F.H., Galvão, L.S., Streher, A.S., Phillips, O.L., Gloor, E., Pugh, T.A.M., Ometto, J.P.H.B., Aragão, L.E.O.C., 2021. Large-scale variations in the dynamics of Amazon forest canopy gaps from airborne lidar data and opportunities for tree mortality estimates. Sci. Rep. 11, 1–15. https://doi.org/10.1038/s41598-020-80809-w
Davies, S.J., Abiem, I., Abu Salim, K., Aguilar, S., Allen, D., Alonso, A., Anderson-Teixeira, K., Andrade, A., Arellano, G., Ashton, P.S., Baker, P.J., Baker, M.E., Baltzer, J.L., Basset, Y., Bissiengou, P., Bohlman, S., Bourg, N.A., Brockelman, W.Y., Bunyavejchewin, S., Burslem, D.F.R.P., Cao, M., Cárdenas, D., Chang, L.W., Chang-Yang, C.H., Chao, K.J., Chao, W.C., Chapman, H., Chen, Y.Y., Chisholm, R.A., Chu, C., Chuyong, G., Clay, K., Comita, L.S., Condit, R., Cordell, S., Dattaraja, H.S., de Oliveira, A.A., den Ouden, J., Detto, M., Dick, C., Du, X., Duque, Á., Ediriweera, S., Ellis, E.C., Obiang, N.L.E., Esufali, S., Ewango, C.E.N., Fernando, E.S., Filip, J., Fischer, G.A., Foster, R., Giambelluca, T., Giardina, C., Gilbert, G.S., Gonzalez-Akre, E., Gunatilleke, I.A.U.N., Gunatilleke, C.V.S., Hao, Z., Hau, B.C.H., He, F., Ni, H., Howe, R.W., Hubbell, S.P., Huth, A., Inman-Narahari, F., Itoh, A., Janík, D., Jansen, P.A., Jiang, M., Johnson, D.J., Jones, F.A., Kanzaki, M., Kenfack, D., Kiratiprayoon, S., Král, K., Krizel, L., Lao, S., Larson, A.J., Li, Y., Li, X., Litton, C.M., Liu, Y., Liu, S., Lum, S.K.Y., Luskin, M.S., Lutz, J.A., Luu, H.T., Ma, K., Makana, J.-R., Malhi, Y., Martin, A., McCarthy, C., McMahon, S.M., McShea, W.J., Memiaghe, H., Mi, X., Mitre, D., Mohamad, M., Monks, L., Muller-Landau, H.C., Musili, P.M., Myers, J.A., Nathalang, A., Ngo, K.M., Norden, N., Novotny, V., O'Brien, M.J., Orwig, D., Ostertag, R., Papathanassiou, K., Parker, G.G., Pérez, R., Perfecto, I., Phillips, R.P., Pongpattananurak, N., Pretzsch, H., Ren, H., Reynolds, G., Rodriguez, L.J., Russo, S.E., Sack, L., Sang, W., Shue, J., Singh, A., Song, G.Z.M., Sukumar, R., Sun, I.F., Suresh, H.S., Swenson, N.G., Tan, S., Thomas, S.C., Thomas, D., Thompson, J., Turner, B.L., Uowolo, A., Uriarte, M., Valencia, R., Vandermeer, J., Vicentini, A., Visser, M., Vrska, T., Wang, Xugao, Wang, Xihua, Weiblen, G.D., Whitfeld, T.J.S., Wolf, A., Wright, S.J., Xu, H., Yao, T.L., Yap, S.L., Ye, W., Yu, M., Zhang, M., Zhu, D., Zhu, L., Zimmerman, J.K., Zuleta, D., 2021. ForestGEO: Understanding forest diversity and dynamics through a global observatory network. Biol. Conserv. 253. https://doi.org/10.1016/j.biocon.2020.108907
Davis, S.H., Wali, A., 1994. Indigenous land tenure and tropical forest management in Latin America. Ambio 23, 485–490. https://doi.org/10.2307/4314265
de Langre, E., 2008a. Effects of Wind on Plants. Annu. Rev. Fluid Mech. 40, 141–168. https://doi.org/10.1146/annurev.fluid.40.111406.102135
de Langre, E., 2008b. Effects of wind on plants. Annu. Rev. Fluid Mech. 40, 141–168. https://doi.org/10.1146/annurev.fluid.40.111406.102135
De Santana, R.A.S., Dias-Júnior, C.Q., Do Vale, R.S., Tóta, J., Fitzjarrald, D.R., 2017. Observing and Modeling the Vertical Wind Profile at Multiple Sites in and above the Amazon Rain Forest Canopy. Adv. Meteorol. 2017. https://doi.org/10.1155/2017/5436157
de Toledo, J.J., Magnusson, W.E., Castilho, C. V., Nascimento, H.E.M., 2012. Tree mode of death in Central Amazonia: Effects of soil and topography on tree mortality associated with storm disturbances. For. Ecol. Manage. 263, 253–261. https://doi.org/10.1016/j.foreco.2011.09.017
DeAngelis, D.L., Grimm, V., 2014. Individual-based models in ecology after four decades. F1000Prime Rep. 6. https://doi.org/10.12703/p6-39
Ding, Y., Zang, R., Letcher, S.G., Liu, S., He, F., 2012. Disturbance regime changes the trait distribution, phylogenetic structure and community assembly of tropical rain forests. Oikos 121, 1263–1270. https://doi.org/10.1111/j.1600-0706.2011.19992.x
Disney, M., 2018. Terrestrial LiDAR: a three-dimensional revolution in how we look at trees. New Phytol. 222, 1736–1741. https://doi.org/10.1111/nph.15517
Disney, M.I., Boni Vicari, M., Burt, A., Calders, K., Lewis, S.L., Raumonen, P., Wilkes, P., 2018. Weighing trees with lasers: Advances, challenges and opportunities. Interface Focus 8. https://doi.org/10.1098/rsfs.2017.0048
Domingues, T.F., Martinelli, L.A., Ehleringer, J.R., 2014. Seasonal patterns of leaf-level photosynthetic gas exchange in an eastern Amazonian rain forest. Plant Ecol. Divers. 7, 189–203. https://doi.org/10.1080/17550874.2012.748849
Domingues, T.F., Meir, P., Feldpausch, T.R., Saiz, G., Veenendaal, E.M., Schrodt, F., Bird, M., Djagbletey, G., Hien, F., Compaore, H., Diallo, A., Grace, J., Lloyd, J., 2010. Co-limitation of photosynthetic capacity by nitrogen and phosphorus in West Africa woodlands. Plant, Cell Environ. 33, 959–980. https://doi.org/10.1111/j.1365-3040.2010.02119.x
Dorman, J.L., Sellers, P.J., 1989. A global climatology of albedo, roughness length and stomatal resistance for atmospheric general circulation models as represented by the Simple Biosphere Model (SiB). J. Appl. Meteorol. 28, 833–855. https://doi.org/10.1175/1520-0450(1989)028<0833:AGCOAR>2.0.CO;2
Dowdy, A.J., Qi, L., Jones, D., Ramsay, H., Fawcett, R., Kuleshov, Y., 2012. Tropical cyclone climatology of

the South Pacific Ocean and its relationship to El Niño-Southern oscillation. J. Clim. 25, 6108–6122. https://doi.org/10.1175/JCLI-D-11-00647.1
Dowle, M., Srinivasan, A., 2020. data.table: Extension of `data.frame`.
Dunham, R.A., Cameron, A.D., 2000. Crown, stem and wood properties of wind-damaged and undamaged Sitka spruce. For. Ecol. Manage. 135, 73–81. https://doi.org/10.1016/S0378-1127(00)00299-1
Duperat, M., Gardiner, B., Ruel, J.C., 2021. Testing an individual tree wind damage risk model in a naturally regenerated balsam fir stand: Potential impact of thinning on the level of risk. Forestry 94, 141–150. https://doi.org/10.1093/forestry/cpaa023
Dupuy, L., Fourcaud, T., Stokes, A., 2005. A numerical investigation into the influence of soil type and root architecture on tree anchorage. Plant Soil 278, 119–134. https://doi.org/10.1007/s11104-005-7577-2
Edwards, D.P., Socolar, J.B., Mills, S.C., Burivalova, Z., Koh, L.P., Wilcove, D.S., 2019. Conservation of Tropical Forests in the Anthropocene. Curr. Biol. 29, R1008–R1020. https://doi.org/10.1016/j.cub.2019.08.026
Ellison, D., Morris, C.E., Locatelli, B., Sheil, D., Cohen, J., Murdiyarso, D., Gutierrez, V., Noordwijk, M. van, Creed, I.F., Pokorny, J., Gaveau, D., Spracklen, D. V., Tobella, A.B., Ilstedt, U., Teuling, A.J., Gebrehiwot, S.G., Sands, D.C., Muys, B., Verbist, B., Springgay, E., Sugandi, Y., Sullivan, C.A., 2017. Trees, forests and water: Cool insights for a hot world. Glob. Environ. Chang. 43, 51–61. https://doi.org/10.1016/j.gloenvcha.2017.01.002
Emanuel, K., Sobel, A., 2013. Response of tropical sea surface temperature, precipitation, and tropical cyclone-related variables to changes in global and local forcing. J. Adv. Model. Earth Syst. 5, 447–458. https://doi.org/10.1002/jame.20032
ESA, 2017. Land Cover CCI Product User Guide Version 2. Tech. Rep.
Espírito-Santo, F.D.B., Gloor, M., Keller, M., Malhi, Y., Saatchi, S., Nelson, B., Junior, R.C.O., Pereira, C., Lloyd, J., Frolking, S., Palace, M., Shimabukuro, Y.E., Duarte, V., Mendoza, A.M., López-González, G., Baker, T.R., Feldpausch, T.R., Brienen, R.J.W., Asner, G.P., Boyd, D.S., Phillips, O.L., 2014. Size and frequency of natural forest disturbances and the Amazon forest carbon balance. Nat. Commun. 5, 1–6. https://doi.org/10.1038/ncomms4434
Everham, E.M., Brokaw, N.V.L., 1996. Forest Damage and Recovery from Catastrophic Wind. Bot. Rev. 62, 113–185. https://doi.org/10.1007/BF02857920
Farquhar, G.D., von Caemmerer, S., Berry, J.A., 1980. A biochemical model of photosynthetic CO<Subscript>2</Subscript> assimilation in leaves of C<Subscript>3</Subscript> species. Planta 149, 78–90.
Farr, T.G., Rosen, P.A., Caro, E., Crippen, R., Duren, R., Hensley, S., Kobrick, M., Paller, M., Rodriguez, E., Roth, L., Seal, D., Shaffer, S., Shimada, J., Umland, J., Werner, M., Oskin, M., Burbank, D., Alsdorf, D., 2007. The shuttle radar topography mission, in: Reviews of Geophysics. pp. 1–33. https://doi.org/10.1007/3-540-44818-7_11
Fauset, S., Gloor, M., Fyllas, N.M., Phillips, O.L., Asner, G.P., Baker, T.R., Patrick Bentley, L., Brienen, R.J.W., Christoffersen, B.O., del Aguila-Pasquel, J., Doughty, C.E., Feldpausch, T.R., Galbraith, D.R., Goodman, R.C., Girardin, C.A.J., Honorio Coronado, E.N., Monteagudo, A., Salinas, N., Shenkin, A., Silva-Espejo, J.E., van der Heijden, G., Vasquez, R., Alvarez-Davila, E., Arroyo, L., Barroso, J.G., Brown, F., Castro, W., Cornejo Valverde, F., Davila Cardozo, N., Di Fiore, A., Erwin, T., Huamantupa-Chuquimaco, I., Núñez Vargas, P., Neill, D., Pallqui Camacho, N., Gutierrez, A.P., Peacock, J., Pitman, N., Prieto, A., Restrepo, Z., Rudas, A., Quesada, C.A., Silveira, M., Stropp, J., Terborgh, J., Vieira, S.A., Malhi, Y., 2019. Individual-Based Modeling of Amazon Forests Suggests That Climate Controls Productivity While Traits Control Demography. Front. Earth Sci. 7. https://doi.org/10.3389/feart.2019.00083
Feng, X., Uriarte, M., González, G., Reed, S., Thompson, J., Zimmerman, J.K., Murphy, L., 2018. Improving predictions of tropical forest response to climate change through integration of field studies and ecosystem modeling. Glob. Chang. Biol. 24, e213–e232. https://doi.org/10.1111/gcb.13863
Féret, J.B., Asner, G.P., 2014. Mapping tropical forest canopy diversity using high-fidelity imaging spectroscopy. Ecol. Appl. 24, 1289–1296. https://doi.org/10.1890/13-1824.1
Féret, J.B., Asner, G.P., 2011. Spectroscopic classification of tropical forest species using radiative transfer modeling. Remote Sens. Environ. 115, 2415–2422. https://doi.org/10.1016/j.rse.2011.05.004
Ferraz, A., Saatchi, S., Mallet, C., Meyer, V., 2016. Lidar detection of individual tree size in tropical forests. Remote Sens. Environ. 183, 318–333. https://doi.org/10.1016/j.rse.2016.05.028
Fischer, F.J., Labrière, N., Vincent, G., Hérault, B., Alonso, A., Memiaghe, H., Bissiengou, P., Kenfack, D., Saatchi, S., Chave, J., 2020. A simulation method to infer tree allometry and forest structure from airborne laser scanning and forest inventories. Remote Sens. Environ. 251, 112056. https://doi.org/10.1016/j.rse.2020.112056
Fischer, F.J., Maréchaux, I., Chave, J., 2019. Improving plant allometry by fusing forest models and remote sensing. New Phytol. 223, 1159–1165. https://doi.org/10.1111/nph.15810
Fischer, R., Bohn, F., Dantas de Paula, M., Dislich, C., Groeneveld, J., Gutiérrez, A.G., Kazmierczak, M., Knapp, N., Lehmann, S., Paulick, S., Pütz, S., Rödig, E., Taubert, F., Köhler, P., Huth, A., 2016. Lessons learned from applying a forest gap model to understand ecosystem and carbon dynamics of complex tropical forests. Ecol. Modell. 326, 124–133. https://doi.org/10.1016/j.ecolmodel.2015.11.018

Fischer, R., Rödig, E., Huth, A., 2018. Consequences of a reduced number of plant functional types for the simulation of forest productivity. Forests 9. https://doi.org/10.3390/f9080460
Fisher, R.A., Koven, C.D., Anderegg, W.R.L., Christoffersen, B.O., Dietze, M.C., Farrior, C.E., Holm, J.A., Hurtt, G.C., Knox, R.G., Lawrence, P.J., Lichstein, J.W., Longo, M., Matheny, A.M., Medvigy, D., Muller-Landau, H.C., Powell, T.L., Serbin, S.P., Sato, H., Shuman, J.K., Smith, B., Trugman, A.T., Viskari, T., Verbeeck, H., Weng, E., Xu, C., Xu, X., Zhang, T., Moorcroft, P.R., 2018. Vegetation demographics in Earth System Models: A review of progress and priorities. Glob. Chang. Biol. 24, 35–54. https://doi.org/10.1111/gcb.13910
Fourcaud, T., Ji, J.N., Zhang, Z.Q., Stokes, A., 2008. Understanding the impact of root morphology on overturning mechanisms: A modelling approach. Ann. Bot. 101, 1267–1280. https://doi.org/10.1093/aob/mcm245
Franklin, J., Serra-Diaz, J.M., Syphard, A.D., Regan, H.M., 2016. Global change and terrestrial plant community dynamics. Proc. Natl. Acad. Sci. U. S. A. 113, 3725–3734. https://doi.org/10.1073/pnas.1519911113
Fyllas, N.M., Bentley, L.P., Shenkin, A., Asner, G.P., Atkin, O.K., Díaz, S., Enquist, B.J., Farfan-Rios, W., Gloor, E., Guerrieri, R., Huasco, W.H., Ishida, Y., Martin, R.E., Meir, P., Phillips, O., Salinas, N., Silman, M., Weerasinghe, L.K., Zaragoza-Castells, J., Malhi, Y., 2017. Solar radiation and functional traits explain the decline of forest primary productivity along a tropical elevation gradient. Ecol. Lett. 20, 730–740. https://doi.org/10.1111/ele.12771
Fyllas, N.M., Gloor, E., Mercado, L.M., Sitch, S., Quesada, C.A., Domingues, T.F., Galbraith, D.R., Torre-Lezama, A., Vilanova, E., Ramírez-Angulo, H., Higuchi, N., Neill, D.A., Silveira, M., Ferreira, L., Aymard C., G.A., Malhi, Y., Phillips, O.L., Lloyd, J., 2014. Analysing Amazonian forest productivity using a new individual and trait-based model (TFS v.1). Geosci. Model Dev. 7, 1251–1269. https://doi.org/10.5194/gmd-7-1251-2014
Galbraith, D., Levy, P.E., Sitch, S., Huntingford, C., Cox, P., Williams, M., Meir, P., 2010. Multiple mechanisms of Amazonian forest biomass losses in three dynamic global vegetation models under climate change. New Phytol. 187, 647–665. https://doi.org/10.1111/j.1469-8137.2010.03350.x
Gardiner, B., Berry, P., Moulia, B., 2016. Review: Wind impacts on plant growth, mechanics and damage. Plant Sci. 245, 94–118. https://doi.org/10.1016/j.plantsci.2016.01.006
Gardiner, B.A., Byrne, K., Hale, S., Kamimura, K., Mitchell, S.J., Peltola, H., Ruel, J.-C., 2008. A review of mechanistic modelling of wind damage risk to forests. Forestry 81, 447–463. https://doi.org/10.1093/forestry/cpn022
Gardiner, B.A., Peltola, H., Kellomäki, S., 2000. Comparison of two models for predicting the critical wind speeds required to damage coniferous trees. Ecol. Modell. 129, 1–23. https://doi.org/10.1016/S0304-3800(00)00220-9
Gardiner, B.A., Stagey, G.R., Belcher, R.E., Wood, C.J., 1997. Field and wind tunnel assessments of the implications of respacing and thinning for tree stability. Forestry 70, 233–252. https://doi.org/10.1093/forestry/70.3.233
Gardner, T.A., Barlow, J., Sodhi, N.S., Peres, C.A., 2010. A multi-region assessment of tropical forest biodiversity in a human-modified world. Biol. Conserv. 143, 2293–2300. https://doi.org/10.1016/j.biocon.2010.05.017
Garstang, M., White, S., Shugart, H.H., Halverson, J., 1998. Convective cloud downdrafts as the cause of large blowdowns in the Amazon rainforest. Meteorol. Atmos. Phys. 67, 199–212. https://doi.org/10.1007/BF01277510
Getzin, S., Nuske, R.S., Wiegand, K., 2014. Using unmanned aerial vehicles (UAV) to quantify spatial gap patterns in forests. Remote Sens. 6, 6988–7004. https://doi.org/10.3390/rs6086988
Gilleland, E., Katz, R.W., 2016. {extRemes} 2.0: An Extreme Value Analysis Package in {R}. J. Stat. Softw. 72, 1–39. https://doi.org/10.18637/jss.v072.i08
Gleason, H., 1926. The Individualistic Concept of the Plant Association. Society 53, 7–26.
Goodenough, D.G., Pearlman, J., Chen, H., Dyk, A., Han, T., Li, J., Miller, J., Niemann, K.O., 2004. Forest information from hyperspectral sensing. Int. Geosci. Remote Sens. Symp. 4, 2585–2589. https://doi.org/10.1109/igarss.2004.1369826
Gora, E.M., Burchfield, J.C., Muller-Landau, H.C., Bitzer, P.M., Yanoviak, S.P., 2020. Pantropical geography of lightning-caused disturbance and its implications for tropical forests. Glob. Chang. Biol. 26, 5017–5026. https://doi.org/10.1111/gcb.15227
Goulamoussène, Y., Bedeau, C., Descroix, L., Linguet, L., Hérault, B., 2017. Environmental control of natural gap size distribution in tropical forests. Biogeosciences 14, 353–364. https://doi.org/10.5194/bg-14-353-2017
Grainger, A., 1993. Rates of Deforestation in the Humid Tropics: Estimates and Measurements. Geogr. J. 159, 33. https://doi.org/10.2307/3451487
Green, D.W., Winandy, J.E., Kretschmann, D.E., 1999. Mechanical properties of wood, in: Wood Handbook—Wood as an Engineering Material. USDA Forest Service, Forest Products Laboratory, Madison, WI, USA, pp. 1–45. https://doi.org/10.1126/science.46.1195.516-a
Grime, J.P., 1977. Evidence for the Existence of Three Primary Strategies in Plants and Its Relevance to Ecological and Evolutionary Theory. Am. Nat. 111, 1169–1194.
Guan, K., Pan, M., Li, H., Wolf, A., Wu, J., Medvigy, D., Caylor, K.K., Sheffield, J., Wood, E.F., Malhi, Y.,

Liang, M., Kimball, J.S., Saleska, S.R., Berry, J., Joiner, J., Lyapustin, A.I., 2015. Photosynthetic seasonality of global tropical forests constrained by hydroclimate. Nat. Geosci. 8, 284–289. https://doi.org/10.1038/ngeo2382
Guenther, A., Nicholas, C., Fall, R., Klinger, L., Mckay, W.A., Scholes, B., 1995. A global model of natural volatile organic compound emissions s Raja the balance Triangle changes in the atmospheric accumulation rates of greenhouse Triangle Several inventories of natural and Exposure Assessment global scales have been two classes Fores. J. Geophys. Res. 100, 8873–8892.
Halder, N.K., Merchant, A., Misbahuzzaman, K., Wagner, S., Mukul, S.A., 2021. Why some trees are more vulnerable during catastrophic cyclone events in the Sundarbans mangrove forest of Bangladesh? For. Ecol. Manage. 490, 119117. https://doi.org/10.1016/j.foreco.2021.119117
Hale, S.A., Gardiner, B.A., Peace, A., Nicoll, B.C., Taylor, P., Pizzirani, S., 2015. Comparison and validation of three versions of a forest wind risk model. Environ. Model. Softw. 68, 27–41. https://doi.org/10.1016/j.envsoft.2015.01.016
Hale, S.E., Gardiner, B.A., Wellpott, A., Nicoll, B.C., Achim, A., 2012. Wind loading of trees: Influence of tree size and competition. Eur. J. For. Res. 131, 203–217. https://doi.org/10.1007/s10342-010-0448-2
Hales, T.C., Miniat, C.F., 2017. Soil moisture causes dynamic adjustments to root reinforcement that reduce slope stability. Earth Surf. Process. Landforms 42, 803–813. https://doi.org/10.1002/esp.4039
Hansen, M.C., Krylov, A., Tyukavina, A., Potapov, P. V., Turubanova, S., Zutta, B., Ifo, S., Margono, B., Stolle, F., Moore, R., 2016. Humid tropical forest disturbance alerts using Landsat data. Environ. Res. Lett. 11. https://doi.org/10.1088/1748-9326/11/3/034008
Hansen, M.C., Potapov, P. V., Moore, R., Hancher, M., Turubanova, S.A., Tyukavina, A., Thau, D., Stehman, S. V., Goetz, S.J., Loveland, T.R., Kommareddy, A., Egorov, A., Chini, L., Justice, C.O., Townshend, J.R.G., 2013. High-resolution global maps of 21st-century forest cover change. Science (80-.). 342, 850–853. https://doi.org/10.1126/science.1244693
Harris, I., Jones, P.D., Osborn, T.J., Lister, D.H., 2014. Updated high-resolution grids of monthly climatic observations - the CRU TS3.10 Dataset. Int. J. Climatol. 34, 623–642. https://doi.org/10.1002/joc.3711
Hartig, F., Dislich, C., Wiegand, T., Huth, A., 2014. Technical note: Approximate bayesian parameterization of a process-based tropical forest model. Biogeosciences 11, 1261–1272. https://doi.org/10.5194/bg-11-1261-2014
Hartig, F., Dyke, J., Hickler, T., Higgins, S.I., O'Hara, R.B., Scheiter, S., Huth, A., 2012. Connecting dynamic vegetation models to data - an inverse perspective. J. Biogeogr. 39, 2240–2252. https://doi.org/10.1111/j.1365-2699.2012.02745.x
Hayashi, M., Saigusa, N., Oguma, H., Yamagata, Y., Takao, G., 2015. Quantitative assessment of the impact of typhoon disturbance on a Japanese forest using satellite laser altimetry. Remote Sens. Environ. 156, 216–225. https://doi.org/10.1016/j.rse.2014.09.028
Henning, D.H., 1998. Buddhism and Deep Ecology: Protection of Spiritual and Cultural Values for Natural Tropical Forests in Asia, in: Personal , Societal , and Ecological Values of Wilderness : Sixth World Wilderness Congress Proceedings on Research, Management, and Allocation. pp. 108–112.
Hijmans, R.J., 2020. raster: Geographic Data Analysis and Modeling.
Hijmans, R.J., 2019. geosphere: Spherical Trigonometry.
Hogan, J.A., Zimmerman, J.K., Thompson, J., Uriarte, M., Swenson, N.G., Condit, R.S., Hubbell, S.P., Johnson, D.J., Sun, I.-F., Chang-Yang, C.H., Su, S.H., Ong, P., Rodriguez, L., Monoy, C.C., Yap, S., Davies, S.J., 2018. The frequency of cyclonic wind storms shapes tropical forest dynamism and functional trait dispersion. Forests 8, 1–27. https://doi.org/10.3390/f9070404
Holm, J.A., Knox, R.G., Zhu, Q., Fisher, R.A., Koven, C.D., Nogueira Lima, A.J., Riley, W.J., Longo, M., Negrón-Juárez, R.I., de Araujo, A.C., Kueppers, L.M., Moorcroft, P.R., Higuchi, N., Chambers, J.Q., 2020. The Central Amazon Biomass Sink Under Current and Future Atmospheric CO2: Predictions From Big-Leaf and Demographic Vegetation Models. J. Geophys. Res. Biogeosciences 125, 1–23. https://doi.org/10.1029/2019JG005500
Huang, S.-C., Lin, Y.-C., Liu, K.-F., Chen, C.-T., 2011. Microplate method for plant total nitrogen and phosphorus analysis. Taiwan. J. Agric. Chem. Food Sci. 49, 19–25.
Huber, N., Bugmann, H., Lafond, V., 2020. Capturing ecological processes in dynamic forest models: why there is no silver bullet to cope with complexity. Ecosphere 11. https://doi.org/10.1002/ecs2.3109
Huber, N., Bugmann, H., Lafond, V., 2018. Global sensitivity analysis of a dynamic vegetation model: Model sensitivity depends on successional time, climate and competitive interactions. Ecol. Modell. 368, 377–390. https://doi.org/10.1016/j.ecolmodel.2017.12.013
Huffman, G.J., Stocker, E.F., Bolvin, D.T., Nelkin, E.J., Tan, J., 2019. GPM IMERG Final Precipitation L3 1 month 0.1 degree x 0.1 degree V06.
Hunter, M.O., Keller, M., Morton, D., Cook, B., Lefsky, M., Ducey, M., Saleska, S., De Oliveira, R.C., Schietti, J., Zang, R., 2015. Structural dynamics of tropical moist forest gaps. PLoS One 10. https://doi.org/10.1371/journal.pone.0132144
Ibanez, T., Keppel, G., Baider, C., Birkinshaw, C., Florens, F.B.V., Laidlaw, M., Menkes, C., Parthasarathy, N., Rajkumar, M., Ratovoson, F., Rasingam, L., Reza, L., Aiba, S. ichiro, Webb, E.L., Zang, R., Birnbaum, P., 2020. Tropical cyclones and island area shape species abundance distributions of local tree communities. Oikos 1–11. https://doi.org/10.1111/oik.07501

Ibanez, T., Keppel, G., Menkes, C., Gillespie, T.W., Lengaigne, M., Rivas-torres, M.M.G., Birnbaum, P., Mangeas, M., Rivas, G., Birnbaum, P., 2019. Globally consistent impact of tropical cyclones on the structure of tropical and subtropical forests. J. Ecol. 107, 279–292. https://doi.org/10.1111/1365-2745.13039

Ichii, K., Suzuki, T., Kato, T., Ito, A., Hajima, T., Ueyama, M., Sasai, T., Hirata, R., Saigusa, N., Ohtani, Y., Takagi, K., 2010. Multi-model analysis of terrestrial carbon cycles in Japan: Limitations and implications of model calibration using eddy flux observations. Biogeosciences 7, 2061–2081. https://doi.org/10.5194/bg-7-2061-2010

Iida, Y., Kohyama, T.S., Swenson, N.G., Su, S.-H., Chen, C.-T., Chiang, J.-M., Sun, I.-F., 2014. Linking functional traits and demographic rates in a subtropical tree community: The importance of size dependency. J. Ecol. 102, 641–650. https://doi.org/10.1111/1365-2745.12221

Inoue, E., 1963. On the Turbulent Structure of Airflow within. J. Meteorol. Soc. Japan. Ser. II 41, 317–326. https://doi.org/10.2151/jmsj1923.41.6_317

Jackson, T., Bunce, A., James, K., Wellpott, A., Van Bloem, S., Achim, A., Gardiner, B., 2021. The motion of trees in the wind: a data synthesis. Biogeosciences 18, 4059–4072.

Jackson, T., Sethi, S., Dellwik, E., Angelou, N., Bunce, A., van Emmerik, T., Duperat, M., Ruel, J.-C., Wellpott, A., Van Bloem, S., Achim, A., Kane, B., Ciruzzi, D., Loheide II, S., James, K., Burcham, D., Moore, J., Schindler, D., Kolbe, S., Wiegmann, K., Rudnicki, M., Lieffers, V., Selker, J., Gougherty, A., Newson, T., Koeser, A., Miesbauer, J., Samelson, R., Wagner, J., Coomes, D., Gardiner, B., 2020. The motion of trees in the wind: a data synthesis. Biogeosciences Discuss. 1–21. https://doi.org/10.5194/bg-2020-427

Jackson, T., Shenkin, A., Kalyan, B., Zionts, J., Calders, K., Origo, N., Disney, M., Burt, A., Raumonen, P., Malhi, Y., Of, S.-M.A.P., Field, T.H.E., 2019a. A New Architectural Perspective on Wind Damage in a Natural Forest. Front. For. Glob. Chang. 1, 1–10. https://doi.org/10.3389/ffgc.2018.00013

Jackson, T., Shenkin, A., Moore, J., Bunce, A., Van Emmerik, T., Kane, B., Burcham, D., James, K., Selker, J., Calders, K., Origo, N., Disney, M., Burt, A., Wilkes, P., Raumonen, P., Gonzalez De Tanago Menaca, J., Lau, A., Herold, M., Goodman, R.C., Fourcaud, T., Malhi, Y., 2019b. An architectural understanding of natural sway frequencies in trees. J. R. Soc. Interface 16. https://doi.org/10.1098/rsif.2019.0116

Jackson, T., Shenkin, A., Wellpott, A., Calders, K., Origo, N., Disney, M., Burt, A., Raumonen, P., Gardiner, B., Herold, M., Fourcaud, T., Malhi, Y., 2019c. Finite element analysis of trees in the wind based on terrestrial laser scanning data. Agric. For. Meteorol. 265, 137–144. https://doi.org/10.1016/j.agrformet.2018.11.014

Jentsch, A., White, P., 2019. A theory of pulse dynamics and disturbance in ecology. Ecology 100, 1–15. https://doi.org/10.1002/ecy.2734

Joetzjer, E., Pillet, M., Ciais, P., Barbier, N., Chave, J., Schlund, M., Maignan, F., Barichivich, J., Luyssaert, S., Hérault, B., von Poncet, F., Poulter, B., 2017. Assimilating satellite-based canopy height within an ecosystem model to estimate aboveground forest biomass. Geophys. Res. Lett. 44, 6823–6832. https://doi.org/10.1002/2017GL074150

Johnson, M.O., Galbraith, D., Gloor, M., De Deurwaerder, H., Guimberteau, M., Rammig, A., Thonicke, K., Verbeeck, H., von Randow, C., Monteagudo, A., Phillips, O.L., Brienen, R.J.W., Feldpausch, T.R., Lopez Gonzalez, G., Fauset, S., Quesada, C.A., Christoffersen, B., Ciais, P., Sampaio, G., Kruijt, B., Meir, P., Moorcroft, P., Zhang, K., Alvarez-Davila, E., Alves de Oliveira, A., Amaral, I., Andrade, A., Aragao, L.E.O.C., Araujo-Murakami, A., Arets, E.J.M.M., Arroyo, L., Aymard, G.A., Baraloto, C., Barroso, J., Bonal, D., Boot, R., Camargo, J., Chave, J., Cogollo, A., Cornejo Valverde, F., Lola da Costa, A.C., Di Fiore, A., Ferreira, L., Higuchi, N., Honorio, E.N., Killeen, T.J., Laurance, S.G., Laurance, W.F., Licona, J., Lovejoy, T., Malhi, Y., Marimon, B., Marimon, B.H., Matos, D.C.L., Mendoza, C., Neill, D.A., Pardo, G., Peña-Claros, M., Pitman, N.C.A., Poorter, L., Prieto, A., Ramirez-Angulo, H., Roopsind, A., Rudas, A., Salomao, R.P., Silveira, M., Stropp, J., ter Steege, H., Terborgh, J., Thomas, R., Toledo, M., Torres-Lezama, A., van der Heijden, G.M.F., Vasquez, R., Guimarães Vieira, I.C., Vilanova, E., Vos, V.A., Baker, T.R., 2016. Variation in stem mortality rates determines patterns of above-ground biomass in Amazonian forests: implications for dynamic global vegetation models. Glob. Chang. Biol. 22, 3996–4013. https://doi.org/10.1111/gcb.13315

Jones, H.G., 2013. Plants and Microclimate: A Quantitative Approach to Environmental Plant Physiology, 3rd ed. Cambridge, UK.

Jucker, T., Caspersen, J., Chave, J., Antin, C., Barbier, N., Bongers, F., Dalponte, M., van Ewijk, K.Y., Forrester, D.I., Haeni, M., Higgins, S.I., Holdaway, R.J., Iida, Y., Lorimer, C., Marshall, P.L., Momo, S., Moncrieff, G.R., Ploton, P., Poorter, L., Rahman, K.A., Schlund, M., Sonké, B., Sterck, F.J., Trugman, A.T., Usoltsev, V.A., Vanderwel, M.C., Waldner, P., Wedeux, B.M.M., Wirth, C., Wöll, H., Woods, M., Xiang, W., Zimmermann, N.E., Coomes, D.A., 2017. Allometric equations for integrating remote sensing imagery into forest monitoring programmes. Glob. Chang. Biol. 23, 177–190. https://doi.org/10.1111/gcb.13388

Kalnay, E., Kanamitsu, M., Kistler, R., Collins, W., Deaven, D., Gandin, L., Iredell, M., Saha, S., White, G., Woollen, J., Zhu, Y., Chelliah, M., Ebisuzaki, W., Higgins, W., Janowiak, J., Mo, K.C., Ropelewski, C., Wang, J., Leetmass, A., Reynolds, R., Jenne, R., Joseph, D., 1996. The NCEP/NCAR 40-year Reanalysis Project. Bull. Am. Meteorol. Soc. 77, 437–471.

Kamimura, K., Gardiner, B.A., Dupont, S., Finnigan, J., 2019. Agent-based modelling of wind damage processes and patterns in forests. Agric. For. Meteorol. 268, 279–288.

https://doi.org/10.1016/j.agrformet.2019.01.020
Kassambara, A., 2020. ggpubr: "ggplot2" Based Publication Ready Plots.
Kattge, J., Bönisch, G., Díaz, S., Lavorel, S., Prentice, I.C., Leadley, P., Tautenhahn, S., Werner, G.D.A., Aakala, T., Abedi, M., Acosta, A.T.R., Adamidis, G.C., Adamson, K., Aiba, M., Albert, C.H., Alcántara, J.M., Alcázar C, C., Aleixo, I., Ali, H., Amiaud, B., Ammer, C., Amoroso, M.M., Anand, M., Anderson, C., Anten, N., Antos, J., Apgaua, D.M.G., Ashman, T.L., Asmara, D.H., Asner, G.P., Aspinwall, M., Atkin, O., Aubin, I., Baastrup-Spohr, L., Bahalkeh, K., Bahn, M., Baker, T., Baker, W.J., Bakker, J.P., Baldocchi, D., Baltzer, J., Banerjee, A., Baranger, A., Barlow, J., Barneche, D.R., Baruch, Z., Bastianelli, D., Battles, J., Bauerle, W., Bauters, M., Bazzato, E., Beckmann, M., Beeckman, H., Beierkuhnlein, C., Bekker, R., Belfry, G., Belluau, M., Beloiu, M., Benavides, R., Benomar, L., Berdugo-Lattke, M.L., Berenguer, E., Bergamin, R., Bergmann, J., Bergmann Carlucci, M., Berner, L., Bernhardt-Römermann, M., Bigler, C., Bjorkman, A.D., Blackman, C., Blanco, C., Blonder, B., Blumenthal, D., Bocanegra-González, K.T., Boeckx, P., Bohlman, S., Böhning-Gaese, K., Boisvert-Marsh, L., Bond, W., Bond-Lamberty, B., Boom, A., Boonman, C.C.F., Bordin, K., Boughton, E.H., Boukili, V., Bowman, D.M.J.S., Bravo, S., Brendel, M.R., Broadley, M.R., Brown, K.A., Bruelheide, H., Brumnich, F., Bruun, H.H., Bruy, D., Buchanan, S.W., Bucher, S.F., Buchmann, N., Buitenwerf, R., Bunker, D.E., Bürger, J., Burrascano, S., Burslem, D.F.R.P., Butterfield, B.J., Byun, C., Marques, M., Scalon, M.C., Caccianiga, M., Cadotte, M., Cailleret, M., Camac, J., Camarero, J.J., Campany, C., Campetella, G., Campos, J.A., Cano-Arboleda, L., Canullo, R., Carbognani, M., Carvalho, F., Casanoves, F., Castagneyrol, B., Catford, J.A., Cavender-Bares, J., Cerabolini, B.E.L., Cervellini, M., Chacón-Madrigal, E., Chapin, K., Chapin, F.S., Chelli, S., Chen, S.C., Chen, A., Cherubini, P., Chianucci, F., Choat, B., Chung, K.S., Chytrý, M., Ciccarelli, D., Coll, L., Collins, C.G., Conti, L., Coomes, D.A., Cornelissen, J.H.C., Cornwell, W.K., Corona, P., Coyea, M., Craine, J., Craven, D., Cromsigt, J.P.G.M., Csecserits, A., Cufar, K., Cuntz, M., da Silva, A.C., Dahlin, K.M., Dainese, M., Dalke, I., Dalle Fratte, M., Dang-Le, A.T., Danihelka, J., Dannoura, M., Dawson, S., de Beer, A.J., De Frutos, A., De Long, J.R., Dechant, B., Delagrange, S., Delpierre, N., Derroire, G., Dias, A.S., Diaz-Toribio, M.H., Dimitrakopoulos, P.G., Dobrowolski, M., Doktor, D., Dřevojan, P., Dong, N., Dransfield, J., Dressler, S., Duarte, L., Ducouret, E., Dullinger, S., Durka, W., Duursma, R., Dymova, O., E-Vojtkó, A., Eckstein, R.L., Ejtehadi, H., Elser, J., Emilio, T., Engemann, K., Erfanian, M.B., Erfmeier, A., Esquivel-Muelbert, A., Esser, G., Estiarte, M., Domingues, T.F., Fagan, W.F., Fagúndez, J., Falster, D.S., Fan, Y., Fang, J., Farris, E., Fazlioglu, F., Feng, Y., Fernandez-Mendez, F., Ferrara, C., Ferreira, J., Fidelis, A., Finegan, B., Firn, J., Flowers, T.J., Flynn, D.F.B., Fontana, V., Forey, E., Forgiarini, C., François, L., Frangipani, M., Frank, D., Frenette-Dussault, C., Freschet, G.T., Fry, E.L., Fyllas, N.M., Mazzochini, G.G., Gachet, S., Gallagher, R., Ganade, G., Ganga, F., García-Palacios, P., Gargaglione, V., Garnier, E., Garrido, J.L., de Gasper, A.L., Gea-Izquierdo, G., Gibson, D., Gillison, A.N., Giroldo, A., Glasenhardt, M.C., Gleason, S., Gliesch, M., Goldberg, E., Göldel, B., Gonzalez-Akre, E., Gonzalez-Andujar, J.L., González-Melo, A., González-Robles, A., Graae, B.J., Granda, E., Graves, S., Green, W.A., Gregor, T., Gross, N., Guerin, G.R., Günther, A., Gutiérrez, A.G., Haddock, L., Haines, A., Hall, J., Hambuckers, A., Han, W., Harrison, S.P., Hattingh, W., Hawes, J.E., He, T., He, P., Heberling, J.M., Helm, A., Hempel, S., Hentschel, J., Hérault, B., Hereş, A.M., Herz, K., Heuertz, M., Hickler, T., Hietz, P., Higuchi, P., Hipp, A.L., Hirons, A., Hock, M., Hogan, J.A., Holl, K., Honnay, O., Hornstein, D., Hou, E., Hough-Snee, N., Hovstad, K.A., Ichie, T., Igić, B., Illa, E., Isaac, M., Ishihara, M., Ivanov, L., Ivanova, L., Iversen, C.M., Izquierdo, J., Jackson, R.B., Jackson, B., Jactel, H., Jagodzinski, A.M., Jandt, U., Jansen, S., Jenkins, T., Jentsch, A., Jespersen, J.R.P., Jiang, G.F., Johansen, J.L., Johnson, D., Jokela, E.J., Joly, C.A., Jordan, G.J., Joseph, G.S., Junaedi, D., Junker, R.R., Justes, E., Kabzems, R., Kane, J., Kaplan, Z., Kattenborn, T., Kavelenova, L., Kearsley, E., Kempel, A., Kenzo, T., Kerkhoff, A., Khalil, M.I., Kinlock, N.L., Kissling, W.D., Kitajima, K., Kitzberger, T., Kjøller, R., Klein, T., Kleyer, M., Klimešová, J., Klipel, J., Kloeppel, B., Klotz, S., Knops, J.M.H., Kohyama, T., Koike, F., Kollmann, J., Komac, B., Komatsu, K., König, C., Kraft, N.J.B., Kramer, K., Kreft, H., Kühn, I., Kumarathunge, D., Kuppler, J., Kurokawa, H., Kurosawa, Y., Kuyah, S., Laclau, J.P., Lafleur, B., Lallai, E., Lamb, E., Lamprecht, A., Larkin, D.J., Laughlin, D., Le Bagousse-Pinguet, Y., le Maire, G., le Roux, P.C., le Roux, E., Lee, T., Lens, F., Lewis, S.L., Lhotsky, B., Li, Y., Li, X., Lichstein, J.W., Liebergesell, M., Lim, J.Y., Lin, Y.S., Linares, J.C., Liu, C., Liu, D., Liu, U., Livingstone, S., Llusià, J., Lohbeck, M., López-García, Á., Lopez-Gonzalez, G., Lososová, Z., Louault, F., Lukács, B.A., Lukeš, P., Luo, Y., Lussu, M., Ma, S., Maciel Rabelo Pereira, C., Mack, M., Maire, V., Mäkelä, A., Mäkinen, H., Malhado, A.C.M., Mallik, A., Manning, P., Manzoni, S., Marchetti, Z., Marchino, L., Marcilio-Silva, V., Marcon, E., Marignani, M., Markesteijn, L., Martin, A., Martínez-Garza, C., Martínez-Vilalta, J., Mašková, T., Mason, K., Mason, N., Massad, T.J., Masse, J., Mayrose, I., McCarthy, J., McCormack, M.L., McCulloh, K., McFadden, I.R., McGill, B.J., McPartland, M.Y., Medeiros, J.S., Medlyn, B., Meerts, P., Mehrabi, Z., Meir, P., Melo, F.P.L., Mencuccini, M., Meredieu, C., Messier, J., Mészáros, I., Metsaranta, J., Michaletz, S.T., Michelaki, C., Migalina, S., Milla, R., Miller, J.E.D., Minden, V., Ming, R., Mokany, K., Moles, A.T., Molnár, A., Molofsky, J., Molz, M., Montgomery, R.A., Monty, A., Moravcová, L., Moreno-Martínez, A., Moretti, M., Mori, A.S., Mori, S., Morris, D., Morrison, J., Mucina, L., Mueller, S., Muir, C.D., Müller, S.C., Munoz, F., Myers-Smith, I.H., Myster, R.W., Nagano, M., Naidu, S., Narayanan, A., Natesan, B., Negoita, L., Nelson, A.S., Neuschulz, E.L., Ni, J., Niedrist, G., Nieto, J., Niinemets, Ü., Nolan, R., Nottebrock, H., Nouvellon, Y., Novakovskiy, A., Nystuen, K.O., O'Grady, A., O'Hara, K.,

O'Reilly-Nugent, A., Oakley, S., Oberhuber, W., Ohtsuka, T., Oliveira, R., Öllerer, K., Olson, M.E., Onipchenko, V., Onoda, Y., Onstein, R.E., Ordonez, J.C., Osada, N., Ostonen, I., Ottaviani, G., Otto, S., Overbeck, G.E., Ozinga, W.A., Pahl, A.T., Paine, C.E.T., Pakeman, R.J., Papageorgiou, A.C., Parfionova, E., Pärtel, M., Patacca, M., Paula, S., Paule, J., Pauli, H., Pausas, J.G., Peco, B., Penuelas, J., Perea, A., Peri, P.L., Petisco-Souza, A.C., Petraglia, A., Petritan, A.M., Phillips, O.L., Pierce, S., Pillar, V.D., Pisek, J., Pomogaybin, A., Poorter, H., Portsmuth, A., Poschlod, P., Potvin, C., Pounds, D., Powell, A.S., Power, S.A., Prinzing, A., Puglielli, G., Pyšek, P., Raevel, V., Rammig, A., Ransijn, J., Ray, C.A., Reich, P.B., Reichstein, M., Reid, D.E.B., Réjou-Méchain, M., de Dios, V.R., Ribeiro, S., Richardson, S., Riibak, K., Rillig, M.C., Riviera, F., Robert, E.M.R., Roberts, S., Robroek, B., Roddy, A., Rodrigues, A.V., Rogers, A., Rollinson, E., Rolo, V., Römermann, C., Ronzhina, D., Roscher, C., Rosell, J.A., Rosenfield, M.F., Rossi, C., Roy, D.B., Royer-Tardif, S., Rüger, N., Ruiz-Peinado, R., Rumpf, S.B., Rusch, G.M., Ryo, M., Sack, L., Saldaña, A., Salgado-Negret, B., Salguero-Gomez, R., Santa-Regina, I., Santacruz-García, A.C., Santos, J., Sardans, J., Schamp, B., Scherer-Lorenzen, M., Schleuning, M., Schmid, B., Schmidt, M., Schmitt, S., Schneider, J. V., Schowanek, S.D., Schrader, J., Schrodt, F., Schuldt, B., Schurr, F., Selaya Garvizu, G., Semchenko, M., Seymour, C., Sfair, J.C., Sharpe, J.M., Sheppard, C.S., Sheremetiev, S., Shiodera, S., Shipley, B., Shovon, T.A., Siebenkäs, A., Sierra, C., Silva, V., Silva, M., Sitzia, T., Sjöman, H., Slot, M., Smith, N.G., Sodhi, D., Soltis, P., Soltis, D., Somers, B., Sonnier, G., Sørensen, M.V., Sosinski, E.E., Soudzilovskaia, N.A., Souza, A.F., Spasojevic, M., Sperandii, M.G., Stan, A.B., Stegen, J., Steinbauer, K., Stephan, J.G., Sterck, F., Stojanovic, D.B., Strydom, T., Suarez, M.L., Svenning, J.C., Svitková, I., Svitok, M., Svoboda, M., Swaine, E., Swenson, N., Tabarelli, M., Takagi, K., Tappeiner, U., Tarifa, R., Tauugourdeau, S., Tavsanoglu, C., te Beest, M., Tedersoo, L., Thiffault, N., Thom, D., Thomas, E., Thompson, K., Thornton, P.E., Thuiller, W., Tichý, L., Tissue, D., Tjoelker, M.G., Tng, D.Y.P., Tobias, J., Török, P., Tarin, T., Torres-Ruiz, J.M., Tóthmérész, B., Treurnicht, M., Trivellone, V., Trolliet, F., Trotsiuk, V., Tsakalos, J.L., Tsiripidis, I., Tysklind, N., Umehara, T., Usoltsev, V., Vadeboncoeur, M., Vaezi, J., Valladares, F., Vamosi, J., van Bodegom, P.M., van Breugel, M., Van Cleemput, E., van de Weg, M., van der Merwe, S., van der Plas, F., van der Sande, M.T., van Kleunen, M., Van Meerbeek, K., Vanderwel, M., Vanselow, K.A., Vårhammar, A., Varone, L., Vasquez Valderrama, M.Y., Vassilev, K., Vellend, M., Veneklaas, E.J., Verbeeck, H., Verheyen, K., Vibrans, A., Vieira, I., Villacís, J., Violle, C., Vivek, P., Wagner, K., Waldram, M., Waldron, A., Walker, A.P., Waller, M., Walther, G., Wang, H., Wang, F., Wang, W., Watkins, H., Watkins, J., Weber, U., Weedon, J.T., Wei, L., Weigelt, P., Weiher, E., Wells, A.W., Wellstein, C., Wenk, E., Westoby, M., Westwood, A., White, P.J., Whitten, M., Williams, M., Winkler, D.E., Winter, K., Womack, C., Wright, I.J., Wright, S.J., Wright, J., Pinho, B.X., Ximenes, F., Yamada, T., Yamaji, K., Yanai, R., Yankov, N., Yguel, B., Zanini, K.J., Zanne, A.E., Zelený, D., Zhao, Y.P., Zheng, Jingming, Zheng, Ji, Ziemińska, K., Zirbel, C.R., Zizka, G., Zo-Bi, I.C., Zotz, G., Wirth, C., 2020. TRY plant trait database – enhanced coverage and open access. Glob. Chang. Biol. 26, 119–188. https://doi.org/10.1111/gcb.14904

Keenan, R.J., Reams, G.A., Achard, F., de Freitas, J. V., Grainger, A., Lindquist, E., 2015. Dynamics of global forest area: Results from the FAO Global Forest Resources Assessment 2015. For. Ecol. Manage. 352, 9–20. https://doi.org/10.1016/j.foreco.2015.06.014

King, M.D., Kaufman, Y.J., Menzel, W.P., Tanré, D., 1992. Remote Sensing of Cloud, Aerosol, and Water Vapor Properties from the Moderate Resolution Imaging Spectrometer (MODIS). IEEE Trans. Geosci. Remote Sens. 30, 2–27. https://doi.org/10.1109/36.124212

Kirscht, M., Rinke, C., 1998. 3D reconstruction of buildings and vegetation from SAR images. Proc. IAPR Work. Mach. Vis. Appl. 228–231.

Kislov, D.E., Korznikov, K.A., 2020. Automatic windthrow detection using very-high-resolution satellite imagery and deep learning. Remote Sens. 12. https://doi.org/10.3390/rs12071145

Kistler, R., Kalnay, E., Collins, W., Saha, S., White, G., Woollen, J., Chelliah, M., Ebisuzaki, W., Kanamitsu, M., Kousky, V., Van Den Dool, H., Jenne, R., Fiorino, M., 2001. The NCEP-NCAR 50-year reanalysis: Monthly means CD-ROM and documentation. Bull. Am. Meteorol. Soc. 82, 247–267. https://doi.org/10.1175/1520-0477(2001)082<0247:TNNYRM>2.3.CO;2

Kitajima, K., Mulkey, S.S., Wright, S.J., 2005. Variation in crown light utilization characteristics among tropical canopy trees. Ann. Bot. 95, 535–547. https://doi.org/10.1093/aob/mci051

Knapp, K.R., Kruk, M.C., Levinson, D.H., Diamond, H.J., Neumann, C.J., 2010. The International Best Track Archive for Climate Stewardship (IBTrACS) Unifying Tropical Cyclone Data. Bull. Am. Meteorol. Soc. 91, 363–376. https://doi.org/10.1175/2009BAMS2755.1

Knapp, N., Fischer, R., Huth, A., 2018. Linking lidar and forest modeling to assess biomass estimation across scales and disturbance states. Remote Sens. Environ. 205, 199–209. https://doi.org/10.1016/j.rse.2017.11.018

Knutson, T.R., Camargo, S.J., Chan, J.C.L.L., Emanuel, K., Ho, C.-H.H., Kossin, J., Mohapatra, M., Satoh, M., Sugi, M., Walsh, K., Wu, L., 2020. Tropical cyclones and climate change assessment: Part II: Projected Response to Anthropogenic Warming Thomas. Bull. Am. Meteorol. Soc. 100, 1987–2007. https://doi.org/10.1175/BAMS-D-18-0189.1

Koch, A., Hubau, W., Lewis, S.L., 2021. Earth System Models Are Not Capturing Present-Day Tropical Forest Carbon Dynamics. Earth's Futur. 9, 1–19. https://doi.org/10.1029/2020EF001874

Köhler, P., Huth, A., 1998. The effects of tree species grouping in tropical rainforest modelling: Simulations

with the individual-based model FORMIND. Ecol. Modell. 109, 301–321. https://doi.org/10.1016/S0304-3800(98)00066-0
Kohyama, T., 1993. Size-Structured Tree Populations in Gap-Dynamic Forest--The Forest Architecture Hypothesis for the Stable Coexistence of Species. J. Ecol. 81, 131. https://doi.org/10.2307/2261230
Kohyama, T., 1992. Size-Structured Multi-Species Model of Rain Forest Trees. Funct. Ecol. 6, 206. https://doi.org/10.2307/2389756
Koven, C., Knox, R., Fisher, R., Chambers, J., Christoffersen, B., Davies, S., Detto, M., Dietze, M., Faybishenko, B., Holm, J., Huang, M., Kovenock, M., Kueppers, L., Lemieux, G., Massoud, E., McDowell, N., Muller-Landau, H., Needham, J., Norby, R., Powell, T., Rogers, A., Serbin, S., Shuman, J., Swann, A., Varadharajan, C., Walker, A., Wright, S.J., Xu, C., 2020. Benchmarking and Parameter Sensitivity of Physiological and Vegetation Dynamics using the Functionally Assembled Terrestrial Ecosystem Simulator (FATES) at Barro Colorado Island, Panama. Biogeosciences Discuss. 1–46. https://doi.org/10.5194/bg-2019-409
Kulakowski, D., Bebi, P., Rixen, C., 2011. The interacting effects of land use change, climate change and suppression of natural disturbances on landscape forest structure in the Swiss Alps. Oikos 120, 216–225. https://doi.org/10.1111/j.1600-0706.2010.18726.x
Kurz, W.A., Stinson, G., Rampley, G.J., Dymond, C.C., Neilson, E.T., 2008. Risk of natural disturbances makes future contribution of Canada's forests to the global carbon cycle highly uncertain. Proc. Natl. Acad. Sci. U. S. A. 105, 1551–1555. https://doi.org/10.1073/pnas.0708133105
Lagarrigues, G., Jabot, F., Lafond, V., Courbaud, B., 2015. Approximate Bayesian computation to recalibrate individual-based models with population data: Illustration with a forest simulation model. Ecol. Modell. 306, 278–286. https://doi.org/10.1016/j.ecolmodel.2014.09.023
Lalic, B., Mihailovic, D.T., Rajkovic, B., Arsenic, I.D., Radlovic, D., 2003. Wind profile within the forest canopy and in the transition layer above it. Environ. Model. Softw. 18, 943–950. https://doi.org/10.1016/S1364-8152(03)00068-9
Laurance, W.F., Curran, T.J., 2008. Impacts of wind disturbance on fragmented tropical forests: A review and synthesis. Austral Ecol. https://doi.org/10.1111/j.1442-9993.2008.01895.x
Lechner, A.M., Foody, G.M., Boyd, D.S., 2020. Applications in Remote Sensing to Forest Ecology and Management. One Earth 2, 405–412. https://doi.org/10.1016/j.oneear.2020.05.001
Lefsky, M.A., Cohen, W.B., Parker, G.G., Harding, D.J., 2002. Lidar remote sensing for ecosystem studies. Bioscience 52, 19–30.
Lehmann, S., Huth, A., 2015. Fast calibration of a dynamic vegetation model with minimum observation data. Ecol. Modell. 301, 98–105. https://doi.org/10.1016/j.ecolmodel.2015.01.013
Lin, T., Vadeboncoeur, M.A., Hamburg, S.P., Lin, K.-C., Wang, L., Chang, C., Hsia, Y., Mcmullen, C.M.M., Liu, C., 2011. Typhoon Disturbance and Forest Dynamics: Lessons from a Northwest Pacific Subtropical Forest. Ecosystems 14, 127–143. https://doi.org/10.1007/s10021-010-9399-1
Lin, T.C., Hogan, J.A., Chang, C. Te, 2020. Tropical Cyclone Ecology: A Scale-Link Perspective. Trends Ecol. Evol. 35, 594–604. https://doi.org/10.1016/j.tree.2020.02.012
Liu, Y., Guo, W., Huang, H., Ge, J., Qiu, B., 2021. Estimating global aerodynamic parameters in 1982–2017 using remote-sensing data and a turbulent transfer model. Remote Sens. Environ. 260, 112428. https://doi.org/10.1016/j.rse.2021.112428
Locatelli, T., Gardiner, B.A., Tarantola, S., Nicoll, B.C., Bonnefond, J.M., Garrigou, D., Kamimura, K., Patenaude, G., 2016. Modelling wind risk to Eucalyptus globulus (Labill.) stands. For. Ecol. Manage. 365, 159–173. https://doi.org/10.1016/j.foreco.2015.12.035
Longo, M., Knox, R.G., Medvigy, D.M., Levine, N.M., Dietze, M.C., Kim, Y., Swann, A.L.S., Zhang, K., Rollinson, C.R., Bras, R.L., Wofsy, S.C., Moorcroft, P.R., 2019. The biophysics, ecology, and biogeochemistry of functionally diverse, vertically and horizontally heterogeneous ecosystems: The Ecosystem Demography model, version 2.2-Part 1: Model description. Geosci. Model Dev. 12, 4309–4346. https://doi.org/10.5194/gmd-12-4309-2019
Loubota Panzou, G.J., Fayolle, A., Jucker, T., Phillips, O.L., Bohlman, S., Banin, L.F., Lewis, S.L., Affum-Baffoe, K., Alves, L.F., Antin, C., Arets, E., Arroyo, L., Baker, T.R., Barbier, N., Beeckman, H., Berger, U., Bocko, Y.E., Bongers, F., Bowers, S., Brade, T., Brondizio, E.S., Chantrain, A., Chave, J., Compaore, H., Coomes, D.A., Diallo, A., Dias, A.S., Dimobe, K., Djagbletey, G.D., Domingues, T., Doucet, J.L., Drouet, T., Forni, E., Godlee, J.L., Goodman, R.C., Gourlet-Fleury, S., Hien, F., Iida, Y., Ilondea, B.A., Ilunga Muledi, J., Jacques, P., Kuyah, S., López-Portillo, J., Loumeto, J.J., Marimon-Junior, B.H., Marimon, B.S., Mensah, S., Mitchard, E.T.A., Moncrieff, G.R., Narayanan, A., O'Brien, S.T., Ouedraogo, K., Palace, M.W., Pelissier, R., Ploton, P., Poorter, L., Ryan, C.M., Saiz, G., dos Santos, K., Schlund, M., Sellan, G., Sonke, B., Sterck, F., Thibaut, Q., Van Hoef, Y., Veenendaal, E., Vovides, A.G., Xu, Y., Yao, T.L., Feldpausch, T.R., 2021. Pantropical variability in tree crown allometry. Glob. Ecol. Biogeogr. 30, 459–475. https://doi.org/10.1111/geb.13231
Lu, X., Yu, H., Yang, X., Li, X., 2017. Estimating Tropical Cyclone Size in the Northwestern Pacific from Geostationary Satellite Infrared Images. Remote Sens. 9, 728. https://doi.org/10.3390/rs9070728
Lucas, T.A., Doña, R.A., Jiang, W., Johns, G.C., Mann, D.J., Seubert, C., Noah, N.B., Willens, C.H., Davis, S.D., 2017. An individual-based model of chaparral vegetation response to frequent wildfires. Theor. Ecol. 10, 217–233. https://doi.org/10.1007/s12080-016-0324-x

Lugo, A.E., 2008. Visible and invisible effects of hurricanes on forest ecosystems: An international review. Austral Ecol. 33, 368–398. https://doi.org/10.1111/j.1442-9993.2008.01894.x
Lugo, A.E., Rogers, C.S., Nixon, S.W., 2000. Hurricanes, Coral Reefs and Rainforests: Resistance, Ruin and Recovery in the Caribbean. AMBIO A J. Hum. Environ. 29, 106–114. https://doi.org/10.1579/0044-7447-29.2.106
Ma, H., Zeng, J., Chen, N., Zhang, X., Cosh, M.H., Wang, W., 2019. Satellite surface soil moisture from SMAP, SMOS, AMSR2 and ESA CCI: A comprehensive assessment using global ground-based observations. Remote Sens. Environ. 231, 111215. https://doi.org/10.1016/j.rse.2019.111215
Ma, J., Shugart, H.H., Yan, X., Cao, C., Wu, S., Fang, J., 2017. Evaluating carbon fluxes of global forest ecosystems by using an individual tree-based model FORCCHN. Sci. Total Environ. 586, 939–951. https://doi.org/10.1016/j.scitotenv.2017.02.073
Maaß, N., Kaleschke, L., Tian-Kunze, X., Drusch, M., 2013. Snow thickness retrieval over thick Arctic sea ice using SMOS satellite data. Cryosphere 7, 1971–1989. https://doi.org/10.5194/tc-7-1971-2013
Madani, N., Parazoo, N.C., 2020. Global Monthly GPP from an Improved Light Use Efficiency Model, 1982-2016 [WWW Document]. URL https://daac.ornl.gov/cgi-bin/dsviewer.pl?ds_id=1789 (accessed 12.14.20).
Magnabosco Marra, D., Chambers, J.Q., Higuchi, N., Trumbore, S.E., Ribeiro, G.H.P.M., Dos Santos, J., Negrón-Juárez, R.I., Reu, B., Wirth, C., 2014. Large-scale wind disturbances promote tree diversity in a Central Amazon forest. PLoS One 9. https://doi.org/10.1371/journal.pone.0103711
Magnabosco Marra, D., Trumbore, S.E., Higuchi, N., Ribeiro, G.H.P.M., Negrón-Juárez, R.I., Holzwarth, F., Rifai, S.W., dos Santos, J., Lima, A.J.N., Kinupp, V.F., Chambers, J.Q., Wirth, C., 2018. Windthrows control biomass patterns and functional composition of Amazon forests. Glob. Chang. Biol. 24, 5867–5881. https://doi.org/10.1111/gcb.14457
Malhi, Y., Aragão, L.E.O.C., Galbraith, D., Huntingford, C., Fisher, R., Zelazowski, P., Sitch, S., Mcsweeney, C., Meir, P., 2009. Exploring the likelihood and mechanism of a climate-change-induced dieback of the. PNAS 106, 20610–20615.
Malhi, Y., Doughty, C., Galbraith, D., 2011. The allocation of ecosystem net primary productivity in tropical forests. Philos. Trans. R. Soc. B Biol. Sci. 366, 3225–3245. https://doi.org/10.1098/rstb.2011.0062
Malhi, Y., Doughty, C.E., Goldsmith, G.R., Metcalfe, D.B., Girardin, C.A.J., Marthews, T.R., del Aguila-Pasquel, J., Aragão, L.E.O.C., Araujo-Murakami, A., Brando, P., da Costa, A.C.L., Silva-Espejo, J.E., Farfán Amézquita, F., Galbraith, D.R., Quesada, C.A., Rocha, W., Salinas-Revilla, N., Silvério, D., Meir, P., Phillips, O.L., 2015. The linkages between photosynthesis, productivity, growth and biomass in lowland Amazonian forests. Glob. Chang. Biol. 21, 2283–2295. https://doi.org/10.1111/gcb.12859
Malhi, Y., Jackson, T., Bentley, L.P., Lau, A., Shenkin, A., Herold, M., Calders, K., Bartholomeus, H., Disney, M.I., 2018. New perspectives on the ecology of tree structure and tree communities through terrestrial laser scanning. Interface Focus 8. https://doi.org/10.1098/rsfs.2017.0052
Maréchaux, I., Chave, J., 2017. An individual-based forest model to jointly simulate carbon and tree diversity in Amazonia: description and applications. Ecol. Monogr. 87, 632–664. https://doi.org/10.1002/ecm.1271
Maréchaux, I., Langerwisch, F., Huth, A., Bugmann, H., Morin, X., Reyer, C.P.O., Seidl, R., Collalti, A., Dantas de Paula, M., Fischer, R., Gutsch, M., Lexer, M.J., Lischke, H., Rammig, A., Rödig, E., Sakschewski, B., Taubert, F., Thonicke, K., Vacchiano, G., Bohn, F.J., 2021. Tackling unresolved questions in forest ecology: The past and future role of simulation models. Ecol. Evol. 1–25. https://doi.org/10.1002/ece3.7391
McDowell, N., Allen, C.D., Anderson-Teixeira, K.J., Brando, P., Brienen, R., Chambers, J., Christoffersen, B., Davies, S., Doughty, C., Duque, A., Espirito-Santo, F., Fisher, R.A., Fontes, C.G., Galbraith, D., Goodsman, D., Grossiord, C., Hartmann, H., Holm, J., Johnson, D.J., Kassim, A.R., Keller, M., Koven, C., Kueppers, L., Kumagai, T., Malhi, Y., McMahon, S.M., Mencuccini, M., Meir, P., Moorcroft, P., Muller-Landau, H.C., Phillips, O.L., Powell, T., Sierra, C.A., Sperry, J., Warren, J., Xu, C., Xu, X., 2018. Drivers and mechanisms of tree mortality in moist tropical forests. New Phytol. 219, 851–869. https://doi.org/10.1111/nph.15027
McDowell, N.G., Allen, C.D., Anderson-Teixeira, K., Aukema, B.H., Bond-Lamberty, B., Chini, L., Clark, J.S., Dietze, M., Grossiord, C., Hanbury-Brown, A., Hurtt, G.C., Jackson, R.B., Johnson, D.J., Kueppers, L., Lichstein, J.W., Ogle, K., Poulter, B., Pugh, T.A.M., Seidl, R., Turner, M.G., Uriarte, M., Walker, A.P., Xu, C., 2020. Pervasive shifts in forest dynamics in a changing world. Science (80-.). 368. https://doi.org/10.1126/science.aaz9463
McEwan, R.W., Lin, Y.C., Sun, I.F., Hsieh, C.F., Su, S.H., Chang, L.W., Song, G.Z.M., Wang, H.H., Hwong, J.L., Lin, K.-C.C., Yang, K.C., Chiang, J.M., 2011. Topographic and biotic regulation of aboveground carbon storage in subtropical broad-leaved forests of Taiwan. For. Ecol. Manage. 262, 1817–1825. https://doi.org/10.1016/j.foreco.2011.07.028
McGroddy, M., Lawrence, D., Schneider, L., Rogan, J., Zager, I., Schmook, B., 2013. Damage patterns after Hurricane Dean in the southern Yucatán: Has human activity resulted in more resilient forests? For. Ecol. Manage. 310, 812–820. https://doi.org/10.1016/j.foreco.2013.09.027
Medlyn, B.E., De Kauwe, M.G., Zaehle, S., Walker, A.P., Duursma, R.A., Luus, K., Mishurov, M., Pak, B., Smith, B., Wang, Y.P., Yang, X., Crous, K.Y., Drake, J.E., Gimeno, T.E., Macdonald, C.A., Norby, R.J., Power, S.A., Tjoelker, M.G., Ellsworth, D.S., 2016. Using models to guide field experiments: a priori predictions for the CO2 response of a nutrient- and water-limited native Eucalypt woodland. Glob. Chang.

Biol. 22, 2834–2851. https://doi.org/10.1111/gcb.13268
Medlyn, B.E., Duursma, R.A., Eamus, D., Ellsworth, D.S., Prentice, I.C., Barton, C.V.M., Crous, K.Y., De Angelis, P., Freeman, M., Wingate, L., 2011. Reconciling the optimal and empirical approaches to modelling stomatal conductance. Glob. Chang. Biol. 17, 2134–2144. https://doi.org/10.1111/j.1365-2486.2010.02375.x
Mensah, S., Salako, V.K., Seifert, T., 2020. Structural complexity and large-sized trees explain shifting species richness and carbon relationship across vegetation types. Funct. Ecol. 34, 1731–1745. https://doi.org/10.1111/1365-2435.13585
Mercado, L.M., Lloyd, J., Dolman, A.J., Sitch, S., Patiño, S., 2009. Modelling basin-wide variations in Amazon forest productivity - Part 1: Model calibration, evaluation and upscaling functions for canopy photosynthesis. Biogeosciences 6, 1247–1272. https://doi.org/10.5194/bg-6-1247-2009
Merganičová, K., Merganič, J., Lehtonen, A., Vacchiano, G., Sever, M.Z.O., Augustynczik, A.L.D., Grote, R., Kyselová, I., Mäkelä, A., Yousefpour, R., Krejza, J., Collalti, A., Reyer, C.P.O., 2019. Forest carbon allocation modelling under climate change. Tree Physiol. 39, 1937–1960. https://doi.org/10.1093/treephys/tpz105
Mikita, T., Klimánek, M., 2012. Topographic Exposure and its Practical Applications. J. Landsc. Ecol. 3, 42–51. https://doi.org/10.2478/v10285-012-0022-3
Mitchard, E.T.A., 2018. The tropical forest carbon cycle and climate change. Nature 559, 527–534. https://doi.org/10.1038/s41586-018-0300-2
Mitchell, S.J., 2013. Wind as a natural disturbance agent in forests: A synthesis. Forestry 86, 147–157. https://doi.org/10.1093/forestry/cps058
Molto, Q., Hérault, B., Boreux, J.J., Daullet, M., Rousteau, A., Rossi, V., 2014. Predicting tree heights for biomass estimates in tropical forests - A test from French Guiana. Biogeosciences 11, 3121–3130. https://doi.org/10.5194/bg-11-3121-2014
Monteith, J., Unsworth, M., 2008. Principles of environmental physics: plants, animals, and the atmosphere, 3rd ed. Academic Press.
Moon, K., Duff, T.J., Tolhurst, K.G., 2016. Sub-canopy forest winds : understanding wind profiles for fire behaviour simulation. Fire Saf. J. https://doi.org/10.1016/j.firesaf.2016.02.005
Moorcroft, P.R., Hurtt, G.C., Pacala, S.W., 2001. A method for scaling vegetation dynamics: The ecosystem demography model (ED). Ecol. Monogr. 71, 557–586. https://doi.org/10.1890/0012-9615(2001)071[0557:AMFSVD]2.0.CO;2
Moore, J.R., Maguire, D.A., 2008. Simulating the dynamic behavior of Douglas-fir trees under applied loads by the finite element method. Tree Physiol. 28, 75–83. https://doi.org/10.1093/treephys/28.1.75
Morgan, J., Cannell, M.G.R., 1994. Shape of tree stems - A re-examination of the uniform stress hypothesis. Tree Physiol. 14, 49–62. https://doi.org/10.1093/treephys/14.1.49
Mortensen, N.G., Steen, R.O., Morten, N., Heathfield, D.N., Rathmann, O., Nielsen, M., 2001. Wind Atlas Analysis and Application Program: WAsP 7 Help Facility 304.
Murakami, H., Wang, B., Li, T., Kitoh, A., 2013. Projected increase in tropical cyclones near Hawaii. Nat. Clim. Chang. 3, 749–754. https://doi.org/10.1038/nclimate1890
Nakamura, J., Camargo, S.J., Sobel, A.H., Henderson, N., Emanuel, K.A., Kumar, A., LaRow, T.E., Murakami, H., Roberts, M.J., Scoccimarro, E., Vidale, P.L., Wang, H., Wehner, M.F., Zhao, M., 2017. Western North Pacific Tropical Cyclone Model Tracks in Present and Future Climates. J. Geophys. Res. Atmos. 122, 9721–9744. https://doi.org/10.1002/2017JD027007
Negrón-Juárez, R.I., Chambers, J.Q., Hurtt, G.C., Annane, B., Cocke, S., Powell, M., Stott, M., Goosem, S., Metcalfe, D.J., Saatchi, S.S., 2014. Remote sensing assessment of forest disturbance across complex mountainous terrain: The pattern and severity of impacts of tropical cyclone Yasi on Australian rainforests. Remote Sens. 6, 5633–5649. https://doi.org/10.3390/rs6065633
Negrón-Juárez, R.I., Holm, J.A., Marra, D.M., Rifai, S.W., Riley, W.J., Chambers, J.Q., Koven, C.D., Knox, R.G., McGroddy, M.E., Di Vittorio, A. V., Urquiza-Muñoz, J., Tello-Espinoza, R., Muñoz, W.A., Ribeiro, G.H.P.M., Higuchi, N., 2018. Vulnerability of Amazon forests to storm-driven tree mortality. Environ. Res. Lett. 13. https://doi.org/10.1088/1748-9326/aabe9f
Negrón-Juárez, R.I., Jenkins, H.S., Raupp, C.F.M., Riley, W.J., Kueppers, L.M., Marra, D.M., Ribeiro, G.H.P.M., Monteiro, M.T.F., Candido, L.A., Chambers, J.Q., Higuchi, N., 2017. Windthrow variability in central Amazonia. Atmosphere (Basel). 8, 1–17. https://doi.org/10.3390/atmos8020028
Negrón-Juárez, R.I., Koven, C.D., Riley, W.J., Knox, R.G., Chambers, J.Q., 2015. Observed allocations of productivity and biomass, and turnover times in tropical forests are not accurately represented in CMIP5 Earth system models. Environ. Res. Lett. 10. https://doi.org/10.1088/1748-9326/10/6/064017
Newman, E.A., 2019. Disturbance Ecology in the Anthropocene. Front. Ecol. Evol. 7. https://doi.org/10.3389/fevo.2019.00147
Newnham, G.J., Armston, J.D., Calders, K., Disney, M.I., Lovell, J.L., Schaaf, C.B., Strahler, A.H., Mark Danson, F., 2015. Terrestrial laser scanning for plot-scale forest measurement. Curr. For. Reports 1, 239–251. https://doi.org/10.1007/s40725-015-0025-5
Nicoll, B.C., Gardiner, B.A., Rayner, B., Peace, A.J., 2006. Anchorage of coniferous trees in relation to species, soil type, and rooting depth. Can. J. For. Res. 36, 1871–1883. https://doi.org/10.1139/x06-072
Oliva, R., Martín-Neira, M., Corbella, I., Closa, J., Zurita, A., Cabot, F., Khazaal, A., Richaume, P.,

Kainulainen, J., Barbosa, J., Lopes, G., Tenerelli, J., Díez-García, R., González-Gambau, V., Crapolicchio, R., 2020. SMOS third mission reprocessing after 10 years in orbit. Remote Sens. 12, 1–24. https://doi.org/10.3390/rs12101645
Olson, W.S., Kummerow, C.D., Yang, S., Petty, G.W., Tao, W.-K., Bell, T.L., Braun, S.A., Wang, Y., Lang, S.E., Johnson, D.E., Chiu, C., 2006. Precipitation and Latent Heating Distributions from Satellite Passive Microwave Radiometry. Part I: Improved Method and Uncertainties. J. Appl. Meteorol. Climatol. 45, 702–720. https://doi.org/10.1175/JAM2370.1
Osman, N., Barakbah, S.S., 2006. Parameters to predict slope stability-Soil water and root profiles. Ecol. Eng. 28, 90–95. https://doi.org/10.1016/j.ecoleng.2006.04.004
Ostertag, R., Silver, W.L., Lugo, A.E., 2005. Factors affecting mortality and resistance to damage following hurricanes in a rehabilitated subtropical moist forest. Biotropica 37, 16–24. https://doi.org/10.1111/j.1744-7429.2005.04052.x
Pacala, S.W., Canham, C.D., Saponara, J., Silander, J.A., Kobe, R.K., Ribbens, E., 1996. Forest models defined by field measurements: estimation, error analysis and dynamics. Ecol. Monogr. 66, 1–43. https://doi.org/10.2307/2963479
Pan, Y., Birdsey, R.A., Phillips, O.L., Jackson, R.B., 2013. The structure, distribution, and biomass of the world's forests. Annu. Rev. Ecol. Evol. Syst. 44, 593–622. https://doi.org/10.1146/annurev-ecolsys-110512-135914
Pappas, C., Fatichi, S., Burlando, P., 2016. Modeling terrestrial carbon and water dynamics across climatic gradients: Does plant trait diversity matter? New Phytol. 209, 137–151. https://doi.org/10.1111/nph.13590
Pappas, C., Fatichi, S., Leuzinger, S., Wolf, A., Burlando, P., 2013. Sensitivity analysis of a process-based ecosystem model: Pinpointing parameterization and structural issues. J. Geophys. Res. Biogeosciences 118, 505–528. https://doi.org/10.1002/jgrg.20035
Park, D.S.R., Ho, C.H., Chan, J.C.L., Ha, K.J., Kim, H.S., Kim, J., Kim, J.H., 2017. Asymmetric response of tropical cyclone activity to global warming over the North Atlantic and western North Pacific from CMIP5 model projections. Sci. Rep. 7, 1–9. https://doi.org/10.1038/srep41354
Pavlick, R., Drewry, D.T., Bohn, K., Reu, B., Kleidon, A., 2013. The Jena Diversity-Dynamic Global Vegetation Model (JeDi-DGVM): a diverse approach to representing terrestrial biogeography and biogeochemistry based on plant functional trade-offs. Biogeosciences 10, 4137–4177. https://doi.org/10.5194/bg-10-4137-2013
Peereman, J., Hogan, J.A., Lin, T.C., 2020. Landscape representation by a permanent forest plot and alternative plot designs in a Typhoon Hotspot, Fushan, Taiwan. Remote Sens. 12. https://doi.org/10.3390/rs12040660
Peltola, H., Kellomäki, S., Hassinen, A., Granander, M., 2000. Mechanical stability of Scots pine, Norway spruce and birch: An analysis of tree-pulling experiments in Finland. For. Ecol. Manage. 135, 143–153. https://doi.org/10.1016/S0378-1127(00)00306-6
Pérez-Harguindeguy, N., Díaz, S., Garnier, E., Lavorel, S., Poorter, H., Jaureguiberry, P., Bret-Harte, M.S., Cornwell, W.K., Craine, J.M., Gurvich, D.E., Urcelay, C., Veneklaas, E.J., Reich, P.B., Poorter, L., Wright, I.J., Ray, P., Enrico, L., Pausas, J.G., De Vos, A.C., Buchmann, N., Funes, G., Quétier, F., Hodgson, J.G., Thompson, K., Morgan, H.D., Ter Steege, H., Van Der Heijden, M.G.A., Sack, L., Blonder, B., Poschlod, P., Vaieretti, M. V., Conti, G., Staver, A.C., Aquino, S., Cornelissen, J.H.C., 2013. New handbook for standardised measurement of plant functional traits worldwide. Aust. J. Bot. 61, 167–234. https://doi.org/10.1071/BT12225
Peterson, C.J., Claassen, V., 2013. An evaluation of the stability of Quercus lobata and Populus fremontii on river levees assessed using static winching tests. Forestry 86, 201–209. https://doi.org/10.1093/forestry/cps080
Peterson, C.J., Ribeiro, G.H.P. de M., Negrón-Juárez, R., Marra, D.M., Chambers, J.Q., Higuchi, N., Lima, A., Cannon, J.B., 2019. Critical wind speeds suggest wind could be an important disturbance agent in Amazonian forests. For. An Int. J. For. Res. 92, 444–459. https://doi.org/10.1093/forestry/cpz025
Pianosi, F., Beven, K., Freer, J., Hall, J.W., Rougier, J., Stephenson, D.B., Wagener, T., 2016. Sensitivity analysis of environmental models: A systematic review with practical workflow. Environ. Model. Softw. 79, 214–232. https://doi.org/10.1016/j.envsoft.2016.02.008
Pickett, S.T.A., White, P.S., 1985. The ecology of natural disturbance and patch dynamics. New York, New York, USA.
Pierce, D., 2019. ncdf4: Interface to Unidata netCDF (Version 4 or Earlier) Format Data Files.
Pivato, D., Dupont, S., Brunet, Y., 2014. A simple tree swaying model for forest motion in windstorm conditions. Trees 28, 281–293. https://doi.org/10.1007/s00468-013-0948-z
Poorter, L., van der Sande, M.T., Arets, E.J.M.M., Ascarrunz, N., Enquist, B., Finegan, B., Licona, J.C., Martínez-Ramos, M., Mazzei, L., Meave, J.A., Muñoz, R., Nytch, C.J., de Oliveira, A.A., Pérez-García, E.A., Prado-Junior, J., Rodríguez-Velázques, J., Ruschel, A.R., Salgado-Negret, B., Schiavini, I., Swenson, N.G., Tenorio, E.A., Thompson, J., Toledo, M., Uriarte, M., Hout, P. van der, Zimmerman, J.K., Peña-Claros, M., 2017. Biodiversity and climate determine the functioning of Neotropical forests. Glob. Ecol. Biogeogr. 26, 1423–1434. https://doi.org/10.1111/geb.12668
Porté, A., Bartelink, H.H., 2002. Modelling mixed forest growth: A review of models for forest management. Ecol. Modell. 150, 141–188. https://doi.org/10.1016/S0304-3800(01)00476-8
Pourrahmati, M.R., Baghdadi, N., Darvishsefat, A.A., Namiranian, M., Gond, V., Bailly, J.S., Zargham, N.,

2018. Mapping lorey's height over Hyrcanian forests of Iran using synergy of ICESat/GLAS and optical images. Eur. J. Remote Sens. 51, 100–115. https://doi.org/10.1080/22797254.2017.1405717
Prentice, I.C., Bondeau, A., Cramer, W., Harrison, S.P., Hickler, T., Lucht, W., Sitch, S., Smith, B., Sykes, M.T., 2007. Dynamic Global Vegetation Modeling: Quantifying Terrestrial Ecosystem Responses to Large-Scale Environmental Change, in: Canadell, J.G., Pataki, D.E., Pitelka, L.F. (Eds.), Terrestrial Ecosystems in a Changing World. Springer Berlin Heidelberg, Berlin, Heidelberg, pp. 175–192. https://doi.org/10.1007/978-3-540-32730-1_15
Prentice, I.C., Liang, X., Medlyn, B.E., Wang, Y.P., 2015. Reliable, robust and realistic: The three R's of next-generation land-surface modelling. Atmos. Chem. Phys. 15, 5987–6005. https://doi.org/10.5194/acp-15-5987-2015
Pretzsch, H., 2019. The effect of tree crown allometry on community dynamics in mixed-species stands versus monocultures. A review and perspectives for modeling and silvicultural regulation. Forests 10. https://doi.org/10.3390/f10090810
Pugh, T.A.M., Arneth, A., Kautz, M., Poulter, B., Smith, B., 2019. Important role of forest disturbances in the global biomass turnover and carbon sinks. Nat. Geosci. 12, 730–735. https://doi.org/10.1038/s41561-019-0427-2
Pulliainen, J.T., Kurvonen, L., Hallikainen, M.T., 1999. Multitemporal behavior of L- and C-band SAR observations of boreal forests. IEEE Trans. Geosci. Remote Sens. 37, 927–937. https://doi.org/10.1109/36.752211
Pulsford, S.A., Lindenmayer, D.B., Driscoll, D.A., 2016. A succession of theories: Purging redundancy from disturbance theory. Biol. Rev. 91, 148–167. https://doi.org/10.1111/brv.12163
QGIS.org, 2021. QGIS Geographic Information System.
Quine, C.P., Gardiner, B.A., 1995. Understanding how the interaction of wind and trees results in windthrow, stem breakage and canopy gap formation, in: Plant Disturbance Ecology: The Process and the Response. pp. 103–156. https://doi.org/10.1016/B978-0-12-088778-1.50006-6
Quine, C.P., Gardiner, B.A., Moore, J., 2021. Wind disturbance in forests: The process of wind created gaps, tree overturning, and stem breakage, Plant Disturbance Ecology. https://doi.org/10.1016/b978-0-12-818813-2.00004-6
R Core Team, 2019. R: A Language and Environment for Statistical Computing.
Rahm, M., Thibault, P., Shapiro, A., Smartt, T., Paloeng, C., Crabbe, S., Farias, P., Carvalho, R., Joubert, P., 2017. Monitoring the impact of gold mining on the forest cover and freshwater in the Guiana Shield. Monit. impact gold Min. For. Cover Freshw. – Ref. year 2015. 20.
Rasband, W.S., n.d. ImageJ.
Raupach, M.R., Antonia, R.A., Rajagopalan, S., 1991. Rough-wall turbulent boundary layers. Appl. Mech. Rev. 44.
Raupach, M.R., Finnigan, J.J., Brunet, Y., 1996. Coherent eddies and turbulence in vegetation canopies: the mixing-layer analogy. Boundary-Layer Meteorol. 78, 351–382. https://doi.org/10.1007/BF00120941
Raupach, M.R., Thom, A.S., 1981. Turbulence in and above plant canopies. Annu. Rev. fluid Mech. Vol. 13 97–129.
Reiche, J., Lucas, R., Mitchell, A.L., Verbesselt, J., Hoekman, D.H., Haarpaintner, J., Kellndorfer, J.M., Rosenqvist, A., Lehmann, E.A., Woodcock, C.E., Seifert, F.M., Herold, M., 2016. Combining satellite data for better tropical forest monitoring. Nat. Clim. Chang. 6, 120–122. https://doi.org/10.1038/nclimate2919
Reiche, J., Mullissa, A., Slagter, B., Gou, Y., Tsendbazar, N.E., Odongo-Braun, C., Vollrath, A., Weisse, M.J., Stolle, F., Pickens, A., Donchyts, G., Clinton, N., Gorelick, N., Herold, M., 2021. Forest disturbance alerts for the Congo Basin using Sentinel-1. Environ. Res. Lett. 16. https://doi.org/10.1088/1748-9326/abd0a8
Reichstein, M., Bahn, M., Ciais, P., Frank, D., Mahecha, M.D., Seneviratne, S.I., Zscheischler, J., Beer, C., Buchmann, N., Frank, D.C., Papale, D., Rammig, A., Smith, P., Thonicke, K., Van Der Velde, M., Vicca, S., Walz, A., Wattenbach, M., 2013. Climate extremes and the carbon cycle. Nature 500, 287–295. https://doi.org/10.1038/nature12350
Rejou-Mechain, M., Tanguy, A., Piponiot, C., Chave, J., Herault, B., 2017. BIOMASS : an {R} package for estimating above-ground biomass and its uncertainty in tropical forests. Methods Ecol. Evol. 8. https://doi.org/10.1111/2041-210X.12753
Restrepo-Coupe, N., Levine, N.M., Christoffersen, B.O., Albert, L.P., Wu, J., Costa, M.H., Galbraith, D., Imbuzeiro, H., Martins, G., da Araujo, A.C., Malhi, Y.S., Zeng, X., Moorcroft, P., Saleska, S.R., 2017. Do dynamic global vegetation models capture the seasonality of carbon fluxes in the Amazon basin? A data-model intercomparison. Glob. Chang. Biol. 23, 191–208. https://doi.org/10.1111/gcb.13442
Reul, N., Tenerelli, J., Chapron, B., Vandemark, D., Quilfen, Y., Kerr, Y., 2012. SMOS satellite L-band radiometer: A new capability for ocean surface remote sensing in hurricanes. J. Geophys. Res. Ocean. 117, 1–24. https://doi.org/10.1029/2011JC007474
Reyer, C., 2015. Forest productivity under environmental change—A review of stand-scale modeling studies. Curr. For. Reports 1, 53–68. https://doi.org/10.1007/s40725-015-0009-5
Rich, P.M., Clark, D.B., Clark, D.A., Oberbauer, S.F., 1993. Long-term study of solar radiation regimes in a tropical wet forest using quantum sensors and hemispherical photography. Agric. For. Meteorol. 65, 107–127. https://doi.org/10.1016/0168-1923(93)90040-O

Rödig, E., Cuntz, M., Heinke, J., Rammig, A., Huth, A., 2017. Spatial heterogeneity of biomass and forest structure of the Amazon rain forest: Linking remote sensing, forest modelling and field inventory. Glob. Ecol. Biogeogr. 26, 1292–1302. https://doi.org/10.1111/geb.12639

Rödig, E., Cuntz, M., Rammig, A., Fischer, R., Taubert, F., Huth, A., 2018. The importance of forest structure for carbon fluxes of the Amazon rainforest. Environ. Res. Lett. 13. https://doi.org/10.1088/1748-9326/aabc61

Rogers, A., Medlyn, B.E., Dukes, J.S., Bonan, G., von Caemmerer, S., Dietze, M.C., Kattge, J., Leakey, A.D.B., Mercado, L.M., Niinemets, Ü., Prentice, I.C., Serbin, S.P., Sitch, S., Way, D.A., Zaehle, S., 2017. A roadmap for improving the representation of photosynthesis in Earth system models. New Phytol. https://doi.org/10.1111/nph.14283

Rudnicki, M., Mitchell, S.J., Novak, M.D., 2004. Wind tunnel measurements of crown streamlining for drag relationships for three conifer species. Can. J. For. Res. 34, 666–676. https://doi.org/10.1139/x03-233

Ruel, J.C., Pin, D., Cooper, K., 1998. Effect of topography on wind behaviour in a complex terrain. Forestry 71, 261–265. https://doi.org/10.1093/forestry/71.3.261

Ryan, M.G., Gower, S.T., Hubbard, R.M., Waring, R.H., Gholz, H.L., Cropper, W.P., Running, S.W., 1995. Woody tissue maintenance respiration of four conifers in contrasting climates. Oecologia 101, 133–140. https://doi.org/10.1007/BF00317276

Sakschewski, B., von Bloh, W., Boit, A., Rammig, A., Kattge, J., Poorter, L., Peñuelas, J., Thonicke, K., 2015. Leaf and stem economics spectra drive diversity of functional plant traits in a dynamic global vegetation model. Glob. Chang. Biol. 21, 2711–2725. https://doi.org/10.1111/gcb.12870

Sato, H., Itoh, A., Kohyama, T., 2007. SEIB-DGVM: A new Dynamic Global Vegetation Model using a spatially explicit individual-based approach. Ecol. Modell. 200, 279–307. https://doi.org/10.1016/j.ecolmodel.2006.09.006

Scheiter, S., Langan, L., Higgins, S.I., 2013. Next-generation dynamic global vegetation models: Learning from community ecology. New Phytol. 198, 957–969. https://doi.org/10.1111/nph.12210

Schelhaas, M.J., Kramer, K., Peltola, H., van der Werf, D.C., Wijdeven, S.M.J., 2007. Introducing tree interactions in wind damage simulation. Ecol. Modell. 207, 197–209. https://doi.org/10.1016/j.ecolmodel.2007.04.025

Schippers, P., Vlam, M., Zuidema, P.A., Sterck, F., 2015. Sapwood allocation in tropical trees: A test of hypotheses. Funct. Plant Biol. 42, 697–709. https://doi.org/10.1071/FP14127

Schmitt, S., Maréchaux, I., Chave, J., Fischer, F.J., Piponiot, C., Traissac, S., Hérault, B., 2020. Functional diversity improves tropical forest resilience: Insights from a long-term virtual experiment. J. Ecol. 108, 831–843. https://doi.org/10.1111/1365-2745.13320

Schulzweida, U., 2019. CDO User Guide (Version 1.9.8) [WWW Document]. https://doi.org/10.5281/zenodo.3539275

Schwartz, N.B., Uriarte, M., Defries, R., Bedka, K.M., Fernandes, K., Gutiérrez-Vélez, V., Pinedo-Vasquez, M.A., 2017. Fragmentation increases wind disturbance impacts on forest structure and carbon stocks in a western Amazonian landscape. Ecol. Appl. 27, 1901–1915. https://doi.org/10.1002/eap.1576

Seidl, R., Fernandes, P.M., Fonseca, T.F., Gillet, F., Jönsson, A.M., Merganičová, K., Netherer, S., Arpaci, A., Bontemps, J.D., Bugmann, H., González-Olabarria, J.R., Lasch, P., Meredieu, C., Moreira, F., Schelhaas, M.J., Mohren, F., 2011a. Modelling natural disturbances in forest ecosystems: A review. Ecol. Modell. 222, 903–924. https://doi.org/10.1016/j.ecolmodel.2010.09.040

Seidl, R., Rammer, W., Blennow, K., 2014. Simulating wind disturbance impacts on forest landscapes: Tree-level heterogeneity matters. Environ. Model. Softw. 51, 1–11. https://doi.org/10.1016/j.envsoft.2013.09.018

Seidl, R., Schelhaas, M.J., Lexer, M.J., 2011b. Unraveling the drivers of intensifying forest disturbance regimes in Europe. Glob. Chang. Biol. 17, 2842–2852. https://doi.org/10.1111/j.1365-2486.2011.02452.x

Seidl, R., Thom, D., Kautz, M., Martin-Benito, D., Peltoniemi, M., Vacchiano, G., Wild, J., Ascoli, D., Petr, M., Honkaniemi, J., Lexer, M.J., Trotsiuk, V., Mairota, P., Svoboda, M., Fabrika, M., Nagel, T.A., Reyer, C.P.O., 2017. Forest disturbances under climate change. Nat. Clim. Chang. 7, 395–402. https://doi.org/10.1038/nclimate3303

Sellers, P.J., Los, S.O., Tucker, C.J., Justice, C.O., Dazlich, D.A., Collatz, G.J., Randall, D.A., 1996. A revised land surface parameterization (SiB2) for atmospheric GCMs. Part II: The generation of global fields of terrestrial biophysical parameters from satellite data. J. Clim. 9, 706–737. https://doi.org/10.1175/1520-0442(1996)009<0706:ARLSPF>2.0.CO;2

Shaw, R.H., Pereira, A.R., 1982. Aerodynamic roughness of a plant canopy: A numerical experiment. Agric. Meteorol. 26, 51–65. https://doi.org/10.1016/0002-1571(82)90057-7

Sheil, D., Wunder, S., 2002. The value of tropical forest to local communities: Complications, caveats, and cautions. Ecol. Soc. 6. https://doi.org/10.5751/es-00458-060209

Shifley, S.R., He, H.S., Lischke, H., Wang, W.J., Jin, W., Gustafson, E.J., Thompson, J.R., Thompson, F.R., Dijak, W.D., Yang, J., 2017. The past and future of modeling forest dynamics: from growth and yield curves to forest landscape models. Landsc. Ecol. 32, 1307–1325. https://doi.org/10.1007/s10980-017-0540-9

Shugart, H.H., 1984. A theory of forest dynamics: The ecological implications of forest succession models. Springer Verlag, New York.

Shugart, H.H., Asner, G.P., Fischer, R., Huth, A., Knapp, N., Le Toan, T., Shuman, J.K., 2015. Computer and remote-sensing infrastructure to enhance large-scale testing of individual-based forest models. Front. Ecol. Environ. 13, 503–511. https://doi.org/10.1890/140327

Shugart, H.H., Wang, B., Fischer, R., Ma, J., Fang, J., Yan, X., Huth, A., Armstrong, A.H., 2018. Gap models and their individual-based relatives in the assessment of the consequences of global change. Environ. Res. Lett. 13. https://doi.org/10.1088/1748-9326/aaaacc

Shugart, H.H., Woodward, F.I., 2001. Global change and the terrestrial biosphere: achievements and challenges. John Wiley & Sons.

Shuman, J.K., Shugart, H.H., Krankina, O.N., 2014. Testing individual-based models of forest dynamics: Issues and an example from the boreal forests of Russia. Ecol. Modell. 293, 102–110. https://doi.org/10.1016/j.ecolmodel.2013.10.028

Shuman, J.K., Tchebakova, N.M., Parfenova, E.I., Soja, A.J., Shugart, H.H., Ershov, D., Holcomb, K., 2015. Forest forecasting with vegetation models across Russia. Can. J. For. Res. 45, 175–184. https://doi.org/10.1139/cjfr-2014-0138

Shuttleworth, W.J., Leuning, R., Black, T.A., Grace, J., Jarvis, P.J., Roberts, J., Jones, H.G., 1989. Micrometeorology of temperate and tropical forest. Phil. Trans. Roy. Soc. Lond. B 324, 299–334. https://doi.org/10.1098/rstb.1989.0050

Simard, M., Pinto, N., Fisher, J.B., Baccini, A., 2011. Mapping forest canopy height globally with spaceborne lidar. J. Geophys. Res. Biogeosciences 116, 1–12. https://doi.org/10.1029/2011JG001708

Stan Development Team, 2016a. Stan Modeling Language Users Guide and Reference Manual, Version 2.14.0 [WWW Document]. URL http://mc-stan.org

Stan Development Team, 2016b. RStan: the R interface to Stan. R package version 2.14.1. [WWW Document]. URL http://mc-stan.org

Stubbs, C.J., Cook, D.D., Niklas, K.J., 2019. A general review of the biomechanics of root anchorage. J. Exp. Bot. 70, 3439–3451. https://doi.org/10.1093/jxb/ery451

Su, S.-H., Chang-Yang, C., Lu, C., Tsui, C., Lin, T., Lin, C., Chiou, W., Kuan, L., Chen, Z., Hsieh, C., 2007. Fushan subtropical forest dynamics plot: tree species characteristics and distribution patterns. Taiwan Forestry Research Institute., Taipei.

Su, S.H., Guan, B.T., Chang-Yang, C.H., Sun, I.F., Wang, H.H., Hsieh, C.F., 2020. Multi-stemming and size enhance survival of dominant tree species in a frequently typhoon-disturbed forest. J. Veg. Sci. 31, 429–439. https://doi.org/10.1111/jvs.12858

Sullivan, M.J.P.P., Lewis, S.L., Affum-Baffoe, K., Castilho, C., Costa, F., Sanchez, A.C., Ewango, C.E.N.N., Hubau, W., Marimon, B., Marimon Jr., B.H., Monteagudo-Mendoza, A., Qie, L., Sonké, B., Martinez, R.V., Baker, T.R., Brienen, R.J.W.W., Feldpausch, T.R., Galbraith, D., Gloor, M., Malhi, Y., Aiba, S.-I.I., Alexiades, M.N., Almeida, E.C., De Oliveira, E.A., Dávila, E.Á., Loayza, P.A., Andrade, A., Vieira, S.A., Aragão, L.E.O.C., Araujo-Murakami, A., Arets, E.J.M.M., Arroyo, L., Ashton, P., Gerardo Aymard, C., Baccaro, F.B., Banin, L.F., Baraloto, C., Camargo, P.B., Barlow, J., Barroso, J., Bastin, J.-F., Batterman, S.A., Beeckman, H., Begne, S.K., Bennett, A.C., Berenguer, E., Berry, N., Blanc, L., Boeckx, P., Bogaert, J., Bonal, D., Bongers, F., Bradford, M., Brearley, F.Q., Brncic, T., Brown, F., Burban, B., Camargo, J.L., Castro, W., Céron, C., Ribeiro, S.C., Moscoso, V.C., Chave, J., Chezeaux, E., Clark, C.J., De Souza, F.C., Collins, M., Comiskey, J.A., Valverde, F.C., Medina, M.C., Da Costa, L., Dančsák, M., Dargie, G.C., Davies, S., Cardozo, N.D., De Haulleville, T., De Medeiros, M.B., Del Aguila Pasquel, J., Derroire, G., Di Fiore, A., Doucet, J.-L., Dourdain, A., Droissart, V., Duque, L.F., Ekoungoulou, R., Elias, F., Erwin, T., Esquivel-Muelbert, A., Fauset, S., Ferreira, J., Llampazo, G.F., Foli, E., Ford, A., Gilpin, M., Hall, J.S., Hamer, K.C., Hamilton, A.C., Harris, D.J., Hart, T.B., Hédl, R., Herault, B., Herrera, R., Higuchi, N., Hladik, A., Coronado, E.H., Huamantupa-Chuquimaco, I., Huasco, W.H., Jeffery, K.J., Jimenez-Rojas, E., Kalamandeen, M., Djuikouo, M.N.K., Kearsley, E., Umetsu, R.K., Kho, L.K., Killeen, T., Kitayama, K., Klitgaard, B., Koch, A., Labrière, N., Laurance, W., Laurance, S., Leal, M.E., Levesley, A., Lima, A.J.N., Lisingo, J., Lopes, A.P., Lopez-Gonzalez, G., Lovejoy, T., Lovett, J.C., Lowe, R., Magnusson, W.E., Malumbres-Olarte, J., Manzatto, Â.G., Marshall, A.R., Marthews, T., De Almeida Reis, S.M., Maycock, C., Melgaço, K., Mendoza, C., Metali, F., Mihindou, V., Milliken, W., Mitchard, E.T.A., Morandi, P.S., Mossman, H.L., Nagy, L., Nascimento, H., Neill, D., Nilus, R., Vargas, P.N., Palacios, W., Camacho, N.P., Peacock, J., Pendry, C., Mora, M.C.P., Pickavance, G.C., Pipoly, J., Pitman, N., Playfair, M., Poorter, L., Poulsen, J.R., Poulsen, A.D., Preziosi, R., Prieto, A., Primack, R.B., Ramírez-Angulo, H., Reitsma, J., Réjou-Méchain, M., Correa, Z.R., De Sousa, T.R., Bayona, L.R., Roopsind, A., Rudas, A., Rutishauser, E., Salim, K.A., Salomão, R.P., Schietti, J., Sheil, D., Silva, R.C., Espejo, J.S., Valeria, C.S., Silveira, M., Simo-Droissart, M., Simon, M.F., Singh, J., Shareva, Y.C.S., Stahl, C., Stropp, J., Sukri, R., Sunderland, T., Svátek, M., Swaine, M.D., Swamy, V., Taedoumg, H., Talbot, J., Taplin, J., Taylor, D., Ter Steege, H., Terborgh, J., Thomas, R., Thomas, S.C., Torres-Lezama, A., Umunay, P., Gamarra, L.V., Van Der Heijden, G., Van Der Hout, P., Van Der Meer, P., Van Nieuwstadt, M., Verbeeck, H., Vernimmen, R., Vicentini, A., Vieira, I.C.G., Torre, E.V., Vleminckx, J., Vos, V.A., Wang, O., White, L.J.T.T., Willcock, S., Woods, J.T., Wortel, V., Young, K., Zagt, R., Zemagho, L., Zuidema, P.A., Zwerts, J.A., Phillips, O.L., Oliveira, E.A. de, Dávila, E.Á., Loayza, P.A., Andrade, A., Vieira, S.A., Aragão, L.E.O.C., Araujo-Murakami, A., Arets, E.J.M.M., Arroyo, L., Ashton, P., C., G.A., Baccaro, F.B., Banin, L.F., Baraloto, C., Camargo, P.B., Barlow, J., Barroso, J., Bastin, J.-F., Batterman, S.A., Beeckman, H.,

Begne, S.K., Bennett, A.C., Berenguer, E., Berry, N., Blanc, L., Boeckx, P., Bogaert, J., Bonal, D., Bongers, F., Bradford, M., Brearley, F.Q., Brncic, T., Brown, F., Burban, B., Camargo, J.L., Castro, W., Céron, C., Ribeiro, S.C., Moscoso, V.C., Chave, J., Chezeaux, E., Clark, C.J., Souza, F.C. De, Collins, M., Comiskey, J.A., Valverde, F.C., Medina, M.C., Costa, L. da, Dan̆cák, M., Dargie, G.C., Davies, S., Cardozo, N.D., Haulleville, T. de, Medeiros, M.B. de, Pasquel, J. del A., Derroire, G., Fiore, A. Di, Doucet, J.-L., Dourdain, A., Droissart, V., Duque, L.F., Ekoungoulou, R., Elias, F., Erwin, T., Esquivel-Muelbert, A., Fauset, S., Ferreira, J., Llampazo, G.F., Foli, E., Ford, A., Gilpin, M., Hall, J.S., Hamer, K.C., Hamilton, A.C., Harris, D.J., Hart, T.B., Hédl, R., Herault, B., Herrera, R., Higuchi, N., Hladik, A., Coronado, E.H., Huamantupa-Chuquimaco, I., Huasco, W.H., Jeffery, K.J., Jimenez-Rojas, E., Kalamandeen, M., Kamdem, M.-N., Kearsley, E., Umetsu, R.K., Kho, L.K., Killeen, T., Kitayama, K., Klitgaard, B., Koch, A., Labrière, N., Laurance, W., Laurance, S., Leal, M.E., Levesley, A., Lima, A.J.N.N., Lisingo, J., Pontes-Lopes, A., Lopez-Gonzalez, G., Lovejoy, T., Lovett, J.C., Lowe, R., Magnusson, W.E., Malumbres-Olarte, J., Manzatto, Â.G., Marimon, Ben Hur, J., Marshall, A.R., Marthews, T., Reis, S.M. de A., Maycock, C., Melgaço, K., Mendoza, C., Metali, F., Mihindou, V., Milliken, W., Mitchard, E.T.A., Morandi, P.S., Mossman, H.L., Nagy, L., Nascimento, H., Neill, D., Nilus, R., Vargas, P.N., Palacios, W., Camacho, N.P., Peacock, J., Pendry, C., Mora, M.C.P., Pickavance, G.C., Pipoly, J., Pitman, N., Playfair, M., Poorter, L., Poulsen, J.R., Poulsen, A.D., Preziosi, R., Prieto, A., Primack, R., Ramírez-Angulo, H., Reitsma, J., Réjou-Méchain, M., Correa, Z.R., Sousa, T.R. de, Bayona, L.R., Roopsind, A., Rudas, A., Rutishauser, E., Salim, K.A., Salomão, R.P., Schietti, J., Sheil, D., Silva, R.C., Espejo, J.S., Valeria, C.S., Silveira, M., Simo-Droissart, M., Simon, M.F., Singh, J., Shareva, Y.C.S., Stahl, C., Stropp, J., Sukri, R., Sunderland, T., Svátek, M., Swaine, M.D., Swamy, V., Taedoumg, H., Talbot, J., Taplin, J., Taylor, D., Steege, H. ter, Terborgh, J., Thomas, R., Thomas, S.C., Torres-Lezama, A., Umunay, P., Gamarra, L.V., Heijden, G. van der, Hout, P. van der, Meer, P.J. van der, Nieuwstadt, M. van, Verbeeck, H., Vernimmen, R., Vicentini, A., Vieira, I.C.G., Torre, E.V., Vleminckx, J., Vos, V.A., Wang, O., White, L.J.T.T., Willcock, S., Woods, J.T., Wortel, V., Young, K., Zagt, R., Zemagho, L., Zuidema, P.A., Zwerts, J.A., Phillips, O.L., C, G.A., Dančák, M., Pasquel, A., Coronado, E.H., 2020. Long-term thermal sensitivity of Earth's tropical forests. Science (80-.). 368, 869–874. https://doi.org/10.1126/science.aaw7578

Tanner, E.V.J., Rodriguez-Sanchez, F., Healey, J.R., Holdaway, R.J., Bellingham, P.J., 2014. Long-term hurricane damage effects on tropical forest tree growth and mortality. Ecology 95, 2974–2983. https://doi.org/10.1890/13-1801.1

Telewski, F.W., 1995. Wind-induced physiological and deveop-mental responses in trees, in: M.P., C., J., G. (Eds.), Wind and Trees. Cambridge University Press, Cambridge, UK, pp. 237–263.

Thom, A.S., 1971. Momentum absorption by vegetation. Q. J. R. Meteorol. Soc. 97, 414–428. https://doi.org/10.1002/qj.49709741404

Thornley, J.H.M., Cannell, M.G.R., 2000. Modelling the components of plant respiration: Representation and realism. Ann. Bot. 85, 55–67. https://doi.org/10.1006/anbo.1999.0997

Toledo, V.M., Ortiz-Espejel, B., Cortés, L., Moguel, P., Ordoñez, M. de J., 2003. The multiple use of tropical forests by indigenous peoples in Mexico: A case of adaptive management. Ecol. Soc. 7. https://doi.org/10.5751/es-00524-070309

Townsend, A.R., Asner, G.P., Cleveland, C.C., 2008. The biogeochemical heterogeneity of tropical forests. Trends Ecol. Evol. 23, 424–431. https://doi.org/10.1016/j.tree.2008.04.009

Trugman, A.T., Anderegg, L.D.L., Wolfe, B.T., Birami, B., Ruehr, N.K., Detto, M., Bartlett, M.K., Anderegg, W.R.L., 2019. Climate and plant trait strategies determine tree carbon allocation to leaves and mediate future forest productivity. Glob. Chang. Biol. 25, 3395–3405. https://doi.org/10.1111/gcb.14680

Turner, M.G., 2010. Disturbance and landscape dynamics in a changing world. Ecology 91, 2833–2849.

Turner, M.G., Dale, V.H., 1998. Comparing Large, Infrequent Disturbances: What Have We Learned? Ecosystems 1, 493–496. https://doi.org/10.1007/s100219900045

Uriarte, M., Canham, C.D., Thompson, J., Zimmerman, J.K., Murphy, L., Sabat, A.M., Fetcher, N., Haines, B.L., 2009. Natural disturbance and human land use as determinants of tropical forest dynamics: Results from a forest simulator. Ecol. Monogr. 79, 423–443. https://doi.org/10.1890/08-0707.1

USGS, 2015. Shuttle radar topography mission (SRTM) 1 Arc-Second global. https://doi.org//10.5066/F7PR7TFT

Valinger, E., Fridman, J., 1999. Models to assess the risk of snow and wind damage in pine, spruce, and birch forests in Sweden. Environ. Manage. 24, 209–217. https://doi.org/10.1007/s002679900227

Van Bloem, S.J., Murphy, P.G., Lugo, A.E., 2007. A link between hurricane-induced tree sprouting, high stem density and short canopy in tropical dry forest. Tree Physiol. 27, 475–480. https://doi.org/10.1093/treephys/27.3.475

Van Der Meer, P.J., Sterck, F.J., Bongers, F., 1998. Tree seedling performance in canopy gaps in a tropical rain forest at Nouragues, French Guiana. J. Trop. Ecol. 14, 119–137. https://doi.org/10.1017/S026646749800011X

Van der Zande, D., Stuckens, J., Verstraeten, W.W., Mereu, S., Muys, B., Coppin, P., 2011. 3D modeling of light interception in heterogeneous forest canopies using ground-based LiDAR data. Int. J. Appl. Earth Obs. Geoinf. 13, 792–800. https://doi.org/10.1016/j.jag.2011.05.005

van Zyl, J., Kim, Y., 2011. Synthetic Aperture Radar (SAR) Imaging Basics, in: Synthetic Aperture Radar

Polarimetry. pp. 1–25. https://doi.org/10.1002/9781118116104.ch1
Vanclay, J.K., Skovsgaard, J.P., 1997. Evaluating forest growth models. Ecol. Modell. 98, 1–12.
Vancutsem, C., Achard, F., Pekel, J.F., Vieilledent, G., Carboni, S., Simonetti, D., Gallego, J., Aragão, L.E.O.C., Nasi, R., 2021. Long-term (1990–2019) monitoring of forest cover changes in the humid tropics. Sci. Adv. 7, 1–22. https://doi.org/10.1126/sciadv.abe1603
Vandecar, K.L., Lawrence, D., Richards, D., Schneider, L., Rogan, J., Schmook, B., Wilbur, H., 2011. High Mortality for Rare Species Following Hurricane Disturbance in the Southern Yucatán. Biotropica 43, 676–684. https://doi.org/10.1111/j.1744-7429.2011.00756.x
Venables, W.N., Ripley, B.D., 2002. Modern Applied Statistics with S, Fourth. ed. Springer, New York.
Vieilledent, G., Courbaud, B., Kunstler, G., Dhôte, J.F., Clark, J.S., 2010. Individual variability in tree allometry determines light resource allocation in forest ecosystems: A hierarchical Bayesian approach. Oecologia 163, 759–773. https://doi.org/10.1007/s00442-010-1581-9
Vieilledent, G., Fischer, F.J., Chave, J., Guibal, D., Langbour, P., Gérard, J., 2018. New formula and conversion factor to compute basic wood density of tree species using a global wood technology database. Am. J. Bot. 105, 1653–1661. https://doi.org/10.1002/ajb2.1175
Viovy, N., 2018. CRUNCEP Version 7 - Atmospheric Forcing Data for the Community Land Model. Research Data Archive at the National Center for Atmospheric Research, Computational and Information Systems Laboratory. [WWW Document]. URL http://rda.ucar.edu/datasets/ds314.3/ (accessed 5.4.17).
Vollsinger, S., Mitchell, S.J., Byrne, K.E., Novak, M.D., Rudnicki, M., 2005. Wind tunnel measurements of crown streamlining and drag relationships for several hardwood species. Can. J. For. Res. 35, 1238–1249. https://doi.org/10.1139/x05-051
Wagner, F.H., Hérault, B., Bonal, D., Stahl, C., Anderson, L.O., Baker, T.R., Sebastian Becker, G., Beeckman, H., Boanerges Souza, D., Cesar Botosso, P., Bowman, D.M.J.S., Bräuning, A., Brede, B., Irving Brown, F., Julio Camarero, J., Camargo, P.B., Cardoso, F.C.G., Carvalho, F.A., Castro, W., Koloski Chagas, R., Chave, J., Chidumayo, E.N., Clark, D.A., Regina Capellotto Costa, F., Couralet, C., Henrique Da Silva Mauricio, P., Dalitz, H., Resende De Castro, V., Milani, J.E.D.F., Consuelo De Oliveira, E., De Souza Arruda, L., Devineau, J.L., Drew, D.M., Dünisch, O., Durigan, G., Elifuraha, E., Fedele, M., Ferreira Fedele, L., Figueiredo Filho, A., Finger, C.A.G., César Franco, A., Jnior, L.F., Galvão, F., Gebrekirstos, A., Gliniars, R., Maurício Lima De Alencastro Graça, P., Griffiths, A.D., Grogan, J., Guan, K., Homeier, J., Raquel Kanieski, M., Khoon Kho, L., Koenig, J., Valerio Kohler, S., Krepkowski, J., Lemos-Filho, J.P., Lieberman, D., Eugene Lieberman, M., Sergio Lisi, C., Longhi Santos, T., Ayala, J.L.L., Eijji Maeda, E., Malhi, Y., Maria, V.R.B., Marques, M.C.M., Marques, R., Maza Chamba, H., Mbwambo, L., Liana Lisboa Melgaço, K., Angela Mendivelso, H., Murphy, B.P., O'Brien, J.J., F. Oberbauer, S., Okada, N., Plissier, R., Prior, L.D., Alejandro Roig, F., Ross, M., Rodrigo Rossatto, D., Rossi, V., Rowland, L., Rutishauser, E., Santana, H., Schulze, M., Selhorst, D., Rodrigues Silva, W., Silveira, M., Spannl, S., Swaine, M.D., Toledo, J.J., Miranda Toledo, M., Toledo, M., Toma, T., Tomazello Filho, M., Ignacio Valdez Hernández, J., Verbesselt, J., Aparecida Vieira, S., Vincent, G., Volkmer De Castilho, C., Volland, F., Worbes, M., Lea Bolzan Zanon, M., Aragão, L.E.O.C., 2016. Climate seasonality limits leaf carbon assimilation and wood productivity in tropical forests. Biogeosciences 13, 2537–2562. https://doi.org/10.5194/bg-13-2537-2016
Walker, L.R., 1995. Timing of Post-Hurricane Tree Mortality in Puerto Rico. J. Trop. Ecol. 11, 315–320. https://doi.org/10.1017/S0266467400008786
Walker, L.R., 1991. Tree Damage and Recovery from Hurricane Hugo in Luquillo Experimental Forest, Puerto Rico. Biotropica 23, 379–385. https://doi.org/10.2307/2388255
Walsh, K.J.E., Mcbride, J.L., Klotzbach, P.J., Balachandran, S., Camargo, S.J., Holland, G., Knutson, T.R., Kossin, J.P., Lee, T. cheung, Sobel, A., Sugi, M., 2016. Tropical cyclones and climate change. Wiley Interdiscip. Rev. Clim. Chang. 7, 65–89. https://doi.org/10.1002/wcc.371
Wang, W.M., Li, Z.L., Su, H.B., 2007. Comparison of leaf angle distribution functions: Effects on extinction coefficient and fraction of sunlit foliage. Agric. For. Meteorol. 143, 106–122. https://doi.org/10.1016/j.agrformet.2006.12.003
Webb, E.L., van de Bult, M., Fa'aumu, S., Webb, R.C., Tualaulelei, A., Carrasco, L.R., 2014. Factors Affecting Tropical Tree Damage and Survival after Catastrophic Wind Disturbance. Biotropica 46, 32–41. https://doi.org/10.1111/btp.12067
Weber, H.C., Lok, C.C.F., Davidson, N.E., Xiao, Y., 2014. Objective Estimation of the Radius of the Outermost Closed Isobar in Tropical Cyclones. Trop. Cyclone Res. Rev. 3, 1–21. https://doi.org/10.6057/2014TCRR01.01
Weishampel, J.F., Urban, D.L., Shugart, H.H., Smith, J.B.J., 1992. Semivariograms from a forest transect gap model compared with remotely sensed data. J. Veg. Sci. 3, 521–526. https://doi.org/10.2307/3235808
Wenger, S.J., Olden, J.D., 2012. Assessing transferability of ecological models: An underappreciated aspect of statistical validation. Methods Ecol. Evol. 3, 260–267. https://doi.org/10.1111/j.2041-210X.2011.00170.x
Wickham, H., 2020. tidyr: Tidy Messy Data.
Wickham, H., 2016. ggplot2: Elegant Graphics for Data Analysis. Springer-Verlag New York.
Widlowski, J.L., Pinty, B., Lopatka, M., Atzberger, C., Buzica, D., Chelle, M., Disney, M., Gastellu-Etchegorry, J.P., Gerboles, M., Gobron, N., Grau, E., Huang, H., Kallel, A., Kobayashi, H., Lewis, P.E., Qin, W., Schlerf, M., Stuckens, J., Xie, D., 2013. The fourth radiation transfer model intercomparison (RAMI-IV):

Proficiency testing of canopy reflectance models with ISO-13528. J. Geophys. Res. Atmos. 118, 6869–6890. https://doi.org/10.1002/jgrd.50497
Wiegand, T., Moloney, K.A., 2014. Handbook of Spatial Point-Pattern Analysis in Ecology. Chapman and Hall/CRC Press.
Wilke, C.O., 2020. cowplot: Streamlined Plot Theme and Plot Annotations for "ggplot2". R package.
Woodcock, C.E., Allen, R., Anderson, M., Belward, A., Bindschadler, R., Cohen, W., Gao, F., Goward, S.N., Helder, D., Helmer, E., Nemani, R., Oreopoulos, L., Schott, J., Thenkabail, P.S., Vermote, E.F., Vogelmann, J., Wulder, M.A., Wynne, R., 2008. Free Access to Landsat Imagery. Science (80-.). 320, 1011–1012.
Wright, S.J., 2002. Plant diversity in tropical forests: a review of mechanisms of species coexistence. Oecologia 130, 1–14. https://doi.org/10.1007/s004420100809
Wright, S.J., Kitajima, K., Kraft, N.J.B., Reich, P.B., Wright, I.J., Bunker, D.E., Condit, R.S., Dalling, J.W., Davies, S.J., DíAz, S., Engelbrecht, B.M.J., Harms, K.E., Hubbell, S.P., Marks, C.O., Ruiz-Jaen, M.C., Salvador, C.M., Zanne, A.E., 2010. Functional traits and the growth-mortality trade-off in tropical trees. Ecology 91, 3664–3674. https://doi.org/10.1890/09-2335.1
Xi, W., 2015. Synergistic effects of tropical cyclones on forest ecosystems: a global synthesis. J. For. Res. 26. https://doi.org/10.1007/s11676-015-0018-z
Xi, W., Peet, R.K., 2011. The Complexity of Catastrophic Wind Impacts on Temperate Forests. Recent Hurric. Res. - Clim. Dyn. Soc. Impacts. https://doi.org/10.5772/16167
Yang, M., Défossez, P., Danjon, F., Fourcaud, T., 2014. Tree stability under wind: Simulating uprooting with root breakage using a finite element method. Ann. Bot. 114, 695–709. https://doi.org/10.1093/aob/mcu122
Yang, S., Olson, W.S., Wang, J.J., Bell, T.L., Smith, E.A., Kummerow, C.D., 2006. Precipitation and latent heating distributions from satellite passive microwave radiometry. Part II: Evaluation of estimates using independent data. J. Appl. Meteorol. Climatol. 45, 721–739. https://doi.org/10.1175/JAM2370.1
Yao, A.W., Chiang, J.-M., Mcewan, R., Lin, T.-C., 2015. The effect of typhoon-related defoliation on the ecology of gap dynamics in a subtropical rain forest of Taiwan. J. Veg. Sci. 26, 145–154. https://doi.org/10.1111/jvs.12217
Yap, S.L., Davies, S.J., Condit, R., 2016. Dynamic response of a Philippine dipterocarp forest to typhoon disturbance. J. Veg. Sci. 27, 133–143. https://doi.org/10.1111/jvs.12358
Yates, K.L., Bouchet, P.J., Caley, M.J., Mengersen, K., Randin, C.F., Parnell, S., Fielding, A.H., Bamford, A.J., Ban, S., Barbosa, A.M., Dormann, C.F., Elith, J., Embling, C.B., Ervin, G.N., Fisher, R., Gould, S., Graf, R.F., Gregr, E.J., Halpin, P.N., Heikkinen, R.K., Heinänen, S., Jones, A.R., Krishnakumar, P.K., Lauria, V., Lozano-Montes, H., Mannocci, L., Mellin, C., Mesgaran, M.B., Moreno-Amat, E., Mormede, S., Novaczek, E., Oppel, S., Ortuño Crespo, G., Peterson, A.T., Rapacciuolo, G., Roberts, J.J., Ross, R.E., Scales, K.L., Schoeman, D., Snelgrove, P., Sundblad, G., Thuiller, W., Torres, L.G., Verbruggen, H., Wang, L., Wenger, S., Whittingham, M.J., Zharikov, Y., Zurell, D., Sequeira, A.M.M., 2018. Outstanding Challenges in the Transferability of Ecological Models. Trends Ecol. Evol. 33, 790–802. https://doi.org/10.1016/j.tree.2018.08.001
Yoshimura, J., Sugi, M., Noda, A., 2006. Influence of greenhouse warming on tropical cyclone frequency. J. Meteorol. Soc. Japan 84, 405–428. https://doi.org/10.2151/jmsj.84.405
Zaehle, S., Sitch, S., Smith, B., Hatterman, F., 2005. Effects of parameter uncertainties on the modeling of terrestrial biosphere dynamics. Global Biogeochem. Cycles 19, 1–16. https://doi.org/10.1029/2004GB002395
Zemp, D.C., Schleussner, C.F., Barbosa, H.M.J., Hirota, M., Montade, V., Sampaio, G., Staal, A., Wang-Erlandsson, L., Rammig, A., 2017. Self-amplified Amazon forest loss due to vegetation-atmosphere feedbacks. Nat. Commun. 8. https://doi.org/10.1038/ncomms14681